Engineering safe mutations to protect cells from antibody-based targeted therapy

Inauguraldissertation

zur

Erlangung der Würde eines Doktors der Philosophie

vorgelegt der

Philosophisch-Naturwissenschaftlichen Fakultät

der Universität Basel

von

Anna Devaux

2023

Genehmigt von der Philosophisch-Naturwissenschaftlichen Fakultät
auf Antrag von
Prof. Dr. Lukas Jeker
Prof. Dr. Mihaela Zavolan
Prof. Dr. Nicole Joller

Basel, 13.12.2022

Prof. Dr. Marcel Mayor
The Dean of Faculty

Acknowledgement

First, I would like to thank Prof. Dr. Lukas Jeker for having given me the opportunity to do my PhD in his lab. Thank you for the supervision and the feedbacks about my thesis which helped me to grow as a scientist.

I would also like to thank my PaC committee members, Mihaela Zavolan and Nicole Joller, for the constructive criticisms and for all the feedbacks about my project. Thank you as well for your precious advices about doing a career in science.

The two studies presented here were made possible by the great contribution of Rosalba Lepore. Thank you for your amazing work in designing the variants.

This work would never have been possible without the support of the members of the Jeker lab. Giuseppina, Corinne, Hélène, Aino, I would never have managed to go through the entire journey without your kind support. Our discussions made me to grow professionally and personally and I will always be thankful for that. I would also like to thank Marianne, Madeleine, Emmanuelle, Denis and Marko for all our scientific and not scientific discussions. Our jokes convinced me that scientists can be brilliant and funny at the same time and I really enjoyed learning science with you. Denis, thank you for all your feedbacks about my work and for sharing with me your vision of science, finishing a PhD is more meaningful for me thanks to you. To finish, no experiment would have been possible in this lab without the organization skills of Romina, thank you for keeping the lab in order.

A great contribution to the projects came from our collaborators in Ridgeline. Stefanie, Anna C, Anna H, Alessandro, Iza and Emiel thank you for your amazing contribution to the projects. Amélie and Lisa, it was a great pleasure to elaborate experiments with you, I always enjoyed coming to Ridgeline to discuss with you.

This work would not have been possible without the kind gifts of Mihaela Zavolan and Simona Rossi who provided us the HEK293 cell line and the plasmid pEGFP-N1 vector.

The institute would not be the same without its great facilities. I learned so much from you Emmanuel, Telma, Lorenzo, Gaël, Stella and Jelena about flow cytometry. I always enjoyed spending time with you during my long sorts and I really appreciated your expertise, I knew that I could always trust you with my cells.

Bernd, you were the first to believe in me when I said that I wanted to do a PhD, I will always be thankful for this.

To finish, would like to thank my family for their constant support. I would like to thank you for all the efforts you put into trying to understand my work, even if it was so far away from what you know. It gave me the strength to go to the end of this project. I am also grateful to all my friend inside and outside the institute who helped me to keep in mind what is really important. It is really difficult for me to summarize in few words all the help and the support I got from you. I will just describe the most important: thanks to you, the craziest situations of this PhD turned into very funny stories. It was such a relief to have the opportunity to laugh about them with you.

The last but not least, I would like to thank William. You were on my side for all this doctorate, and I would not have managed the situations the same without your legendary calm. Thank you for your constant support.

Abbreviations

µl	microliter
A	Adenine
ABE	Adenine base editor
ADC	Antibody-drug conjugate
ADCC	Antibody-dependent cell mediated cytotoxicity
AML	Acute myeloid leukemia
B-ALL	B-cell acute lymphocytic leukemia
BEs	Base editors
C	Cytosine
CAR	Chimeric antigen receptor
CBE	Cytosine base editor
CDC	Complement-dependent cytotoxicity
cDNA	Coding DNA
CHO	Chinese hamster ovary
CLL	Chronic lymphocytic leukemia
CML	Chronic myeloid leukemia
CRISPR	Clustered regularly interspaced short palindromic repeats
CRS	Cytokine release syndrome
d	Days
DSBs	Double-strand breaks
ECD	Extracellular domain
Fab	Fragment of antigen binding
FDA	Food and drug administration
Fc	Fragment crystallizable
FCS	Fetal calf serum
FN3	Fibronectin type III
G	Guanine
GFP	Green fluorescent protein
GI	Gastro-intestinal
GM-CSF	Granulocyte macrophage-colony stimulating factor
GvHD	Graft-versus-host disease
GvL	Graft-versus-leukemia
gRNA	Guide RNA
h	Hour
HA	Homology arm
HD	Hodgkin disease
HDR	Homology-directed repair
HDRT	Homology-directed repair template
HEK	Human embryonic kidney
HLA	human leucocyte antigen
HSCs	Hematopoietic stem cells
HSCT	hematopoietic stem cell transplantation
HSPCs	Hematopoietic and progenitor stem cells

Igs	Immunoglobulins
IL-3	Interleukin 3
IL-3Rα	IL-3 receptor alpha-chain
JAK	Janus kinase
KO	Knock-out
KI	Knock-in
mAbs	Monoclonal antibodies
MDS	Myelodysplastic syndrome
MFI	Mean fluorescence intensity
ml	Milliliter
MPPs	Multipotent progenitors
MRD	Measurable residual disease
NLS	Nuclear localization signal
NGS	Next-generation sequencing
NHEJ	Non-homologous end joining
NHD	Non-Hodgkin disease
NK	Natural killer
nt	Nucleotide
PAM	Protospacer adjacent motif
PBS	Phosphate buffered saline
PCD	Plasma cell disorder
PCR	Polymerase chain reaction
pDCs	Plasmacytoid dendritic cells
PGA	Poly-l-glutamic acid
PEs	Prime editors
RNPs	Ribonucleoprotein particles
RT	Room temperature
s	Second
SAP	Saporin toxin
scFv	Single-chain variable fragments
SCID	Severe combined immunodeficiency
sgRNA	Single guide RNA
STAT	Signal transducer and activator of transcription proteins
Strep-PE	Streptavidin-phycoerythrin
T	Thymine
TALEN	Transcription activator-like effector nucleases
TCE	T-cell engager
TCR	T-cell receptor
TLS	Tumor lysis syndrome
U	Uracil
UGI	Uracil DNA glycosylase inhibitor
VH	Variable heavy chain
VL	Variable light chain
VKL	Variable kappa light chain
vs.	Versus
WT	Wild-type
ZFNs	Zinc finger nucleases

Index

Abstract

Therapeutic depletion of diseased cells using antibody-based targeted therapies such as monoclonal antibodies (mAbs), antibody-drug conjugates (ADCs), T cell engagers (TCEs) or chimeric antigen receptor (CAR)-T cells is very effective for hematologic diseases. However, shared expression of antigens between diseased and healthy cells bears the risk for collateral killing of healthy cells leading to unwanted side-effects. For instance, myeloid tumor cells and hematopoietic stem and progenitor cells (HSPCs) express very similar surface proteins resulting in a risk for extensive myelotoxicity upon targeted depletion. If the healthy cell is essential (e.g. HSPCs) then such co-expression may constitute a major, possibly insurmountable, barrier. In order to enable therapeutic targeting of such proteins, it was proposed to transplant engineered hematopoietic stem cells in which the target was removed. However, since removing the protein abolishes its function, this approach is limited to redundant proteins. Here, we show feasibility for shielding the therapeutic cells from antibody-based targeted therapy while preserving the expression of the targeted receptors with two proteins. In chapter I we showed that CD123, the interleukin-3 (IL-3) receptor alpha-chain, could be engineered to protect cells from targeted depletion. We identified several CD123 point mutations which protected *in vitro* from antibody dependent cellular cytotoxicity, TCE and CAR T-cells killing. Preserved function of two shielding variants was shown *in vitro* using the IL-3 dependent cell line TF-1 and *in vivo* using engineered HSPCs. In chapter II, we showed that a second protein, CD45, the protein tyrosine phosphatase receptor type C, could be engineered into primary human T cells to shield them from ADC killing. To finish, we optimized genome engineering of CD45 mutations using base editors. We showed that point mutations could be introduced with strategies other than CRISPR/Cas9 and homology-directed repair engineering, demonstrating that multiple genome engineering approaches could be employed to shield cells.

Introduction

1- Blood cells originate from the bone marrow in a highly regulated process

1.1- Hematopoiesis allows the development of multiple cell types

Hematopoiesis is the process which allows to daily produce and replenish blood cells. Every hour, hematopoietic stem cells (HSCs) and their progeny generate $1x10^9$ erythrocytes and $1x10^8$ leucocytes [1]. Studies on blood cells' origins started in mice with the observation that injection of bone marrow cells into lethally irradiated mice rescued them from death through a reconstitution of the full hematopoietic system by the donor cells [2]. Later, studies showed the proliferation capacity [3] and the ability of the bone marrow cells to reconstitute different cell lineages[4], explaining how these cells can refurbish a full hematopoietic system.

Two populations of bone marrow cells were identified by Osawa et al: the HSCs and the multipotent progenitors (MPPs) [5]. HSCs were associated with the markers $CD34^-KIT^+SCA\text{-}1^+Lin^-$ and allowed long term reconstitution of the blood system. Injection of a single cell with this profile was enough to reconstitute the lymphohematopoietic system for more than 3 months. The MPPs were identified with the markers $CD34^+KIT^+SCA\text{-}l^+Lin^-$ and gave multilineage reconstitution but not self-renewal. These cells were shown to be derived from HSCs, demonstrating that HSCs are able to reconstitute all blood cells after a differentiation process in which they progressively lose their self-renewal capacity [5]. Other markers were found to be associated with HSCs ($CD150^+$, $CD48^-$ [6], $CD135^-$ [7]) and allowed to classify cells according to their level of differentiation (**Figure 1**).

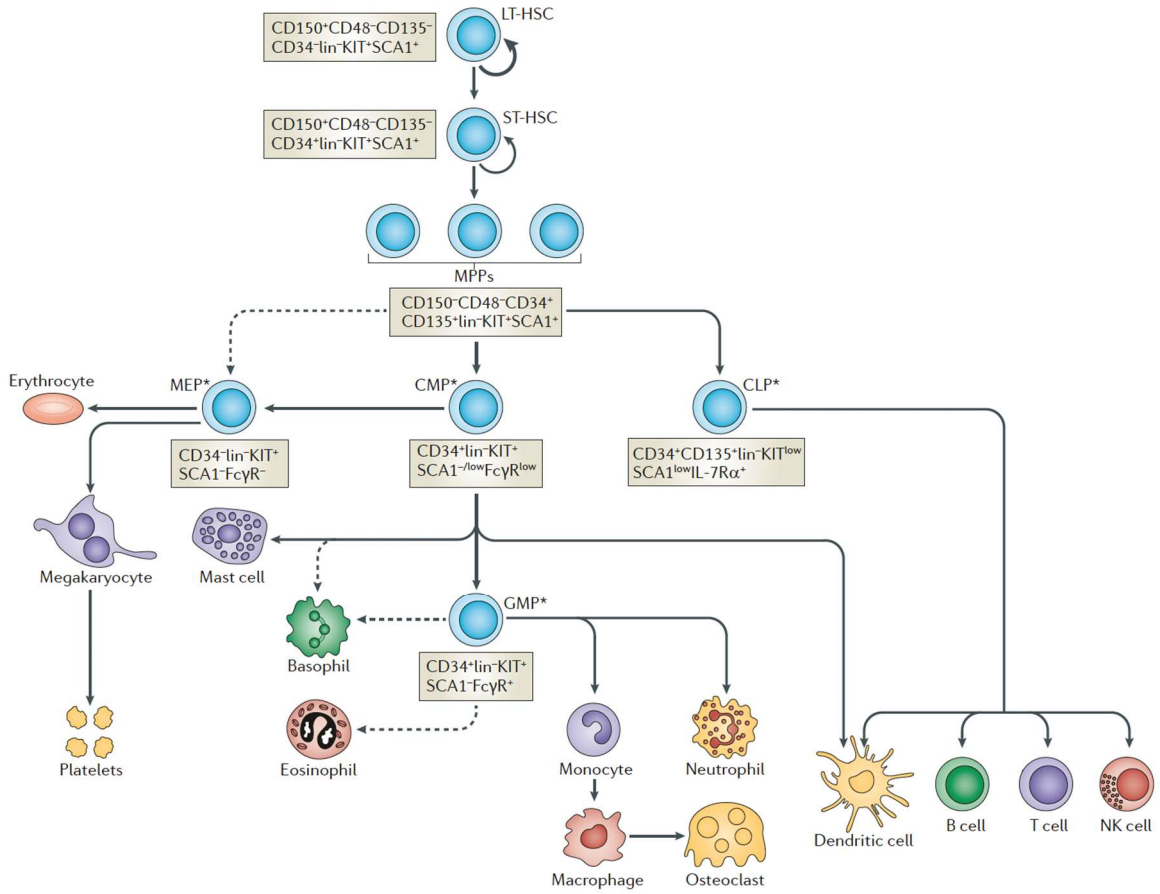

Figure 1: Hematopoiesis in the adult bone marrow

All hematopoietic cells originate from HSCs which can be differentiated into two types of cells: Long-Term reconstituting HSCs (LT-HSCs), which present self-renewal capacities and multi-lineage differentiation potential, and Short-Term reconstituting HSCs (ST-HSCs) which have lower self-renewal potential and start to differentiate into MPPs. Several subsets of MPPs were described in literature but they are not all shown here. MPPs differentiate into common lymphoid progenitor (CLP), common myeloid progenitor (CMP), megakaryocytes-erythrocyte progenitor (MEP) and granulocyte-monocyte progenitor (GMP). Dotted arrows show a potential origin of the cells. NK, natural killer. Figure taken from [1] *license No. 5415260182945*

Early in hematopoiesis, the MPPs $CD34^+KIT^+SCA\text{-}1^+Lin^-$ commit into the lymphoid or the myeloid lineages. Once a progenitor cell is engaged in a lineage, it cannot change anymore and will continue to differentiate within this lineage. The lymphoid lineage includes T cells, B cells and natural killer (NK) cells while the myeloid lineage comprises megakaryocytes, erythrocytes, mast cells, basophils, eosinophils, monocytes and neutrophils [8] (**Figure 1**). Only the dendritic cells can be issued from both lineages. At the end of the differentiation process, the fully differentiated cells can be identified with cellular markers. Markers are cell surface

proteins with specific functions. Some cellular markers are specific for a unique cell type. This is the case for CD3 which is expressed only on T cells, CD19 on B cells or CD14 on monocytes. Other are shared between several differentiated cells, for instance CD16 which is expressed on monocytes, neutrophils and NK cells. In addition, some markers are shared within cells lineage and are thus expressed in differentiated and less differentiated cells. This is the case for CD33 which was found in all the cells of the myeloid lineages. The most broadly expressed marker is CD45 as it was detected on all nucleated cells of the hematopoietic system [9].

1.2- Hematopoiesis relies on the environment of the HSCs

Hematopoiesis needs the appropriate environment for proper conservation and differentiation of the cells. A complex network of various cells forms the niche which supports HSCs [10] [1]. This environment comprises mesenchymal stroma cells [11], osteoclast [12], nerve cells [13], vascular structure [6], adipocytes [14] and macrophages [15]. Each cell type contributes to the self-renewal, the dormancy or the localization of the HSCs in the niche.

In addition, differentiation of HSCs into progenitors and cell lineages requires the help from cytokines. Cytokines can be differentiated between interleukins, colony-stimulating factors, interferons, erythropoietin and thrombopoietin. They signal through binding to cytokine receptors expressed at the surface of hematopoietic cells and support survival and differentiation steps (**Figure 2**).

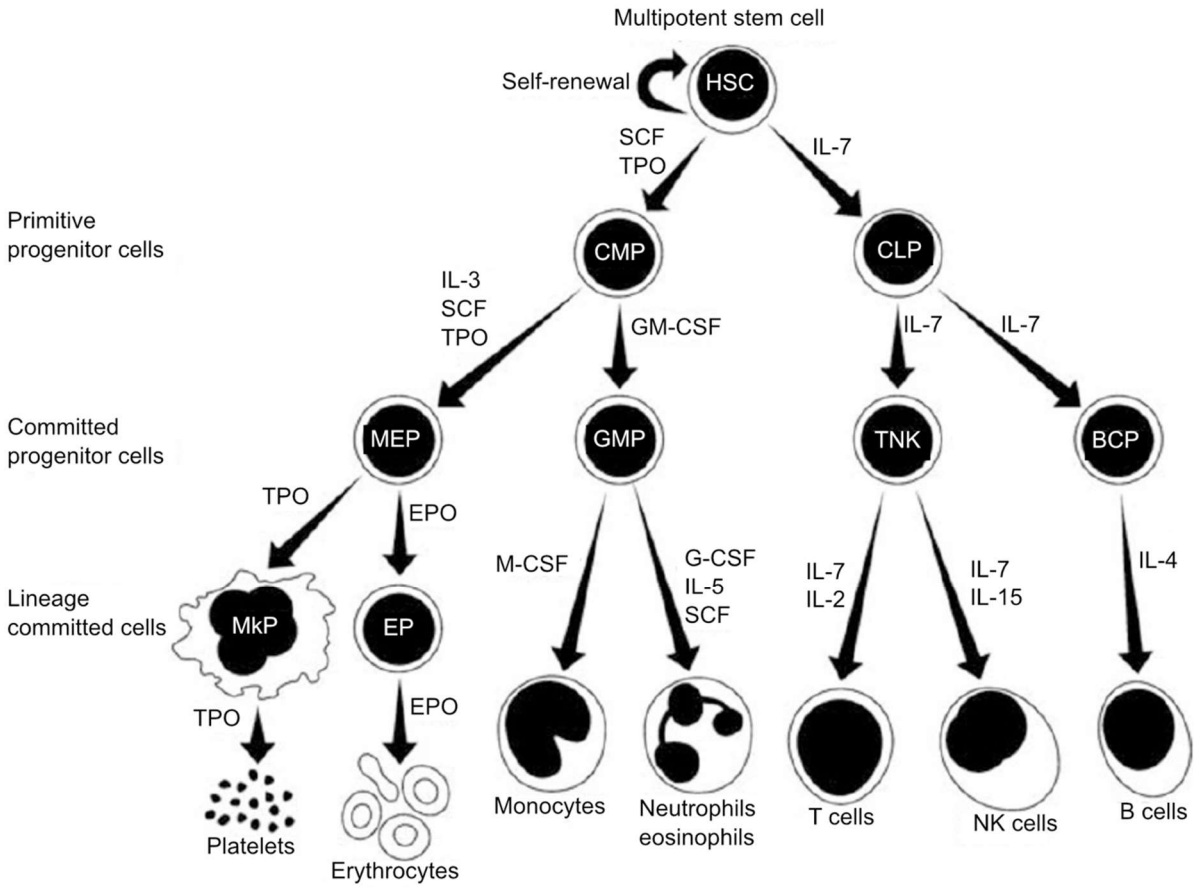

Figure 2: The role of cytokines in hematopoiesis

Points at which cytokines act to provide survival, proliferation an d in some cases differentiative signals. TNK, T-cell natural killer cell progenitor. BCP, B-cell progenitor. MkP, megakaryocyte progenitor. EP, Erythropoietic progenitor. TPO, Thrombopoietin. EPO, Erythropoietin. Figure taken from [16] *license No: 5415340949608*

Thus, hematopoiesis is a highly controlled process, regulated by the HSCs environment, which can regenerate the full hematopoietic system starting from only one undifferentiated cell.

1.3- Dysfunctions of different blood cell types lead to various outcomes

Blood cells dysfunctions can lead to diseases. Dysfunctions will lead to different outcome depending on the cells affected. For instance, diseases affecting red blood cells' function will cause anemia, while dysfunctions affecting the immune cells will lead to immunodeficiencies. Finally, tumorigenic cells can arise at any step of hematopoiesis, leading to two types of cancers: myeloid malignancies, which includes acute myeloid leukemia (AML), myelodysplastic syndrome (MDS), myeloproliferative neoplasm and chronic myeloid leukemia (CML); and lymphoid malignancies which include chronic lymphocytic leukemia

(CLL), T-cell acute lymphocytic leukemia, B-cell acute lymphocytic leukemia (B-ALL), plasma cell disorder (PCD), Hodgkin disease (HD) and non-Hodgkin disease (NHD)[17]

2- HSCT is potentially curative for many blood disorders but is associated with toxicities

2.1- Current conditioning strategies are toxic due to off-target effect

All of blood diseases can theoretically be cured with hematopoietic stem cell transplantation (HSCT) which aims to eradicate all the defective cells and to "reset" the hematopoietic system with injection of healthy HSCs [18]. In clinic, HSCT involves several steps (**Figure 3**).

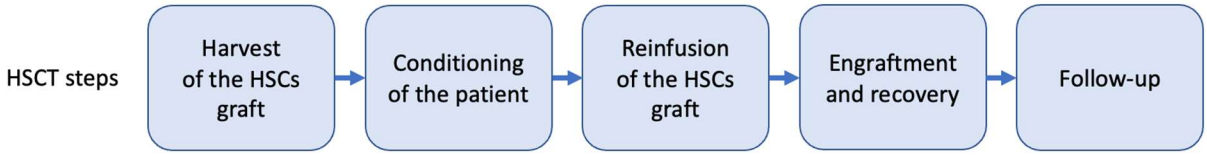

Figure 3: steps of HSCTs

Adapted from [19]

This treatment strategy is very promising as it is potentially curative. However, many complications arise from the conditioning step. The conditioning regimen is a preparative step coming before the injection of the graft which aims to eradicate the diseased cells [20]. Conditioning regimen are very efficient depleting strategies which can be given as chemotherapy or irradiation, each of them affecting differently the cells. For instance, irradiation reaches sites not accessed by chemotherapy [20]. However, conditioning regimens are unspecific and thus have a very high off-target toxicity to any dividing cells [21] [20]. Due to their lack of specificity, they were shown to be toxic for the heart, bladder, kidney, lungs, liver and gastro-intestinal (GI) tract. Irradiation was also shown to be harmful for the hematopoietic niche, impairing engraftment of the new HSCs [22]. Thus, this preparative step is so toxic that few patients can tolerate high dose conditioning regimen, but high doses are necessary in the case of cancer to kill all diseased cells.

2.2- Grafts can be associated with toxicities due to HLA mismatches

Unspecificity of conditioning leads to the depletion of HSCs. This is why it was suggested to rescue patient from this toxicity by HSCT, allowing the use of higher doses of conditioning while preserving patient's life [18]. The two current strategies of HSCs transplantation consist in

autologous and allogeneic transplantations. In autologous transplantation, the patients are transplanted with their own HSCs. This strategy is mainly used for lymphoid malignancies arising from differentiated cells (ie PCD, HD, NHD) [17]. The HSCs of the patients are healthy and can be used as graft, allowing the use of highly toxic conditioning. However, the grafts can be contaminated with tumor cells, contributing to relapses.

The second type of transplantation consists in the allogeneic transplantation, where the graft HSCs are taken from a donor. In case of cancers arising from immature cells diseases such as AML, MDS and ALL, the HSCs from the patient cannot be used as a graft as they can be themselves diseased. Therefore, cells must be taken from someone else, which comes with complications. Nowadays, graft HSCs are often harvested from a donor via injection of granulocyte colony stimulating factor which frees HSCs from bone marrow and mobilizes them to circulate in blood [23]. Peripheral blood stem cells are then extracted from the donor by leukapheresis, together with white blood cells such as T cells [24]. Thus, patients receive as graft a mixture of HSCs and white blood cells containing mature T cells. However, the injection of this cell mixture from a donor comes with a major risk: the rejection by the host or donor T lymphocytes of the cells of the other person. This rejection is due to a lack of histocompatibility. Histocompatibility is determined by the human leucocyte antigens (HLA) I and II and HLAs I are expressed at the surface of all cells. If the HLAs of the patient and of the donor are too different, the T cells from the donor or from the host can react. When the reaction is done by the host lymphocytes against the graft cells, this is host-versus-graft disease, leading to graft rejection. When the killing is done by the grafted lymphocytes on the host cells, this is graft-versus-host disease (GvHD) [20]. Nowadays, transplantations are performed with HSCs grafts taken from HLA-matched donors, reducing the risk of rejection and of GvHD. However, only the grafts of identical tween protect from these risks. Therefore, graft rejection is prevented by the depletion of the host lymphocytes, which are killed by the conditioning regimen together with the disease cells [20]. Despite the risk of GvHD, donor lymphocytes are kept as they are part of the cancer depleting strategy.

Allogeneic transplantation is advantageous for the treatment of cancers as the graft from the donor will help killing the tumor cells when the conditioning is not efficient enough [20]. Conditioning regimen such as chemotherapy is usually mostly toxic for proliferative cells. However, as malignant stem cells are quiescent, they are less sensitive to the conditioning and can lead to relapse. Thus, depleting these cells can be done with help of donor T lymphocytes [20]. The consequence but unexpected side effect of GvHD is that patients developing this disease have reduced cancer relapses. The alloreactive mature T cells which attack the host react

against the cancer cells, allowing the graft-versus-leukemia (GvL) effect [25]. GvL is an interesting strategy as it allows to deplete cancer stem cells without increasing the conditioning doses, protecting the patients from this toxicity. However, GvHD is a major risk of allogeneic transplantation. This immune reaction of donor T cells can lead to severe symptoms involving the skin and the GI tract and would be deadly if not treated [26].

2.3- HSCT is so far not used to its full extent for the treatment of cancers

Through the HSCT process, patients can experience many types of toxicities associated with the early conditioning step (**Figure 4**).

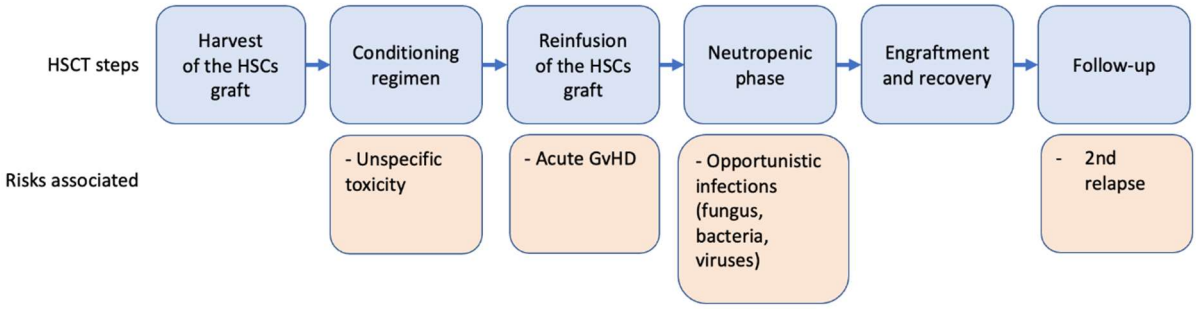

Figure 4: Complications associated with conditioning steps of HSCTs in cancers treatments
Adapted from [19]

First, GvHD is accentuated by the injury induced by the conditioning regimen[20]. Then, following myeloablation, patients experience neutropenia which render them vulnerable to all types of bacterial, fungal, virus infections[27] and arising of new cancers[28]. The recovery of the innate immunity usually takes place in the months following the transplantation, while the recovery of the adaptive immunity takes 1-2 years [29]. Moreover, conditioning itself when used at high doses can trigger the arising of a secondary cancer from cells which did not belong to the original tumor [28].

In order to protect patients from the different toxicities and side-effects of the conditioning, preparative regimens can be given at different intensities: myeloablative, reduced intensity and non-myeloablative [18]. However, this does not work for cancers. If the conditioning regimen is not intense enough, some residual leukemic cells can remain in the bone marrow. When residual leukemic cells are detected despite a disappearance of all cancer signs, they are quantified as the measurable residual disease (MRD). A high level of MRD can be a sign that the patient will relapse[30]. Thus, use of conditioning to eradicate cancer cells faces a paradox:

too few will lead to a high level of MRD and risk of relapse, while too much will be toxic and even lead to the generation of new cancer cells

HSCT is a promising treatment for hematological cancers because it is potentially curative. However, while in 2013 it was estimated that 156 099 patients will develop hematological malignancies [31], only 39 209 HSCT were actually performed [32]. Indeed, due to the risks associated with this strategy, and particularly with conditioning, other treatments are preferred. Unfortunately, many malignant blood diseases have no other alternative than to be treated with HSCT. Thus, fragile patients who cannot tolerate a high intensity of conditioning will relapse and we currently do not have any solution to cure these patients. This is why it is worth pursuing the development of new strategies: if we could reduce the unspecific toxicity of the conditioning while preserving a high depletion of cancer cells, HSCT would become a safe solution to cure all blood cancers.

3- Targeted therapies deplete specifically cancer cells with low off-target toxicity

3.1- Depleting antibody-based targeted therapies use antibodies' properties to target killing

More than 100 years ago, Paul Ehrlich emitted the idea of killing specifically cancer cells while sparing the others thanks to "magic bullets" [33]. This concept motivated lots of research as targeting cancer cells only would be much less toxic than chemotherapy or irradiation. Following this idea, targeted therapies were developed to reach specific molecules differentially expressed in cancer cells compared to healthy cells. Molecules differentially expressed in cancer can be classified into different categories: cell surface antigens, growth factors/receptors/signal transduction pathways, cell cycle inhibitors, apoptosis inducers and angiogenesis inducer [34]. Among these molecules, cell surface antigens are targets of choice as they can potentially be recognized by monoclonal antibodies (mAbs). Then, antibodies can be engineered into cancer depleting therapies, enabling a specific killing of cells through targeting their cell surface proteins.

In blood cancers, few cell surface antigens are specific of cancer cells. However, we saw that hematological malignancies arise from different cell subsets and that subsets of hematopoietic cells express different cell markers. Thus, these markers can be used to target cell depletion with antibodies, killing only the tumor cells and the cell subset associated. Such a system would be much more specific than the current conditioning with chemotherapy and would have many advantages: in addition to a reduced general toxicity on many organs, the incoming HSCs would find a healthier niche and likely engraftment will be faster. Then, the patient would

experience a faster posttransplant reconstitution and therefore will hopefully have a reduced neutropenia. Thus, antibody-based depletion therapies could be a safer alternative to high dose conditioning for the treatment of blood cancers.

Depleting antibody-based targeted therapies rely on antibodies' inner properties to target specifically antigens. These properties make antibodies, which are also known as immunoglobulins (Igs), a unique type of proteins highly used to develop treatments. Igs are heterodimeric molecules comprising two functional parts: the fragment of antigen binding (Fab) which contains the variable parts of the antibody and the fragment crystallizable (Fc) region which contains the constant part (**Figure 5**).

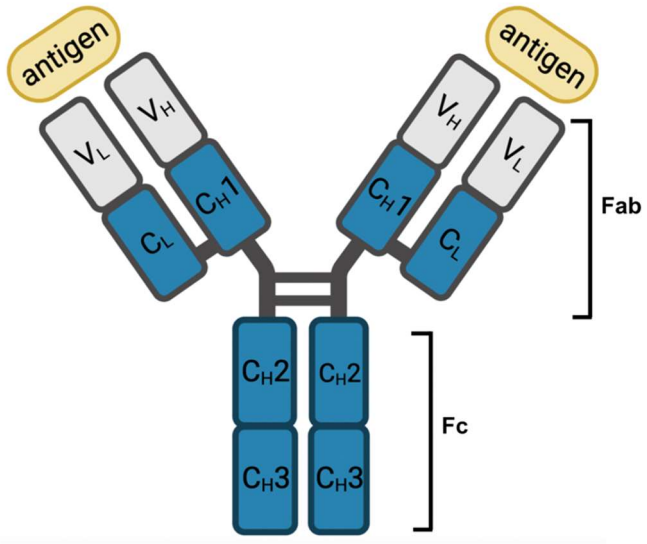

Figure 5: Antibody structure

Antibodies are heterodimers of two chains, the heavy ($_H$) and the light chain ($_L$). Each of these chain comprises constant (blue, C) and variable (gray, V) parts. The variable light chain (V_L) and the variable heavy chain (V_H) bind the antigen (yellow). Fab: Fragment of Antigen binding. Fc: Fragment crystallizable. Figure created with BioRender.com

The variable regions of the Fab encode for the complementary-determining regions which allow specific recognition of the target. The structure of the Fc part determines the class of the Ig among the 5 human ones: IgM, IgE, IgA, IgD or IgG. The Fc part makes the link with the rest of the immune system. It triggers cytotoxicity performed by the complement, the complement-dependent cytotoxicity (CDC). It can also trigger the cytotoxicity performed by immune cells: the antibody dependent cellular cytotoxicity (ADCC) and the antibody-dependent cellular phagocytosis [33]. Thus, the specificity of Igs allows to recognize specific proteins on a cell, e.g. CD19, CD3, and thus to identify specific cells subsets. To conclude,

mAbs have very interesting properties to develop depleting targeted therapies for blood cancers.

3.2- mAbs, ADCs, TCEs and CAR-T cells deplete cancer cells with high potency

Some antibody-based targeted therapies have already shown spectacular results on the treatment of B-cell malignancies with the targeting the cell marker CD19 [35] [36] [37]. These strategies involved antibody-based targeted therapies combined with reduced conditioning intensities [36] or without conditioning at all [35]. They led to the complete remission of the patients, showing that antibody-based targeted therapies could offer a less toxic alternative to HSCT to cure blood cancers.

So far, 4 depleting antibody-based targeted therapies modalities were successful in treating blood cancer and thus were approved by regulatory agencies: the mAbs, the antibody drug conjugates (ADCs), the T-cell engagers (TCEs) and the chimeric antigen receptor (CAR)-T cells (**Figure 6**)

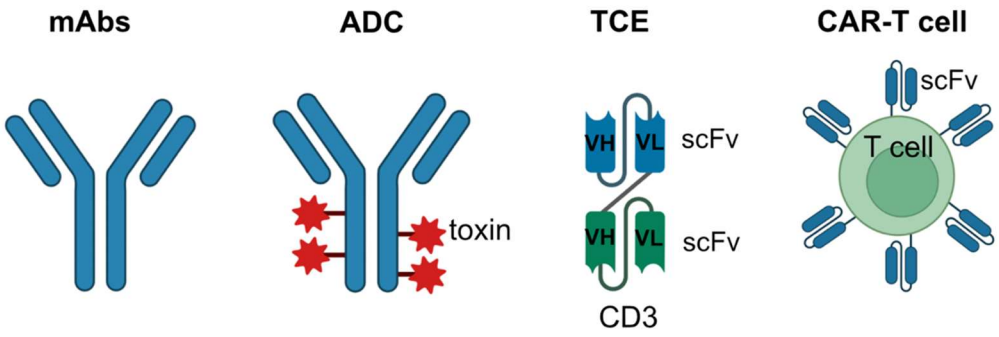

Figure 6: Formats of antibody-based targeted therapies for cell depletion

mAbs designed for cell depletion induce cytotoxicity by triggering ADCC. ADCs induce cytotoxicity by internalization of the toxins into the target cell. TCEs induce cytotoxicity by bridging T cells to their target. CAR-T cells induce cytotoxicity by activating the engineered T cell. Figure created with BioRender.com

Each antibody-based targeted therapy modality has its own advantages and drawbacks.

Depleting mAbs kill cancer cells by triggering CDC or ADCC (**Figure 6**). CDC is activated by binding of the Fc region to the complement protein C1q, while ADCC is activated by attachment of Fc region to the FcγRIIIa of NK cells (CD16A) [33]. Triggering of ADCC can be further improved by increasing the affinity of the Fc part of the antibody to its receptors. This can be done by selecting a specific IgG subclass [38] or by glycoengineering the Fc part [39]. MAbs have the advantage to be easy to produce and cost effective compared to other antibody-based

targeted therapies modalities. However, they need a functional immune system and thus can be not potent enough for killing in some cases.

Depletion potency of mAbs can be increased by attaching cytotoxic toxins to their Fc part, generating ADCs (**Figure 6**). ADCs are complex molecules which can kill cells independently of a functional immune system. They target a cytotoxic payload to cells expressing a specific antigen. Following their internalization, they release their cytotoxic payload, killing the target cell. Thus, internalization is a key property for this format to work [40]. The currently most used toxins are anti-mitotic tubulin disruptors and DNA damaging agents [41]. Efficiency of an ADC depends on several components: the antibody, the choice of target, the type of drug and its attachment strategy, making the design of a functional ADC a complex process [40 41]. Therefore, it is difficult to predict what will lead them to release their toxin. This explains why this depleting modality is often associated with a high off-tumor on-target, due to the uncontrolled separation of the toxin and the mAbs in non-targeted tissues.

In the search of different modes of action for cell depletion it was observed that T cell could function as serial killer of cancer cells [42]. These cells have such a high killing potency that they need to be restricted by the HLA dependency and mechanisms of immune tolerance to prevent autoimmunity. Following this observation, antibodies-based strategies were designed to bridge the T cells with target cells, triggering the killing of the target cells independently of these restrictions. These antibodies-based strategies were named bispecific antibodies and consisted in a construct made of a fusion of two antibody variable parts. While one part of the bispecific antibody recognized an element of the T cell receptor (eg CD3), enabling activation of the T cells, the other part recognized the target. The first T cells re-direction was done in 1985 with the engineering of an antibody targeting T-cell receptor (TCR) to another targeting the Thy-1.1 antigen, showing targeted killing of tumor cell lines [43]. Many types of bispecific constructs were generated since then. In this work we will discuss only the TCE as this format was approved by regulatory agencies. TCEs are composed of two single-chain variable fragments (scFv) fused together, one binding to CD3 on T cells and the other one the antigen (**Figure 6**) [41]. They were shown to be extremely effective: the anti-CD19 blinatumomab was shown to cure patient from B-ALL without help of conditioning [35]. However, this high killing potency has drawbacks, over-activation of T cells can lead to the uncontrolled release of cytokines known as cytokine release syndrome (CRS), which is life-threatening for the patients [42]. Thus, TCEs can be very effective, but they have limitations. In addition, they need functional T cells and their access is limited to areas accessible for antibodies, they cannot infiltrate tissues as well as T cells can do.

A more efficient T cells bridging strategy would be to have the antibody variable region directly attached to the surface of the T cells through a specific receptor. In addition to the advantages of the HLA independency and the breaking of immune tolerance seen with TCE, this therapy could exploit the property of T cells to infiltrate the tissues and to stay as memory, keeping the cancer on check years after injection. This would be interesting compared to the antibodies format as these latter are quickly eliminated from the body (i.e. the mAbs rituximab is eliminated in about 27 days [44] while the TCE blinatumomab is eliminated in 1.42 h [45]). Such an idea was tested in 1989 by a team who inserted in T cells the variable chains of a specific antibody in front of TCR constant parts, showing specific killing of the target cells [46]. This idea was further developed with the construction of a receptor in which scFv were attached to the TCR constant part ζ and γ, showing T cell targeted killing [47]. Today, the receptor is optimized in several versions and this concept is named CAR-T cells [48]. CAR-T cells are the most potent antibody-based targeted therapy as they have the possibility to stay long-term in the patients, keeping the tumor in check. Remarkably, therapeutic cell persistence was observed up to a decade [49]. This is explained by the permanent presentation of the CD19-CAR antigen, mainly due to the production of pre-B cells by HSCs [48]. However, similarly to TCE, this treatment strategy involves CRS [42]. A summary of advantages and drawbacks of each strategy is displayed in **Table 1**.

Table 1: Summary of advantages and drawbacks of each depleting antibody-based targeted therapy used to treat blood malignancies

Targeted therapy	Advantages	Drawbacks	Selected reviews
IgG	Easy to manufacture Cost-effective	Need functional immune system Less efficient than T cells to travel through tissues	[41] [33]
ADC	More specific than chemotherapy Work in absence of functional immune system	High off-target and organ toxicity due to toxin release Complex to design Less efficient than T cells to travel through tissues	[41] [40]
TCE	Trigger T cell activation Highly efficient	Short half-life Cytokine release syndrome Need functional T cells Less efficient than T cells to travel through tissues	[42] [41]
CAR-T cells	Trigger T cell activation Highly efficient Persist in the organism	Cytokine release syndrome Expensive and complex to manufacture	[48] [42]

To conclude, different modalities can be used to target specific markers at the surface of cancer cells. Antibody-based targeted therapies present a promising alternative to conditioning for the treatment of blood cancers.

4- Healthy cells can be shielded from the off-tumor on-target effect of targeted therapies

4.1- Targeted therapies can be limited by their off-tumor on-target activity

Mabs, ADCs, TCEs and CAR-T cells deplete all cells sharing their antigen. Thus, healthy cells can be killed by the therapy, leading to what is known as the off-tumor on-target effect. This effect is well illustrated by the use of CAR-T cells for the treatment of B cells malignancies [49] [36] [37]. Despite the major success of the therapy, remaining B cell aplasia was observed for some cases more than 3 years after infusion [49] [36] [37]. Thus, even if targeted therapies are more specific

and less toxic than currently used conditioning strategies, they are still toxic as they deplete cell subsets without differentiating healthy from cancer cells.

Humans can survive without B cells if they receive regular injections of immunoglobulins [50], which make the off-tumor on-target toxicity acceptable when B cells markers are targeted. However, in other blood cancers such as AML, antigens expressed at the surface of cancer cells are mostly shared with HSCs [51] [52]. Use of life-long depleting antibody-based targeted therapy to kill cancer cells would therefore be myelotoxic. For instance, it was demonstrated that targeting CD123 and CD33 with CAR-T cells, two targets expressed in AML and on HSCs, led to myeloablation in xenografted mouse models [53] [54]. Due to this fear of toxicity, most of the depleting antibody-based targeted therapies accepted so far by the US food and drug administration (FDA) for hematological diseases target B cells antigens only (CD19, CD20, BCMA, CD22) (**Table 2**), and clinical trials for CD123 require to have a matched allogeneic donor ready if needed (NCT03114670).

Table 2: Depleting antibody-based targeted therapies approved by FDA for the treatment of hematological malignancies in 2021

Targeted therapy	Name	Target	Application
IgG	Tafasitamab	CD19	B cell lymphoma
	Rituximab	CD20	NHD/CLL
	Ofatumumab	CD20	CLL
	Obinutuzumab	CD20	CLL, Follicular Lymphoma
	Daratumumab	CD38	Multiple myeloma
	Isatuximab	CD38	Multiple myeloma
	Alemtuzumab	CD52	CLL
ADC	Belantamab mafodotin	BCMA	Multiple myeloma
	Loncastuximab tesirine	CD19	B cell lymphoma
	Tositumomab-I131 (radioconjugated)	CD20	B cell non-Hodgkin lymphoma
	Ibritumomab tiuxetan (radioconjugated)	CD20	NHD
	Inotuzumab ozogamicin	CD22	B-ALL
	Moxetumomab pasudotox	CD22	Hairy cell leukemia
	Brentuximab vedotin	CD30	Hodgkin lymphoma and systemic anaplastic large cell lymphoma
	Gemtuzumab ozogamicin	CD33	AML
	Polatuzumab vedotin	CD79b	B cell lymphoma
TCE	Teclistamab	BCMA, CD3	Multiple myeloma
	Blinatumomab	CD19,CD3	ALL
	Mosunetuzumab	CD20, CD3	Follicular lymphoma
CAR-T	Tisagenlecleucel	CD19	ALL [55]
	Axicabtagene ciloleucel	CD19	Large B cell lymphoma [55]
	Brexucabtagene autoleucel	CD19	Mantle cell lymphoma [55]
	Lisocabtagene maraleucel	CD19	Large B cell lymphoma [55]
	Idecabtagene vicleucel	BCMA	Multiple myeloma [56]
	Ciltacabtagene autoleucel	BCMA	Multiple myeloma [56]

The Antibody Society. Therapeutic monoclonal antibodies approved or in regulatory review. (26.09.2022); www.antibodysociety.org/antibody-therapeutics-product-data, [55] [56]

Thus, despite the achievement in treating B cell cancers, these strategies could not be adapted to other blood tumors due to the risk of HSCs depletion. To adapt targeted therapies to tumor expressing HSCs antigens, new approaches need to be developed.

4.2- Knock-out of targeted therapies' antigens shields cells from off-tumor on-target toxicity

In order to treat tumor cells bearing shared HSC antigens without myeloablation, depleting antibody-based targeted therapies need a way to differentiate healthy HSCs from cancer cells. To do so, several teams suggested to engineer healthy HSCs *ex vivo* to shield them from the

therapy, before to re-inject them into the patient. They suggested to shield them by removing the targeted antigen with a knock-out (KO) of the protein. This created a new therapeutic strategy comprising two products, the antigen-specific depleter (mAb, TCE, CAR-T cells, ADC) and the donor shielded HSCs (**Figure 7**).

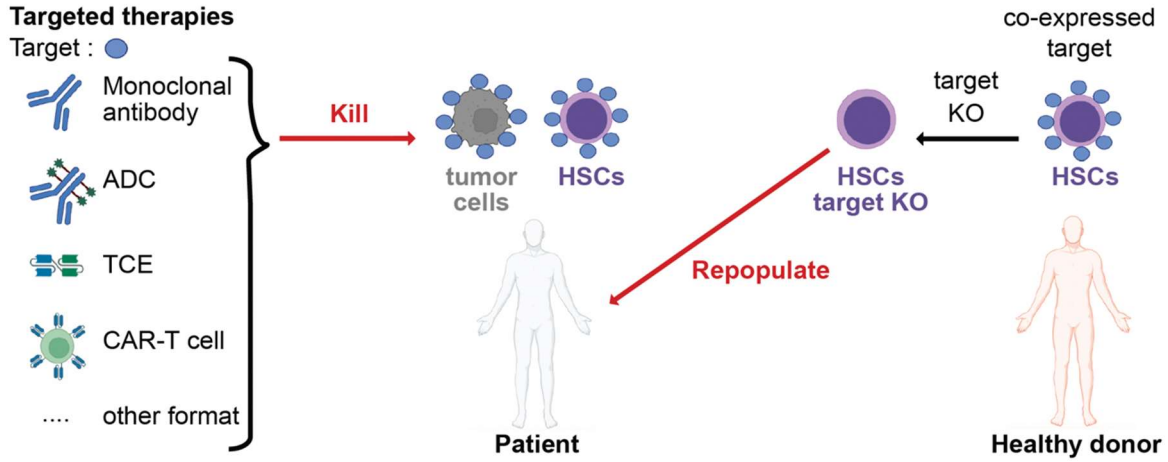

Figure 7: Combination product of KO HSCs/Immunotherapies strategy

Left: Depleting antibody-based targeted therapies are injected into the patient and deplete cells presenting their targeted antigen: cancer cells and HSCs. Right: Healthy HSCs are taken from a matched donor and genome engineered in order to remove targeted antigen from their surface. Targeted therapy and shielded HSCs are injected together in the patient. Figure inspired from [57]

First proof-of-concept of this combination product was done with the target CD33. CD33 is a transmembrane receptor of the Siglec family expressed on all cells of the myeloid lineage and identified as a target of choice for AML [58]. Two research groups made a KO of CD33 in human HSCs with clustered regularly interspaced short palindromic repeats (CRISPR)/Cas9 and co-injected the cells in immunodeficient mice with CD33 CAR-T cells. Engineered HSCs showed multilineage engraftment in the peripheral blood and shielding from CD33 CAR-T cells killing [57 59].

A different study suggested to cut out the exon2 (V-set part) of CD33 at the endogenous level, resulting in the expression of a short, naturally occurring isoform of the protein[60]. The exon 2 is the target of all the anti-CD33 antibodies currently tested in clinical trial, which are derivatives of the gentuzumab ozogamicin (**Table 2**). Therefore, these engineered HSCs will be virtually protected from all the new CD33 targeted therapies arising. *In vivo*, engineered cells showed engraftment of all lineages and protection from the anti-CD33 antibody

gentuzumab ozogamicin, demonstrating the functionality and the shielding of the CD33 shorter isoform [60].

CD7 is found at the surface of T and NK cells [61] and it is one of the earliest marker of T cells development [62], but it is also found on the surface of HSCs [61]. Targeting CD7 with depleting therapies would kill cancer cells together with HSCs, T and NK cells. Similarly to the strategy presented above with CD33, Kim et al knocked-out CD7 in HSCs with CRISPR/Cas9 [63] [61] and showed that the CD7 KO T and NK cells which developed after CD7 KO HSCs engraftment in mice were still functional. In addition, CD7 KO cells were protected from CD7 antibody-based targeted therapy depletion [61].

To conclude, off-tumor on-target killing of depleting antibody-based targeted therapies on donor HSCs can be avoided with target KO in therapeutic cells. The combination product of targeted therapy/shielded HSCs would have many advantages for the treatment of blood cancers as: (i) it would allow to target new antigens so far undruggable due to off-tumor on-target toxicity (ii) it would allow to target antigens with high toxicity, increasing chances to kill all cancer stem cells, (iii) it would allow to use the depleting therapy even after the HSCT and to treat relapsing cells.

However, this system relies on KO, meaning that only dispensable proteins can be targeted. This is problematic as few proteins are really unnecessary and a dispensable protein can be downregulated by cancer cells, leading to relapses. This is why we suggest a different shielding strategy. Instead of a KO, we propose to introduce point mutations in the antigen target, preserving the function of the protein while disrupting the binding of the antibody-based targeted therapy. This strategy would allow to target proteins that could not be knocked-out due to their important role in cell function, increasing the number of available targets. Moreover, this would be advantageous for the treatment of cancers as important proteins have less chances to be downregulated by tumor cells. However, such a strategy needs an efficient way to introduce point mutations in the genome of HSCs.

5- Shielding is allowed by genome engineering

5.1- Several genome engineering strategies are available

Shielding of HSCs with antigens modification relies on the introduction of mutations in the genome of the cells. Recently, many strategies to engineer the genome of cells arose and it is now a challenge to adapt them for HSCs. Nonetheless, developing genome engineering

strategies for HSCs is worthy considering all the innovative treatments it would allow. For instance, it was shown that engineering of hematopoietic stem and progenitor cells (HSPCs) could rescue sickle cell disease in mice [64].

Each genome engineering technology consist in a complex system which can recognize a specific area of the genome and cut it to insert mutations (**Figure 8**).

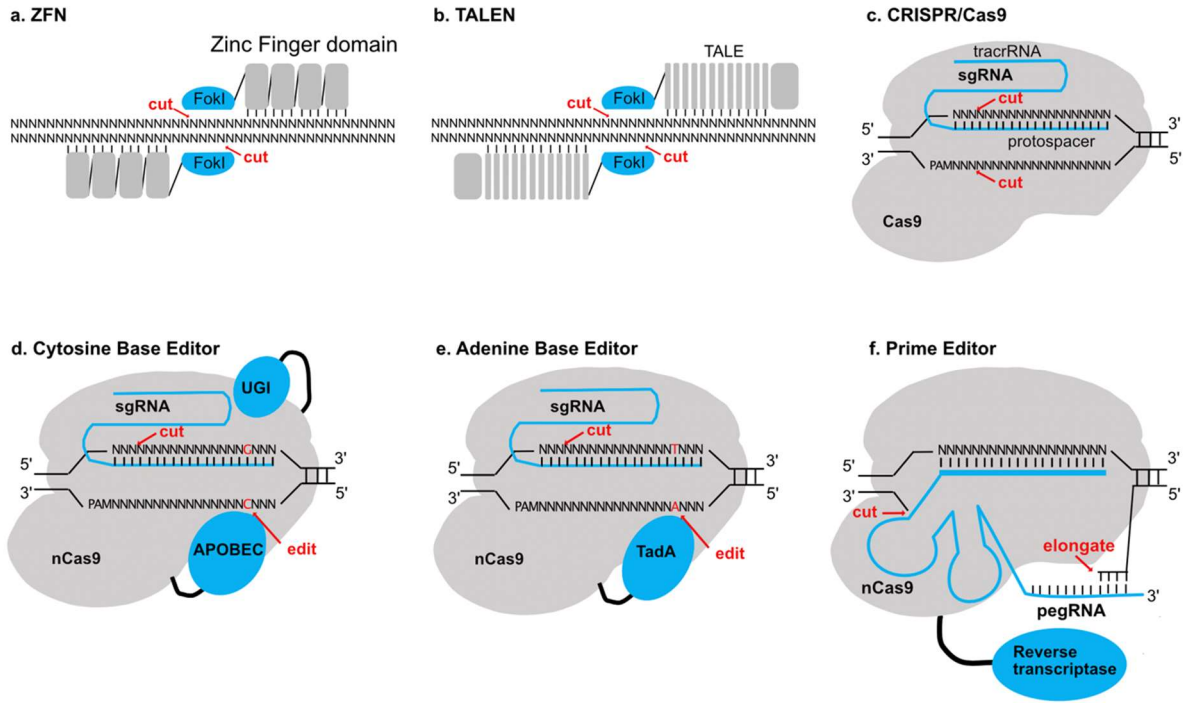

Figure 8: Schematic representation of the different systems available for genome engineering

***a**. Zinc-Finger Nuclease (ZFNs). ZFNs cut two strands of DNA in pairs using the FokI restriction enzyme. **b**. Transcription activator-like effector nucleases (TALEN). TALEN cuts two strands of DNA in pairs using the FokI restriction enzyme. **c.** CRISPR/Cas9. CRISPR/Cas9 cuts two strands of DNA after recognition of the protospacer adjacent motif (PAM) sequence (NGG) next to the protospacer. **d**. Cytosine Base Editor. Cut one strand of DNA and deaminase cytosines on the other strand with the help of APOBEC. Uracil DNA glycosylase inhibitor (UGI) prevents the correction of the deamination by the base excision repair pathway **e.** Adenine Base Editor. Cut one strand of DNA and deaminase Adenines on the other strand with the help of TadA. **f.** Prime Editor (PE). PE cut one strand of DNA and anneal it to its pegRNA. Cut DNA is then elongated by the reverse transcriptase according to the sequence of the pegRNA, inserting mutations. Figure inspired from* [66 67 68 69 70 72]

The first strategy developed consisted in zinc finger nucleases (ZFNs) which are composed of Zinc Finger DNA-binding domains coupled to the restriction enzyme FokI (**Figure 8a**) [65]. Recognition of a specific DNA sequence is allowed by the zinc finger domains, each of them

binding 3 consecutive base pairs of DNA. Then, the two FokI cut the DNA, allowing the generation of a double strand breaks (DSBs). ZFNs need to be designed in pairs with binding sites in close proximity in order to cleave both DNA strands [66]. Thus, targeting a precise site in the genome is resource intensive as it demands engineering of two chimeric nucleases.

Transcription activator-like effector nucleases (TALEN) are a similar technology using transcription activator-like effectors of plant instead of Zinc Finger DNA-binding domains (**Figure 8b**). Each TALEN molecule is composed of a repeat of modules binding one DNA base pair via 2 amino acids. As ZFNs, TALENs cleave DNA in pairs and demand expensive optimization [67].

Discovery of CRISPR/Cas9 system in *S. pyrogenes* allowed a major step forward in the development of genome engineering technologies. CRISPR/Cas9 consist in a Cas9 endonuclease complexed to a guide RNA (gRNA) composed of a protospacer recognizing the cutting site and of a tracrRNA allowing the formation of a complex between Cas9 and the gRNA. CRISPR/Cas9 leads to a cleavage of dsDNA when the protospacer recognize a region located near a protospacer adjacent motif (PAM) (**Figure 8c**) [68]. This system was a major improvement in terms of flexibility compared to ZFNs and TALENs as there is no need of protein engineering to target different DNA localizations, only design of new protospacers. The main limitation for this system is the need of the PAM, necessary for the cut of Cas9 [68].

This technology was derived into base editors (BEs), which have the advantage to edit nucleotides (nt) while cutting only one strand of the DNA. Base editors are system composed of a nickase Cas9 and a deaminase allowing nucleotides deamination from C to T for the cytosine base editors (CBE) [69] (**Figure 8d**) and from A to G for the adenine base editors (ABE) [70] (**Figure 8e**). They were used to develop the concept of CRISPR-STOP: genes were silenced through nonsense mutations introduced by nucleotide deamination [71].

The last system developed to introduce mutations in the endogenous DNA is prime editors (PEs) (**Figure 8f**). PEs consists in a nickase Cas9 fused to a reverse transcriptase and targeted by a RNA, the pegRNA[72]. Similarly to BEs, PEs do not generate DSBs. They use the reverse transcriptase to reverse transcribe the pegRNA template into DNA which is then used as a repair template [72]. Comparisons of the advantages and drawbacks of each system is presented in **Table 3**.

Table 3: Advantages and drawbacks of genome engineering systems for use in therapies

Editing system	Pro	Cons
ZFN	Very flexible in terms of regions targeted Almost no off-target Insertion of big templates by HDR	DSBs Expensive Complicated to produce
TALEN	Very flexible in terms of regions targeted Almost no off-target Insertion of big templates by HDR	DSBs Expensive Complicated to produce
CRISPR/Cas9	Very flexible in terms of regions targeted Easy to produce Insertion of big templates by HDR	DSBs Off-target Limited efficiency of HDR
Base editing	No DSBs Less off target High efficiency (depending on target)	Less flexible than CRISPR/Cas9 (need of a PAM near an editing windows) Bystander editing Insert point mutations only
Prime editing	No DSBs Very flexible in terms of regions targeted Less off-target	Difficult to scale-up to many targets (lot of optimisations required) Designed for smallmutations mainly (twin PEs to be tested for big templates)

5.2- DSBs can be repaired with different pathways

Technologies of ZFN, TALEN, and CRISPR/Cas9 introduce DSBs into the DNA, which can be repaired mainly with two different mechanisms, non-homologous end joining (NHEJ) or homologous directed repair (HDR), leading to different outcomes [73].

NHEJ is the most frequent process. It can occur at any step of the cell cycle but happens most often in the G0/G1 and G2. Its fast kinetics is an advantage as it allows to rapidly resolve the DSBs, avoiding chromosomal translocation[73]. However, this process is error-prone and will result in loss or addition of nucleotides called "indels", leading to the introduction of a nonsense mutation[74]. Therefore, it is preferable to avoid the use of this mechanism in therapeutic cells.

HDR mechanism repairs the DSBs following a template. Usually, the sister chromatin of the cut strand is used, resolving the DSBs without introduction of mutations. This mechanism can

be used to introduce precise knock-in (KI) mutations. An HDR template (HDRT) consisting in a DNA strand containing mutations and homology arms (HA) similar to the targeted gene can be inserted into the cell nucleus. Thus, following this template, the mutations are integrated into the gene by HDR [74]. This mechanism is predominant when the chromatin is unpacked, in the mid-S and mid-G2 cell cycle[75]. Summary of steps and proteins involved in the two processed is displayed in **Figure 9**.

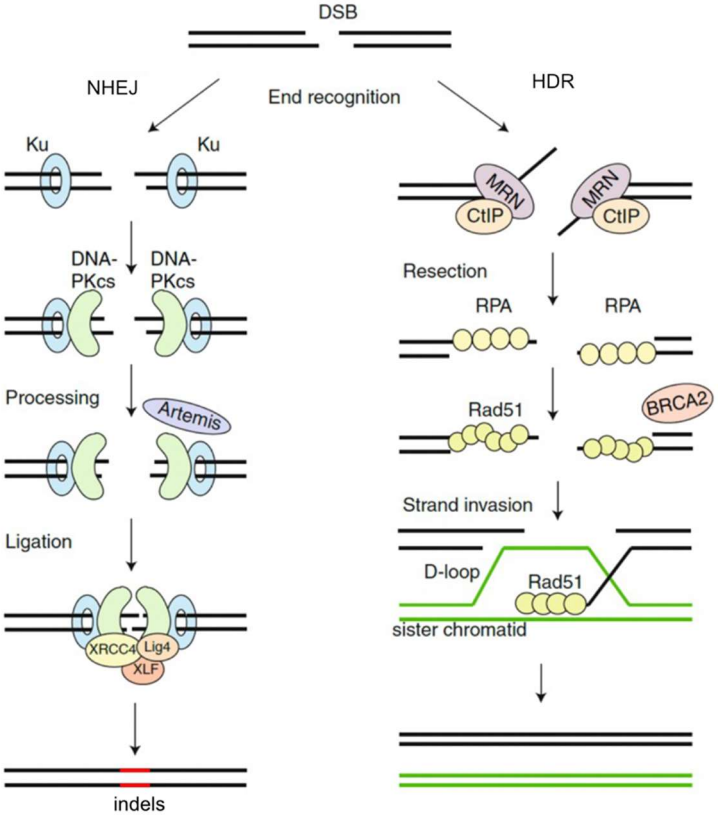

Figure 9: mechanisms involved in NHEJ and HR repair processes

NHEJ: Repair by NHEJ starts with binding of the Ku protein to the DNA ends of the DSBs. Binding of Ku allows the recruitment of DNA-PKcs and of the Artemis nuclease which edits the DNA ends to make them compatible. Then the X-ray repair cross-complementing protein 4 (XRCC4), the DNA Ligase 4 (Lig4) and the XLF-repair factor complex to resolve the break. This repair mechanism inserts indels. HDR: The MRN protein complex and CtIP bind to the DNA ends of the DSBs and generate single strand DNA (ssDNA). ssDNA is recognized by replication protein A (RPA), which allows the recruitment of Rad51and of Breast cancer type 2 susceptibility protein (BRCA2). Rad51 allow strand invasion of the ssDNA on the sister chromatin template. The D-loop is extended and terminated, allowing the resolution of the DSBs without introduction of indels. Figure adapted from [76]

5.3- Is genome engineering of HSCs safe?

Safety of human HSCs engineering is in constant re-evaluation due to the lack of long-term studies on genetically modified HSCs. Haapaniemi et al showed that insertion of CRISPR/Cas9 in cell lines selected for cells with a defect of the p53 pathway. In normal cells, the DSBs induced by Cas9 should activate p53, leading to a growth arrest and death of the cells. However, when Cas9 is inserted into the cells for genome engineering, only the cells surviving the process are used. Consequently, these cells may have a less functional p53 growth arrest [77]. This pathway is essential to preserve from cancer development as it has been found mutated in more that 50% of all human cancers. Having cells surviving Cas9 treatment can be a sign of a defect in this essential pathway, leading to the development of cancers later[78].

Another issue with using CRISPR/Cas9 is the stochasticity of the DNA repair. DSBs is most of the time repaired by NHEJ, leading to uncontrolled repair[74]. Such lack of control of the repair can be problematic as the new protein can potentially present a gain-of-function, and become oncogenic. In addition, CRISPR/Cas9 can cut in off-target sites due to the flexibility of protospacers recognition [79]. If off-target cuts happen in two different chromosomes, this can lead to chromosomes recombination which also increases risks of cancer genesis[74].

To summarize, avoiding the random repair of DNA would enhance safety of the patients. Two strategies can be used to make a KO without random repair: base editing, which was already used to introduce STOP mutations by deamination [71], and prime editing [72].

Aim and objectives of the thesis

In this work, we tested the feasibility of inserting point mutations in the antigens of antibody-based targeted therapies. We aimed to disrupt the binding of the antibody but to preserve the functionality of the protein.

- In a first project we aimed to design CD123 variants shielding cells from CD123-targeted therapies.

- In a second project we aimed to design CD45 variants shielding cells from CD45-targeted therapies.

- In a third project we aimed to optimise BE strategy as it may be safer than CRISPR/Cas9 to introduce point mutations into the genome of cells. We asked if we could edit the CD45 endogenous locus with BEs in the area of the variants.

Chapter I:
Design of CD123 variants shielding from CD123-targeted therapies

I.1- Introduction

In this chapter, we aimed to design CD123 variants shielding cells from CD123-targeted therapies. CD123 is the interleukin 3 (IL-3) receptor alpha-chain (IL-3Rα). Upon IL-3 binding, the heterodimer complexes with CD131 and signals through the Janus kinase (JAK)/ signal transducer and activator of transcription proteins (STAT) pathway. On which cells CD123 is expressed remains controversial. The receptor seems to be transiently expressed on undifferentiated hematopoietic cells because IL-3 was shown to stimulate *in vitro* the proliferation and development of HSCs into mast cells, basophils, neutrophils, eosinophils, macrophages, erythrocytes, megakaryocytes, and dendritic cells [80]. *In vivo*, analysis of cell markers showed that CD123 is highly expressed on plasmacytoid dendritic cells (pDCs) and injection of IL-3 led to the activation of basophils and of mast cells [80 81]. However, the function of this receptor can be diverted by cancer cells: CD123 was shown to be up-regulated on some AML cells [80] and was often found expressed on leukemic stem cells [82]. In addition, in the blastic plasmacytoid dendritic cell neoplasm, which is a cancer of pDCs, CD123 is expressed in 100% of cases [83]. Therefore, this cytokine receptor is an interesting target for myeloid cancer therapies. MAbs [84 85], Bispecific antibodies [86 87], CAR-T cells [88 89 90 91] , and other formats were engineered to target the protein in cancer treatment strategies, demonstrating the feasibility to target this receptor with antibody-based strategies efficiently. However, whether targeting CD123 depletes HSCs together with cancer cells is still debated. While some studies claimed that anti-CD123 therapies do not deplete HSCs [84 89], others showed that injection of CD123 targeted therapies can lead to myeloablation [87 53]. This myeloablation could be interesting as it was shown that host HSCs need to be depleted to make space for the graft before HSCT [92]. Thus, shielding cells from CD123 targeted therapies would have double interests: it would allow the use of high doses of targeted therapy without toxicity on shielded HSCs and the same therapy could be used as conditioning regimen, depleting HSCs and cancer cells together before HSCT.

In addition, the crystal structure of CD123 bound to the anti-CD123 CSL362 was published [93]. We could use this work as a basis to identify the amino acids involved in the binding of CSL362 and to design variants abolishing this binding. To conclude, we chose CD123 as a promising target to develop the shielding concept. We expected that the available information enables the rationale design of shielding but function preserving variants. In addition, its expression pattern on cancer cells and HSCs could lead to clinical translation of identified shielding variants.

I.2- Aims and objectives of the chapter

We asked if CD123 variants could be used for shielding from CSL362-derived targeted therapies in a highly collaborative project. In order to answer this question, we set up several aims:

- Design *in silico* CD123 variants shielding from the anti-CD123 CSL362 binding (done by R. L)
- Stably express the designed variants in human embryonic kidney (HEK) 293 and test the loss-of-binding of CSL362 by flow cytometry (done by me, A.D, in collaboration with C. E and E. L)
- Assess *in vitro* the shielding of the variants from ADCC (done by me, A. D in collaboration with A. W), TCE and CAR-T cells killing (done by E. L)
- Compare the biophysical properties of the variants with the non-modified form of the protein (done by A. C, A. S and A. H)
- Test the functionality of the variants in a relevant cell line (done by me, A. D)
- Engineer the variants into HSPCs and assess the engraftment of the modified cells in mice to test the functionality of the variants *in vivo* (done by R. M and A. DA)

E. L., R.M and me, A. D designed and performed experiments.

I.3- Submitted manuscript

Epitope Engineered Human Haematopoietic Stem Cells are Shielded from CD123-targeted Immunotherapy

Emmanuelle Landmann*1,2, Anna Devaux*1,2, Rosalba Lepore*1,2,5,6, Romina Marone*1,2, Corinne Engdahl 1,2, Giuseppina Capoferri 1,2, Alessandro Dell'Aglio 1,2, Amélie Wiederkehr 6, Alessandro Sinopoli 6, Valentin Do Sacramento 5, Anna Haydn 6, Laura Garcia-Prat 5, Christopher Divsalar 6, Anna Camus 5, Liwen Xu 7, Lorenza Bordoli 3, 4, Torsten Schwede 3, 4, Matthew Porteus 7, Stefanie Urlinger 5,6 and Lukas T. Jeker 1,2

* These authors contributed equally

1) Department of Biomedicine, Basel University Hospital and University of Basel, Hebelstrasse 20, CH-4031 Basel, Switzerland
2) Transplantation Immunology & Nephrology, Basel University Hospital, Petersgraben 4, CH-4031 Basel, Switzerland
3) Biozentrum, University of Basel, Spitalstrasse 41, CH-4056 Basel, Switzerland
4) SIB Swiss Institute of Bioinformatics, Spitalstrasse 41, CH-4056 Basel, Switzerland
5) Cimeio Therapeutics AG, Aeschenvorstadt 36, CH-4051 Basel, Switzerland
6) Ridgeline Discovery GmbH, Aeschenvorstadt 36, CH-4051, Switzerland

7) Department of Pediatrics, Stanford University School of Medicine, Stanford CA 94305, USA.

Author Correspondence:

Lukas T. Jeker, MD, PhD

Department of Biomedicine, Basel University Hospital and University of Basel, Hebelstrasse 20, CH-4031 Basel, Switzerland

E-mail: lukas.jeker@unibas.ch

+41 61 328 50 27

30 Keywords

31 Haematopoietic stem cell transplantation (HSCT); targeted immunotherapy; CD123, genome

32 engineering; CRISPR/Cas9; acute myeloid malignancy (AML); molecular shield; epitope

33 engineering

Summary

Targeted eradication of transformed or otherwise dysregulated cells using monoclonal antibodies (mAb), T cell engagers (TCE) or chimeric antigen receptor (CAR) cells is very effective for haematologic diseases. Unlike the breakthrough progress achieved for B cell malignancies, there is a pressing need to find suitable antigens for immunotherapy of myeloid malignancies. CD123, the interleukin-3 (IL-3) receptor alpha-chain, is highly expressed in various haematological malignancies, including acute myeloid leukemia (AML) and blastic plasmacytoid dendritic cell neoplasm (BPDCN). However, shared expression of CD123 on healthy haematopoietic stem and progenitor cells (HSPCs) bears the risk for extensive myelotoxicity upon targeted depletion. Here, we demonstrate that rationally designed, epitope engineered HSPCs were completely shielded from CD123-targeted immunotherapy but remained fully functional. Thus, molecularly shielded HSPCs could allow tumor-selective targeted immunotherapy and in parallel enable rebuilding a fully functional haematopoietic system. We envision that this approach is broadly applicable, could render undruggable targets accessible to immunotherapy and will allow continued, posttransplant immunotherapy for instance to treat minimal residual disease (MRD) or be used as a salvage therapy. More generally, epitope shielding will be applicable for replacement of other cell types including the many immune cells which are currently being considered for engineered cellular therapies.

Introduction

Targeted cell depletion represents a medical standard of care for several liquid malignancies, autoimmune diseases and prevention or treatment of acute rejection in organ transplantation. Depleting antibodies are mostly IgG but other highly effective targeted immunotherapies work through different mode of action (MoA) and include various antibody-derived molecular formats such as antibody drug conjugates (ADC), radioimmunoconjugates, T cell engagers (TCE) or chimeric antigen receptor (CAR) bearing cells[1-3]. In the past decade the latter have emerged as a highly effective, programmable cell depletion modality with very high response rates in B cell malignancies and more recently systemic lupus erythematodes[4-9]. The persistence of CD19 CAR T cells can be reliably measured by assessing the duration of B cell aplasia after infusion [5,10,11]. In children and young adults with B-ALL it appears that persistence of CAR T cells is an important requirement for cure[12]. Hence, various strategies to increase CAR T longevity are explored[13,14]. Although high depletion efficiencies can lead to long-term remission, they are associated with the risk for prolonged B cell aplasia due to indiscriminate killing of both normal and tumor B cells, respectively[9,15]. In fact, CAR T cells can persist for a decade and result in years-long B cell aplasia[16]. Such deep purging of a cell type is only acceptable if the depleted cell is dispensable and/or its function can be replaced. Thus, a key to the CAR T field's success was the availability of B cell-restricted target antigens (e.g. CD19) and the possibility to mitigate the loss of co-targeted healthy B cells through infusions of immunoglobulins (IVIG). Given the clinical benefit and the commercial availability of CAR T cells as well as other effective cell depleting modalities, the number of patients at risk for iatrogenic long-term immunodeficiencies through highly efficacious cell depleting therapies are expected to continue to increase rapidly.

Unlike the breakthrough progress achieved for B cell malignancies there is a pressing need to find suitable antigens for immunotherapy of myeloid malignancies and particularly acute

77 myeloid leukemia (AML)[17]. Targeting myeloid malignancies is especially challenging
78 however, since AML displays high clonal heterogeneity, being composed of cells with highly
79 variable surface protein expression[12,17-19]. Importantly, leukemia stem cells (LSCs) which are
80 phenotypically very similar to HSCs are important targets in (AML)[20]. Therefore, most AML
81 candidate targets are co-expressed by HSPCs[17,18]. As a consequence, the risk of
82 myelosuppression associated with myeloid-cell targeted CAR T therapy likely limited the
83 number of clinical trials for AML compared to B cell targeted CAR T trials[12,21]. Despite major
84 efforts, single targets with an expression profile as favorable as CD19 could not be identified
85 in AML[17]. Therefore, the paucity or mere absence of cancer-restricted surface proteins
86 constitutes a critical barrier to antigen-specific immunotherapy[11,12,22].
87 A number of solutions have been proposed to overcome the limitations of shared target antigens
88 that underly on-target off-tumor toxicity. Affinity tuning, i.e. reducing a CAR's affinity, can
89 increase the selectivity towards cells with a high antigen expression[23]; transient CAR
90 expression (delivery as mRNA) temporally limits CAR activity; and CAR T therapies targeting
91 essential cells, particularly HSPCs, could be used as a bridge to transplant[21,24,25]. However,
92 sparing cells with low antigen expression creates a risk for antigen$^{-/lo}$ relapse[12,26] and the need
93 to remove an effective CAR T therapy targeting HSPCs is neither economically nor
94 scientifically appealing. Therefore, three groups proposed a radical solution: removing the
95 target antigen partially or entirely in HSPCs before haematopoietic stem cell transplantation
96 (HSCT) prevents binding of the immunotherapy to the HSPCs and their progeny and thus
97 creates a synthetic tumor-selectivity[27-29]. Preclinical studies demonstrate the feasibility for
98 CD33 and clinical trials will be informative for translation (clinicaltrial.gov NCT04849910)[27-
99 29]. However, the number of truly dispensable antigens is likely limited. Moreover, targeting
100 dispensable proteins may favor antigen negative cancer relapses, a phenomenon known to limit
101 long-term outcome of CAR T therapies[26]. Therefore, deliberately targeting essential proteins

would be preferrable to reduce the risk for antigen escape. However, this is impossible with a knock-out (KO) approach.

Here, we aimed to engineer HSPCs expressing an endogenous protein variant that completely shields the cells from targeted immunotherapy while preserving its function. The interleukin-3 receptor α chain (IL3RA; CD123) regulates proliferation and differentiation of HSPCs[30], is often expressed on AML LSCs and blasts from relapses[31] and hence is associated with a poor outcome of the disease. Therefore, CD123 constitutes a promising target for AML[19,21] for which multiple therapeutics are being explored preclinically and clinically including IL-3 bound to diphteria toxin[32], monoclonal antibodies (mAb) blocking IL-3 [33] or engineered for enhanced antibody dependent cellular cytotoxicity (ADCC)[34], an antibody drug conjugate (ADC)[35] and bispecific TCEs, e.g. a CSL362/OKT3-TCE[36,37]. Despite the promising on target toxicity, many of these therapies displayed cytotoxicity towards HSPCs, monocytes, basophils and plasmacytoid dendritic cells (pDCs)[19,21,36]. Thus, protecting HSPCs from the immunotherapies is desirable but due to CD123's role in HSPC biology a KO approach may result in impaired immune function. We identified multiple single amino acid (aa) substitutions that shielded from ADCC, TCE and CAR T cell killing while preserving CD123 function. These variants enabled selective TCE-mediated tumor killing while engineered HSPCs were unaffected. We envision that this approach is broadly applicable, could render undruggable targets accessible to immunotherapy and will allow continued, posttransplant immunotherapy for instance to treat minimal residual disease (MRD) or be used as a salvage therapy.

Results

Figure 1: Rational design of human CD123 protein variants to shield from targeted immunotherapy

CD123 variants were designed *in silico*. We aimed to identify protein variants that are structurally and functionally tolerated, i.e., variants that exhibit a similar structure to wildtype (WT) CD123, that preserve the ability to bind IL-3 and elicit IL-3 mediated downstream cell signaling, but are otherwise shielded from the CSL362 antibody or a similar antigen binding moiety. To this aim, available experimentally determined three-dimensional structures of CD123 in different states were used to identify the protein regions involved in binding to CSL362 and IL-3. As previously described[38], the CSL362 epitope is located at the N-terminal domain (NTD) of CD123 (**Fig. 1a**), where the CSL362 fragment antigen binding (Fab) binds both the "open" and "closed" conformations of the NTD. Based on structural analysis, we identified several CD123 residues as part of the antibody-antigen interface and involved in direct intermolecular interactions with the CSL362 complementarity-determining regions (CDRs) in both conformational states: T48, D49, E51, A56, D57, Y58, S59, M60, P61, R84, V85, A86, N87, P89, F90, S91. Most of these amino acid sites show differential exposure to solvent upon binding of the CSL362 antibody, with residues E51, S59, P61, and R84 switching from highly exposed to buried (**Fig. 1b**). E51, S59 and R84 were selected as critical sites for the CSL362 binding (**Fig. 1c**) and most likely safe for mutagenesis. In contrast, P61 is likely relevant for IL-3 binding due to its close interatomic distance to IL-3 residues and therefore was excluded from further analysis. Comprehensive mutagenesis was performed *in silico* and the mutational effect estimated as statistical energy difference (ΔE) (**Fig. 1d**) with particular focus on the three key residues (**Fig. 1e**) and candidate variants selected upon ranking for decreasing ΔE, for a total of 28 variants (**Fig. 1f**).

Figure 2: Preserved expression of engineered CD123 variants despite abolished binding to the monoclonal antibody MIRG123

We used a CSL362 IgG1 biosimilar (MIRG123) to experimentally validate its binding to the in silico designed CD123 variants. We generated HEK-293 cells stably expressing human wildtype CD123 (HEK-CD123) or individually harbouring each of the 28 selected amino acid substitutions at positions E51, S59 and R84 (**Fig. 1f**). Using flow cytometry we concomitantly quantified MIRG123 binding as well as preserved expression of the variants by staining with the control anti-CD123 mAb clone 6H6, whose binding to CD123 does not interfere with MIRG123 (**Fig. 2a**). The results revealed a drastic reduction of MIRG123 binding to most candidate CD123 variants, and abolished binding to almost half (13/28) of them. Based on the dual staining characteristics to mAbs 6H6 and MIRG123 each variant was categorized as either a non-binding (< 1% double staining to 6H6/MIRG123, 13 variants, blue), weak (1-20%, 12 variants, orange) or strong (> 20%, 3 variants, red) binding variant (**Fig. 2b**). The latter showed comparable binding to HEK-CD123. Among the weak binding variants, MIRG123 mostly bound the highest CD123 expressing cells. These results demonstrate the feasibility to rationally design single amino acid substitutions that completely disrupt the binding of a candidate antibody while preserving the expression of the engineered protein.

Figure 3: Cells expressing engineered CD123 variants are shielded from multiple targeted immunotherapy modalities in vitro

Next, we explored whether the non-binding variants were protected from MIRG123-mediated cytotoxicity either in the format of a mAb (ADCC), a bispecific TCE or human CAR T cells (**Fig. 3a**). First, we tested whether the CD123 variants were shielded from MIRG123-triggered ADCC using an FcγRIIIa expressing reporter cell line. Target cell binding of the test antibody leads to activation of a luminescence signal in the reporter cells through Fc-mediated activation

of the FcγRIIIa receptor. High luminescence was measured in the presence of unmodified antigen (HEK-CD123) as well as all strong binding variants (**Fig. 3b**). In contrast and consistent with the flow cytometry data (**Fig. 2a-b**) 12/13 non-binding variants did not induce any ADCC signal above background detected in control cells devoid of CD123 (HEK; lower dashed line) with the exception of S59Y which induced minimal activity. Weak binders showed an intermediate ADCC activity. Thus, ADCC signals positively correlated with the flow cytometry data.

Encouraged by these results, we investigated whether the non-binding variants would also protect from more potent immunotherapies such as TCEs and CAR T cells which result in cytotoxicity at a lower antigen density than ADCC-inducing mAbs[39]. First, we co-cultured CD123 expressing HEK-293 cells and human T cells with and without the CSL362/OKT3-TCE (TCE)[37]. After 3 days of co-culture, T cells clustered in the presence of HEK-CD123 and TCE, whereas clusters were neither seen with the non-binding variant E51K (or any of the other non-binding variants) nor with the target cells devoid of CD123 (HEK) (**Fig. 3c**). In line with these findings, neither HEK cells nor cell lines expressing non-binding CD123 variants were subject to TCE-mediated cytotoxicity. In contrast, some weak binding CD123 variants induced limited cytotoxicity while control HEK-CD123 and strong-binding variants were lysed in the presence of the TCE (**Fig. 3d**). Consistent with these results, upregulation of the activation marker CD69 above background was only detected in T cells in co-culture with HEK-CD123 but not with E51K or HEK (**Fig. 3e**) or any of the non-binding CD123 variants (**Fig. 3f, Extended data Fig. 1a**). In contrast, the frequency of $CD69^+$ T cells increased in the presence of some weak binding variants and was comparable between HEK-CD123 and the strong binding variants. Both $CD4^+$ and $CD8^+$ T cells were activated but $CD8^+$ T cells displayed a higher proportion of activated $CD8^+CD69^+$ effector T cells (**Extended data Fig. 1b-c**).

196 Likewise, secreted IFN□ was only detected in the co-culture supernatants from highly
197 activated T cells triggered by strong antigen binding (**Extended data Fig. 1d**).
198 As a third modality of CD123-targeting immunotherapies we investigated CAR T cells. We
199 used non-viral CRISPR/Cas9-mediated homology directed repair (HDR) to integrate a second-
200 generation CSL362-derived CD123-specific CAR (123CAR) into the T cell receptor □
201 constant region (*TRAC*) (**Extended data. Fig. 2a**). Up to 9% of all electroporated $CD4^+$ and
202 $CD8^+$ T cells expressed the 123CAR as assessed by GFP (**Extended data Fig. 2b-d**). Correct
203 123CAR integration at the *TRAC* locus was confirmed by Sanger sequencing (**Extended data**
204 **Fig. 2e**). GFP^+123CAR T cells were purified by flow cytometry, expanded and subsequently
205 used for in vitro cytotoxicity assays. CAR-less control T cells or 123CAR T cells were co-
206 cultured for 24h with the CD123 variant expressing target cell lines. Within hours, 123CAR T
207 cells clustered around HEK-CD123 cells, whereas neither HEK nor E51K triggered 123CAR
208 T clustering (**Fig. 3g**). As observed for ADCC and TCE, 12/13 non-binding CD123 variants
209 were shielded from cytotoxicity (**Fig. 3h**). The only exception was again S59Y which induced
210 cytotoxicity (**Fig. 3h**) and IFN□ □secretion (**Extended data Fig. 2i**). In contrast and different
211 to the results observed for ADCC and TCE, both, weak and strong binding variants triggered
212 strong cytotoxicity (**Fig. 3h**) and IFN□ secretion (**Extended data Fig. 2i**). In accordance,
213 neither HEK nor E51K increased the proportion of activated $CD69^+$ 123CAR T cells above
214 background whereas the frequency of $CD69^+$ 123CAR increased in response to unmodified
215 CD123 (**Fig. 3i**). The exceptions were S59F and S59Y which both induced CD69 upregulation
216 in $CD4^+$ and $CD8^+$ 123CAR T cells, respectively (**Fig. 3j; Extended data Fig. 2f-h**). However,
217 among the non-binders, only S59Y concomitantly induced CD69 upregulation, IFN□ secretion
218 and cytotoxicity whereas S59F resulted in isolated CD69 upregulation but neither IFN□
219 secretion nor cytotoxicity. Thus, in contrast to ADCC and TCE where antibody and T cell
220 effector function correlated well with antibody binding as determined by flow cytometry (**Fig.**

3b-f, Fig. 2b), weak binding CD123 variants induced 123CAR T responses comparable to strong-binding CD123 variants. These findings suggest that CAR T cells are more potent than ADCC and TCE and even weak binding can result in CAR T activation and elimination of target cells. In summary, we demonstrate that a series of single amino acid substitutions in CD123 are sufficient to completely prevent the activity of an ADCC-inducing mAb, a TCE and a CAR T cell. This suggests that such variant proteins - when engineered into the genome of target cells - might provide protection from different targeted immunotherapy.

Figure 4: Biophysical characterization of selected CD123 protein variants

To characterize the effect of the introduced point mutations on the protein biophysical properties, the extracellular domains (ECD, amino acids 19-305) of selected CD123 variants were synthesized as soluble proteins. Real time interaction with the immobilized CSL362 was measured using Bio-Layer Interferometry (BLI) at increasing concentrations of soluble CD123 ECD variants. Wildtype CD123 associated rapidly to the antibody CSL362 in a dose-dependent manner (**Fig. 4a**). In contrast, no interaction was observed up to 300nM of the soluble analyte CD123 E51T, a variant characterized as a non-binder by flow cytometry (**Fig. 4a, Fig. 2b**). Similarly, no association to CSL362 was observed for other non-binding variants, including E51K, S59P, S59E, S59F, S59R and R84E). Residual CSL362 association was detected at different concentrations of the weak-binding variants E51A, E51Q, R84T and R84Q (**Fig. 4b**). Consistent with the shielding assays (**Fig. 3b-j**), S59Y showed similar residual binding as weak-binders. Importantly, the association to the control antibody 6H6 was preserved in all tested variants, except for R84E (**Fig. 4c**). Next, we assessed the functionality of the variants in terms of binding to IL-3, i.e. the physiologic ligand of CD123, to the immobilized CD123 variants. All tested variants bound to increasing concentrations of IL-3, with S59P and R84E displaying a modest reduction in IL-3 binding (**Fig. 4d**). Lastly, protein thermal stability was

assessed by differential scanning fluorimetry (DSF) analysis. Most CD123 variants demonstrated a thermostability comparable to CD123 WT with an unfolding temperature (Tm) of 50°C. In contrast, R84E induced a higher fluorescence signal at ambient temperature and featured a lower Tm (43°C) (**Fig. 4e**). Since R84E showed reduced binding to 6H6, IL-3 and a lower thermal stability compared to wildtype, it was excluded from further experiments. In summary, we identified several protein variants harboring single amino acid substitutions at two different residues (E51T, E51K, S59E, S59R) that entirely abolish binding to MIRG123 but preserve protein stability, binding to the control mAb 6H6 and the receptor's natural ligand IL-3.

Figure 5: Cells expressing CD123 variants E51K and E51T are functional, engraft and differentiate in vivo

Since we used a cell-free system to establish that the selected CD123 variants preserved dose-dependent binding of IL-3, we next aimed to investigate the functionality of E51K and E51T in intact cells. We used CRISPR/Cas9-mediated HDR to engineer the variants into the human erythroleukemia cell line TF-1 whose proliferation and survival is IL-3- or GM-CSF-dependent[40] (**Fig. 5a**). The genetically engineered cells were cultured with increasing concentrations of IL-3. WT TF-1 displayed IL-3-dependent growth and the two KI populations E51K and E51T demonstrated near overlapping growth curves indicating intact IL-3 sensing and signaling. In contrast, KO sorted cells proliferated considerably less (**Fig. 5b**). To test the blocking effect of MIRG123, we cultured the cells with a fixed IL-3 concentration but increasing amounts of MIRG123. As reported in a comparable system using BaF3 cells[38], WT cells showed a dose-dependent growth inhibition and died in the presence of antibody concentrations ≥ 0.036nM. In contrast, E51K and E51T KI cells proliferated irrespective of the

MIRG123 concentration. KO cells were not affected by MIRG123 but displayed decreased survival compared to WT, E51K or E51T (**Fig. 5c**).

Next, we aimed to engineer clinically relevant HSPCs that can potentially be used to provide a patient with a CD123 immunotherapy-resistant haematopoietic system. We used reagents close to GMP-grade with the goal to provide scientific proof of concept with the potential for clinical translation. To this end, we engineered the variants E51K and E51T into mobilized, $CD34^+$ enriched peripheral blood HSPCs from healthy donors. $CD34^+$ HSPCs were electroporated with high fidelity SpCas9 RNPs and single strand oligodeoxynucleotides (ssODNs). CD123 expression was monitored using flow cytometry with the mAbs MIRG123 and 6H6 two and five days post electroporation, respectively (**Fig. 5d, Extended data Fig. 3a**). In comparison to non-electroporated WT cells (no EP) electroporation per se did not alter CD123 expression (EP) whereas cells receiving RNPs displayed an increased fraction of $MIRG123^-6H6^-$ (KO) cells. HSPCs receiving RNP together with the E51K or E51T HDRTs displayed a distinctly different FACS profile. Over time a population with retained 6H6 but abolished MIRG123 binding ($MIRG123^-6H6^+$) gradually appeared (from 7-8% on day 2 to 25-32% on day 5), suggesting that these were E51K or E51T KI HSPCs (**Fig. 5d**). Importantly, $CD34^+CD38^-CD90^+CD45RA^-$ cells (HSCs) displayed similar editing rates as the bulk $CD34^+$ HSPCs suggesting that long-term repopulating HSCs (LT-HSC) and multipotent progenitors MPP1 and MPP2 were edited at similar frequencies (**Fig. 5e, Extended data Fig. 3b**). Sanger sequencing of these cells confirmed correct editing of E51 (GAG) to K (AAG) or T (ACC). Of note, EP and KO samples mainly displayed WT sequences suggesting that CD123 KO cells were lost, possibly due to a competitive disadvantage compared to WT cells (**Fig. 5f**). To investigate whether the variants E51K and E51T preserved IL-3 signaling we analyzed pSTAT5 in KI HSPCs. We used AAV6-mediated HDR as an orthogonal approach to engineer the KI variants. IL-3 induced a strong p-STAT5 signal in both control HSPCs (non-edited and

CCR5 edited) as well as E51K and E51T KI HSPCs (**Fig. 5g**). In contrast, CD123 KO cells displayed strongly reduced p-STAT5 signaling. To further characterize the functionality of the engineered HSPCs, we analyzed their in vitro differentiation potential in a colony forming assay. The relative distribution of colonies representing different lineages (BFU-E & CFU-E, CFU-G/GM and CFU-GEMM) was comparable among all genotypes independent of IL-3 (**Fig. 5h**). In addition, also non-virally edited HSPCs displayed an equal differentiation into $CD33^+$ myeloid and GlycophorinA $(GlyA)^+$ erythroid cells (**Fig. 5i**). Thus, E51K and E51T variants were efficiently engineered into HSPCs using two orthogonal approaches and resulted in functional CD123 receptor expression with intact IL-3 signaling and normal in vitro differentiation capacity.

Next, we tested *in vivo* engraftment and differentiation potential. We injected non-virally edited HSPCs (EP, KO, E51K and E51T, respectively) into sublethally irradiated NSG mice. After 15 weeks, all mice of the different groups showed engraftment of $hCD45^+$ cells in peripheral blood and bone marrow (**Fig. 5j**). E51K and E51T groups displayed a reduced human chimerism which was more pronounced in blood than bone marrow. This was most likely due to the editing with ssODN which typically resulted in lower viability of the edited HSPCs compared to EP or KO groups. This was also reflected by a reduced frequency of human HSCs in the bone marrow (**Fig. 5k**). However, within the $hCD45^+$ cells, all four groups displayed comparable multi-lineage differentiation in blood (**Fig. 5l**). Finally, we aimed to analyze the presence of KI cells among haematopoietic cells with strong CD123 expression. Therefore, we analyzed CD123 on pDCs (gating strategy **Extended data Fig. 3c**). Although pDC numbers were very low, a few of the typical $MIRG123^-6H6^+$ KI cells were only present in the mice injected with E51K or E51T HSPCs (**Fig. 5m**). Thus, engineered HSPCs harboring single amino acid substitutions engrafted in vivo and differentiated into multiple cell types including

pDCs which had high CD123 expression but did not bind the surrogate therapeutic antibody MIRG123.

Figure 6: Engineered HSPCs enable tumor-selective CD123 immunotherapy

After establishing efficient engineering and preserved function of E51K and E51T in HSPCs we sought to investigate resistance of engineered HSPCs to CD123-targeted immunotherapy. First, we co-cultured edited HSPCs ($CD34^+$) and autologous T cells ($CD3^+$) together with the CSL362/OKT3-TCE. Non-engineered $CD34^+$ HSPCs were depleted (EP, +TCE: 9%) in comparison to the control condition without TCE (EP, -TCE: 53%). In contrast, $CD34^+$ E51K and E51T HSPCs were only mildly reduced in the presence of autologous T cells and the TCE (**Fig. 6a**). Since HSPC KI engineering usually remained < 40% (**Fig. 5d**), a 2-fold reduction of $CD34^+$ HSPCs would be expected due to killing of unedited, CD123 expressing HSPCs. To verify which cells were specifically eliminated we compared the staining profile of CD123 on the remaining $CD34^+$ HSPCs after co-culture. The number of control (EP) HSPCs co-cultured with T cells and TCE were strongly reduced but the staining profile of CD123 expression was comparable to control EP HSPCs co-cultured without TCE. In contrast, E51K and E51T HSPCs were readily detectable in wells co-cultured with T cells and TCE. However, CD123 only stained 6H6 but not MIRG123 ($MIRG123^-6H6^+$) indicating selective depletion of CD123 WT expressing HSPCs. As a consequence, $MIRG123^-6H6^+$ HSPCs were enriched in TCE treated wells compared to wells without TCE (**Fig. 6b**). To exclude possible artifacts due to epitope masking by remaining CSL362/OKT3-TCE that could block MIRG123 binding, we FACS-sorted HSPCs on the day of analysis based on 6H6 staining. Sanger sequencing confirmed that EP HSPCs ($6H6^-$ and $6H6^+$) and $6H6^-$ cells sorted from E51K and E51T HSPCs were primarily WT. Thus, these are HSPCs that have a CD123 WT genotype but do not express CD123. In contrast, sorted $6H6^+$ KI HSPCs were almost purely E51K (AAG) or E51T (ACC),

respectively (**Fig. 6c**). Thus, E51K and E51T expressing HSPCs withstood CD123-targeted TCE-mediated cytotoxicity leading to an enrichment of edited KI HSPCs. Finally, we co-cultured the CD123 expressing AML cell line MOLM-14 with engineered HSPCs to determine whether the molecular shield could indeed provide protection from CD123-targeted immunotherapy. Co-culture of HSPCs with autologous T cells and TCE resulted in a 90% reduction of MOLM-14 cells compared to cells without TCE. Similarly, unprotected $CD34^+$ HSPCs (EP) were strongly reduced whereas E51K and E51T HSPCs persisted (**Fig. 6d**). Analysis of CD123 expression confirmed depletion of remaining unedited HSPCs and a strong enrichment of E51K and E51T KI cells as observed without tumor cells (**Fig. 6e**). Thus, epitope engineered, shielded HSPCs are functional but resistant to CD123-targeted immunotherapy and thereby enable tumor-selective targeting.

Discussion

HSCT is a potentially curative approach for haematologic diseases. A conditioning phase prepares the transplantation of autologous or allogeneic HSCs which, after engraftment, will rebuild a new haematopoietic and immune system. The conditioning serves to remove host HSCs and can kill tumor cells when HSCT is applied for malignant diseases. However, current untargeted cytotoxic conditioning regimens have been directly or indirectly associated with transplant related morbidity and mortality. With the advent of highly effective targeted depleting agents such as mAbs, ADCs, TCEs and CAR T cells it may become possible to replace untargeted conditioning and tumor control by antigen-specific immunotherapy[25,41-44]. However, the absence of suitable antigens constitutes a major impediment to progress in this field[11,12,22]. In particular, targeting LSCs would be highly desirable to treat AML but the risk for myelosuppression arising from shared antigen expression of LSCs and healthy HSCs precludes a continuous posttransplant therapy[25]. As a compromise, it was proposed to use CAR T cells directed against CD123 or CD117 to purge tumor cells and HSCs alike, followed by myeloablative conditioning to remove the CAR T cells before HSCT[21,24,25]. Thus, the targeted immunotherapy would be limited to the pretransplant period and only serve as a bridge-to-transplant. However, the ability to continue immunotherapy posttransplant would be highly desirable to eliminate MRD and prevent relapse.

We previously used genome engineering to substitute single amino acids in surface proteins of murine T cells which completely abolished binding of specific mAbs[45]. Since we converted protein variants known to have exchangeable function (aka congenic markers) the results suggested that engineering a minimal alteration in surface proteins could enable safe cell shielding for therapeutic purposes. To enable HSCT with continuous antigen-specific immunotherapy, we engineered human HSPCs to express epitope engineered CD123 and demonstrate that these cells are both shielded and functional, respectively. We used structural

information to identify at least one aa substitution that completely abrogated mAb binding for 3 separate residues. This is important since it increases the chances that an appropriate genome engineering strategy can be found to safely and efficiently insert a variant into primary therapeutic cells. The choice of the most suitable genome engineering approach will depend on the desired aa substitution and cell type. To establish feasibility, we employed CRISPR/Cas9-mediated HDR which provides flexibility through a DNA template. Despite some shortcomings such as cellular toxicity, HDR-mediated HSPC editing is safe and clinically relevant[46,47]. Nevertheless, more recently developed genome engineering approaches provide additional options. Specifically, base editing is well tolerated, can achieve very high editing efficiencies in HSPCs and is suitable for multiplex editing[48]. However, base editors have more constraints than HDR since they typically convert A-›G or C-›T, have PAM restrictions and a limited editing window that can result in unwanted bystander editing. As a consequence, base editing can only install a fraction of desired codon changes for a particular aa change. In contrast, prime editing provides a templated approach that also avoids dsDNA breaks and provides the greatest flexibility to install any desired codon change[48]. However, efficient prime editing in HPSCs has yet to be reported.

Information about naturally occurring polymorphisms without known disease association (e.g. CD123 E51K) could inform variant choice from a safety perspective. For instance, although IL-3 binding to CD123 E51K may be slightly reduced compared to WT CD123 (**Fig. 4d**), it appears that different binding strengths to IL-3 may be biologically tolerated. Theoretically, allogeneic HSPC donors could be pre-screened for such variants which would provide shielding without the need to engineer the cells. However, practically, most polymorphisms are likely too rare since HSPCs also have to be matched for HLA. Conversely, this indicates that some patients receiving therapeutic cell depleting agents may be non-responders due to genetic variation. Remarkably, our results show that a single aa substitution is sufficient to

protect from mAb (ADCC), TCE and even CAR T cells. Thus, shielded HSPCs or other therapeutic cells could be combined with a broad range of available cell depleting agents. However, our data shows that careful characterization of the variants for potential clinical translation is important. For instance, although R84E shielded from all tested depletion modalities, it showed signs of reduced stability. Furthermore, S59P and R84E both showed reduced IL-3 binding and therefore were not further pursued. In addition, the degree of binding reduction will be relevant for the choice of the MoA of the depleter. For instance, S59Y, R84T and R84Q protected from ADCC and TCE but led to substantial killing by the CAR T cells. It is noteworthy that the CAR T response was rather digital with non-binders being protected whereas weak binders resulted in strong CAR T activation and cytotoxicity. In contrast, responses to weak binders were more analogue for ADCC and TCE resulting in much more limited killing. Thus, the therapeutic window created by a shielding variant will be a function of the binding reduction between the WT and the engineered variant, the expression on the target cells (which may be dynamic) as well as the efficacy of the depleting agent. In some cases, e.g. when a blocking Ab is used, residual binding of the shielding variant may be acceptable. In others, when the variant is to be paired with a highly effective depleter, the non-binding must be more stringent.

In order to fully exploit the advantage of combining shielded HSPCs with targeted immunotherapy, the function of the antigen should be preserved[11]. Our results show that selected shielded CD123 variants preserved IL-3 binding, signaling (p-STAT5) and IL-3 dose-dependent growth. Furthermore, engineered KI HSPCs differentiated normally in vitro, engrafted and displayed multi-lineage differentiation potential in vivo. Thus, molecularly shielded HSPCs could allow tumor-selective CD123 targeted immunotherapy and in parallel enable rebuilding a CD123 variant-expressing haematopoietic system. For instance, CD123 targeting therapies are clinically successful for the treatment of BPDCN, a pDC-derived

neoplasm. However, also healthy pDCs strongly express CD123 and therefore will be depleted by any effective CD123 immunotherapy. Yet, pDCs are primary producers of type I interferon and hence anti-viral immunity. Their importance was recently illustrated for the protective immunity against SARS-CoV-2 [49]. Therefore, transplanting CD123-shielded HSPCs may in the future potentially allow to fully restore immunity with a completely functional haematopoietic system while simultaneously allowing efficient tumor immunotherapy. More broadly, we envision that function-preserving but shielding variants could be identified for other proteins that currently cannot safely be targeted. For instance, directed ablation of HSPCs or more generally haematopoiesis has been a long-standing goal to improve HSCT[11] and could be applied beyond malignancies. CD117 and CD45 are promising targets but current approaches are limited to short-term depletion[24,25,41-44]. Targeting CD45 could be applied to systemic autoimmune diseases but it is currently unknown whether short-term depletion will be sufficient and clinically tolerated[42,50,51]. Shielded CD45 variants could enable a gradual replacement of the haematopoietic system including autoreactive lymphocytes. Other applications could include T cell malignancies since T cell deficiency results in unacceptably severe immunosuppression and T cell function cannot readily be replaced. Finally, epitope shielding could open up development of new immunotherapies against as yet unidentified targets and may be applicable for replacement of other cell types e.g. T, B and the many other immune cells which are currently being considered for engineered cellular therapies[11].

Acknowledgements

We acknowledge the contributions of the following research core facilities at the University of Basel and the Department of Biomedicine: the teams of the animal facility for expert animal husbandry and the flow cytometry core facility for excellent support. We thank Marko Hasiuk for gRNA design; Jonathan Knowles for critical reading of the manuscript; Dario Neri and Mihaela Zavolan for sharing reagents; This project has received funding from the European Research Council (ERC) under the European Union's Horizon 2020 research and innovation programme (grant agreement No. 818806).

Author contributions

These authors contributed equally: E.L., A.D., R.L., R.M.; E.L., A.D., R.M. designed and performed experiments, analyzed data and wrote the manuscript; R.L. performed computational analysis and wrote the manuscript; C.E., A.W., L.G.P., L.X. performed experiments and analyzed data; G.C. performed experiments and produced the TCE; A.DA. performed in vivo experiments; A.S., A.H., A.C. performed protein stability experiments; V.DS., C.D. performed HSPC isolation; L.B. performed initial computational analysis; T.S. supervised computational analysis; M.P. supervised AAV experiments; S.U. designed and supervised experiments; L.T.J. conceived the study, supervised experiments, acquired funding and wrote the manuscript. All authors read and approved the manuscript.

Declaration of interests

Funding: Research was supported by the European Research Council (L.T.J.). Sponsored research agreement with Cimeio Therapeutics AG (Cimeio) (L.T.J. and M.P.). Cimeio scientists actively contributed to the research and are therefore listed as co-authors. Decision to publish was the sole responsibility of L.T.J. L.T.J.'s employer, the Basel University Hospital,

receives financial compensation for L.T.J.'s consulting. Employment: Ridgeline Discovery GmbH: R.L., A.W., A.S., A.H., C.D., S.U.; Cimeio Therapeutics AG: R.L., V.DS., L.G.P., A.C., S.U.. Personal financial interests: L.T.J.: co-founder, board member of Cimeio. Holding Cimeio equity: University of Basel, R.L., A.W., A.S., V.DS., A.H., L.G.P., C.D., A.C., S.U., L.T.J.; inventors on a patent application related to the findings reported here: E.L., A.D., R.L., R.M., A.W., A.S., A.H., A.C., S.U., L.T.J.

Data availability Statement

Datasets are available from the corresponding author on reasonable request.

Materials and Methods

All antibody sequences, gRNAs, oligos and flow cytometry antibodies used in the study are listed in Extended data table.

Structural dataset and computational design of CD123 protein variants

Experimentally determined three-dimensional structures of the CD123 protein were retrieved from the PDB and include (i) the CD123-CSL362 complex in open and closed conformation (PDB ID: 4JZJ[1]), (ii) the CD123-IL-3 binary complex (PDB ID: 5UV8[2]), (iii) the CD123 unbound structure extracted from the complex in open and closed conformation. Given the structure of the complexes, the CSL362 and IL-3 epitopes were defined as the sets of CD123 residues having at least one atom within 4Å to any CSL362 and IL-3 atoms, respectively. Per-residue relative solvent accessibility area was computed using the Lee & Richards algorithm[3] implemented in FreeSASA[4], using default parameters and upon removing crystallographic waters, sugars and ions. Comprehensive mutagenesis was performed *in silico* using the EVmutation sequence-specific probabilistic model[5] and the mutational effect, defined as statistical energy difference ΔE, estimated using the epistatic coevolutionary analysis framework[6s8]. For a given mutant, the ΔE is computed as the sum of differences of the constraints on individual amino acid sites plus the sum of differences of the coupling parameters computed for all pairs of sites involving the mutated site. In order to quantify the total epistatic constraint acting on a given amino acid site of interest, evolutionary coupling analysis was run on a multiple sequence alignment (MSA) spanning the entire CD123 sequence. The MSA was built using five iterations of the jackhammer HMM search algorithm against the non-redundant UniProtKB database[9] and default significance score for inclusion of homologous sequences. As values of ΔE below, equal and above 0 correspond to putatively

beneficial, neutral, and deleterious effects, respectively, variants at a given site were selected upon ranking for decreasing ΔE.

Eukaryotic cell lines

Freestyle CHO-S cells were purchased from Thermo Scientific (Cat#R80007) and were expanded in PowerCHO 2 Serum-free Medium (Lonza BELN12-771Q) supplemented with GlutaMAX (Gibco), HT supplement (Cat# 41065012) and antibiotic-antimycotic (Cat#15240062), to a maximum density of $20x10^6$ cells/ml. TF-1 were purchased from DSMZ (Cat#ACC334) and maintained in RPMI-1640 media supplemented with 10% heat-inactivated FCS (Gibco Life Technologies), 2mM GlutaMAX and 2ng/ml hGM-CSF (215-GM, Bio-Techne). HEK-293 cells were a kind gift of M. Zavolan (Biozentrum Basel) and cultured in Dulbecco's Modified Eagle's Medium - high glucose (Sigma-Aldrich) supplemented with 10% heat-inactivated FCS and 2mM GlutaMAX. MOLM-14 were purchased from DSMZ (Cat#ACC777) and K-562 were purchased from ATCC (Cat#CCL243). Both cell lines were maintained in RPMI-1640 media supplemented with 10% heat-inactivated FCS (Gibco Life Technologies) and 2mM GlutaMAX. All cell lines were freshly thawed and passaged 3-6 times prior to use.

Cloning and expression of recombinant wildtype human CD123 and its variants

Full length cDNA of human CD123 (NM_002183.2) was obtained from a pCMV3 vector (Cat#HG10518-M, Sino Biological). The Hygromycin sequence was replaced by a Neomycin resistance cassette by Gibson Assembly. *The point mutations of the human CD123 variants were introduced into the vector using PCR (see Extended data table).* $2x10^6$ HEK-293 cells were electroporated with the pCMV3 vector encoding CD123 wildtype or its variants using the Neon Transfection System (ThermoFisher; 1100V, 20ms, 2pulses). To generate stable cell

lines Geneticin G418 (50mg/ml; BioConcept) was added to the cell culture medium at a concentration of 350µg/ml.

Cloning and expression of the monoclonal antibody CSL362 biosimilar (MIRG123)

The heavy and kappa light chain variable regions (VH and VKL) of CSL362 were derived from the CSL362/OKT3-TCE[10]. To generate the monoclonal IgG1 antibody CSL362 biosimilar MIRG123 the VH and VKL sequences were cloned into AbVec2.0-IGHG1 (Addgene plasmid # 80795) and AbVec1.1-IGKC (Addgene plasmid # 80796), respectively, kindly provided by Hedda Wardemann[11]. $2x10^9$ Freestyle CHO-S cells were resuspended in 500ml ProCHO 4 Protein-free Medium (Lonza, Cat#BEBP12-029; supplemented with 1XHT, GlutaMAX, antibiotic-antimycotic) and co-transfected with both plasmids (0.6mg each) using 5mg polyethyleneimine (PEI, Polysciences, Cat#23966). The cells were expanded under constant rolling (140rpm) at 31°C, 5% CO_2 for 6 days. The Freestyle CHO-S cells were pelleted and the filtered supernatant (0.22□m filter) was applied on a Protein A column for purification. CSL362 biosimilar was eluted with 0.1M glycine (pH=2.2), 0.5ml fractions were collected and OD_{280} was measured using a Nanodrop spectrophotometer. The high-concentration fractions were pooled and dialyzed twice overnight in PBS.

Expression and purification of CSL362/OKT3-TCE

The design of the CSL362/OKT3-TCE was recently described[10] and the plasmid was a kind gift from D. Neri (ETH Zurich). Freestyle CHO-S producer cells were transfected using PEI (as described above) with 1.7mg TCE DNA. Following 6 days of expansion the filtered cell culture supernatant was applied to a 5ml Ni-NTA column (ThermoFisher) prewashed with 100ml washing solution (PBS, 150mM NaCl, 5mM Imidazole, pH7.4) for protein purification. The eluted and dialysed TCE was filtered (0.22□m) and stored in aliquots (1mg/ml) at -80°C.

Flow cytometry and cell sorting

Flow cytometry was performed on BD LSRFortessa with the BD FACSDiva Software, and the data was analysed with FlowJo Software. Antibodies used for flow cytometry can be found in the Extended data table. For cell sorting the cells were pelleted and resuspended in FACS Buffer (PBS + 2%FCS) supplemented with 1mM EDTA, and sorting was performed either on BD FACSAria or BD FACSMelody Cell Sorter. The control cells were also subjected to the sorting process.

Primary human T cell isolation and culture

Leucocyte Buffy coats from anonymous healthy human donors were purchased from the blood donation center Basel (Blutspendezentrum SRK beider Basel, BSZ). Peripheral blood mononuclear cells (PBMCs) were isolated by density centrifugation using SepMate tubes (Stemcell technologies) and the density gradient medium Ficoll-Paque (GE Healthcare) according to the manufacturer's protocol. Human T cells were purified (> 96% purity) by magnetic negative selection using an EasySep Human T Cell Isolation Kit (Cat#17951, Stemcell Technologies) according to the manufacturer's instruction. If frozen PBMCs were used, T cells were isolated after thawing and cultured in supplemented media without stimulation overnight. T cells were cultured in RPMI-1640 Medium (Sigma-Aldrich) supplemented with 10% heat-inactivated human serum (AB^+, male; purchased from BSZ Basel), 10mM HEPES (Sigma-Aldrich), 2mM GlutaMAX, 1mM Sodium Pyruvate, 0.05mM 2-Mercaptoethanol, 1% MEM Non-essential amino acids (100x) (all Gibco Life Technologies) and IL-2 150U/ml (Proleukin, University Hospital Basel). The medium and IL-2 was replenished every 2 days, and the cells were kept at a cell density of $1x10^6$ cells/ml.

ADCC assay (FcγRIIIa activation assay)

ADCC assay was performed using the ADCC Reporter Bioassays, V Variant (Promega, Cat#G7015) according to the manufacturer's instructions. Target cells HEK-293 expressing the CD123 variants were seeded in white 96 well-plate clear bottom at 4400 cells/100µl culture medium. At day 1, medium was removed and effector cells (Jurkat/FcγRIIIa/NFAT-Luc cells; E:T ratio 12:1) and MIRG123 antibody (final concentration 1µg/ml) were added and incubated for 5h at 37 °C 5% CO_2. The emitted luminescence was read 10min after the addition of Bio-Glo Luciferase Assay Reagent (Promega) using the PHERAstart FSX (BMG LABTECH) program Luc-Glo (LUM), GainA=3600, Optic module=LUMplus. Raji cells incubated with 1µg/ml of anti-CD20 antibody rituximab were used as positive control.

In vitro TCE-mediated killing assay with primary T cells

For the TCE killing assays the HEK-293 target cells were co-cultured together with human effector T cells and the CD3/CSL365-TCE at an effector to target ratio of 10:1 for 72 h. One day prior to co-culture HEK, HEK-CD123 and the HEK expressing the CD123 variants were stained with CellTraceViolet (CTV) according to the manufacturer's protocol. The following day effector T cells were added with the TCE at a concentration of 300ng/ml and kept for 72h at 37 °C. Cytotoxic activity and activation of T cells were analyzed by flow-cytometry. Specific killing was calculated as follows: (1-No. alive target cells with TCE/No. alive target cells without TCE)*100. Cell morphology was assessed with the light microscope Axio Vert.A1 (Zeiss) at 20x magnification.

Design and production of the CD123CAR HDRT

The CAR T cells were generated by co-electroporation of CRISPR-Cas9 Ribonucleoproteins (RNPs) specific for the *TRAC* locus and a double-stranded DNA HDR template (HDRT). The HDRT encoding a second-generation CD123-specific CAR with the scFv of clone CSL362,

606 the CD8□ hinge and transmembrane domain (Gen CD8A ENSG00000153563), the
607 intracellular signaling moieties 4-1BB (Gen TNFRSF9 ENSG00000049249) and CD3ζ (Gen
608 CD247 ENSG00000198821), as well as the fluorescent reporter protein GFP (for full sequence
609 see Extended data table). It is flanked by symmetric arms of homology (300 bp) complementary
610 to the *TRAC* locus Exon 1. The construct was synthesized by GenScript® and the plasmid was
611 used as template for PCR amplification (Kapa Hifi Hotstart Ready Mix, Cat#F-530-L, Roche).
612 The PCR amplicon was purified with NucleoSpin Gel and PCR clean-up kit (Macherey-Nagel)
613 according to the manufacturer's instruction and the correct size was verified by gel. The HDRT
614 was then condensed to a final concentration of 1µg/µl using vacuum concentration, and stored
615 at -20°C until usage.
616
617 Engineering primary CD123CAR T cells.
618 Protocols for human CRISPR/Cas9-mediated genome engineering are based on *Roth et al.*[12,13]
619 In short, Cas9 RNPs were freshly generated prior to each electroporation. Thawed crRNA and
620 tracrRNA (purchased from IDT Technologies, at 200µM) were mixed in a 1:1 molar ratio
621 (120pmol each), denatured at 95°C for 5min, and annealed at room temperature (RT) for 10 to
622 20min to complex a 80µM gRNA solution. Poly-Glutamic Acid (PGA; 15-50 kDa at
623 100mg/ml; Sigma-Aldrich) was added to the gRNA in a 0.8:1 volume ratio[14]. To complex
624 RNPs, 60pmol recombinant Cas9 (University of California Berkeley at 40µM) was mixed with
625 the gRNA (molar ratio Cas9:gRNA = 1:2) and incubated for 20min at RT in the dark. Prior to
626 electroporation isolated human T cells were activated for 48h with CD3/CD28 Dynabeads
627 (Thermofisher) at a cell to beads ratio 1:1 together with the recombinant human cytokines IL-
628 2 (150U/ml), IL-7 (5ng/ml; R&D Systems) and IL-15 (5ng/ml; R&D systems). Electroporation
629 was performed with the 4D-Nucleofector™ system (Lonza) with Program EH-115. Following
630 activation, the T cells were de-beaded using an EasySep™ magnet and $1x10^6$ cells were

resuspended in 20µl Lonza supplemented P3 electroporation buffer. HDRT (3-4µg) and RNPs (60pmol) were mixed separately and incubated for 5min. The cells were added to the mix and the total volume was transferred to the 16-well Nucleocuvette Strips. Immediately following electroporation 80µl of prewarmed supplemented medium was added to each cuvette and incubated at 37°C. After 20min, the cells were transferred into 48-well culture plates and replenished wit IL-2 500U/ml. Following flow-sorting at day 3 to 5 post-electroporation the cells were expanded for 5 to 6 days until used for the subsequent experiments. Control T cells were electroporated with an incomplete RNP (missing the specific crRNA), otherwise processed as the CAR T cells.

In vitro human CD123CAR killing assay.

The day before the co-culture HEK-293 target cells were stained with CTV and kept in supplemented human medium overnight. The flow-sorted, expanded GFP^+ CAR T cells and control cells were added to the target cells in an effector to target ratio 10:1 and co-cultured for 24h. Specific killing and T cell activation was measured by flow cytometry. Specific killing was calculated according to the indicated formula: (1-No. alive target cells in co-culture with CAR T cells/No. alive target cells in co-culture with control cells)*100. Using the microscope Axio Vert.A1 (Zeiss) cell morphology was recorded.

Human cytokine measurement (ELISA)

IFN□ was measured from the supernatants of the co-culture experiments (TCE / CAR) using the colorimetric ELISA MAX Standard Set Human IFN□ kit (BioLegend) according to the manufacturer's instruction. The optical density was read at 450 nm with the microplate reader. A standard curve calculated from standard dilutions was run in duplicates with every experiment.

Genomic DNA extraction and sequencing from human T cells, eukaryotic cell lines and HSPCs

Genomic DNA was extracted using the QuickExtract™ (Biosearch technologies; QE09050) according to the manufacturer's instruction. Alternatively, cells were lysed in Tail Lysis Buffer (100 mM Tris [pH 8.5], 5 mM Na-EDTA, 0.2% SDS, 200 mM NaCl) containing Proteinase K (0.1 µg; Sigma-Aldrich) at 56 °C (1000 rpm). The DNA was precipitated with isopropanol (1:1 volume ratio), and washed in 70% ethanol. The genomic DNA concentration was measured with a NanoDrop™ device (Thermo Fisher). PCR was performed using either GoTaq G2 Green Master Mix (Cat#M782B, Promega) or Kapa Hifi Hotstart Ready Mix. Sanger Sequencing was performed at Microsynth AG Switzerland. Sequences were analysed using MegAlign Pro (DNASTAR).

Bio-Layer Interferometry (BLI) measurement of binding

All BLI measurements were performed either on an Octet Red96e (ForteBio) or on an Octet R8 (Sartorius). The extracellular domain (ECD) of CD123 WT and variants were produced and purified by Icosagen.

CSL362 hIgG1 binding to CD123 WT ECD and variants

Binding of antibody CSL362 hIgG1 to CD123 WT ECD and variants (analytes in solution) was performed at low (50nM) and high (300nM) concentration of analyte. Antibody CSL362 hIgG1 (captured ligand) was captured by Anti-Human Fc capture biosensor (AHC) (Sartorius, PN: 18-5060) for 300s at 0.5µg/mL. Analytes CD123 WT ECD and variants were titrated at 7 concentrations (1:2 dilution series) from 50nM to 0.78nM and from 300nM to 4.7nM. Association to analyte was monitored for 300s and dissociation for 600s or 900s. Double reference subtraction was performed against buffer only and biosensor loaded with a negative hIgG1 control. Regeneration was performed in 10mM Gly-HCl pH1.7. Data were analyzed

using the Octet Data Analysis software HT 12.0. Data were fitted to a 1:1 binding model. Kinetic rates k_a and k_d were globally fitted.

6H6 mIgG1 binding to CD123 WT ECD and variants

Binding of antibody 6H6 mIgG1 (Biolegend, PN: 306002; captured ligand) to CD123 WT ECD and variants (analytes in solution) was performed using Streptavidin capture biosensor (SA) (Sartorius, PN: 18-5019). CaptureSelect™ Biotin Anti-LC-kappa (Murine) (Thermo Fischer, PN: 7103152100) was captured for 600s at 1µg/mL on SA tips. Those biosensors were then used to capture antibody 6H6 mIgG1 for 300s at 2.5µg/mL. Analytes CD123 WT ECD and variants were titrated at 7 concentrations from 50 to 1.56nM. Association to analyte was monitored for 300s and dissociation for 600s. Buffer only well was used as reference. Regeneration was performed in 10mM Gly-HCl pH1.7. Data were analyzed using the Octet Data Analysis software HT 12.0. Data were fitted (when possible) to a 1:1 binding model. Kinetic rates k_a and k_d were globally fitted.

IL-3 binding to CD123 WT ECD and variants

Binding of IL-3 (Sino Biological, PN: 11858-H08H) (analyte in solution) to CD123 WT ECD and variants (captured ligands) was performed using Streptavidin capture biosensor (SA) (Sartorius, PN: 18-5019). CD123 WT ECD and variants were biotinylated using Biotinylation kit Type B (Abcam, PN: ab201796) following manufacturer instructions. Biotinylated CD123 WT ECD. and variants (ligands) were captured on SA tips for 1000s at 3µg/mL concentration. Analyte IL-3 was titrated at 7 concentrations from 500 to 7.8nM in PBS pH7.4. Association to analyte was monitored for 300s and dissociation for 120s. Buffer only well was used as reference. No regeneration was performed, and a new set of tips was used for each biotinylated captured ligand. Data were analyzed using the Octet Data Analysis software HT12.0. Due to the fast on/off nature of the interaction data were analyzed using Steady state analysis.

Thermal stability analysis

Differential Scanning Fluorimetry (DSF) analysis were performed on a Bio-Rad CFX96 Touch Deep Well RT PCR Detection System. Sypro Orange 5000X in DMSO (Sigma, PN: S5692) was used at a final concentration of 5X. Temperature gradient was performed from 25 to 95°C in increment of 1.5°C in a reaction volume of 20µL. "FRET" scan mode was used to monitor fluorescence. All samples were analyzed at a final concentration of 0.25mg/mL in triplicate in PBS pH7.4. The temperature of protein unfolding transition (Tm) was calculated using the 1st derivative method.

Engineering of TF-1 cells expressing CD123 variants and functional assays thereof

RNPs were freshly prepared as outlined above. 50pmol ssDNA HDRT (180bp length, Ultramer DNA Oligonucleotides, synthetized by IDT) were added to the RNPs. Per reaction $0.2x10^6$ TF-1 cells were re-suspended in 10µl R buffer (Neon™ Transfection System) and electroporated using the Neon® Transfection System (1200V, 40ms, 1pulse). Following an expansion period of 12 days the edited cells were flow sorted based on the binding to MIRG123 and 6H6: WT ($MIRG123^+6H6^+$), KO ($MIRG123^-6H6^-$) and KI ($MIRG123^-6H6^+$).

To test responsiveness of TF-1 cells to human IL-3, $0.18x10^5$ sorted cells were distributed into white 96 well-plate clear bottom tissue-culture treated (Greiner) and different IL-3 concentrations indicated in **Fig. 5b** were added. In certain experiments MIRG123 was added in the concentrations shown in **Fig. 5c**. After 3 days, proliferation was assessed using CellTiter-Glo® 2.0 (Cat#G9241, Promega) according to the manufacturer's protocol. Luminescence was assessed with the Synergy H1 (BioTek) with an integration time of 1s.

Non-virally CRISPR/Cas9 mediated engineering of HSPCs

Leukopaks were purchased from CytoCare and HSPCs were isolated by the LP-34 Process using the CliniMACS Prodigy (Miltenyi). HSPCs were thawed in HSC-Brew GMP Basal Medium (Miltenyi) supplemented with HSC-Brew GMP Supplement, 2% human serum albumin, 100ng/mL Stem Cell Factor (SCF), 100ng/mL Thrombopoietin (TPO), 100ng/mL Fms-like tyrosine kinase 3 ligand (Flt3L) and 60ng/mL IL-3 (Miltenyi) at a concentration of $0.5x10^6$ cells/ml. Cells were electroporated 2 days later. gRNAs were freshly prepared as outlined above, but 50 µM crRNA and tracrRNA were used to form the gRNA and complexed with 1µM Spyfi Cas9 (Aldevron at 61.889 µM) at a molar ratio Cas9:gRNA = 1:2 and incubated for 20 min at RT. As control, incomplete RNPs lacking the site-specific crRNA were generated. During the RNPs complexing, HSPCs were collected, washed twice with electroporation buffer (Miltenyi) and resuspend in electroporation buffer at $1x10^6$ cells/90 µl. Cells were then mixed with 5µl RNP and ssDNA HDRT encoding the variants (5µl corresponding to 500 pmol) and the whole volume was transferred into the electroporation nucleocuvette. Electroporation was performed with the CliniMACS Prodigy (600V 100µs burst / 400V 750µs square). Immediately after electroporation the cells were transferred to a 6 well plate and rested for 20 minutes at RT. After 20min, 2mL of pre-warmed HSC medium supplemented with 100ng/mL SCF, 100ng/mL TPO and 100ng/mL Flt3L was added and the plate was incubated at 37°C.

CD123 and CCR5 gene editing with CRISPR/Cas9 and rAAV6 virus

$CD34^+$ HSPC culture condition

Plerixafor mobilized peripheral blood $CD34^+$ HSPCs were purchased from AllCells (Alameda, CA, USA). The cells were thawed per manufacturer's instructions and were cultured at 37°C, 5% CO2, and 5% O2. Cell culture medium was GMP SCGM medium from CellGenix (Portsmouth, NH, USA) supplemented with human cytokine (PeproTech, Rocky Hill, NJ,

USA) cocktail containing SCF 100ng/ml, TPO 100ng/ml, Flt3L 100ng/ml, and IL-6 100ng/ml. UM171 (35nM) (StemCell Technologies, Vancouver, Canada), streptomycin (20mg/ml) and penicillin (20U/ml) were added into the cell culture medium.

CD123 and CCR5 gene editing procedure

HSPCs were cultured and pre-stimulated for 72 hours after thaw and before gene editing. Chemically modified CD123 sgRNA and CCR5 sgRNA were synthesized by Synthego Corporation (Redwood City, CA, USA). SpyFi Cas9 was purchased from Aldevron, LLC (Fargo, ND, USA). CD123-E51K and CD123-E51T donor rAAV6 virus was purchased from SignaGen Laboratories (Frederick, MD, USA). CCR5-KO donor rAAV6 virus was produced in HEK-293T cells and was purified with AAVpro Purification Kit (TakaRa, San Jose, CA, USA). Electroporation of the RNP complex was performed using the Lonza 4D-Nucleofector (Lonza Group Ltd, Alpharetta, GA, USA) in P3 Primary Cell Solution with program DZ-100. Donor rAAV6 virus was immediately dispensed onto electroporated cells at multiplicity of infection (MOI) of $2.5x10^3$ vector genomes (vg) per cell for CD123 and $5.0x10^3$ vg per cell for CCR5 based on the titers determined by ddPCR. The cells were then divided into two halves at $2.5x10^5$ cells/ml. One half was plated in SCGM medium supplemented with cytokines and 10ng/ml IL-3 (PeproTech, Rocky Hill, NJ, USA) as +IL-3 treatment. The other half was plated in SCGM medium supplemented with cytokines only as -IL-3 treatment. After incubation for 24 hours, a medium change was performed to remove residual rAAV6 virus. The $CD34^+$ HSPCs were cultured for up to 8 days for quantification of gene editing events, CFU assays and pSTAT5 staining and FACS analysis.

Methylcellulose colony formation unit (CFU) assay

CFU assay was started at 48h post gene editing. For each condition, 1.1mL of semi-solid methylcellulose medium (StemCell Technologies, Seattle, WA, USA) containing 300 cells and

with 10ng/ml IL-3 (+IL-3 treatment) or without IL-3 (-IL-3 treatment) were plated in a well of a SmartDish (StemCell Technologies, Seattle, WA, USA) in duplicates. The cells were incubated at 37 °C, 5% O2 and 5% CO2 for 14 days. The resulting progenitor colonies were counted and scored with STEMVision analysis (StemCell Technologies, Seattle, WA, USA) per manufacturer's instruction.

pSTAT5 staining

On day 8 post gene editing, all cells were switched to growth medium without IL-3 for IL-3 starvation. After 1-day IL-3 starvation, for +IL-3 treatment, 10ng/ml IL-3 was added back to the cells which were originally cultured in +IL-3 medium. For -IL-3 treatment, IL-3 was not added into the cells which were originally cultured in -IL-3 medium. All cell cultures were incubated for 1h and then were subjected to pSTAT5 staining. Briefly, after 1h incubation, cells were lysed and fixed in BD Phosflow Lyse/Fix Buffer and then were permeabilized with BD Phosflow Perm Buffer III (BD Biosciences, San Jose, CA, USA) following manufacturer's instruction. The permeabilized cells were stained with Alexa 647 Mouse-anti-human Stat5 (pY694) antibody in PBS at RT for 1h. Alexa 647 Mouse isotype IgG (BD Pharmingen, San Jose, CA, USA) was used as a negative control. K-562 cells which were not subjected to IL-3 treatment nor IL-3 stimulation was stained with the same pSTAT5 antibody as a positive control. After staining, cells were washed with PBS and then were subjected to CytoFLEX Flow Cytometer (Beckman Coulter Life Sciences, Brea, CA) for FACS analysis.

Differentiation of non-virally edited HSPCs in vitro

Two days after electroporation cells were stained with the antibodies 6H6-BV650 and MIRG123-bio/Strep-PE and FACS sorted as WT ($MIRG123^{+}6H6^{+}$), KO ($MIRG123^{-}6H6^{-}$) and KI ($MIRG123^{-}6H6^{+}$). Sorted cells were resuspended in StemPro media (Gibco) containing

StemPro Nutrients, LDL 50ng/mL, P/S 1%, Glutamine 1%, Flt3 20ng/mL, TPO 50ng/mL, IL-6 50ng/mL, IL-3 10ng/mL, IL-2 10ng/mL, IL-7 20ng/mL, IL-11 50ng/mL, EPO 3ng/mL, GM-CSF 20ng/mL, SCF 100ng/m, and $0.21x10^4$ cells/well were plated in a 96 well plate. After 7 days cells were collected, stained for CD33 and GlyA/CD235a and acquired on a FACS Lyria.

Mice

All animal work was performed in accordance with the federal and cantonal laws of Switzerland. Protocols were approved by the Animal Research Commission of the Canton of Basel-Stadt, Switzerland. All mice were housed in a specific pathogen-free (SPF) condition in accordance with institutional guidelines and ethical regulations. NSG (stock# 005557) female mice were purchased from Jackson Laboratories. The HSPCs were edited as described above. One day after electroporation cells were collected, washed and resuspended in PBS at $10x10^6$ live cells/ml. Recipient female mice (3 weeks old) were irradiated the day before with 200cGy. Chimerism was analysed after 6 and 10 weeks in the blood by flow cytometry. Mice were euthanized 15 weeks after humanization.

In vitro TCE-mediated killing assay of non-virally engineered HSPCs

For the TCE killing assays the HSPCs were edited as described above. Autologous human T cells were isolated from PBMCs as abovementioned and cultured overnight in supplemented media without stimulation. Two days after electroporation edited HSPCs were co-cultured in a 96 U-bottom plate together with human effector T cells at an effector to target ratio of 3:1 and the CD3/CSL362-TCE at 100ng/ml for 72 h at 37 °C. In a set of experiments MOLM-14 (labelled with CTV according to the manufacturer's instruction) were added to the autologous T cells and edited HSPCs at an effector to target to tumor ratio of 3:0.5:0.5 together with the CD3/CSL365-TCE (100ng/ml). Cytotoxic activity (specific killing and elimination of non-

edited HSCs) were analysed by flow-cytometry. Specific killing was calculated as follows: (1-No. alive target cells with TCE/No. alive target cells without TCE)*100.

Statistical Analysis

Statistical Analysis was performed on Prism 9.1.2 software (GraphPad). Number of donors and replicates are found within each figure legend.

References

1 Carter, P. J. & Rajpal, A. Designing antibodies as therapeutics. *Cell* **185**, 2789-2805, doi:10.1016/j.cell.2022.05.029 (2022).

2 Globerson Levin, A., Riviere, I., Eshhar, Z. & Sadelain, M. CAR T cells: Building on the CD19 paradigm. *Eur J Immunol* **51**, 2151-2163, doi:10.1002/eji.202049064 (2021).

3 June, C. H., O'Connor, R. S., Kawalekar, O. U., Ghassemi, S. & Milone, M. C. CAR T cell immunotherapy for human cancer. *Science* **359**, 1361-1365, doi:10.1126/science.aar6711 (2018).

4 Lee, D. W. *et al.* T cells expressing CD19 chimeric antigen receptors for acute lymphoblastic leukaemia in children and young adults: a phase 1 dose-escalation trial. *Lancet* **385**, 517-528, doi:10.1016/S0140-6736(14)61403-3 (2015).

5 Kochenderfer, J. N. *et al.* Eradication of B-lineage cells and regression of lymphoma in a patient treated with autologous T cells genetically engineered to recognize CD19. *Blood* **116**, 4099-4102, doi:10.1182/blood-2010-04-281931 (2010).

6 Brentjens, R. J. *et al.* Safety and persistence of adoptively transferred autologous CD19-targeted T cells in patients with relapsed or chemotherapy refractory B-cell leukemias. *Blood* **118**, 4817-4828, doi:10.1182/blood-2011-04-348540 (2011).

7 Kalos, M. *et al.* T cells with chimeric antigen receptors have potent antitumor effects and can establish memory in patients with advanced leukemia. *Sci Transl Med* **3**, 95ra73, doi:10.1126/scitranslmed.3002842 (2011).

8 Mougiakakos, D. *et al.* CD19-Targeted CAR T Cells in Refractory Systemic Lupus Erythematosus. *N Engl J Med* **385**, 567-569, doi:10.1056/NEJMc2107725 (2021).

9 Porter, D. L., Levine, B. L., Kalos, M., Bagg, A. & June, C. H. Chimeric antigen receptor-modified T cells in chronic lymphoid leukemia. *N Engl J Med* **365**, 725-733, doi:10.1056/NEJMoa1103849 (2011).

10 Paszkiewicz, P. J. *et al.* Targeted antibody-mediated depletion of murine CD19 CAR T cells permanently reverses B cell aplasia. *J Clin Invest* **126**, 4262-4272, doi:10.1172/JCI84813 (2016).

11 Finck, A. V., Blanchard, T., Roselle, C. P., Golinelli, G. & June, C. H. Engineered cellular immunotherapies in cancer and beyond. *Nat Med* **28**, 678-689, doi:10.1038/s41591-022-01765-8 (2022).

12 Majzner, R. G. & Mackall, C. L. Clinical lessons learned from the first leg of the CAR T cell journey. *Nat Med* **25**, 1341-1355, doi:10.1038/s41591-019-0564-6 (2019).

13 Eyquem, J. *et al.* Targeting a CAR to the TRAC locus with CRISPR/Cas9 enhances tumour rejection. *Nature* **543**, 113-117, doi:10.1038/nature21405 (2017).

14 Lynn, R. C. *et al.* c-Jun overexpression in CAR T cells induces exhaustion resistance. *Nature* **576**, 293-300, doi:10.1038/s41586-019-1805-z (2019).

15 Maude, S. L. *et al.* Chimeric antigen receptor T cells for sustained remissions in leukemia. *N Engl J Med* **371**, 1507-1517, doi:10.1056/NEJMoa1407222 (2014).

16 Melenhorst, J. J. *et al.* Decade-long leukaemia remissions with persistence of CD4(+) CAR T cells. *Nature* **602**, 503-509, doi:10.1038/s41586-021-04390-6 (2022).

17 Perna, F. *et al.* Integrating Proteomics and Transcriptomics for Systematic Combinatorial Chimeric Antigen Receptor Therapy of AML. *Cancer Cell* **32**, 506-519 e505, doi:10.1016/j.ccell.2017.09.004 (2017).

18 Haubner, S. *et al.* Coexpression profile of leukemic stem cell markers for combinatorial targeted therapy in AML. *Leukemia* **33**, 64-74, doi:10.1038/s41375-018-0180-3 (2019).

19 Baroni, M. L. *et al.* 41BB-based and CD28-based CD123-redirected T-cells ablate human normal hematopoiesis in vivo. *J Immunother Cancer* **8**, doi:10.1136/jitc-2020-000845 (2020).

20 Zeng, A. G. X. *et al.* A cellular hierarchy framework for understanding heterogeneity and predicting drug response in acute myeloid leukemia. *Nat Med* **28**, 1212-1223, doi:10.1038/s41591-022-01819-x (2022).

21 Gill, S. *et al.* Preclinical targeting of human acute myeloid leukemia and myeloablation using chimeric antigen receptor-modified T cells. *Blood* **123**, 2343-2354, doi:10.1182/blood-2013-09-529537 (2014).

22 Irving, M., Zoete, V., Bassani-Sternberg, M. & Coukos, G. A roadmap for driving CAR T cells toward the oncogenic immunopeptidome. *Cancer Cell* **40**, 20-22, doi:10.1016/j.ccell.2021.12.011 (2022).

23 Mause, E. R. V., Atanackovic, D., Lim, C. S. & Luetkens, T. Roadmap to affinity-tuned antibodies for enhanced chimeric antigen receptor T cell function and selectivity. *Trends Biotechnol* **40**, 875-890, doi:10.1016/j.tibtech.2021.12.009 (2022).

24 Arai, Y. *et al.* Myeloid Conditioning with c-kit-Targeted CAR-T Cells Enables Donor Stem Cell Engraftment. *Mol Ther* **26**, 1181-1197, doi:10.1016/j.ymthe.2018.03.003 (2018).

25 Myburgh, R. *et al.* Anti-human CD117 CAR T-cells efficiently eliminate healthy and malignant CD117-expressing hematopoietic cells. *Leukemia* **34**, 2688-2703, doi:10.1038/s41375-020-0818-9 (2020).

26 Majzner, R. G. & Mackall, C. L. Tumor Antigen Escape from CAR T-cell Therapy. *Cancer Discov* **8**, 1219-1226, doi:10.1158/2159-8290.CD-18-0442 (2018).

27 Kim, M. Y. *et al.* Genetic Inactivation of CD33 in Hematopoietic Stem Cells to Enable CAR T Cell Immunotherapy for Acute Myeloid Leukemia. *Cell* **173**, 1439-1453 e1419, doi:10.1016/j.cell.2018.05.013 (2018).

28 Borot, F. *et al.* Gene-edited stem cells enable CD33-directed immune therapy for myeloid malignancies. *Proc Natl Acad Sci U S A* **116**, 11978-11987, doi:10.1073/pnas.1819992116 (2019).

29 Humbert, O. *et al.* Engineering resistance to CD33-targeted immunotherapy in normal hematopoiesis by CRISPR/Cas9-deletion of CD33 exon 2. *Leukemia* **33**, 762-808, doi:10.1038/s41375-018-0277-8 (2019).

30 Emerson, S. G., Yang, Y. C., Clark, S. C. & Long, M. W. Human recombinant granulocyte-macrophage colony stimulating factor and interleukin 3 have overlapping but distinct hematopoietic activities. *J Clin Invest* **82**, 1282-1287, doi:10.1172/JCI113727 (1988).

31 Jordan, C. T. *et al.* The interleukin-3 receptor alpha chain is a unique marker for human acute myelogenous leukemia stem cells. *Leukemia* **14**, 1777-1784, doi:10.1038/sj.leu.2401903 (2000).

32 Liu, T. F. *et al.* Diphtheria toxin fused to variant interleukin-3 provides enhanced binding to the interleukin-3 receptor and more potent leukemia cell cytotoxicity. *Exp Hematol* **32**, 277-281, doi:10.1016/j.exphem.2003.11.010 (2004).

33 Roberts, A. W. *et al.* A phase I study of anti-CD123 monocional antibody (mAb) CSL360 targeting leukemia stem cells (LSC) in AML. *J Clin Oncol* **28**, doi:DOI 10.1200/jco.2010.28.15_suppl.e13012 (2010).

34 Busfield, S. J. *et al.* Targeting of acute myeloid leukemia in vitro and in vivo with an anti-CD123 mAb engineered for optimal ADCC. *Leukemia* **28**, 2213-2221, doi:10.1038/leu.2014.128 (2014).

929 35 Kovtun, Y. *et al.* A CD123-targeting antibody-drug conjugate, IMGN632, designed to
930 eradicate AML while sparing normal bone marrow cells. *Blood Adv* **2**, 848-858,
931 doi:10.1182/bloodadvances.2018017517 (2018).
932 36 Chichili, G. R. *et al.* A CD3xCD123 bispecific DART for redirecting host T cells to
933 myelogenous leukemia: preclinical activity and safety in nonhuman primates. *Sci*
934 *Transl Med* **7**, 289ra282, doi:10.1126/scitranslmed.aaa5693 (2015).
935 37 Hutmacher, C. *et al.* Development of a novel fully-human anti-CD123 antibody to
936 target acute myeloid leukemia. *Leuk Res* **84**, 106178,
937 doi:10.1016/j.leukres.2019.106178 (2019).
938 38 Broughton, S. E. *et al.* Dual mechanism of interleukin-3 receptor blockade by an anti-
939 cancer antibody. *Cell Rep* **8**, 410-419, doi:10.1016/j.celrep.2014.06.038 (2014).
940 39 Strohl, W. R. & Naso, M. Bispecific T-Cell Redirection versus Chimeric Antigen
941 Receptor (CAR)-T Cells as Approaches to Kill Cancer Cells. *Antibodies (Basel)* **8**,
942 doi:10.3390/antib8030041 (2019).
943 40 Kitamura, T. *et al.* Establishment and characterization of a unique human cell line that
944 proliferates dependently on GM-CSF, IL-3, or erythropoietin. *J Cell Physiol* **140**,
945 323-334, doi:10.1002/jcp.1041400219 (1989).
946 41 Czechowicz, A., Kraft, D., Weissman, I. L. & Bhattacharya, D. Efficient
947 transplantation via antibody-based clearance of hematopoietic stem cell niches.
948 *Science* **318**, 1296-1299, doi:10.1126/science.1149726 (2007).
949 42 Palchaudhuri, R. *et al.* Non-genotoxic conditioning for hematopoietic stem cell
950 transplantation using a hematopoietic-cell-specific internalizing immunotoxin. *Nat*
951 *Biotechnol* **34**, 738-745, doi:10.1038/nbt.3584 (2016).
952 43 Li, Z., Czechowicz, A., Scheck, A., Rossi, D. J. & Murphy, P. M. Hematopoietic
953 chimerism and donor-specific skin allograft tolerance after non-genotoxic CD117

antibody-drug-conjugate conditioning in MHC-mismatched allotransplantation. *Nat Commun* **10**, 616, doi:10.1038/s41467-018-08202-w (2019).

44 Czechowicz, A. *et al.* Selective hematopoietic stem cell ablation using CD117-antibody-drug-conjugates enables safe and effective transplantation with immunity preservation. *Nat Commun* **10**, 617, doi:10.1038/s41467-018-08201-x (2019).

45 Kornete, M., Marone, R. & Jeker, L. T. Highly Efficient and Versatile Plasmid-Based Gene Editing in Primary T Cells. *J Immunol* **200**, 2489-2501, doi:10.4049/jimmunol.1701121 (2018).

46 Dever, D. P. *et al.* CRISPR/Cas9 beta-globin gene targeting in human haematopoietic stem cells. *Nature* **539**, 384-389, doi:10.1038/nature20134 (2016).

47 Cromer, M. K. *et al.* Ultra-deep sequencing validates safety of CRISPR/Cas9 genome editing in human hematopoietic stem and progenitor cells. *Nat Commun* **13**, 4724, doi:10.1038/s41467-022-32233-z (2022).

48 Anzalone, A. V., Koblan, L. W. & Liu, D. R. Genome editing with CRISPR-Cas nucleases, base editors, transposases and prime editors. *Nat Biotechnol* **38**, 824-844, doi:10.1038/s41587-020-0561-9 (2020).

49 Asano, T. *et al.* X-linked recessive TLR7 deficiency in ~1% of men under 60 years old with life-threatening COVID-19. *Sci Immunol* **6**, doi:10.1126/sciimmunol.abl4348 (2021).

50 Persaud, S. P. *et al.* Antibody-drug conjugates plus Janus kinase inhibitors enable MHC-mismatched allogeneic hematopoietic stem cell transplantation. *J Clin Invest* **131**, doi:10.1172/JCI145501 (2021).

51 Saha, A. *et al.* A CD45-targeted antibody-drug conjugate successfully conditions for allogeneic hematopoietic stem cell transplantation in mice. *Blood* **139**, 1743-1759, doi:10.1182/blood.2021012366 (2022).

Method reference

1 Broughton, S. E. *et al.* Dual mechanism of interleukin-3 receptor blockade by an anti-cancer antibody. *Cell Rep* **8**, 410-419 (2014). https://doi.org:10.1016/j.celrep.2014.06.038

2 Broughton, S. E. *et al.* A dual role for the N-terminal domain of the IL-3 receptor in cell signalling. *Nat Commun* **9**, 386 (2018). https://doi.org:10.1038/s41467-017-02633-7

3 Lee, B. & Richards, F. M. The interpretation of protein structures: estimation of static accessibility. *J Mol Biol* **55**, 379-400 (1971). https://doi.org:10.1016/0022-2836(71)90324-x

4 Mitternacht, S. FreeSASA: An open source C library for solvent accessible surface area calculations. *F1000Res* **5**, 189 (2016). https://doi.org:10.12688/f1000research.7931.1

5 Hopf, T. A. *et al.* Mutation effects predicted from sequence co-variation. *Nat Biotechnol* **35**, 128-135 (2017). https://doi.org:10.1038/nbt.3769

6 Hopf, T. A. *et al.* The EVcouplings Python framework for coevolutionary sequence analysis. *Bioinformatics* **35**, 1582-1584 (2019). https://doi.org:10.1093/bioinformatics/bty862

7 Ekeberg, M., Lovkvist, C., Lan, Y., Weigt, M. & Aurell, E. Improved contact prediction in proteins: using pseudolikelihoods to infer Potts models. *Phys Rev E Stat Nonlin Soft Matter Phys* **87**, 012707 (2013). https://doi.org:10.1103/PhysRevE.87.012707

8 Dunn, S. D., Wahl, L. M. & Gloor, G. B. Mutual information without the influence of phylogeny or entropy dramatically improves residue contact prediction. *Bioinformatics* **24**, 333-340 (2008). https://doi.org:10.1093/bioinformatics/btm604

9 Suzek, B. E. *et al.* UniRef clusters: a comprehensive and scalable alternative for improving sequence similarity searches. *Bioinformatics* **31**, 926-932 (2015). https://doi.org:10.1093/bioinformatics/btu739

10 Hutmacher, C. *et al.* Development of a novel fully-human anti-CD123 antibody to target acute myeloid leukemia. *Leuk Res* **84**, 106178 (2019). https://doi.org:10.1016/j.leukres.2019.106178

11 Tiller, T. *et al.* Efficient generation of monoclonal antibodies from single human B cells by single cell RT-PCR and expression vector cloning. *J Immunol Methods* **329**, 112-124 (2008). https://doi.org:10.1016/j.jim.2007.09.017

12 Roth, T. L. *et al.* Reprogramming human T cell function and specificity with non-viral genome targeting. *Nature* **559**, 405-409 (2018). https://doi.org:10.1038/s41586-018-0326-5

13 Roth, T. L. *et al.* Pooled Knockin Targeting for Genome Engineering of Cellular Immunotherapies. *Cell* **181**, 728-744 e721 (2020). https://doi.org:10.1016/j.cell.2020.03.039

14 Nguyen, D. N. *et al.* Polymer-stabilized Cas9 nanoparticles and modified repair templates increase genome editing efficiency. *Nat Biotechnol* **38**, 44-49 (2020). https://doi.org:10.1038/s41587-019-0325-6

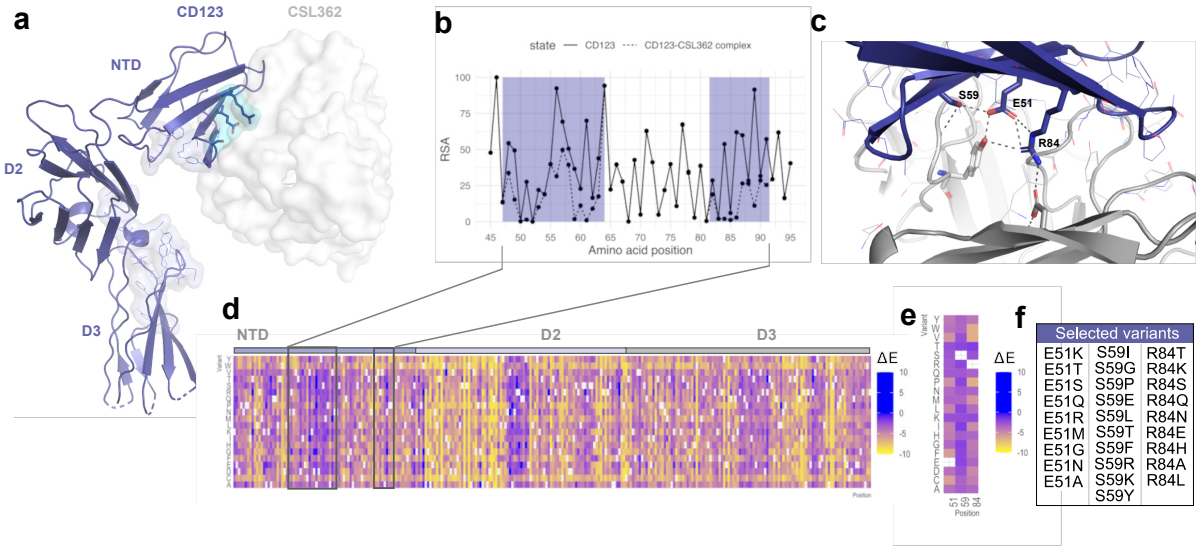

Figure 1. Rational design of human CD123 protein variants to shield from targeted immunotherapy

a, Crystal structure of the CD123-CSL362 complex in open conformation (PDB ID: 4JZJ[38]). CD123 is shown as ribbons. The CSL362 antibody variable domain is shown as white surface. CD123 amino acid residues involved in IL-3 binding are highlighted as lines and in light-blue. **b**, Per-residue relative solvent accessibility (RSA) computed on the CSL362-free (solid line) and CSL362-bound (dashed line) states based on the X-ray structure of the CD123-CSL362 complex (PDB ID: 4JZJ). RSA data are shown for the N-terminal domain. The CSL362 epitope region is highlighted by blue rectangles. **c**, Amino acid residues at the interface of the CD123-CSL362 complex are highlighted as lines and sticks. Side chain mediated intermolecular contacts are shown as dashed black lines. **d**, The predicted ΔE mutational landscape of CD123 is shown as a heatmap for the full extracellular domain (residue range 20-305, x-axis) and **e**, selected amino acid positions: E51, S59 and R84. Heatmap color ranges from yellow (ΔE <0, predicted damaging) to blue (ΔE ≥0, predicted neutral or beneficial). **f**, Selected amino acid variants at residues E51, S59, R84 sorted by decreasing ΔE values.

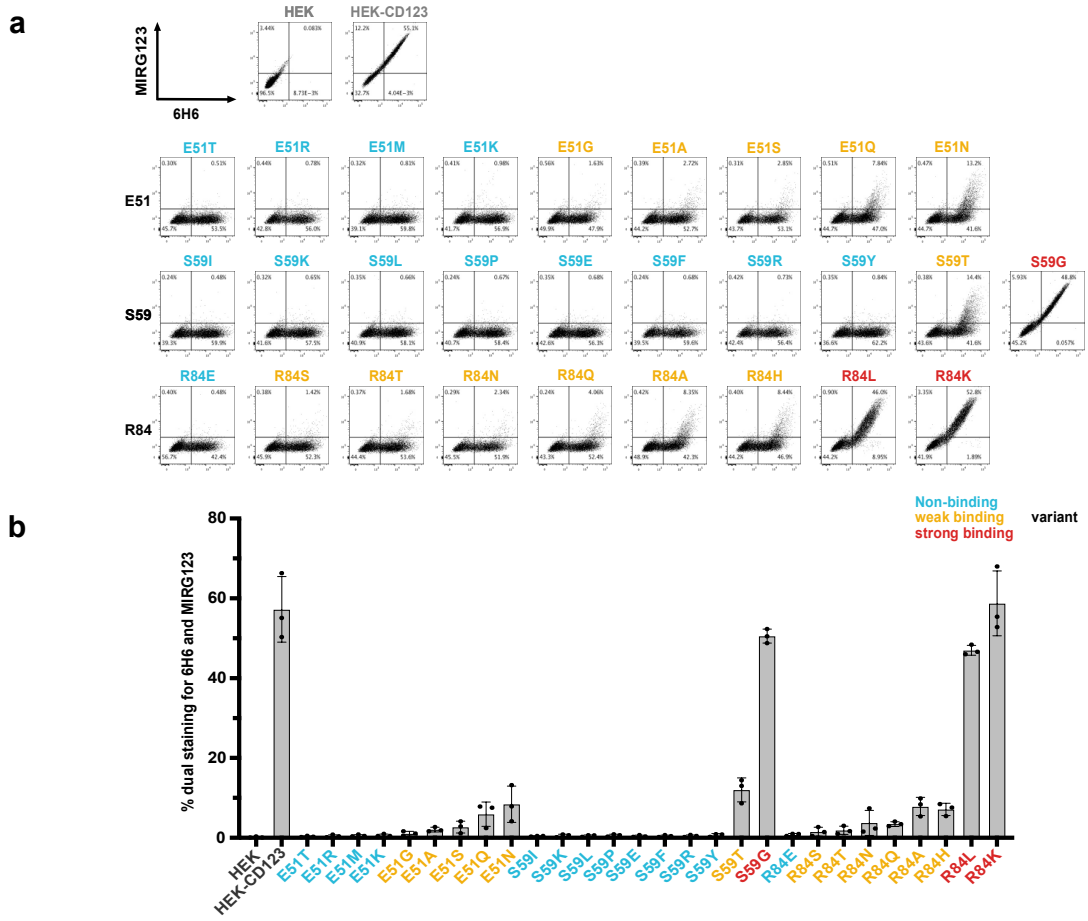

Figure 2: Preserved expression of engineered CD123 variants despite abolished binding to the monoclonal antibody MIRG123

a, Flow cytometry plots and **b,** summarizing bar graph showing binding of the anti-human CD123 antibody MIRG123 (biosimilar of CSL362) and the control clone 6H6 to wildtype CD123 and its 28 variants stably expressed in HEK-293 cells. Variants were categorized based on the dual staining to MIRG123 and 6H6 as non-binding (blue, <1% dual staining), weak (orange, 1-20%) or strong (red, >20%) binding variants. Control conditions (grey) are HEK-293 cells stably expressing wildtype CD123 (HEK-CD123) and non-transduced HEK-293 cells (HEK). Error bars: mean ± SD. Each symbol represents an individual experiment. Data in **a** is representative of three independent experiments.

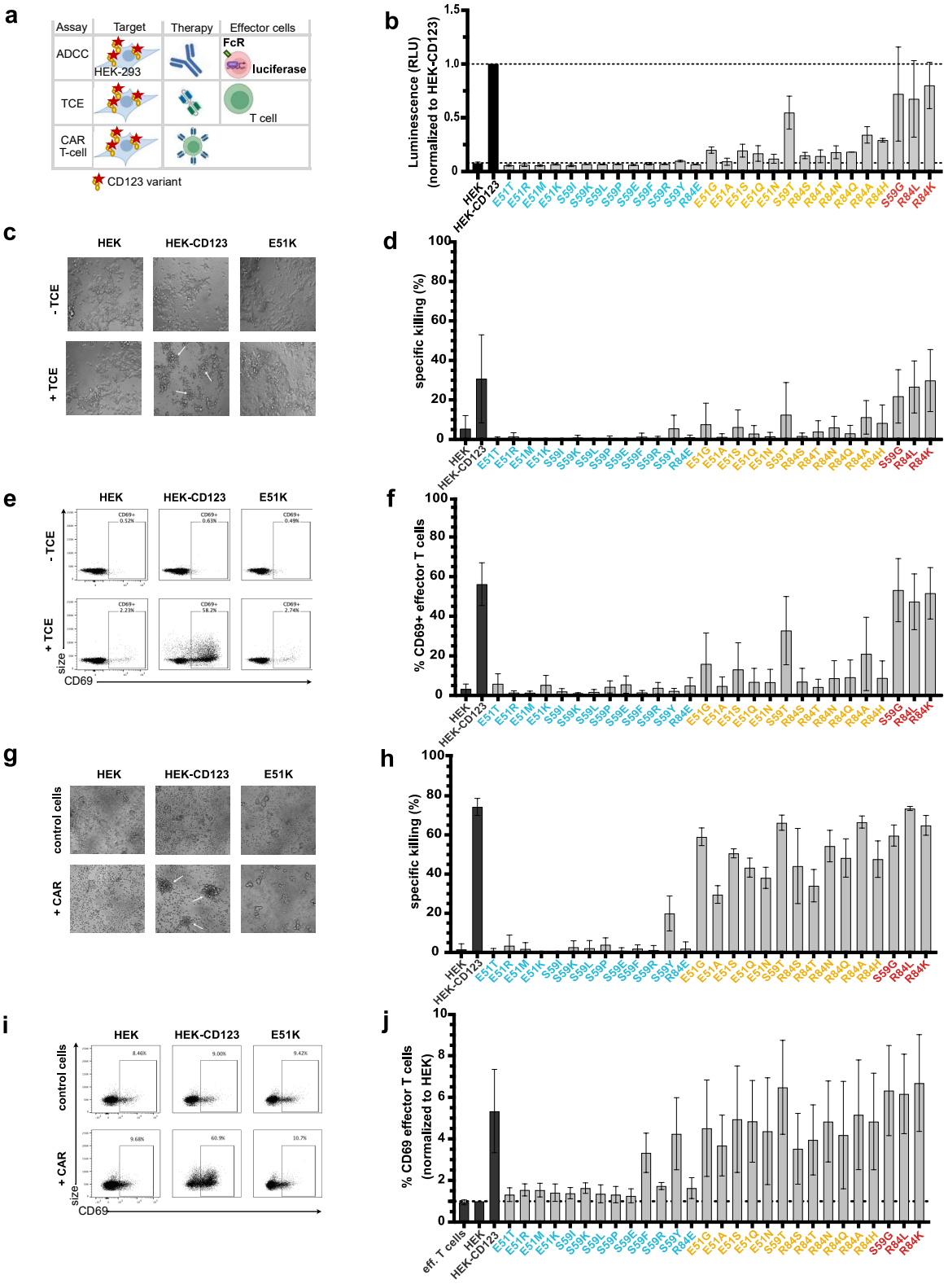
a
Assay
Target
Therapy
Effector cells
ADCC
HEK-293
FcR
luciferase
TCE
T cell
CAR T-cell
CD123 variant
b
Luminescence (RLU) (normalized to HEK-CD123)
c
HEK
HEK-CD123
E51K
- TCE
+ TCE
d
specific killing (%)
e
size
CD69
f
% CD69+ effector T cells
g
control cells
+ CAR
h
i
j
% CD69 effector T cells (normalized to HEK)
eff. T cells
HEK
HEK-CD123
E51T
E51R
E51M
E51K
S59I
S59K
S59L
S59P
S59E
S59F
S59R
S59Y
R84E
E51G
E51A
E51S
E51Q
E51N
S59T
R84S
R84T
R84N
R84Q
R84A
R84H
S59G
R84L
R84K

Figure 3: Cells expressing engineered CD123 variants are shielded from multiple targeted immunotherapy modalities *in vitro*

a, Schematic to assess shielding of CD123 expressing cells from three targeted immunotherapies (ADCC, TCE, CAR T-cell) in vitro. **b,** MIRG123-induced ADCC measured by luminescence of the effector cell line Jurkat/FcγRIIIa/NFAT-Luc following co-culture with HEK, HEK-CD123 or the CD123 variants. Luminescence signal normalized to the culture with HEK-CD123 (top dashed line). Data of 2 independent experiments. **c-f,** 3-day co-culture of effector T cells and HEK-293 expressing CD123 and its variants with and without CSL362/OKT3-TCE (TCE). Data represent 5 independent blood donors and experiments with 2 technical replicates per group. **c,** Representative images (Magnification 20x) after 3-day co-culture with HEK, HEK-CD123 or E51K with and without TCE. White arrows indicate cell clustering. **d,** Specific TCE-mediated killing of HEK-293 cells or its variants. **e,** Representative flow cytometry plots indicating CD69-expression in effector T cells without (top) and with (bottom) TCE after 3 days co-cultures with HEK, HEK-CD123 and the variant E51K. **f,** Frequency of CD69-expressing $CD3^+$ effector T cells after 3 days. **g-j,** Human 123CAR T cells were co-cultured with the target cells HEK, HEK-CD123 or its variants for 24h. Control T cells were electroporated with an HDRT, but incomplete RNP. Data from 3 independent blood donors and experiments with 2 technical replicates per group. **g,** Representative microscopy images (Magnification 20x) after 1 day with white arrows indicating cell clustering. **h,** Specific killing of target cells measured by flow cytometry at day 1 of co-culture. **i,** Representative FACS plots and **j,** summary of $CD69^+$ 123CAR T cells either alone (effector T cells) or in the presence of HEK, HEK-CD123 or all CD123 variants after 24h co-culture. The data are normalized to %$CD69^+$cells in the presence of HEK target cells. **b-j,** Error bars: mean ± SD.

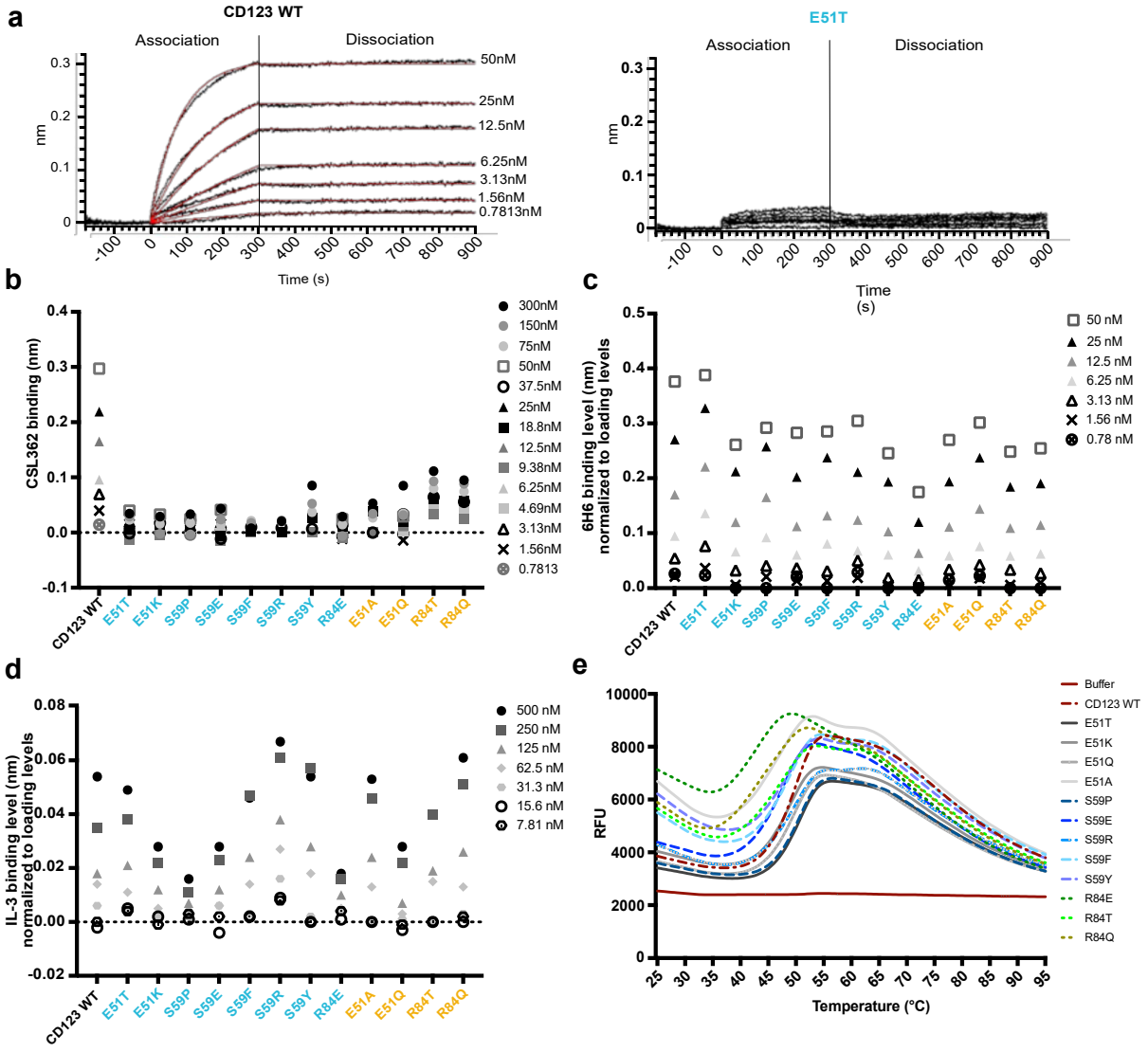

Figure 4: Biophysical characterization of selected CD123 protein variants

a, Binding of CSL362 to recombinant extracellular domain (ECD) of CD123 WT (**left**) and CD123 E51T (**right**) at increasing concentrations measured of CSL362 by Bio-Layer Interferometry. **b**, Binding levels of CD123 WT and its variants at different concentrations to captured CSL362 at 280s. CD123 WT reaches its saturation to CSL362 at 50nM, therefore higher concentrations were not measured. **c,** Binding levels of CD123 WT and its variants to the captured antibody 6H6 (normalized to the loading level of 6H6) at 250s. **d,** Binding levels of IL-3 to biotinylated CD123 WT and variants (normalized to loading levels of biotinylated CD123 WT and its variants) at 250s. **e,** Thermal unfolding (Relative Fluorescence Unit, RFU) of CD123 WT and variants measured by Differential Scanning Fluorimetry (DSF) with increasing temperatures.

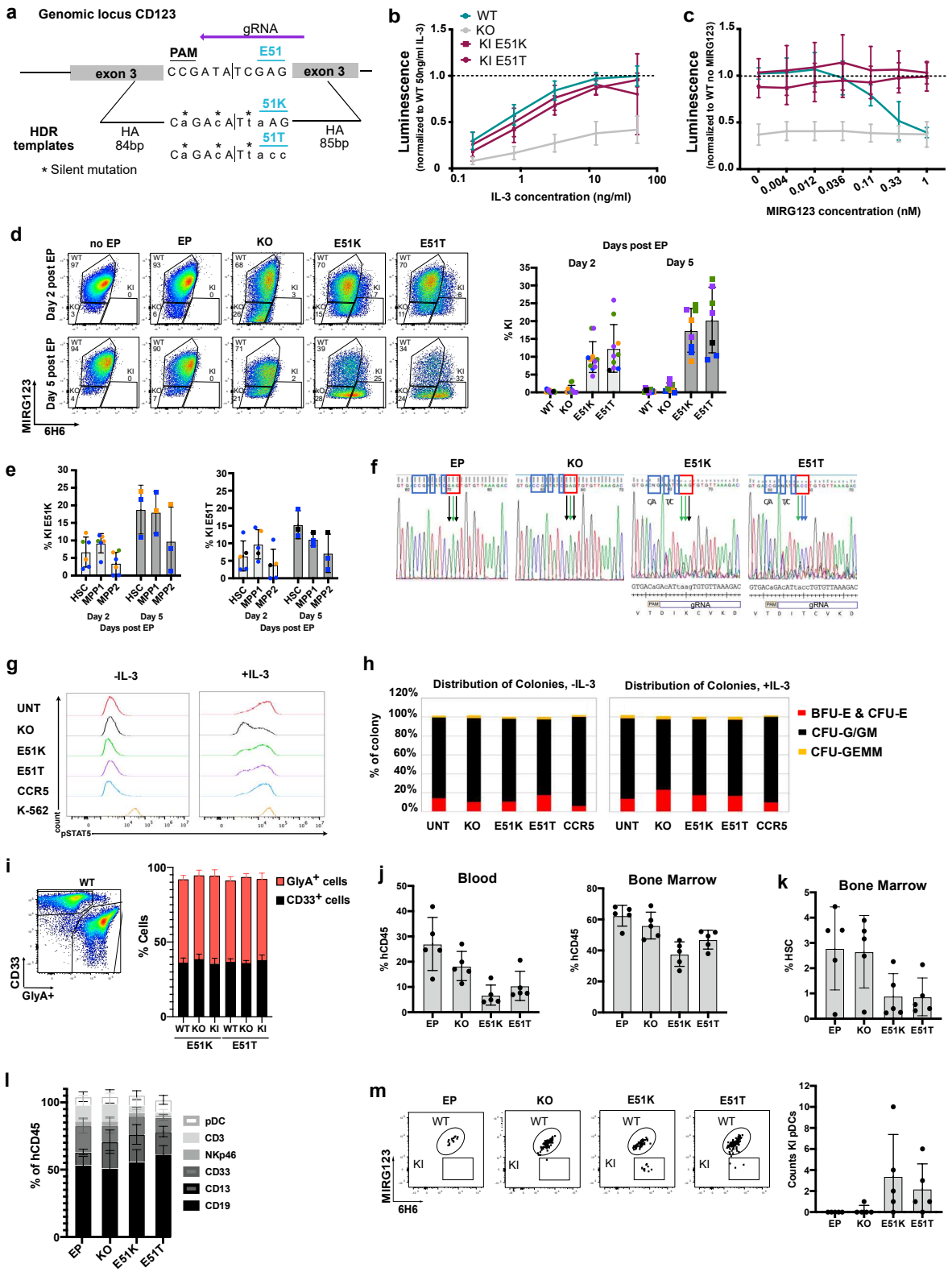
a
Genomic locus CD123
gRNA
PAM
E51
exon 3
CCGATA|TCGAG
exon 3
51K
CaGAcA|TtaAG
HDR templates
HA 84bp
HA 85bp
51T
CaGAcA|Ttacc
* Silent mutation
b
WT
KO
KI E51K
KI E51T
Luminescence (normalized to WT 50ng/ml IL-3)
IL-3 concentration (ng/ml)
c
Luminescence (normalized to WT no MIRG123)
MIRG123 concentration (nM)
d
no EP
EP
KO
E51K
E51T
Day 2 post EP
Day 5 post EP
MIRG123
6H6
Days post EP
Day 2
Day 5
% KI
e
% KI E51K
% KI E51T
HSC
MPP1
MPP2
Day 2
Day 5
Days post EP
f
EP
KO
E51K
E51T
gRNA
g
-IL-3
+IL-3
UNT
KO
E51K
E51T
CCR5
K-562
count
pSTAT5
h
Distribution of Colonies, -IL-3
Distribution of Colonies, +IL-3
% of colony
BFU-E & CFU-E
CFU-G/GM
CFU-GEMM
UNT
KO
E51K
E51T
CCR5
i
WT
CD33
GlyA+
% Cells
GlyA+ cells
CD33+ cells
WT KO KI WT KO KI
E51K
E51T
j
Blood
Bone Marrow
% hCD45
EP
KO
E51K
E51T
k
Bone Marrow
% HSC
l
% of hCD45
pDC
CD3
NKp46
CD33
CD13
CD19
m
EP
KO
E51K
E51T
WT
KI
MIRG123
6H6
Counts KI pDCs

Fig. 5. Cells expressing CD123 variants E51K and E51T are functional, engraft and differentiate in vivo
a, Schematic of HDR templates design for insertion of variants K and T at position 51. **b-c,** Engineered TF-1 cells were sorted based on the binding to the anti-CD123 mAbs 6H6 and MIRG123 (WT MIRG123^{+}6H6^{+}, KO MIRG123^{-}6H6^{-}, KI MIRG123^{-}6H6^{+}) and cultured for three days **b,** with increasing concentrations of IL-3, or in **c,** with 2.5ng/ml IL-3 in the presence of increasing concentrations of MIRG123. Viable cells were quantified by luminescence and results normalized to WT cells cultured with 50ng/ml IL-3 (**a**) or to WT cells cultured without MIRG123 (**b**). Data from 4 independent experiments. **d-f,** Characterization of non-virally CRISPR/Cas9-edited human CD34^{+} HSPCs. Data from 5 individual donors (each a color) performed in 4 independent experiments with 2 to 4 technical replicates. **d, left** Representative flow cytometry plots showing binding (%) of the anti-human CD123 antibody clones 6H6 and MIRG123 to edited CD34^{+} HSPCs two and five days after electroporation (EP). **right** Frequency of KI cells (MIRG123^{-}6H6^{+}) two and five days after electroporation. No EP (WT HSPC cells), EP (cells electroporated with incomplete RNPs), KO (electroporation with RNP only), CD123 E51K or E51T variants (electroporated with according HDRT). **e,** Quantification of the KI population in long-term repopulating HSCs (LT-HSC; CD34^{+}CD38^{-}CD90^{+}CD45RA^{-}), multipotent progenitor 1 (MPP1; CD34^{+}CD38^{-}CD90^{-}CD45RA^{-}) and MPP2 (CD34^{+}CD38^{-}CD90^{-}CD45RA^{+}). Gating strategy depicted in Extended data Fig. 3b. **f**, Representative Sanger sequencing of the CD123 locus 2 days post-editing of control (EP), KO, E51K and E51T conditions. Blue box: silent mutations, red box: E51K and E51T AA substitutions. WT and crRNA sequences indicated below chromatogram. **g,** Representative histogram of phosphorylated STAT5 upon exposure to IL-3 (10ng/ml) in AAV6-edited HSPCs. CCR5 KO was used as negative, and K-562 cells as positive control. Data represents two independent experiments. **h,** In vitro differentiation of AAV6-edited HSPCs with and without IL-3. Colony Forming Units (erythroid: BFU-E & CFU-E, granulocytes/monocytes: CFU-G/GM and myeloid progenitors: CFU-GEMM) were scored based on morphological characteristics. Data from two independent experiments. **i, left** Representative flow cytometry and **right** frequency of GlycophorinA (GlyA)$^{+}$ and CD33^{+} non-virally edited HSPCs seven days after sorting and culturing in high cytokine medium. Myeloid lineage: CD33^{+} Erythroid lineage: GlyA^{+}. One experiment performed in triplicates. **j-m,** In vivo engraftment and differentiation potential of non-virally engineered HSPCs expressing E51K and E51T variants measured 15 weeks after injection in NSG mice. One experiment with 4 mice per group. **j,** Human chimerism (% hCD45^{+}) in blood (**left**) and bone marrow (**right**). **k,** Proportion of CD90^{+}CD45RA^{-} HSCs in the bone marrow. **l**, Multi-lineage differentiation in blood. **m, left** Representative dot plot of MIRG123^{-}6H6^{+} KI pDCs in blood. **right** Absolute number of pDCs within edited HSPCs. Gating strategy to identify pDCs depicted in Extended data Fig. 3c. **a-m,** Error bars: mean ± SD.

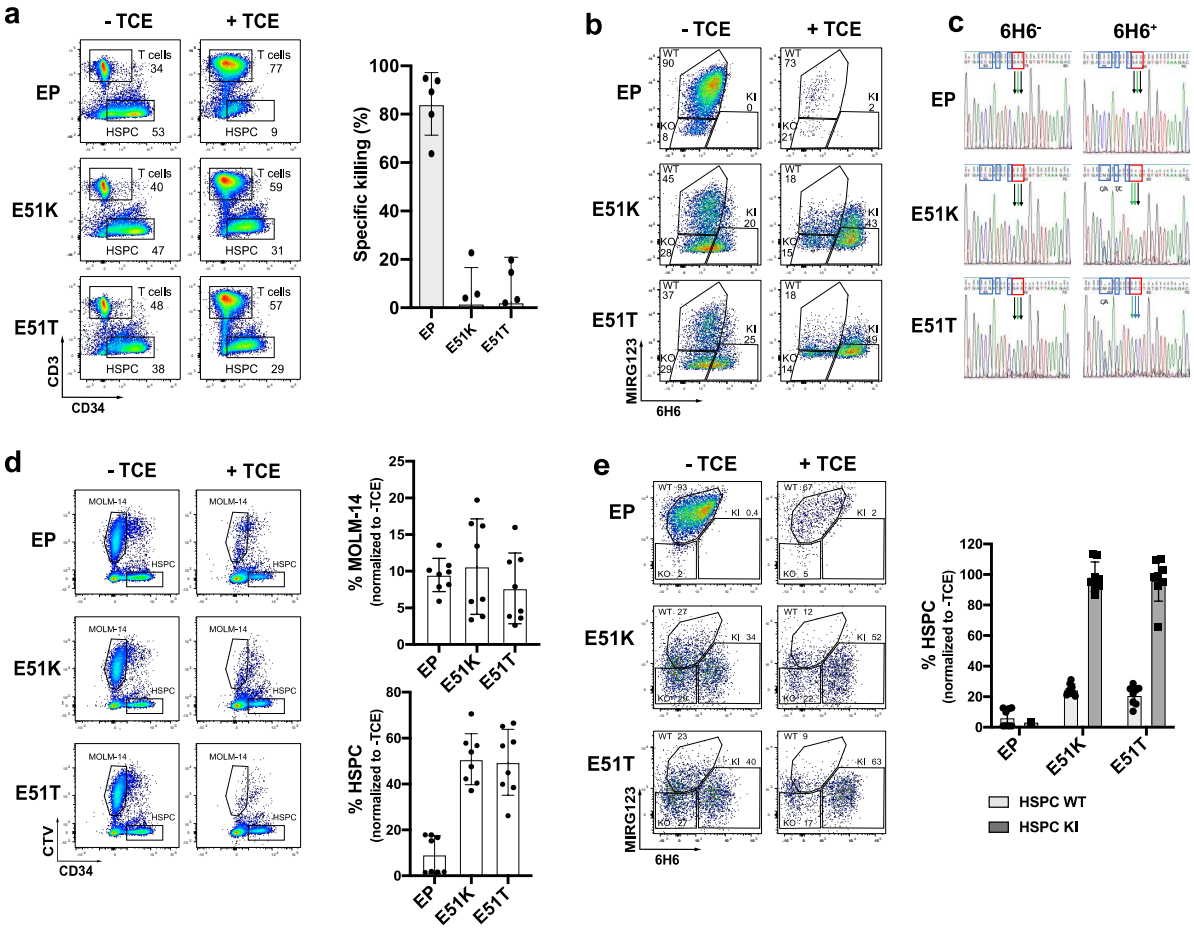

Figure 6: Engineered HSPCs enable tumor-selective CD123 immunotherapy

a-c, Non-virally edited HSPCs cultured with autologous T cells with or without CSL362/OKT3-TCE (100ng/ml) for 3 days. Control condition (EP) are electroporated but non-edited HSPCs. Data from 2 individual donors performed in 3 independent experiments with 1 or 2 replicates per experiment. **a, left** Representative dot plot indicating proportion (%) of autologous $CD3^+$T cells and $CD34^+$ HSPCs in different conditions on day 3 of co-culture. **right** Specific TCE-mediated killing of HSPCs at day 3. **b**, FACS plots illustrating fraction (%) of edited HSPCs at the end of the co-culture based on the binding characteristics to the mAb MIRG123 and 6H6. **c,** Sanger Sequencing chromatogram of FACS-sorted $6H6^+$ and $6H6^-$ HSPCs on day 3 of co-culture. Blue boxes: silent mutations, red boxes: E51K and E51T AA substitutions. **d-e,** 3-days co-culture of non-virally engineered $CD34^+$ HSPCs, AML cells MOLM-14 (CTV-labelled) and autologous T cells with and without TCE. Data represents one independent donor performed in two experiment each with quadruplicate replicates. **d, left** Representative dot plots indicating MOLM-14 and $CD34^+$ HSPCs with or without TCE at day 3. **Right** Relative number of MOLM-14 (top) and HSPC cells (bottom). Data normalized to co-culture without TCE. **e, left** Representative dot plot showing the ratio (%) of edited HSPCs and **right** Relative number of HSPC WT and KI at the end of the co-culture. Data is normalized to the condition without TCE. HSC WT: $MIRG123^+6H6^+$, HSC KI: $MIRG123^-6H6^+$. **a-e,** Error bars: mean ± SD.

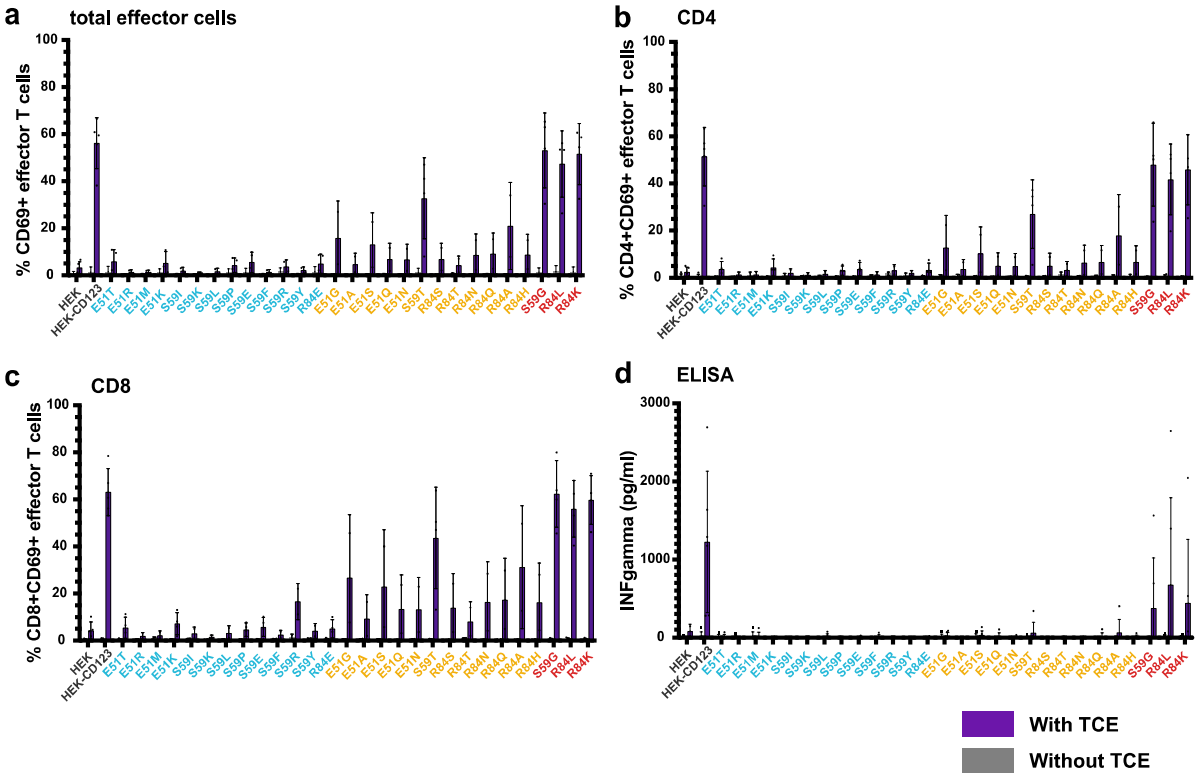

Extended data Fig. 1

72 hours co-culture of human effector T cells with HEK, HEK-CD123 and CD123 variants (E:T = 10:1) in the presence of the CSL362/OKT3-TCE (300ng/ml). Summary of flow cytometry CD69⁺ total (**a**), gated CD4⁺ (**b**), and CD8⁺ (**c**) effector T cells after 3 days co-culture with (purple) and without (grey) TCE. Data from 5 independent donors and experiments with 2 technical replicates per group. **d,** IFNgamma secretion measured by ELISA in co-culture supernatants at 72h. **a-d,** Data from 4 blood donors and experiments with 2 technical replicates per group. Error bars: mean ± SD.

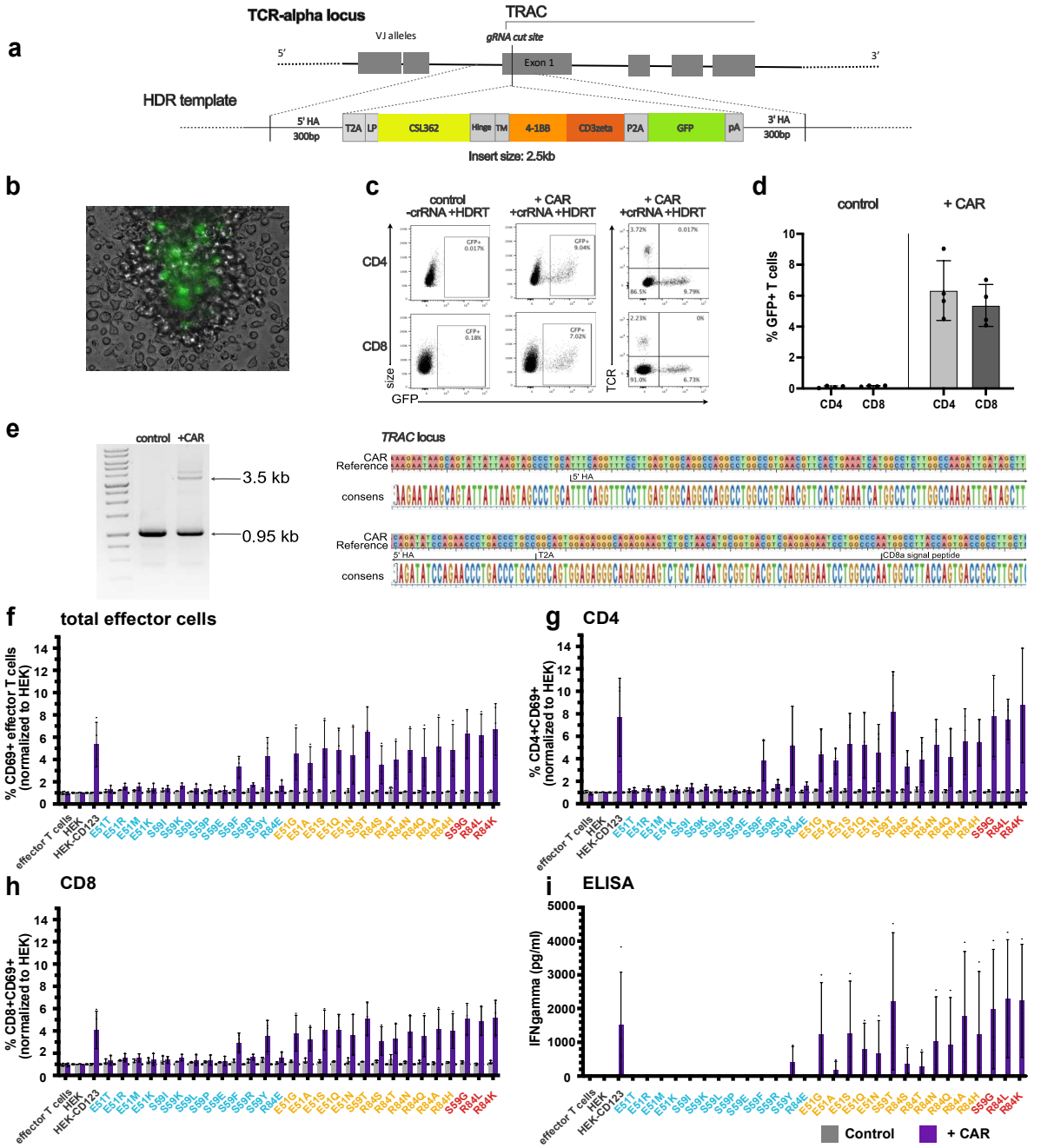

Extended data Fig. 2

a, Non-viral HDR-mediated integration of the CD123-specific second-generation CAR into Exon 1 of the *TRAC* locus using CRISPR/Cas9. **b,** Representative microscopy image (magnification 40x) day 4 post-electroporation showing GFP$^+$ cells expressing the CAR-encoding template. **c,** Flow cytometry plots highlighting CAR insertion into the *TRAC* locus represented by fluorescent intensity of GFP with disrupted endogenous TCR expression in primary human gated CD4$^+$ and CD8$^+$ T cells. **d,** Mean knock-in efficiency of the CAR-encoding template in gated CD4$^+$ and CD8$^+$ T cells in "control" and "+CAR" cells at day 4-5. Data from 4 independent donors and experiments. **e, left** Gel image and **right** Sanger Sequencing results confirming correct HDRT integration at the *TRAC* locus in flow-sorted GFP$^+$ CAR cells using PCR with primers annealing outside both arms of homology. Reference refers to the designed sequence in SeqBuilderPro (DNASTAR). **f-i,** 123CAR T cells (purple) or control cells (grey) were co-cultured with HEK, HEK-CD123 or its variants at an effector to target ratio of 10:1 for 24h. Summary of flow cytometry data indicating percentage of CD69$^+$ total (**f**), gated CD4$^+$ (**g**), or CD8$^+$ (**h**) "control" (grey) or "+ CAR" (purple) T cells after 24h co-culture.**i.** Quantification of IFNg in supernatants of 24h co-cultures using ELISA. Error bars: mean ± SD. Data from 3 independent donors and experiments with 2 technical replicates per group.

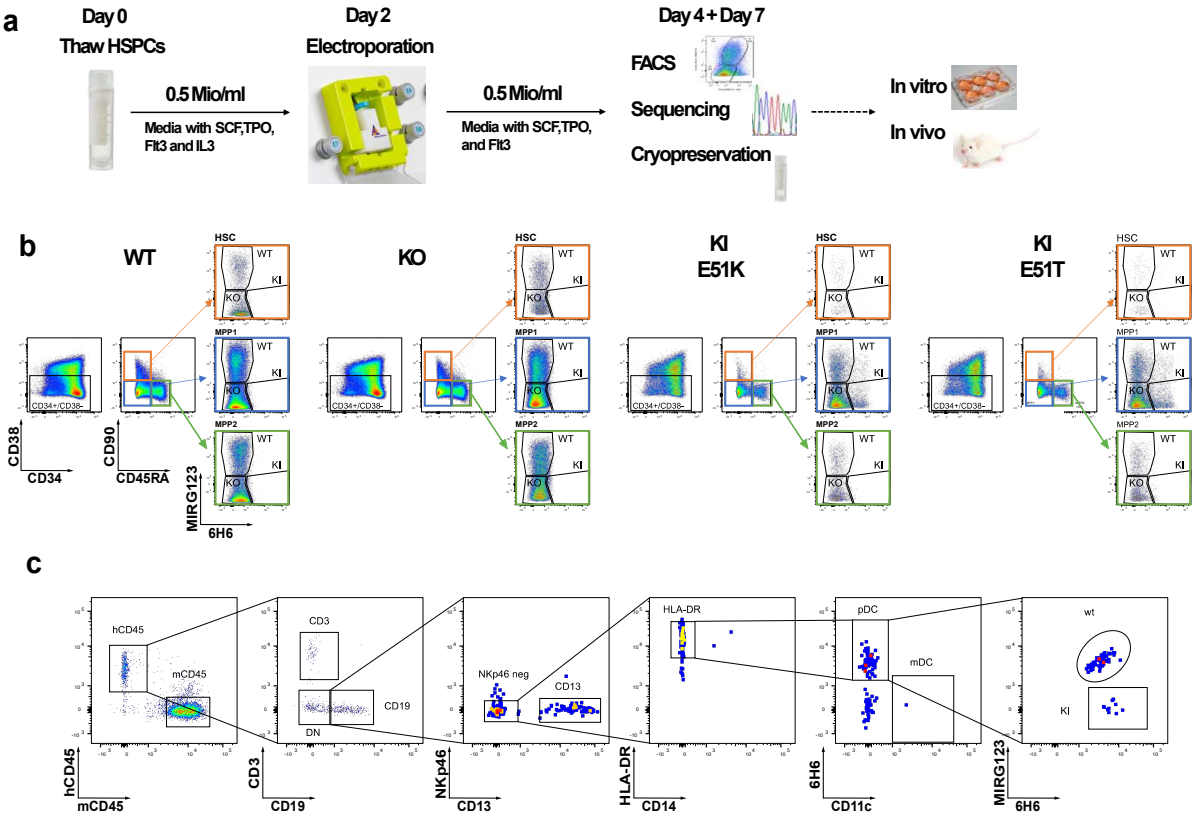

Extended data Fig. 3

a. Experimental design of non-viral CRISPR/Cas9-mediated HDR engineering of mobilized CD34$^+$ enriched peripheral blood HSPCs using GMP-compatible protocol with the CliniMACS Prodigy (Miltenyi). **b.** Gating strategy to monitor CD123 expression in HSC (orange, CD34$^+$CD38$^-$CD90$^+$CD45RA$^-$), multipotent progenitor 1 (MPP1; blue; CD34$^+$CD38$^-$CD90$^-$CD45RA$^-$) and MPP2 (green; CD34$^+$CD38$^-$CD90$^-$CD45RA$^+$) using the mAbs MIRG123 and 6H6 two and five days post electroporation. WT MIRG123$^+$6H6$^+$, KO MIRG123$^-$6H6$^-$, KI MIRG123$^-$6H6$^+$ **c.** Gating strategy to identify pDCs 15weeks after injection of edited HSPCs in NSG mice.

I.4- Additional results

In this part, we will present the additional results associated to the manuscript included before. First, we will present the optimization of the genome engineering protocol which allowed to KI E51K and E51T in the CD123 locus of TF-1 cells. Then, we will present the sort and the sequencing of the cells which were used in the functionally analysis of CD123 variants presented in **I.3, Figure 5b-c**. In a last part, we will show the culture of the engineered TF-1 in selective conditions with IL-3 and MIRG123.

I.4.1- Engineering of CD123 variants in TF-1 cells for functional assays

I.4.1.1- TF-1 cell line is a good in vitro model for assessment of CD123 functionality and sensitivity to MIRG123 blocking

In the first part of the chapter, we showed *in silico* design and selection of 12 CD123 variants resulting in loss-of-binding of the antibody MIRG123 and protection from killing by ADCC, TCE and CAR-T cells. Therefore, we needed to test their preserved functionality. Several models could be used to test CD123 functionality *in vitro*. For instance, Broughton et al used the Ba/F3 which is a mouse cell line cytokine-dependent. The authors transduced the cells with recombinant human CD123 and CD131 before to measure their response to IL-3. As we did not have expertise in transduction in the lab and we could not efficiently transfect the cells, we looked for other models [93]. TF-1 is a human erythroid cell line that depends on cytokine signaling to proliferate. Both IL-3 and granulocyte macrophage-colony stimulating factor (GM-CSF) were shown to be able to induce survival and proliferation in these cells [94]. Therefore, we aimed to assess functionality of CD123 by measuring the TF-1 response to IL-3. First, we set up a culture of TF-1 cells with increasing amounts of IL-3 and we measured the quantity of living cells after 3 days. Amount of living cells was deduced by a quantitation of the adenosine triphosphate present in each well, measured by luminescence with CellTiter-Glo® (**Figure 10a**).

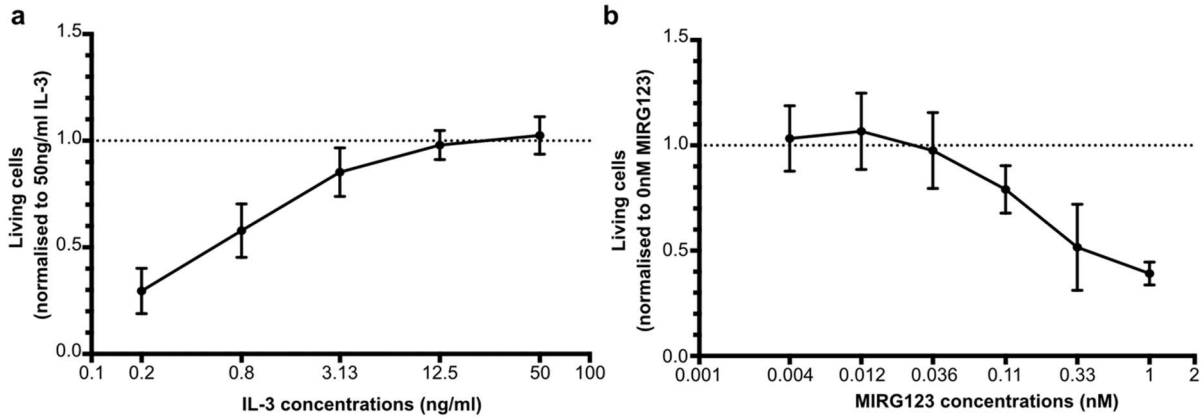

Figure 10: TF-1 sensitivity to IL-3 and MIRG123

***a**. IL-3 response of TF-1 measured by luminescence after 3 days of culture with increasing concentrations of IL-3. Luminescence for each IL-3 concentration was normalized to the condition 50nng/ml IL-3 **b**. IL-3 response of TF-1 measured by luminescence after 3 days of culture with 2.5ng/ml IL-3 and increasing concentrations of MIRG123. Luminescence for each MIRG123 concentration was normalized to the condition 0nM MIRG123. Data represent mean ± s.e.m (3 independent experiments)*

We observed a dose-dependent response of TF-1 cells and no response when no cytokine was provided, confirming the dependence of TF-1 on IL-3. Following IL-3 binding to its receptor, the formation of a heterocomplex composed of IL-3, CD123 and CD131 is necessary to trigger JAK/STAT activation. CSL362 blocks the formation of this complex[93] and MIRG123 is a biosimilar of CSL362. Therefore, in presence of MIRG123, the IL-3 signal should no longer be transmitted. In a further assay we wanted to test the blocking effect of MIRG123 *in vitro*. We determined in another experiment that the EC50 of IL-3 on TF-1 is 2.5ng/ml (data not shown). We therefore cultured TF-1 cells with a constant concentration of IL-3 (2.5 ng/ml) but with increasing concentrations of MIRG123 (**Figure 10b**). We observed reduced luminescence when increased concentrations of MIRG123 were added. These results show a reduced response to IL-3 signaling. Thus, we validated the choice of the TF-1 cell line as an *in vitro* model to assess the functionality of the CD123 variants and the shielding from MIRG123 binding.

I.4.1.2- TF-1 cells can be genetically engineered with CD123 variants

In a further step we wanted to engineer the selected variants into the CD123 endogenous gene of TF-1 using CRISPR/Cas9. We aimed to use later the engineered cells to assess functionality of the variants.

First, we needed to establish a protocol to electroporate ribonucleoprotein particles (RNPs) into TF-1 cells as we could not find any published literature. We screened several buffers and pulses conditions with the Lonza nucleofector 4D and with the Neon electroporator. The latter was the most efficient (data not shown). In order to reach a high KO efficiency, we compared RNPs electroporation with and without poly-l-glutamic acid (PGA) as it was shown to increase KO efficiency in several types of cells such as T cells, B cells and HSCs [95]. We observed that addition of PGA was beneficial and this optimization allowed us to establish a highly efficient protocol for RNPs electroporation in TF-1.

In order to efficiently engineer the E51 position with CRISPR/Cas9 by HDR, we first needed to identify gRNAs efficiently cutting as close as possible to the site to mutate. Indeed, it was shown that KI efficiency is increased when the cut of the Cas9 is close to the site to edit [96]. As we worked with high fidelity SpCas9 we designed 4 gRNAs with NGG PAM. Using our optimized protocol, we electroporated the TF-1 cells with these gRNAs complexed as RNPs (**Figure 11**).

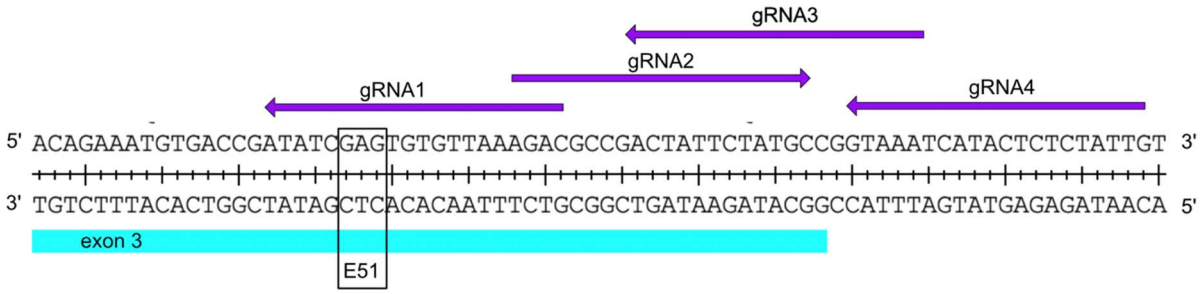

Figure 11: Localization of gRNA1-4 in exon 3 of CD123

Blue indicates the exon 3 of CD123. Purple corresponds to the protospacer sequences

7-8 days later, we analyzed CD123 expression by flow cytometry using antibodies MIRG123 and 6H6 labeled with different fluorochromes (**Figure 12**).

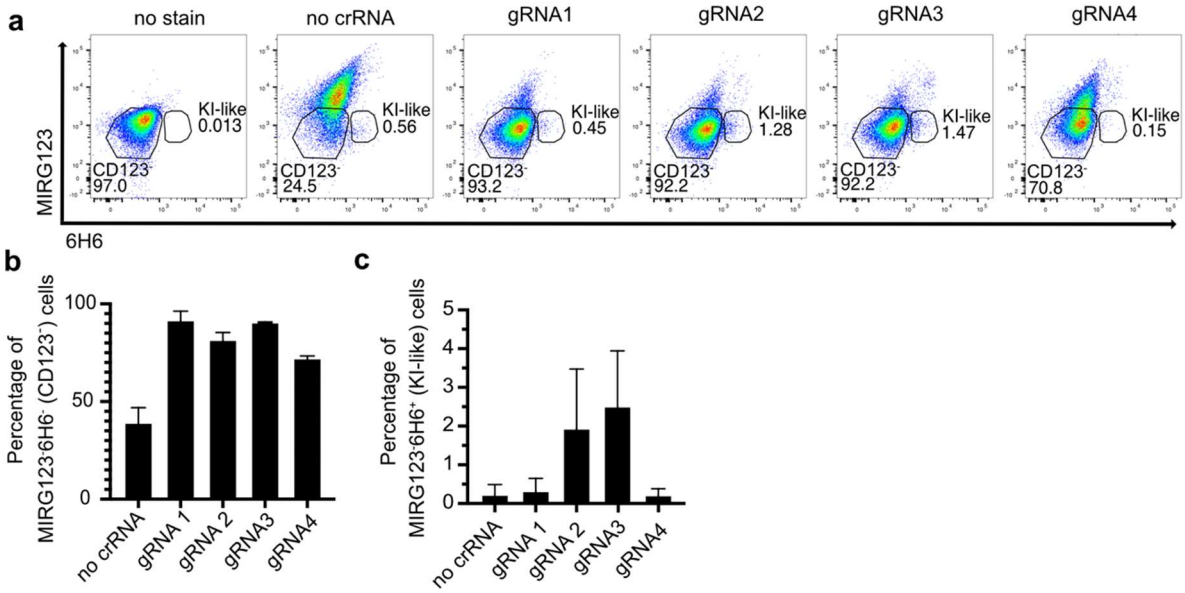

Figure 12: screening of gRNA close to E51 position for CD123 cutting

***a**. Representative flow cytometry plots of TF-1 cells electroporated with RNPs targeting CD123 close to the E51 codon 7 days after electroporation. **b**. Percentage of CD123$^-$ cells for each electroporation condition measured 7 days after electroporation. **c**. Percentage of "KI-like" cells for each electroporation condition measured 7 days after electroporation. no crRNA: cells electroporated with incomplete RNPs missing crRNA. Data represent mean ± s.e.m (3 independent experiments)*

First, we identified the CD123$^-$ population (MIRG123$^-$6H6$^-$) on the unstained TF-1. Then, we analyzed expression of CD123 at the surface of the cells. In TF-1 cells mock electroporated with incomplete RNPs (no crRNA) we observed CD123 expression but the mean fluorescence intensity (MFI) was low compared to what was observed in HSPCs in the manuscript presented before (**I.3**). We noticed an increase of the proportion of CD123$^-$ cells when the gRNAs were electroporated. For instance, electroporation with gRNA1 resulted in > 90% of CD123$^-$ cells. The least efficient gRNA was the number 4 with a CD123$^-$ population representing only 70% of the pool after electroporation (**Figure 12a-b**). Interestingly, staining with MIRG123 and 6H6 allowed us to identify a small population of cells marked as MIRG123$^-$6H6$^+$. This profile means that the cells bind 6H6, so express the protein, but without binding MIRG123. This staining profile is expected for the variants, where the cells should lose the binding to MIRG123 only. However, in this experiment we did not intend to insert any variant. We supposed that this population was due to the repair of the DSBs by NHEJ. Its random repair mechanism could have led to in-frame repair with removal of amino acids in the epitope of MIRG123, disturbing the binding of the antibody. Therefore, we named this population "KI-

like" as it showed the flow cytometry profile expected for a KI, but we don't know the sequences. In further experiments we planned to do KI of E51K and E51T and to use the MIRG123^{-}6H6^{+} profile to identify the cells correctly engineered by flow cytometry. Therefore, we selected the gRNA which led to the lowest "KI-like" population, the gRNA1.

Next, we aimed to engineer E51K and E51T in endogenous CD123 gene of TF-1 cells by electroporation of RNPs and HDRTs. Design of the two templates encoding for E51K and E51T is presented in the first part of **I.3, Figure 5a**. Briefly, we designed the HDRT with symmetric homology arms of 90bp around the cut of the Cas9. Between these HAs, we designed an insert containing the E51K or the E51T mutation, a PAM mutation and additional silent mutations. We introduced PAM mutations because it avoids recutting and it was previously reported to increase HDR efficiency [96]. In addition, Bak et al reported that if the template sequence is too similar to wild-type (WT), repair machinery can switch to using the WT sequence and do not integrate the full template [96]. Thus, we decided to introduce silent mutations between the E51K/E51T mutations and the PAM mutations in order to maximize the chances to have all the modifications integrated together (**Figure 13**).

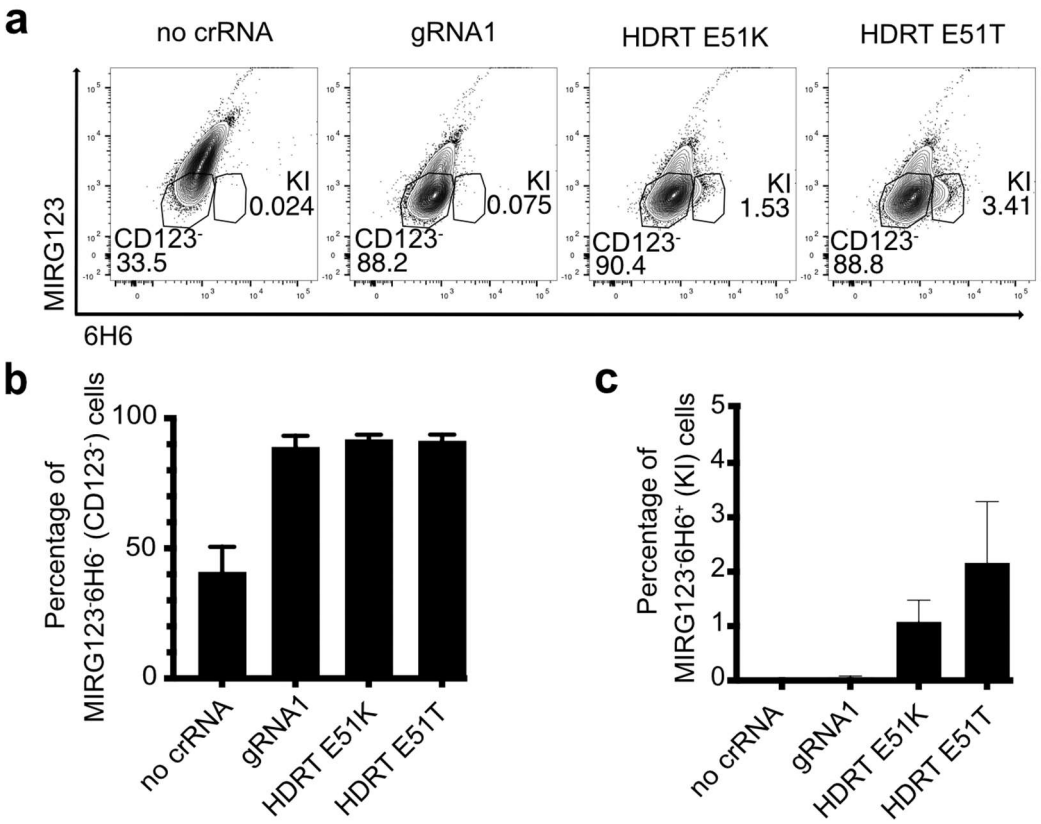

Figure 13: KI efficiencies of E51K and E51T in TF-1

a. *Representative flow cytometry plots of TF-1 cells electroporated with RNPs targeting CD123 and HDRTs encoding for E51K and E51T 7 days after electroporation.* ***b****. Percentage of CD123$^-$ cells for each condition 7 days after electroporation.* ***c****. Percentage of KI cells for each condition 7 days after electroporation. no crRNA: cells electroporated with incomplete RNPs missing crRNA. HDRT E51K: cells electroporated with RNPs and HDRT encoding for E51K. HDRT E51T: cells electroporated with RNPs and HDRT encoding for E51T. Data represent mean ± s.e.m (3 independent experiments)*

Similarly to what we observed in the previous experiment, electroporation of TF-1 cells with RNPs complexed to gRNA1 allowed a high KO efficiency (around 90% of cells are CD123$^-$). This efficiency was conserved when the cells were electroporated with RNPs and HDRTs encoding for E51K or E51T as more than 85% of cells lost the expression of CD123 (**Figure 13a-b**). Small populations of MIRG123$^-$6H6$^+$ (KI) cells were observed when the cells were electroporated with the HDRTs. The KI population for E51K represented around 1% of the cell pool while the KI population for E51T represented almost 2% (**Figure 13a-c**). This KI efficiency was low but could be an underestimation due to the low MFI of CD123 in these cells. To conclude, we saw by flow cytometry that variants E51K and E51T were engineered

into TF-1 cells. However, this analysis was phenotypic and to use these cells in further analysis we needed to validate the KI by sequencing.

I.4.1.3- Flow cytometry sorting allowed enrichment of engineered populations

In order to test the functionality of CD123 variants, we asked if cells engineered with the mutations would respond similarly to non-modified cells to IL-3 signaling and if CD123 KO cells would be able to respond to IL-3. In addition, we asked if the cells expressing the CD123 variants would be protected from the blocking effect of MIRG123 and proliferate in presence of the antibody.

The KI frequency in the electroporated bulks was too low to test directly the functionality of the E51K and E51T variants. First, we tried to generate cell lines by sorting single engineered cells. However, we ran into technical issues and the sorted clones showed variability. Thus, we went back to oligoclonal freshly engineered cells. We electroporated TF-1 cells with RNPs and HDRTs and sorted from the pool of electroporated cells the cells with a WT profile ($MIRG123^{+}6H6^{+}$), the cells with a KO profile ($MIRG123^{-}6H6^{-}$) and the cells with a KI profile ($MIRG123^{-}6H6^{+}$) (**Figure 14**).

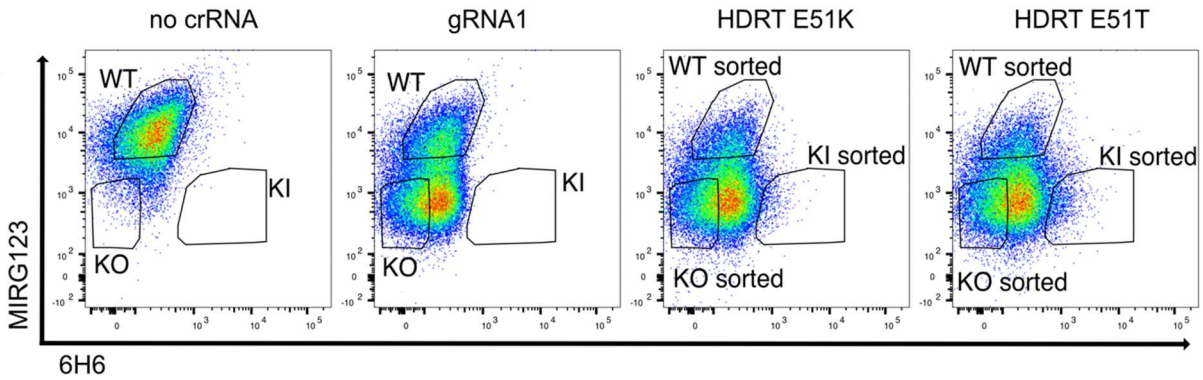

Figure 14: Representative flow cytometry plots for gating strategy used to sort WT, KO and KI cells

Representative flow cytometry plots of TF-1 electroporated with RNPs and HDRTs encoding for E51K and E51T. WT cells were identified with $MIRG123^{+}6H6^{+}$ staining, KO cells were identified with $MIRG123^{-}6H6^{-}$ staining and KI cells were identified with $MIRG123^{-}6H6^{+}$ staining. Cells were sorted only from the pools HDRT E51K and HDRT E51T as WT ($MIRG123^{+}6H6^{+}$), KO ($MIRG123^{-}6H6^{-}$), KI ($MIRG123^{-}6H6^{+}$)

Sorted pools of cells were sequenced by Sanger sequencing in order to confirm the editing of the locus (**Figure 15**).

a.

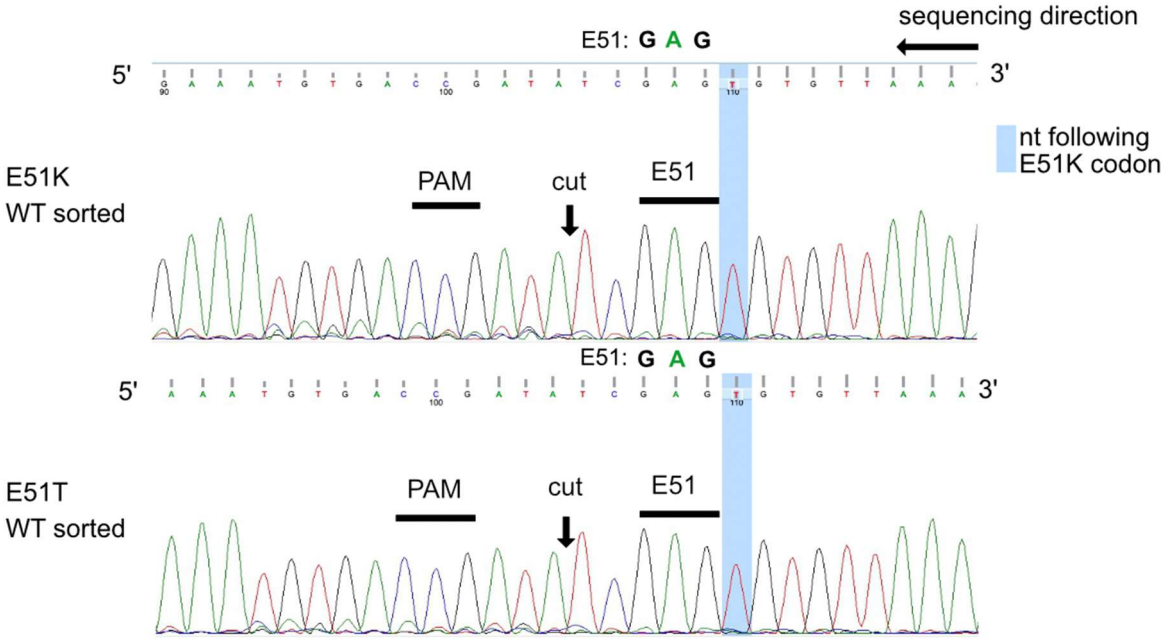
sequencing direction
E51: G A G
5'
3'
nt following
E51K codon
E51K
WT sorted
PAM
cut
E51
E51: G A G
5'
3'
E51T
WT sorted
PAM
cut
E51

b.

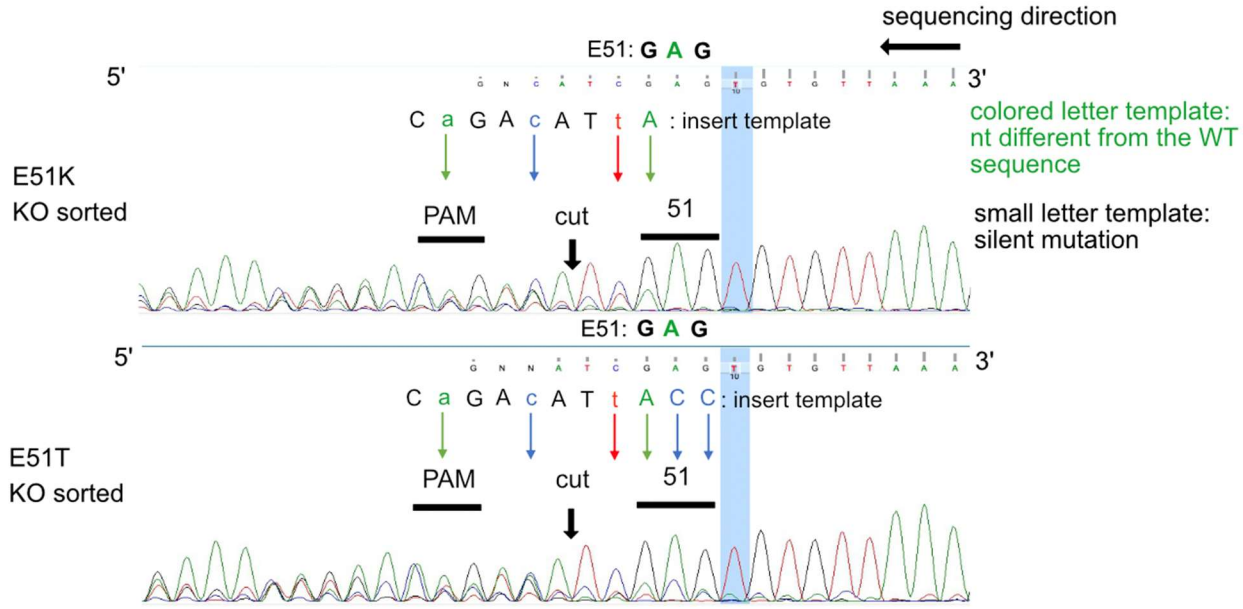
sequencing direction
E51: G A G
5'
3'
C a G A c A T t A : insert template
colored letter template:
nt different from the WT
sequence
E51K
KO sorted
PAM
cut
51
small letter template:
silent mutation
E51: G A G
5'
3'
C a G A c A T t A C C: insert template
E51T
KO sorted
PAM
cut
51

c.

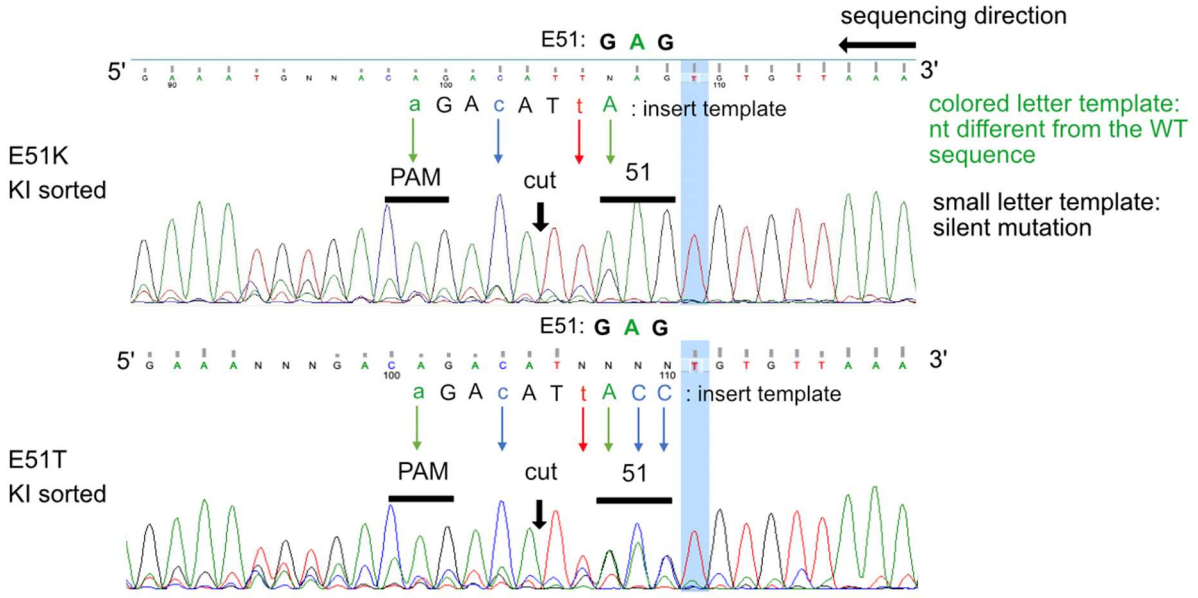

Figure 15: Representative Sanger sequencing of sorted WT, KO and KI cells after E51K and E51T engineering

*Sanger sequencing chromatograms of cell pools sorted as WT (MIRG123^{+}6H6^{+}) (**a**), KO (MIRG123^{-}6H6^{-}) (**b**) and KI (MIRG123^{-}6H6^{+}) (**c**) after genome engineering with E51K and E51T HDRTs. PAM indicates the PAM sequence of the protospacer. Cut indicates the localization of the Cas9 cut performed after recognition of the PAM sequence. E51 and 51 indicates the three nucleotides involved in the 51 codon. Insert template indicates the sequence of the HDRT which is not homology arms. Dark letter in the insert template are nucleotides similar to the WT sequence.*

All loci were sequenced from the 3' extremity. In the cells sorted as WT, the chromatogram showed a majority of WT sequences (**Figure 15a**). In contrast, the cells sorted as KO displayed a superposition of sequences starting around the Cas9 cut (**Figure 15b**). This overlap of sequences indicates that the cells repaired the DSBs with indels. Thus, the loss of CD123 protein observed with flow cytometry (**Figure 14**) was confirmed on the genomic level. Sanger sequencing of pooled cells has to be interpreted with caution due to overlapping signals. Despite this, a KI sequence could clearly be identified in the pools of cells sorted as KO: AAG signal in E51K KO and ACC signal in E51T KO (**Figure 15b**). Thus, it seemed that the cells sorted in the "KO" gate contained some "KI" cells. We supposed that these "KI" cells were engineered but did not express CD123 when the sort was performed. Thus, we concluded that our KO sorted pool was enriched for KO cells but was not pure. To finish, the KI sorted pools

contain a majority of KI cells since the HDRT sequence are the most abundant ones (**Figure 15c**). However, these pools seem to contains other sequences which we could not analysis further due to the lack of separation. One strategy to separate better the sequences could have been to use the next-generation sequencing (NGS) technique. However, we only wanted to confirm enrichment of the engineered population in a cost-effective way. This semi-quantitative data was therefore enough for us.
To conclude, the data supports that we have relatively pure WT population but KO and KI are enriched. The presence of unwanted cells in the KO and KI sorted pools needs to be taken into consideration when interpreting the functional experiments.

Thus, we enriched the WT, KO and KI population following electroporation, allowing the use of the cells in further IL-3 response assays. These assays were performed in the first part of this chapter (**I.3, Figure 5b-c**) and showed functionality and shielding of E51K and E51T variants. However, the response of KI cells to IL-3 was slightly lower than WT cells, and the KO cells showed a low response to the cytokine. Much of these results could be explained by the impurities observed with sequencing.

I.4.2- Knock-in of CD123 variants can be an advantage in culture with IL-3 and MIRG123

In a next set of experiments, we aimed to test whether engineered variants could be exploited to enrich KI cells. We engineered TF-1 cells with E51K and E51T and cultured the mix of WT, KO and KI cells with GM-CSF, IL-3, or IL-3 and MIRG123. TF-1 cells grow IL-3 dependent but can also grow with GM-CSF alone. Thus, WT, KO and KI cells should respond similarly to GM-CSF. We hypothesized that KI could have a passive selective advantage if a selective pressure would be exogenously applied. Therefore, only WT and KI cells should be able to respond to IL-3 signaling while only KI cells should be able to respond to IL-3 signaling in presence of MIRG123 (**Figure 16**).

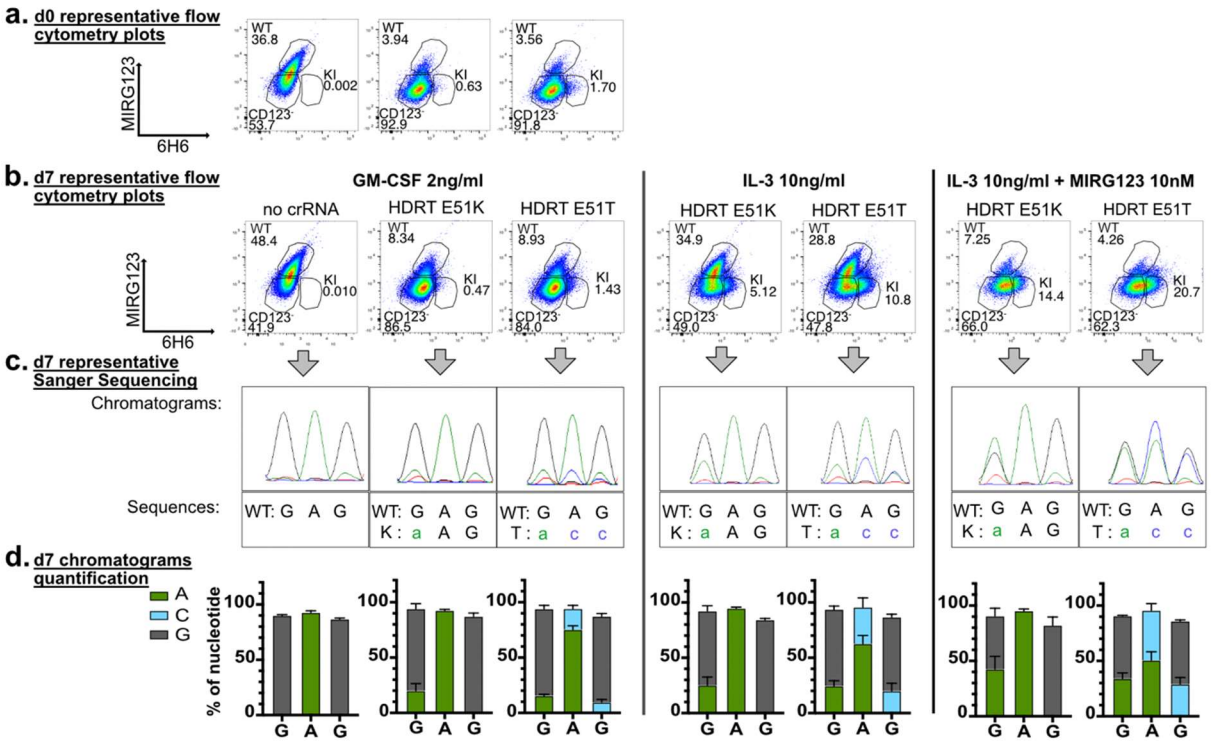

Figure 16: Enrichment profile of electroporated TF-1 with E51K and E51T variants after 7 days in culture with GM-CSF, IL-3 or IL-3+MIRG123

***a**. Representative flow cytometry plots of TF-1 electroporated with RNPs and HDRTs encoding for E51K and E51T at d0. **b.** Representative flow cytometry plots of TF-1 electroporated with RNPs and HDRTs encoding for E51K and E51T and kept in culture with 2ng/ml GM/CSF, 10ng/ml IL-3 or 10ng/ml IL-3 + 10nM MIRG123 for 7 days. **c**. Representative Sanger sequencing chromatograms of TF-1 electroporated with RNPs and HDRTs encoding for E51K and E51T and kept in culture with 2ng/ml GM/CSF, 10ng/ml IL-3 or 10ng/ml IL-3 + 10nM MIRG123 for 7 days. **d**. Percentage of nucleotide at each position of the codon 51 after enrichment in 2ng/ml GM/CSF, 10ng/ml IL-3 or 10ng/ml IL-3 + 10nM MIRG123 for 7 days. Data represent mean ± s.e.m (4 independent experiments)*

After seven days of culture, we observed that the relative frequencies of WT, $CD123^-$ or KI population remained constant compared to the day 0 of the experiment when the cells were cultured in GM-CSF (**Figure 16a-b**). This was confirmed by Sanger sequencing, the representative chromatograms of E51K and E51T HDRT conditions showed a majority of KO sequences (data no shown) and low KI signal (AAG for 51K and ACC for 51T) at the codon 51 (**Figure 16c**). When the cells were cultured with IL-3, the relative frequencies of the KI and WT populations increased compared to the cell pools cultured with GM-CSF (**Figure 16b**). This was confirmed by Sanger sequencing as we observed a raise of KI sequence compared to the same cells cultured with GM-CSF (**Figure 16c**). We also observed an increase of the WT

sequence (data not shown). When the electroporated cells were cultured with IL-3 and MIRG123, the relative frequency of the KI was further enriched compared to the other culture conditions (**Figure 16b**). This observation was confirmed with Sanger sequencing (**Figure 16c**).

In order to reinforce the observations of sequence enrichment (**Figure 16c**), we used EditR [97] to quantify the amount of nucleotide signal recorded for each position for several experiments. Quantification of nucleotides signals confirmed enrichment of the KI sequences when the cells were cultured with IL-3 and IL-3 + MIRG123 (**Figure 16d**). With this experiment we showed that in selective culture conditions, when IL-3 is the only cytokine, WT and KI have an advantage over the KO cells. The variant receptors should be functionally neutral and give advantage only by disrupting the binding of MIRG123. When IL-3 was the only cytokine and MIRG123 was present, we observed that KI have an advantage over WT cells. To conclude, KI provides the possibility for further enrichment by selective blockade, this principle could be used for therapeutical purposes.

In the previously described enrichment experiment, the blocking of CD123 was done with the antibody clone MIRG123. However, for the flow cytometry staining, the same clone MIRG123 biotinylated (MIRG123-biot) was used with streptavidin-phycoerythrin (strep-PE). Therefore, to exclude a technical artifact, we asked if the absence of WT ($MIRG123^{+}6H6^{+}$) cells after culture in IL-3 and MIRG123 could be due to epitope masking (**Figure 16b**). The enrichment by DNA sequencing demonstrates a true enrichment. Nevertheless, we aimed to determine if there was a superimposed artifact. To determine how much residual MIRG123 was bound on day 7 we repeated the enrichment culture with MIRG123-biot instead of MIRG123. The residual antibody bound to the cells was determined by direct staining with strep-PE (**Figure 17**).

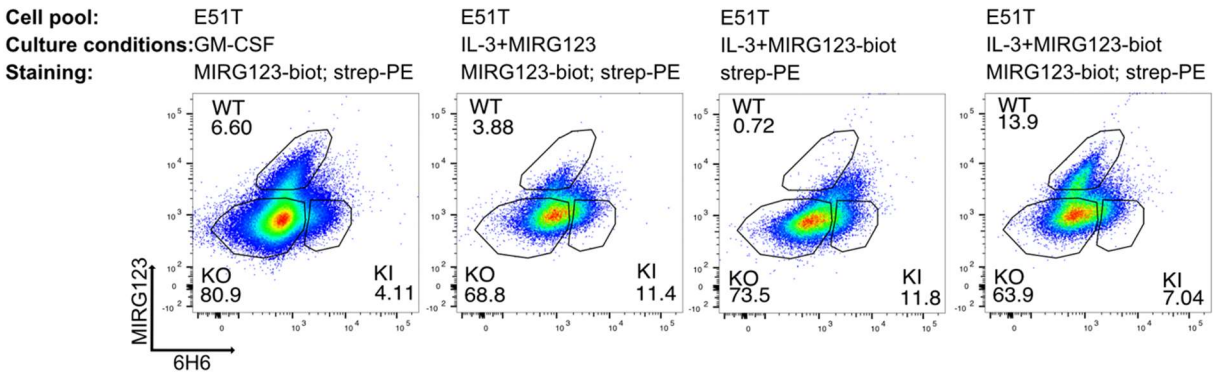

Figure 17: Blocking assessment of MIRG123-biot with MIRG123

Representative flow cytometry plot of TF-1 cells electroporated with RNPs and HDRT encoding for E51K cultured 7 days with 10ng/ml IL-3 + 10nM MIRG123 or 10ng/ml IL-3 + 10nM MIRG123-biot and stained with MIRG123-biot and strep-PE or strep-PE only (2 independent experiments).

We observed around 3% of WT cells in the conditions where MIRG123-biot binding was blocked by MIRG123. When the cells were cultured with IL-3 + MIRG123-biot and stained with strep-PE only, we observed a small population with a low PE fluorescence. It seems that with the concentration of MIRG123-biot used, not all CD123 was bound. Therefore, we cultured the cells with IL-3 + MIRG123-biot and restrained with MIRG123-biot in order to make sure that all CD123 protein present at the surface will be detected. More sites were bound and we observed around 13% of WT cells. Thus, this experiment showed us that we missed WT cells in the flow cytometry analysis due to the blocking of the detection antibody.

To conclude, we developed a new electroporation protocol which allowed us to engineer E51K and E51T variants in the endogenous CD123 of TF-1 cells. TF-1 genetically engineered with E51K and E51T variants responded to IL-3 in absence and in presence of MIRG123, demonstrating the functionality and the shielding capacities of the variants. In a further experiment, we demonstrated the passive advantage of the variants in selective conditions. When IL-3 was the only cytokine and MIRG123 was present, only E51K and E51T could respond to IL-3 and thus had an advantage over WT and KO cells. These results obtained in cell line form the basis for further validation in primary cells which is advantageous as HSPCs, the cells we aim to shield, are more difficult to get and therefore more precious.

I.5- Methods

IL-3 enrichment assay

TF-1 cells electroporated with RNPs and HDRTs were grown for 12 days before enrichment assay. The day before the assay, sorted cells were adjusted to $0.5x10^6$ cells/ml in fresh media. The day of the assay, cells were dispersed in 1 ml of medium at the concentration $0.4x10^6$ cells/ml. Each electroporation condition (no crRNA, gRNA1, HDRT E51K, HDRT E51T) was tested for growth in three different media: growth in medium supplemented with GM-CSF 2 ng/ml (RPMI-1640, 10% fetal calf serum (FCS), 2 mM GlutaMAX™ and 2 ng/ml GM-CSF), growth in medium supplemented with 10 ng/ml IL-3 (RPMI-1640, 10% FCS, 2 mM GlutaMAX™ and 10 ng/ml IL-3), growth in medium supplemented with 10 ng/ml IL-3 and 10 nM MIRG123 (RPMI-1640, 10% FCS, 2 mM GlutaMAX™, 10 ng/ml IL-3 and 10 nM MIRG123). At day 2 after the start of the assay, 400 µl of culture were removed and 400 µl of fresh medium were added for all the conditions. Four days after the start of the assay, the conditions no crRNA, gRNA1, HDRT E51K, HDRT E51T cultured with hGM-CSF and the condition no crRNA cultured in IL-3 were diluted ten times in fresh medium. The other conditions were diluted as at day 2. At day 0 and 7, cells were analyzed for CD123 variants expression by flow cytometry. The day of the measurement, in order to avoid downregulation of CD123 due to incubation of the cells with IL-3, 200 µl of cell culture of all conditions were washed with phosphate buffered saline (PBS) and re-suspended in 200 µl of medium with 2 ng/ml GM-CSF for 7 h of incubation before flow cytometry. Cells were stained with the antibodies 6H6-Bv650 and MIRG123-biot/strep-PE and gDNA was extracted for sequencing analysis of the enriched bulks at day 7.

Chapter II:
Design of CD45 variants shielding from CD45-targeted therapies

II.1- Introduction

In this chapter, we aimed to design CD45 variants shielding cells from CD45-targeted therapies. CD45, the protein tyrosine phosphatase receptor type C, is a large surface protein composed of a highly glycosylated extracellular domain (ECD) and of an intracellular domain consisting of two phosphatase domains, D1 and D2. Between D1 and D2, only D1 is enzymatically active[98]. Several isoforms of CD45, CD45RO, CD45RA, CD45RB, CD45RC and CD45RAB are expressed by human cells. They are generated by differential splicing of the highly O-glycosylated exons 4 (A), 5 (B), 6 (C), or none of them (RO) (**Figure 18**).

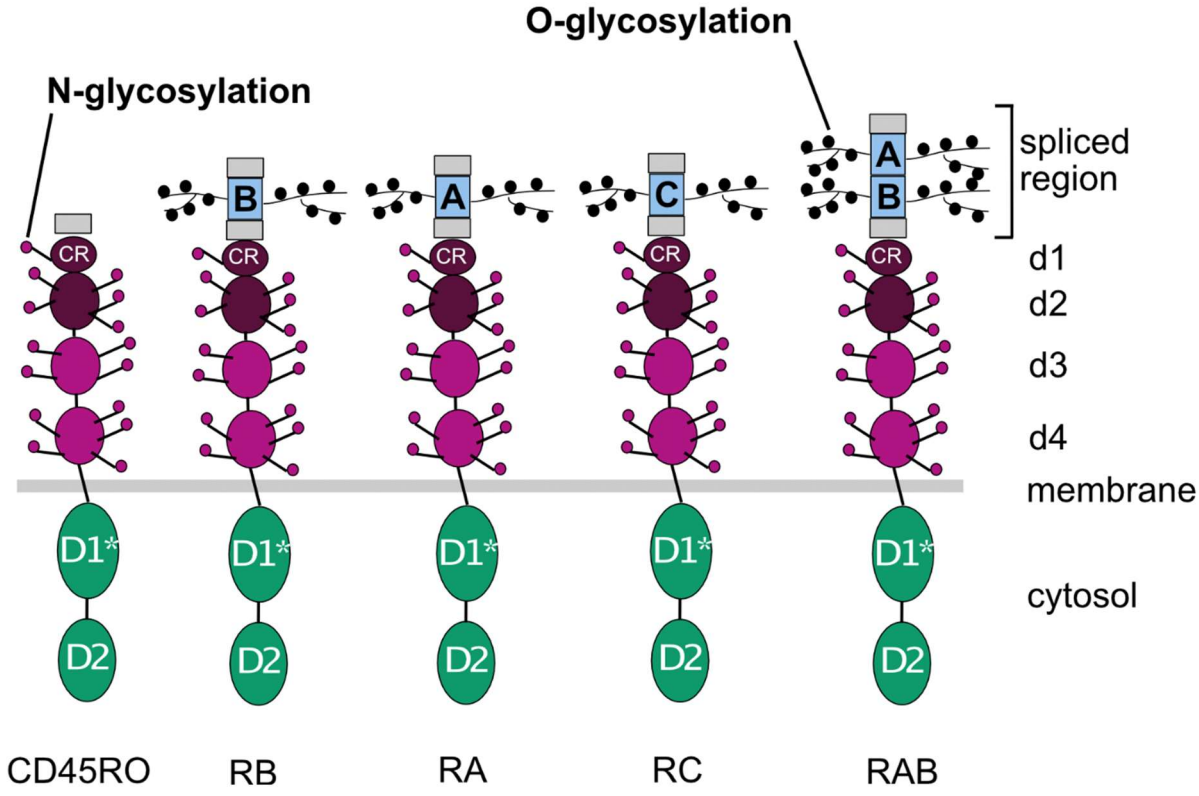

Figure 18: Schematic representation of human CD45 isoforms

On the intra-cellular part, D1 (green, catalytically active) and D2 (green, catalytically inactive) are phosphatase domains. On the extracellular part, d1 and d2 show degenerated topology of fibronectin type III (FN3) domain (dark pink) and d1 is cysteine rich (CR). d3 and d4 are FN3 domains (light pink). A (exon 4), B (exon 5), C (exon 6) are the alternatively spliced exons (blue). Figure adapted from* [99] [100]

CD45 is expressed in all nucleated hematopoietic cells [98] and represents up to 10% of the cell surface area [101]. Thus, this protein is interesting to target in targeted therapies for many reasons: (i) its high expression will increase the binding and the killing efficiency of the antibody-based

targeted therapy; (ii) its broad expression would allow to deplete HSCs and lymphocytes together with targeted therapies in one conditioning regimen; (iii) its expression on all hematopoietic cell lineages would allow to target different cancer types with a single immunotherapy; (iv) its broad and high expression suggests that the protein is important for the cells' function, reducing the possibility for cancer cells to downregulate it and to escape.

Indeed, CD45 is a phosphatase involved in many pathways. It was shown to interact with TCR [102], the Src-Family protein kinases Lck, Fyn and Lyn and to play an important role for the dephosphorylation of JAK after cytokine signaling through the JAK/STAT pathway [101]. Thus, CD45 is an important protein for various cell processes. It should be difficult for cancer cells to downregulate it without impairing the viability of the cells, so anti-CD45 targeted therapies could be used to prevent relapses. Therefore, the protein was already tested in several clinical trials. Most of the current strategies involve the anti-CD45 BC8 clone bound to different radionuclides (^{90}Y, ^{211}At and ^{131}I) and are used for conditioning before reconstitution with HSCT. These therapies indicate the feasibility to target this receptor with antibody-based strategies and show that targeting CD45 can efficiently deplete HSCs. Thus, development of CD45 shielding variants would have many interests: it would support the use of high doses of targeted therapy without toxicity on graft HSCs and the therapy could be continuously applied, preventing from relapses. However, shielding will not work with radioligands as they deplete all cells located around their target. Strategies to protect cells would need to be developed together with immunotherapies without bystanders' activity such as ADCs, TCEs or CAR-T cells.

Data from murine models demonstrate that CD45 can potentially tolerate mutations. The mouse CD45 protein naturally exists in two isoforms, CD45.1 and CD45.2 which differ by 6nt in the extracellular domain [103] [104]. Among those, a single amino acid substitution results in the specific recognition of the two isoforms by two distinct antibody clones. It was demonstrated by competitive bone marrow transplantation that CD45.1 and CD45.2 are functionally equivalent [105]. Thus, congenic markers in mice are informative that mutating the human CD45 protein may be possible without impact on its function. Collectively, CD45 represents a promising target for the development of shielding strategies.

II.2- Aims and objectives of the chapter

In this chapter, we asked if CD45 variants could be used for shielding from anti-CD45 targeted therapies. In order to answer this question, we set up several aims:

- Design *in silico* functional CD45 variants in an area that could be used as an epitope (done by R. L)
- Establish a system for high expression of recombinant CD45 variants
- Screen CD45 variants vs. anti-CD45 antibodies to identify pairs of antibody/variant leading to loss-of-binding of the antibodies
- Use the antibody/variants pairs identified to generate antibody-based targeted therapies targeting CD45
- Test if engineering of variants can protect cells *in vitro* from killing by the targeted therapy generated

II.3- Results

II.3.1- Design of CD45 variants

The protein CD45 would be a good candidate for the development of targeted therapy and for allele engineering in humans. Where could we design the mutation to shield cells from antibody-based targeted therapies?

We knew that CD45 can be alternatively spliced and we aimed to create variants that will be present even if the cells express different isoforms. Therefore, we focused on regions of the ECD not modified by the alternative splicing [99]. The non-spliced part of the protein is composed of 4 highly N-glycosylated domains d1, d2, d3, d4 (**Figure 18**). In order to identify candidate mutation sites without screening extensively the full ECD of the protein, we collaborated with Prof. Schwede and R. L. The laboratory of Prof. Schwede is specialized in computational modelling of 3D protein structures and the use of these structures to deduce protein functions. First, we decided together to narrow down the area of potential mutations and we started by selecting a domain where we could design them. d3 and d4 are classical evolutionarily conserved Fibronectin type III (FN3) domains [106], a structure used in 2% of animal proteins [107]. To avoid the risk for cross-reactivity with other FN3 containing proteins, we decided to ignore these domains. Unlike d3 and d4, d1 and d2 show degenerate topology of FN3 domains [108], therefore we decided to focus on them. The d2 extracellular domain was shown to be the target of several antibodies [106] and is known in mice to be targeted by the antibodies recognizing the CD45.1 and the CD45.2 isoform [104], we decided to design mutations in this domain. To design amino acids substitutions inside, we used the following three criteria: (i) The amino acids needed to be accessible for a ligand, (ii) They should not be evolutionarily conserved, meaning that they were likely tolerating mutagenesis, (iii) The insertion of the mutation should be possible with available CRISPR/Cas9 tools. Following these criteria, R. L selected several positions where we could insert mutations. For each of these positions, she ran several computational tools (ie STRUM[109], META [110]) predicting the conservation of the stability of the protein (ddG) following substitutions. Amino acids keeping the stability of the protein (ddG>0) were selected. This analysis gave us eventually six possible substitutions, all located in the d2 domain and replacing the amino acids E329 and T330. Two substitutions were designed for E329: E329I and E329K and four for T330: T330E, T330D, T330R and T330K. We added to this list of variants one mutation which could be potentially edited by base editors, T330I, and one variant which was experimentally identified by R. M: F331_T332del.

The amino acids E329, T330, F331 and T332 are part of a loop protruding outside of the d2 domain of CD45 (**Figure 19**)

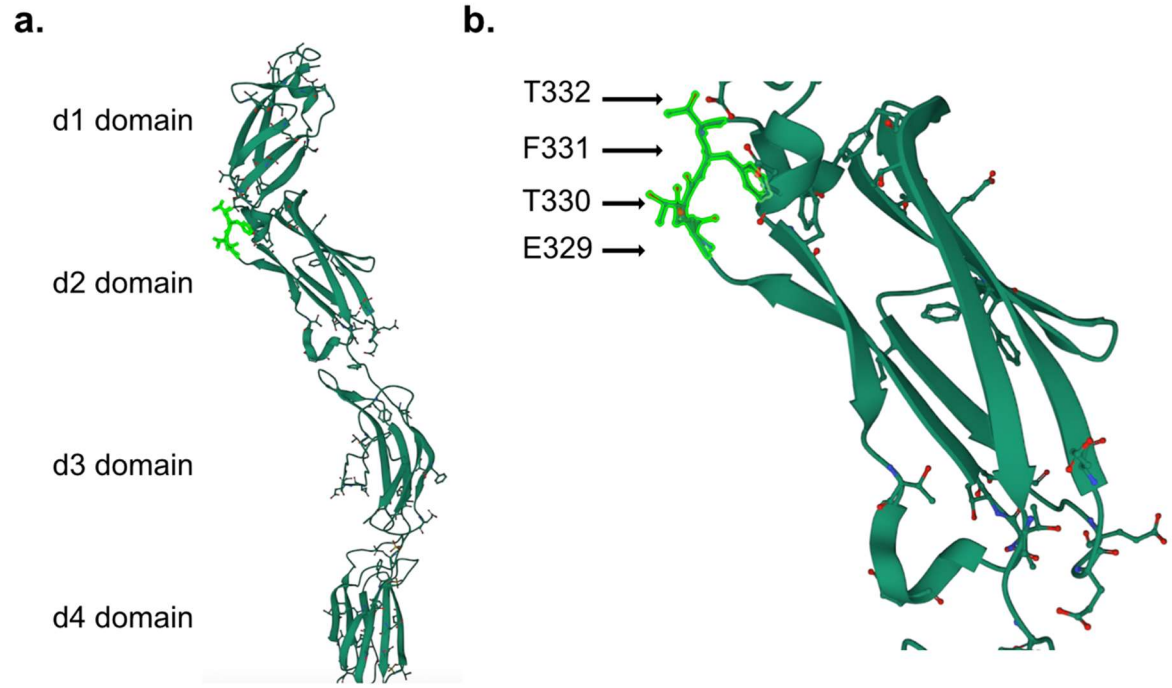

Figure 19: Localization of E329, T330, F331 and T332 in the CD45 structure

***a**. Crystal structure of the human CD45 with the 4 domains annotated and the amino acids F, T and E displayed as "balls and sticks". The four amino acids E329, T330, F331 and T332 are highlighted in light green in the d2 domain. **b**. d2 domain with the E329, T330, F331 and T332 highlighted in light green in the protruding loop. PDB ID: 5FMV* [108]

Loops are good to engineer since the risk to disrupt the overall protein stability is rather low. Thus, our analysis allowed us to design mutations in a region that can tolerate to be mutated, increasing the chance to have in our selection functional variants.

II.3.2- K562 CD45KO cells allow high expression of CD45 variants

II.3.2.1- HEK293 cells are not favorable for expression of recombinant CD45

In order to identify a combination of variant/antibody that would disrupt the binding of the antibody, we needed a system allowing similar expression of all the variants to screen antibody candidates against them. We tested the HEK293 cells system as these cells are not of hematopoietic origin, therefore don't express CD45 and are in addition easy to transfect. First, we assessed transient expression of the two CD45 isoforms CD45RABC and CD45RO. We

observed a higher MFI but also more CD45 positive cells (60% estimated) for CD45RO compared to CD45RABC (**Figure 20**), we therefore decided to introduce the designed variants into the CD45RO isoform.

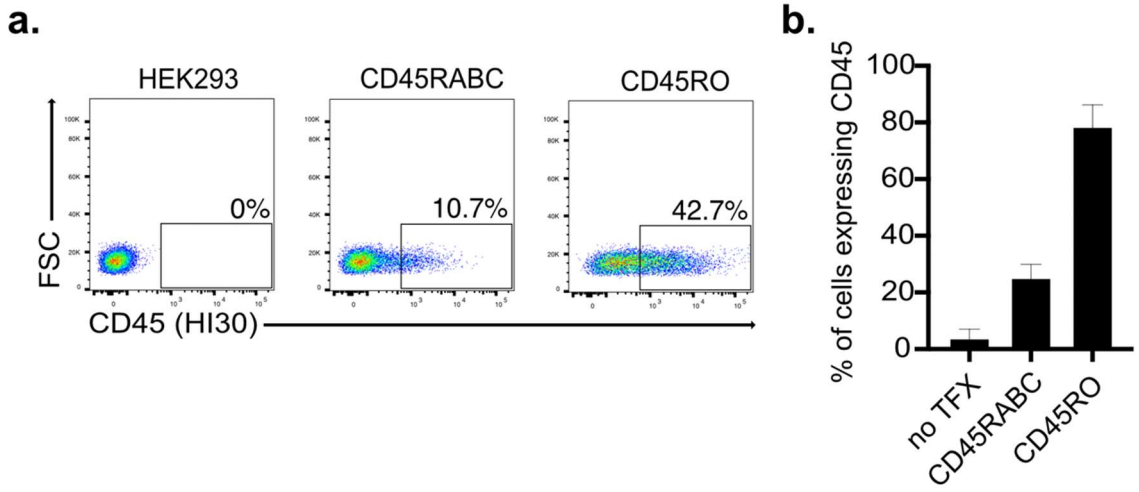

Figure 20: Transient expression of CD45 isoforms RO and RABC in HEK293 cells

***a**. Representative flow cytometry plots of CD45 isoforms expression in HEK293. HEK293: cells mock electroporated. CD45RABC: HEK cells electroporated with CD45RABC plasmid. CD45RO: cells electroporated with CD45RO plasmid. Flow cytometry staining done using the anti-CD45 antibody clone HI30.* ***b**. Percentage of HEK293 cells expressing recombinant CD45. Data represent mean ± s.e.m (3 independent experiments)*

Efficiencies of transient transfections can slightly vary between experiments. In order to work with cells expressing constant and similar levels of the variants, we aimed to generate stable HEK293 cell lines. The eight plasmids encoding for CD45 variants were co-electroporated with a plasmid encoding for the G418 resistance gene in order to select the stable cell lines by antibiotic resistance (**Figure 21**).

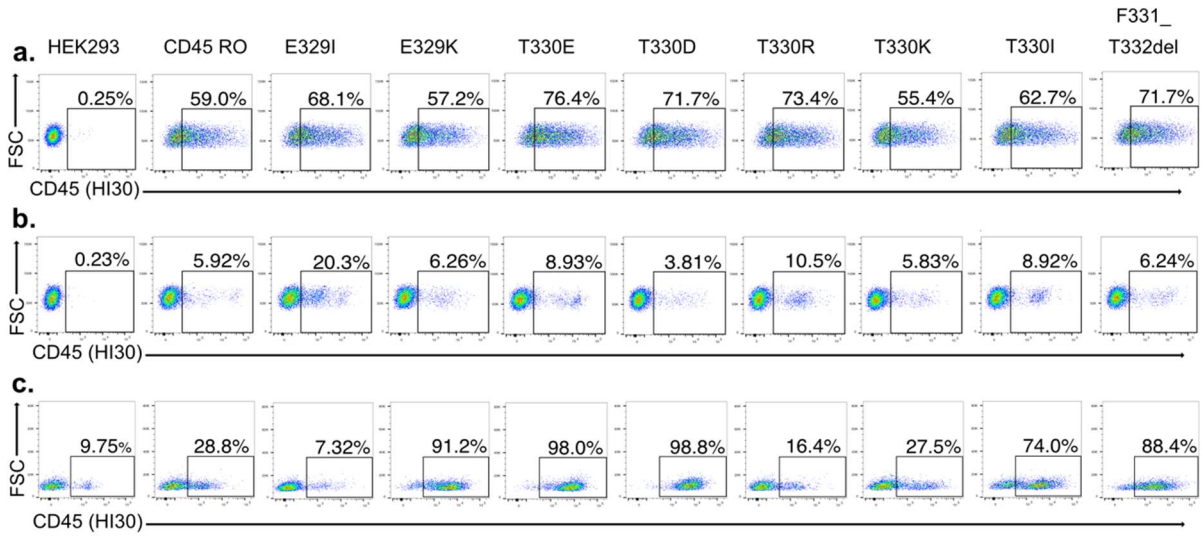

Figure 21: HEK293 do not conserve CD45 variants expression after G418 selection

***a**. Representative flow cytometry plots of CD45 variants expression 2 days after electroporation. **b**. Representative flow cytometry plots of CD45 variants expression 10 days after G418 selection. CD45$^+$ cells sorted by flow cytometry **c**. Representative flow cytometry plots of CD45 variants expression profile 40 days after sort of CD45$^+$ cells. Flow cytometry analysis of CD45 expression performed with the anti-CD45 antibody clone HI30*

We observed similar expression of the variants 2 days after electroporation (**Figure 21a**). However, 10 days after G418 selection, very few cells retained the expression of the protein (**Figure 21b**). The few cells expressing the variants were sorted for high expression of CD45, but we observed a high variability of expression between the variant cell lines obtained after expansion (**Figure 21c**). Thus, despite the fact that all variants showed similar expression after electroporation, we did not manage to isolate cells highly expressing the protein for all the variants. As expression of the unmodified CD45RO was also lost, we supposed that the instability of expression was not due to the instability of the variants but rather to the cell line system. Low expression of recombinant CD45 in HEK293 cells was previously observed in other studies [111] [105]. Therefore, we concluded that HEK293 is not a system adapted for the expression of this protein.

CD45 is a highly glycosylated protein and Pulido and Sanchez-Madrid showed that glycosylation of CD45 is required for cell surface expression [112]. Moreover, Medzihradsky et al showed that glycosylation of a protein is tissue-specific [113]. We reasoned that CD45 expression could improve in cells of hematopoietic origin as CD45 is usually expressed on all nucleated hematopoietic cells. Thus, we tried to express CD45 variants in the K562 cell line.

II.3.2.2- KO of CD45 in K562 cells allows high re-expression of CD45 variants

K562 cell line was isolated from a patient with CML [114]. Thus, as CD45 is highly expressed on all nucleated blood cells [115], we expected that K562 cells would express high levels of the protein, which we confirmed experimentally (**Figure 22a**). Then, in order to generate a cell system allowing a high expression of CD45 variants, we knocked-out CD45 in the $CD45^+$ cells, generating the K562 CD45KO cell bulk (**Figure 22**).

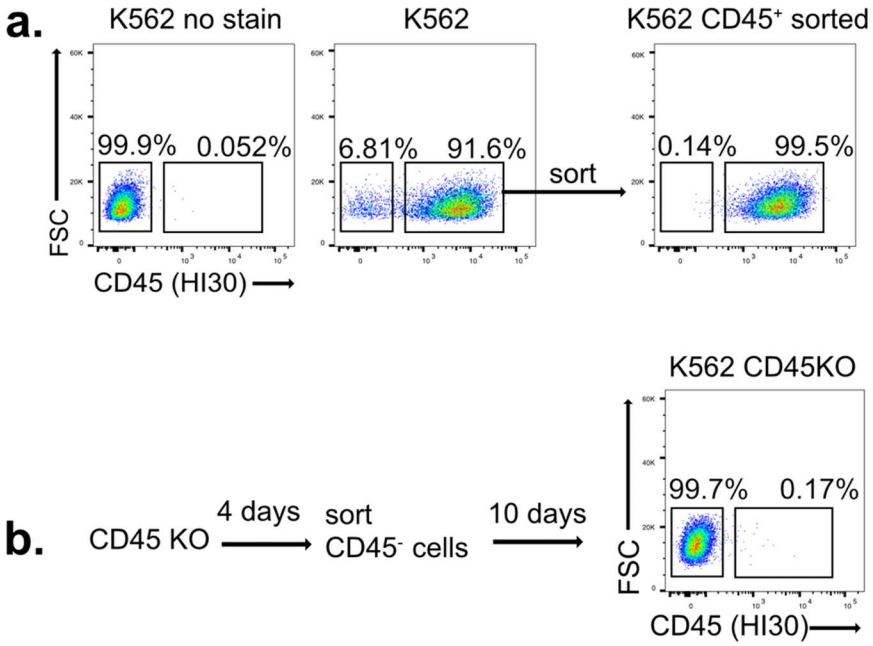

Figure 22: Generation of the K562 CD45KO cell bulk

***a**. Representative flow cytometry plot of K562 before and after sort of $CD45^+$ cells **b**. Representative flow cytometry plot of $CD45^+$ sorted K562 10 days after electroporation with RNPs. Cells were analyzed for CD45 expression with anti-CD45 HI30*

Staining of K562 with anti-CD45 showed two populations. The majority of cells expressed CD45 (91.6%) while a small population (6.81%) did not express it. We purified the $CD45^+$ cells (**Figure 22a**) and we electroporated them with RNPs coupled to a gRNA targeting CD45 (**Figure 22b**). Following electroporation, we sorted the cells having lost expression of CD45 ($CD45^-$) and we obtained a pool of cells highly enriched for CD45KO (99.7%) which we named K562 CD45KO (**Figure 22b**).

Next, we tested whether the K562 CD45KO cells would indeed express more homogenously CD45 variants than HEK293. K562 CD45KO cells were transiently electroporated with the plasmids encoding for the variants (**Figure 23**).

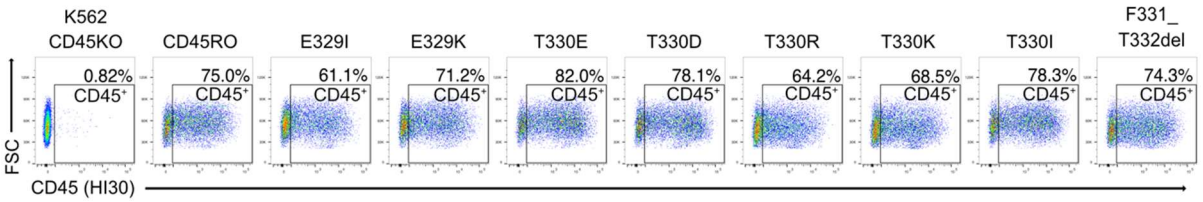

Figure 23: Expression of recombinant CD45 variants in K562 CD45KO cells

Representative flow cytometry plots of CD45 variants expression 24 h after K562 CD45KO electroporation. Flow cytometry analysis of CD45 expression performed with the anti-CD45 antibody clone HI30.

All CD45 isoforms (variant and non-modified) were highly expressed in K562 CD45KO cells. However, for all isoforms, we did not observe a $CD45^+$ population clearly separated from the $CD45^-$ population. Instead, we observed an heterogenous expression of the protein. This heterogeneity between cells electroporated with the same plasmid can be due to different amounts of plasmid received per cell. Thus, we considered that any cell with binding of anti-CD45 compared to K562 CD45KO, no matter the expression level, was $CD45^+$. After electroporation of K562 CD45KO with the non-modified CD45RO, 75% of cells were $CD45^+$. This percentage was similar for the variants, excepted for E329I which showed 61.1% of $CD45^+$ cells. However, this experiment represents only one repeat, we could not conclude about the low expression. Thus, we demonstrated that we established a robust system for expression of the recombinant variants.

II.3.3- Screening of variants vs. anti-CD45 antibodies revealed the binding properties of the QA17A19 antibody clone

II.3.3.1- Eight good CD45 binders were identified

Next, we aimed to identify existing mAbs that could be used in targeted therapies to target CD45. Then, we intended to show that some of these clones had binding disrupted by the designed CD45 variants. We started with existing antibodies instead of making our own. Therefore, we considered any anti-CD45 available antibody and we identified 12 clones which seemed to be directed at the ECD of the protein: B-A11, BRA-11, F10-89-4, HI30, MEM-28, QA17A19, YAML 501.4, 2D1, 5B1, 5K237, 10B1611 and 15j36. First, we aimed to identify good binders: we transiently expressed non-modified CD45RO and tested by flow cytometry staining of the clones (**Figure 24**).

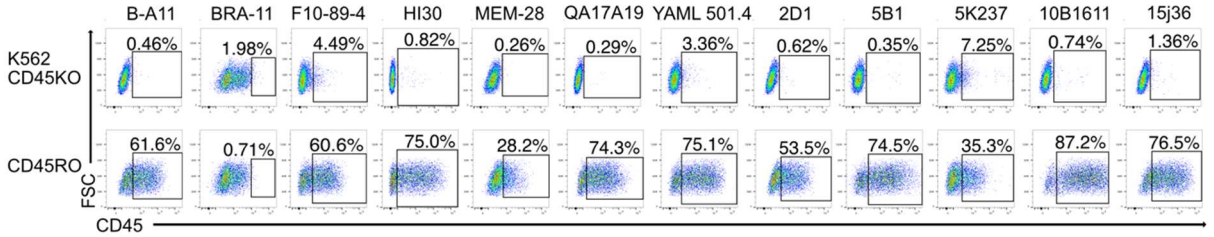

Figure 24: Anti-CD45 antibodies binding to non-modified CD45RO

Representative flow cytometry plots of K562 transiently electroporated with CD45RO and stained with anti-CD45 antibodies. For each clone, gate of positive cells was designed according to the fluorescence of stained non-transfected cells (K562 CD45KO).

In this experiment, we wanted to select antibodies with a high percentage of stained cells and a high fluorescence intensity in order to use them later on CD45 variants. After staining with BRA-11, we did not observe any positive cells, this antibody was not selected for further screening. MEM-28, 2D1 and 5K237 clones showed a low MFI. This told us that these antibodies had likely a low sensitivity to identify difference of staining induced by the variants. We did not select them for further experiments. In contrast, B-A11, F10-89–4, HI30, QA17A19, YAML 501.4, 5B1, 10B1611 and 15j36 showed more than 60% of cells stained and showed a high fluorescence intensity. They likely have a better sensitivity to identify different staining of variants. These clones were selected for further screening with CD45 isoforms.

II.3.3.2- QA17A19 showed loss-of-binding for several variants

Binding of selected antibody clones B-A11, F10-89–4, HI30, QA17A19, YAML 501.4, 5B1, 10B1611 and 15j36 to CD45 variants was tested via flow cytometry (**Figure 25)**. Ten variants were tested. Among them, eight variants were previously described: E329I, E329K, T330E, T330D, T330R, T330K, T330I, and the F331_T332del. As we planned to test the double deletion of F331 and T332, we added the single deletions of F331 and T332 to the screening.

a.

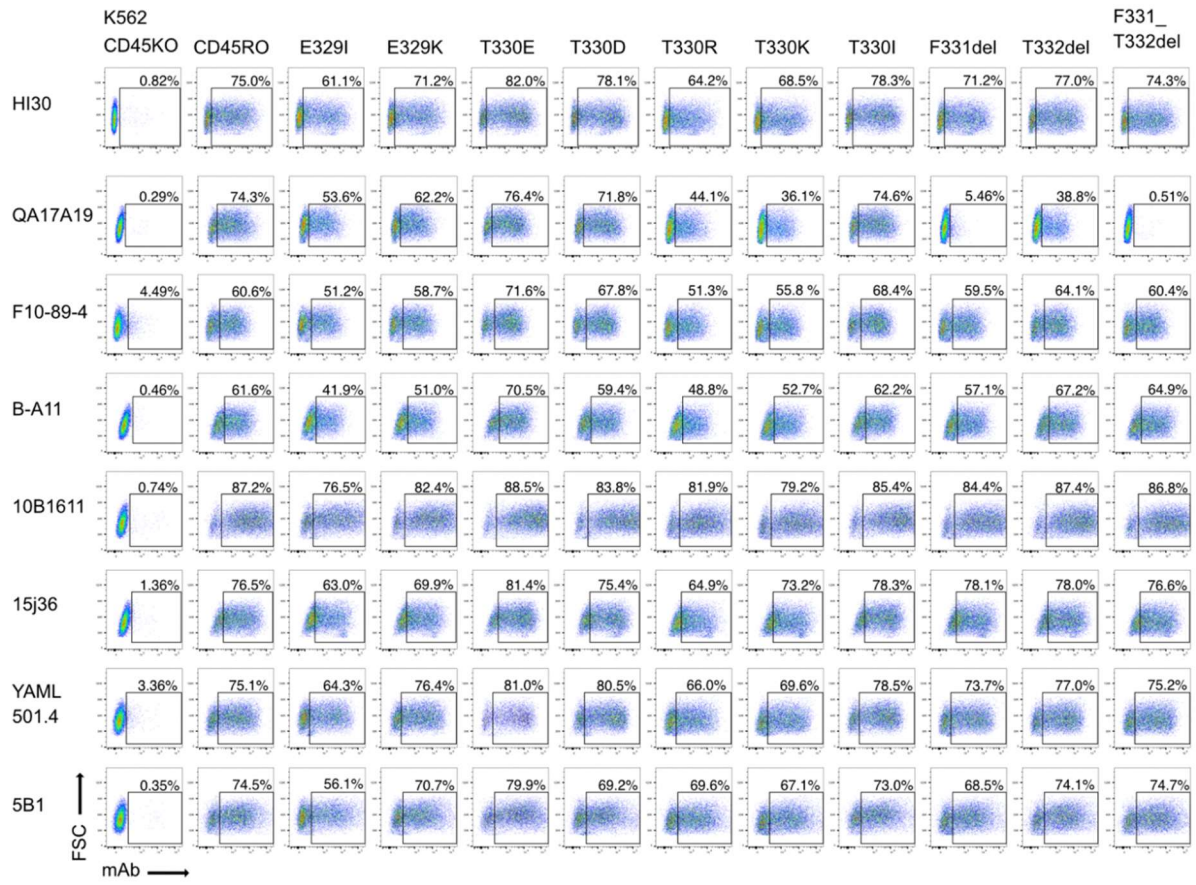
K562 CD45KO
CD45RO
E329I
E329K
T330E
T330D
T330R
T330K
T330I
F331del
T332del
F331_ T332del
HI30
QA17A19
F10-89-4
B-A11
10B1611
15j36
YAML 501.4
5B1
FSC
mAb

b.

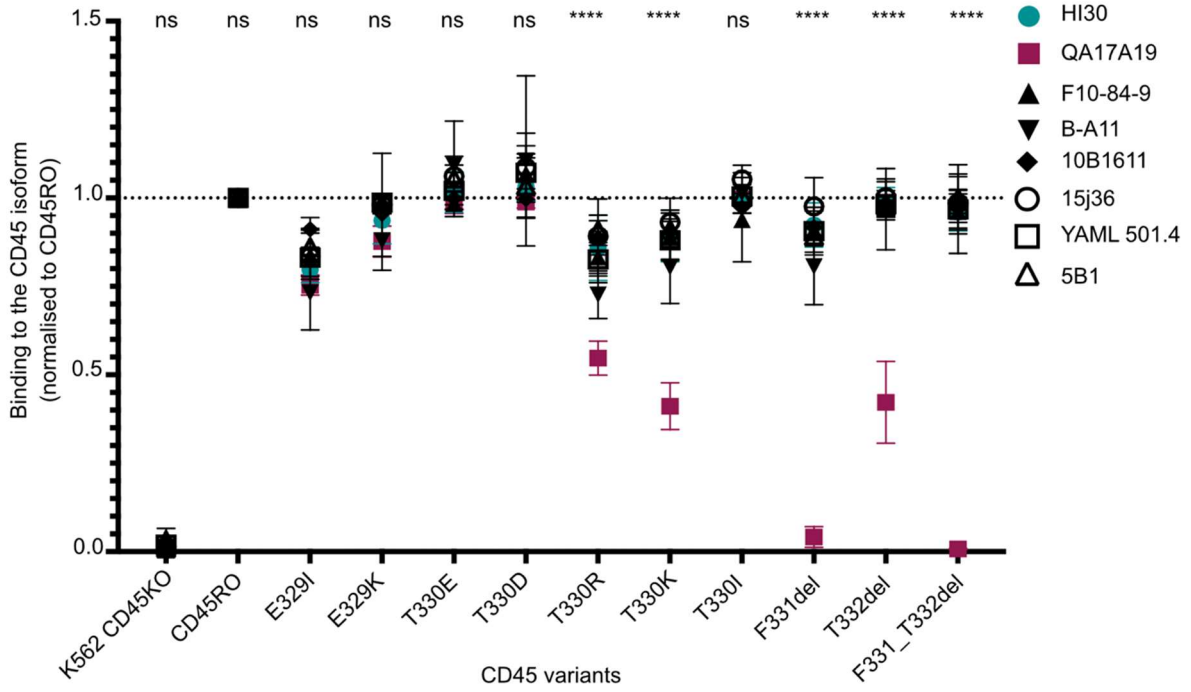
Binding to the CD45 isoform (normalised to CD45RO)
1.5
1.0
0.5
0.0
ns
****
HI30
QA17A19
F10-84-9
B-A11
10B1611
15j36
YAML 501.4
5B1
K562 CD45KO
CD45RO
E329I
E329K
T330E
T330D
T330R
T330K
T330I
F331del
T332del
F331_T332del
CD45 variants

Figure 25: Screening of selected anti-CD45 antibodies on designed variants

***a**. Representative flow cytometry plots of CD45 variants stained with HI30, QA17A19, F10-89-4, B-A11, 10B1611, 15j36, YAML 501.4, 5B1 antibody clones. Cells stained 24 h after electroporation. For each antibody, gate of positive cells was designed according to the fluorescence of stained non-transfected cells (K562 CD45KO).* **b**. *Binding of each clone to the CD45 variants. Binding was calculated as following: percentage of $CD45^+$ cells per variant was normalized to the percentage of $CD45^+$ cells in non-modified CD45RO. Variants were normalized separately for each antibody clone. Data represent mean ± s.e.m (3 independent experiments) **** $P<0.0001$; n.s, not significant. Statistics calculated using two-way ANOVA by comparison of the anti-CD45 clones means to HI30 mean. Statistics displayed here represent comparison of QA17A19 mean to HI30 mean.*

Staining of the non-modified CD45RO by the eight antibody clones showed different percentages of $CD45^+$ cells (**Figure 25a**). For instance, staining with 10B1611 showed around 80% of $CD45^+$ cells across experiments while staining with F10-89-4 showed around 60% of $CD45^+$ cells. Thus, we had to study the antibodies separately. We analyzed loss-of-binding of antibodies using their own staining to CD45RO as reference. To do this, we normalized the percentage of $CD45^+$ cells measured for each variant to the percentage of $CD45^+$ cells measured for unmodified CD45RO. Then, we compared the normalization results for each variant (**Figure 25b**).

One antibody clone that caught our attention was QA17A19. We observed that several mutations affected its binding while the same mutations did not affect the binding of the other clones. Interestingly, the substitution of T330 with R and K affected its binding, while exchange of the same position with E, D or I did not. We aimed to select mutations which would preserve the function of the protein. T330R and T330K were designed with criteria such as preservation of the protein stability or frequent use of the amino acids R and K at this position in different animal species, making the substitutions more likely to preserve the function of the protein. Even if we observed a limited loss-of-binding for these substitutions, we selected QA17A19 together with T330R and T330K for further experiments.

T332del variant reduced binding of QA17A19 while F331del and F331_T332del completely abolished it (**Figure 25b**). These three mutations were selected as well for further experiments.

To conclude, we selected the mutations T330K, T330R, F331del, T332del and F331_T332del and the QA17A19 clone as variant/antibody pairs leading to antibody loss-of-binding. For further experiments we decided to use HI30 as control antibody as we did not observe any impact of the variants on its binding.

II.3.3.3- QA17A19-derived MIRG451 showed high sensitivity to selected variants

We aimed to use the variable parts of QA17A19 to generate targeted therapies targeting CD45. First, we needed to integrate the variable parts of QA17A19 in a known protein format easy to handle. Then, we planned to test and to derive this format into different targeted therapies. Antibodies represent a stable protein format well known and easy to work with, as demonstrated by their massive use. We decided to generate a human chimeric antibody with the variable chains of the mouse QA17A19 and the constant chain of a human antibody. QA17A19 is a commercially available monoclonal mouse antibody provided by Biolegend (Cat# 393402). In order to be able to engineer it, we determined the heavy and light chain sequences by *de novo* sequencing. The purified antibody was sent to the company Rapid Novor Inc which divided the protein in small fragments by enzyme digestions and sequenced the obtained pieces by liquid chromatography with tandem mass spectrometry. Sequenced fragments were aligned and allowed to reconstitute the amino acids order of the variable parts of QA17A19. We turned these amino acid sequences into DNA and cloned them into a human IgG1 backbone [116] in order to generate the human chimeric antibody MIRG451 (**Figure 26**). MIRG451 was produced by transient transfection in chinese hamster ovary (CHO) cells and purified from supernatant with protein A resin.

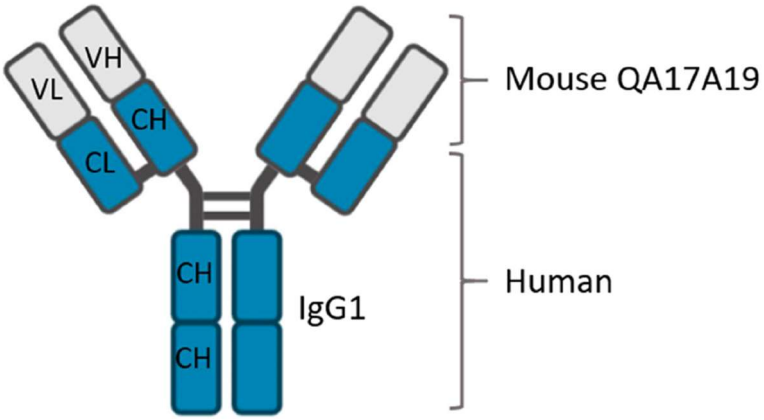

Figure 26: Human chimeric anti-CD45 antibody MIRG451

Anti-CD45 antibody structure and composition. Blue: constant parts of the antibody (human IgG1). Grey: variable parts of the antibody (mouse QA17A19).

Next, we aimed to compare loss-of-binding of QA17A19 and of the newly generated antibody MIRG451. We chose to compare them on the same variants as described before (**Figure 25**) but we also decided to design new variants in order to increase our alternatives for complete

loss-of-binding. According to previous results, amino acid T330, F331 and T332 are involved in QA17A19 binding (**Figure 25**). First, T330 substitutions showed low loss-of-binding of QA17A19. We tested a new substitution, T330A. As we saw previously that the deletion of close amino acids allowed a high loss-of-binding we also tested a deletion of T330. F331 and T332 seem promising amino acids to target as their deletion highly impacted the binding of QA17A19. In collaboration R. L, we designed four substitutions of F331: F331S, F331I, F331L and F331A. We also designed one for T332, T332A. All the variants were screened by flow cytometry with QA17A19 or MIRG451 together with HI30. This latter antibody clone was used as control for protein expression (**Figure 27**).

a.

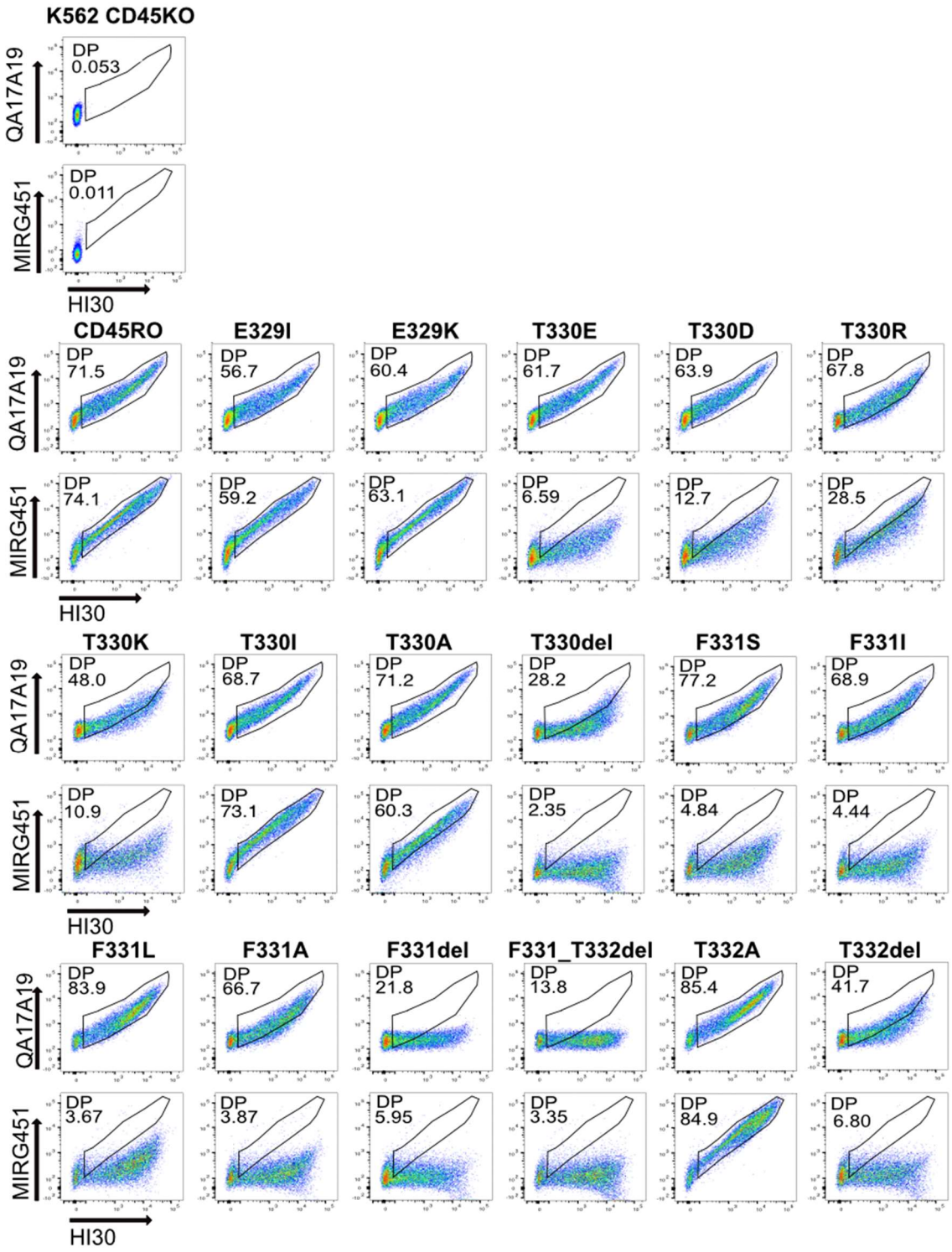
K562 CD45KO
QA17A19
DP 0.053
MIRG451
DP 0.011
HI30
CD45RO
DP 71.5
DP 74.1
E329I
DP 56.7
DP 59.2
E329K
DP 60.4
DP 63.1
T330E
DP 61.7
DP 6.59
T330D
DP 63.9
DP 12.7
T330R
DP 67.8
DP 28.5
T330K
DP 48.0
DP 10.9
T330I
DP 68.7
DP 73.1
T330A
DP 71.2
DP 60.3
T330del
DP 28.2
DP 2.35
F331S
DP 77.2
DP 4.84
F331I
DP 68.9
DP 4.44
F331L
DP 83.9
DP 3.67
F331A
DP 66.7
DP 3.87
F331del
DP 21.8
DP 5.95
F331_T332del
DP 13.8
DP 3.35
T332A
DP 85.4
DP 84.9
T332del
DP 41.7
DP 6.80

b.

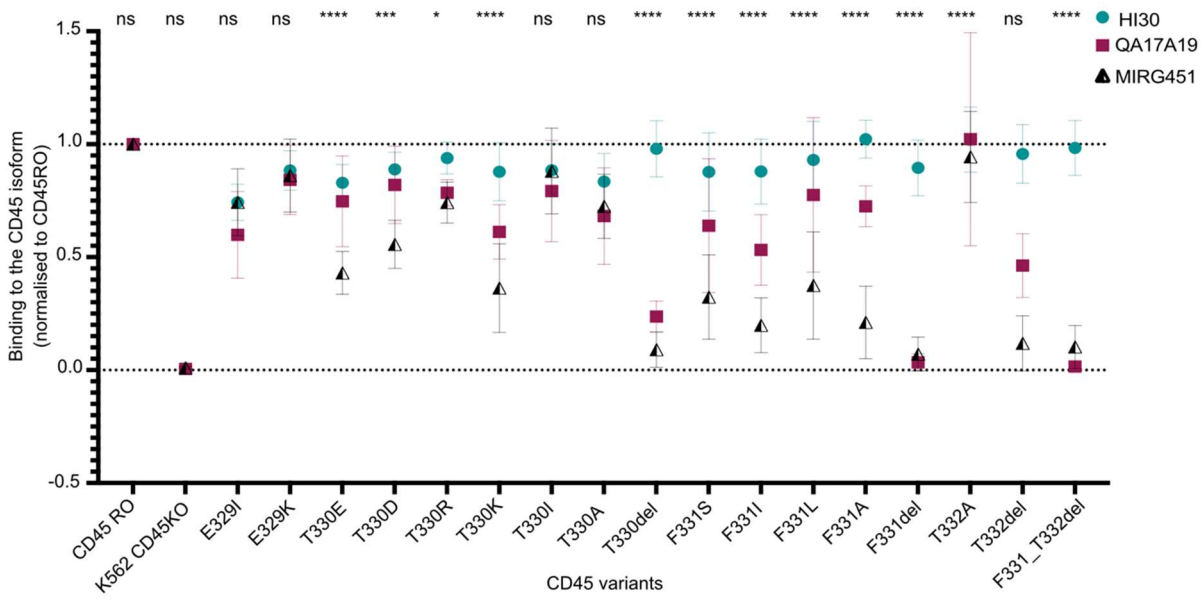

Figure 27: Comparison of MIRG451 and QA17A19 binding on CD45 variants

***a**. Representative flow cytometry plots of K562 CD45KO cells transiently electroporated and stained 24 h later with MIRG451 and HI30 (ctrl) or QA17A19 and HI30 (ctrl). Gate of double positive cells (DP) were designed according to the fluorescence of stained non-transfected cells (K562 CD45KO) and of non-modified CD45RO transfected cells (CD45RO). **b**. Binding of the QA17A19 and MIRG451 to the CD45 variants. For each variant the percentage of $CD45^+$ cells was measured after staining with MIRG451, QA17A19 and HI30. Binding was calculated as following: percentage of $CD45^+$ cells for each variant was normalized to the percentage of $CD45^+$ cells for CD45RO. Each antibody was analyzed separately. Data represent mean ± s.e.m (3 independent experiments) **** P<0.0001; *** P≤ 0.001, ** P≤ 0.01, * P≤ 0.05, n.s, not significant. Statistics calculated using two-way ANOVA with comparison of the anti-CD45 clones means to HI30 mean. Statistics displayed here represent comparison of MIRG451 mean to HI30 mean.*

Since there is a possibility for errors when using mass spectrometry-based sequencing, the amino acid sequence of the variable parts of MIRG451 and QA17A19 may not be 100% identical. In addition, the MIRG451 is a chimeric molecule composed of a human Fc part and a mouse variable part, while QA17A19 is 100% mouse. Thus, we asked if we have differences in binding of the two antibodies. We observed higher loss-of-binding for MIRG451 than for QA17A19 when staining variants. For instance, variants T330E and T330D staining showed significant loss-of-binding of MIRG451 compared with HI30 (**Figure 27**), while we did not observe a significant loss-of-binding of QA17A19 for the same variants (**Figure 25**). For

further experiments, we decided to pick first variants leading to a strong loss-of-binding for the two clones when compared to HI30 binding (**Figure 27**). Therefore, we chose T330del, F331del, T332del and F331_T332del.

This selection contained only deletions. We wanted to include a variant with an amino acid substitution in order to increase the chances to select for a functional variant. Some missense mutation of F331 showed strong effect on the two clones' binding, but F331 is a conserved amino acid according to Dr. R. Lepore's analysis. We wanted to select another amino acid which is less conserved than F331 across species and chose the mutation T330K as it impacts binding of both QA17A19 and MIRG451.

To conclude, our screening strategy of variants vs. antibodies allowed us to identify one antibody which binding was disrupted by several variants. Sequencing of the variable chains of this antibody allowed us generate the new anti-CD45 MIRG451 which showed increased sensitivity to the variants compared to the original clone QA17A19. We selected the variants T330K, T330del, F331del, F331del_T332del and T332del for further *in vitro* proof-of-shielding from MIRG451.

II.3.4- MIRG451-SAP kills primary cells *in vitro*

II.3.4.1- MIRG451 does not induce ADCC activity in vitro

The project is now moving from identification of variant/antibody pair to functional testing. The previous experiments allowed us to generate the MIRG451, an anti-CD45 antibody with binding disrupted by T330K, T330del, F331del, T332del and F331_T332del variants. Next, we wanted to show that MIRG451 could be used to deplete cells and that expression of the variants shielded the cells from killing. First, we wanted to see if MIRG451 could trigger ADCC against cells expressing CD45. MIRG451 could have ADCC activity since it contains human IgG1 Fc known to induce potent killing mechanism. In addition, the Fc part of MIRG451 is identical to the one of MIRG123 described in chapter I. Potency of this Fc part was confirmed by the high ADCC activity measured when MIRG123 was tested on HEK293 cell lines recombinantly expressing CD123 (**I.3, Figure 3b**). In order to assess if MIRG451 could be used to deplete cancer cells via ADCC and to test if the variants T330K, T330del, F331_T332del, F331del and T332del protect healthy cells from killing, we measured ADCC activity on K562 CD45KO transiently transfected with the variants and the unmodified protein (**Figure 28**).

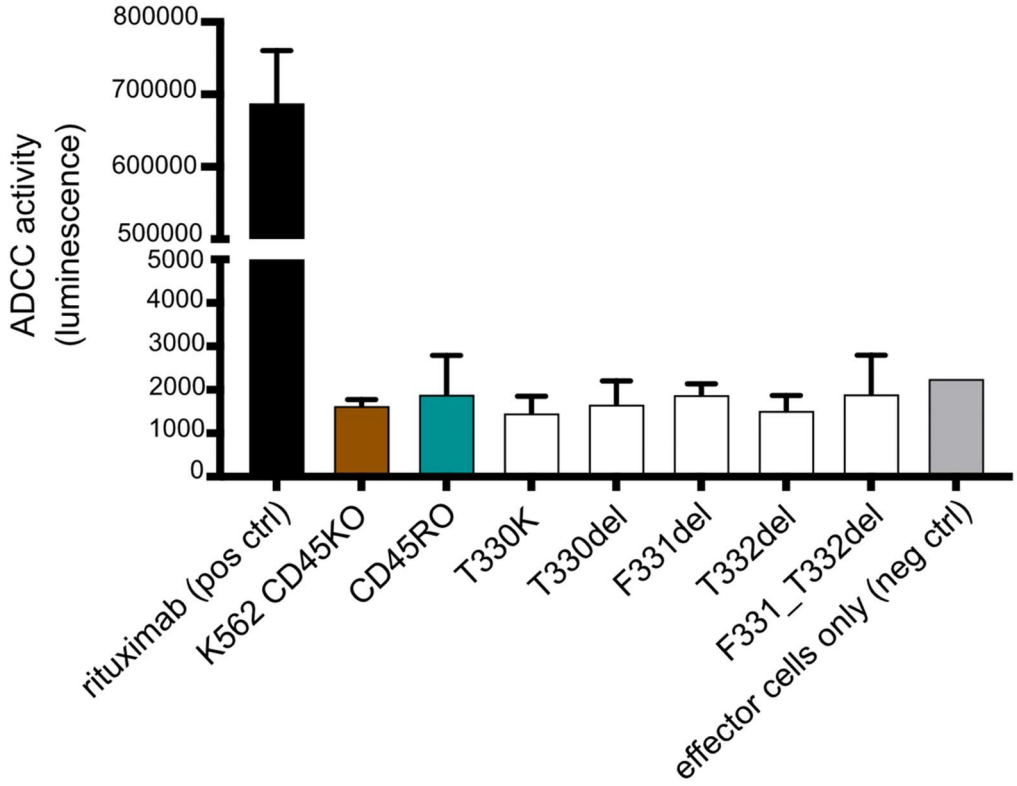

Figure 28: ADCC activity of MIRG451 on CD45 variants

ADCC activity measured after incubation of MIRG451 with K562 CD45KO transiently transfected with CD45 variants and the effector Jurkat cell line. Positive control: rituximab (anti-CD20) mixed with Raji cells and the effector cell line. Negative controls: effector cells without antibody or target cells. Repeats shown here are experimental duplicates and do not show 2 independent experiments.

A high ADCC activity was measured when Rituximab was mixed with Raji cells (positive control). However, when MIRG451 was tested on the cells expressing the non-modified CD45RO, the ADCC measured was similar to the negative control, meaning that MIRG451 is not able to trigger ADCC. Cleary et al showed that epitopes distant of 16 nm from the cell membrane are less able to engage ADCC than epitopes close to the cell membrane (1.5 nm) [117]. CD45RO is a long protein which has an extracellular size of 20-28 nm [118] and the epitope of MIRG451 is located on the d2 domain, about 12 nm from the membrane (PDB ID: 5FMV [108]). Absence of ADCC triggering could be explained here by a too long distance between the epitope and the membrane, therefore we couldn't use ADCC as killing mechanism. Moreover, Li et al showed that the same principle applies for TCE: distant epitopes are not able to correctly trigger T cell activation due to the absence of proper immune synapse formation [119]. We infer that the same principle would apply to CAR-T cells. Thus, we decided to abandon depleting strategies involving the formation of an immune synapse such as ADCC, TCE and CAR-T

cells. Instead, we developped a killing assay with a different mode of action: we decided to use an ADC, which consist in an antibody attached to a toxin, killing the cells upon internalization of the complex.

II.3.4.2- Jurkat cells but not K562 cells are sensitive to MIRG451-SAP

First, we aimed to establish *in vitro* an ADC killing assay depleting a cell line expressing CD45. We planned then to engineer endogenously the selected cell line with the variants and to use the engineered cells to test shielding from ADC killing. Palchaudhuri et al showed killing of Jurkat cells with anti-human CD45 antibody clones MEM-28 and HI30 bound to saporin toxin (SAP) [21], which kills cells by inactivating their ribosomal activity after endocytosis [120]. Thus, we aimed to establish the ADC killing assay with MIRG451 bound to SAP and we tested two human cell lines highly expressing CD45, K562 and Jurkat cells (**Figure 29**).

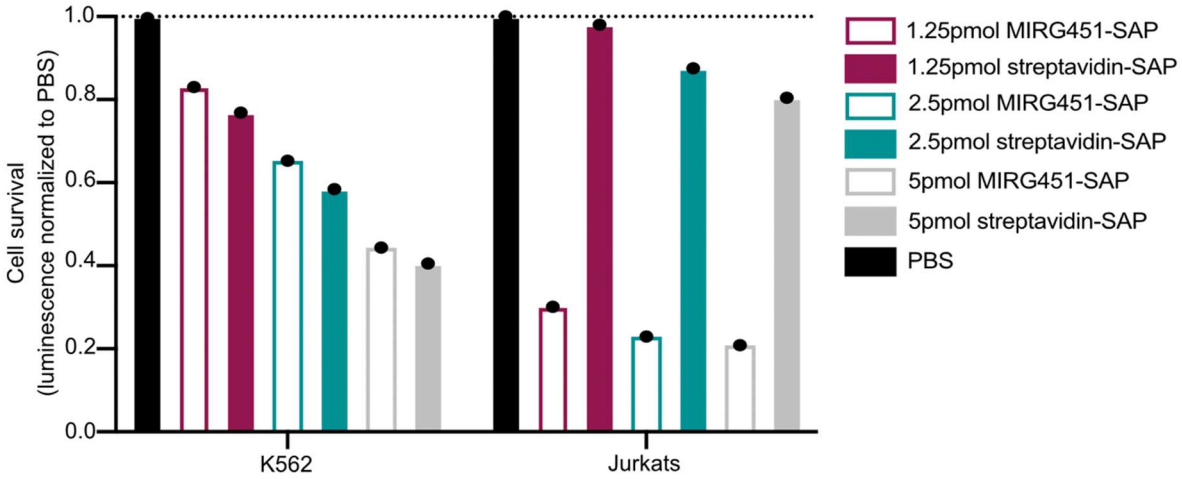

Figure 29: Killing of Jurkat and K562 cells by MIRG451-SAP

Amount of living cells measured after 3 days of incubation with 12.5 nM, 25 nM or 50 nM of MIRG451-SAP or 12.5 nM, 25 nM or 50 nM of unbound streptavidin-SAP. Control cells were incubated with PBS. Amount of living cells was measured by luminescence. For each condition luminescence was normalized to the luminescence measured for cells incubated with PBS.

Interestingly, only Jurkat cells show sensitivity to MIRG451-SAP. K562 were sensitive to the general concentration of toxin in the well, but addition of antibody to target integration of the toxin did not increase the killing. This differential sensitivity was not expected as both cell lines highly express CD45. To establish an *in vitro* assay showing proof-of-shielding of the variants, we selected Jurkat cells and we aimed to engineer the variants into their genome using CRISPR/Cas9 and HDR. Genome engineering of the cells gave a very low efficiency (1.2%,

data not shown) and we did not manage to isolate a cell population expressing the variants. Thus, we decided to not pursue with these cells. As Jurkat cells are a human leukemic T cell line sharing properties with human T cells [121], we inferred from these results that primary human T cells may be sensitive to MIRG451-SAP. Thus, we tested the *in vitro* killing of primary human T cells with the ADC.

II.3.4.3- Primary human T cells are sensitive to MIRG451-SAP

First, we tested the sensitivity of the human T cells by performing a dose titration of MIRG451-SAP (**Figure 30**).

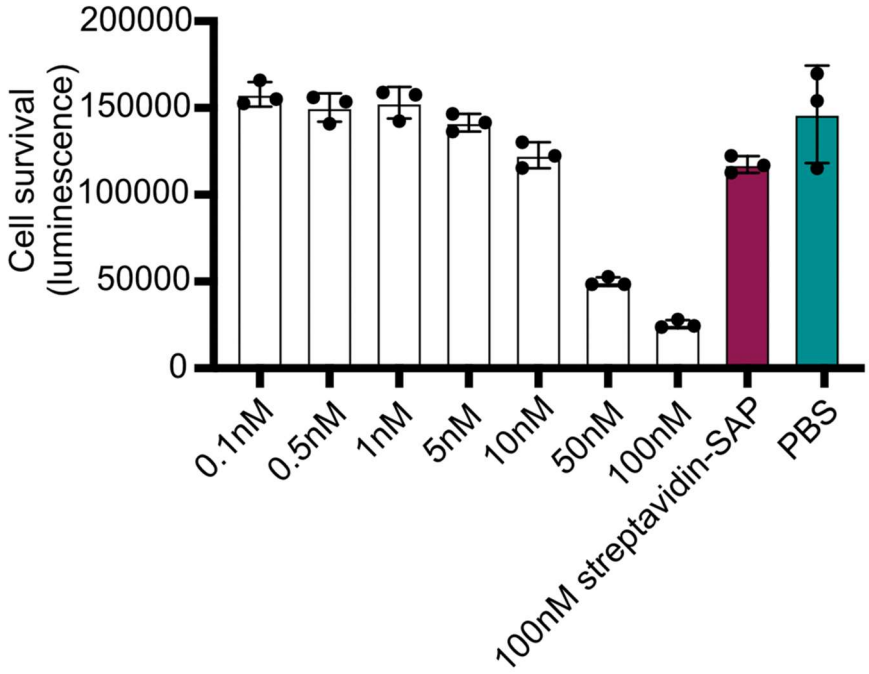

Figure 30: Killing of primary human T cells by MIRG451-SAP

Amount of living T cells measured after 3 days of incubation with increasing concentration of MIRG451-SAP (0.1 nM, 0.5 nM, 1 nM, 5 nM, 10 nM, 100 nM) or unbound streptavidin-SAP (100 nM). Control cells were incubated with PBS. Amount of living cells was measured by luminescence. Repeats shown here are experimental replicates and do not show 3 independent experiments.

We observed a dose-dependent killing of human T cells by MIRG451-SAP, while no killing was observed when the cells were incubated with 100 nM of unbound streptavidin-SAP. Thus, the human T cells are sensitive to MIRG451 targeted SAP. Highest killing efficiencies were observed for 50 nM and 100 nM of MIRG451-SAP with delta of more than 100000 relative light unit between luminescence of cells cultured with PBS and luminescence of cells cultured

with MIR451-SAP. As 50 nM of MIRG451-SAP required less material, we decided to use this concentration for shielding assays with primary human T cells.

II.3.5- CD45 variants engineered human T cells are resistant to MIRG451-SAP cytotoxicity

II.3.5.1- CRISPR/Cas9 and HDRTs allowed efficient engineering of variants in human T cells

We aimed to KI the selected variants into human T cells in order to test their shielding potency from the ADC. First, we needed to achieve a high KI efficiency of the five variants T330K, T330del, F331del, T332del and F331_T332del into primary human T cells using CRISPR/Cas9 driven HDR. The two most important parameters for gRNAs design for KI are: (i) gRNA cutting close to desired mutations [122] and (ii) high cutting efficiency. As determining the best gRNAs is still empiric, we first tested in K562 cells KO efficiency of four gRNAs (gRNA1, gRNA2, gRNA3, gRNA4) targeting the exon 10. We selected the gRNA1 which cuts 7 nucleotides downstream of T330 and gRNA3 which cuts 34 nucleotides downstream of T330 (**Figure 31**) as they both showed high KO efficiency (data not shown, done by R. M).

Figure 31: Schematic of gRNA1 and 3 cutting sites in exon 10 of CD45

gRNA1 and gRNA3 were designed as close as possible to the amino acids of interest.

Next, we wanted to assess KO efficiencies of gRNA1 and gRNA3 in primary human T cells. gRNA1 and gRNA3 were complexed into RNPs and electroporated in primary human T cells. We set up a flow cytometry panel: we stained cells with HI30 and MIRG451. The population MIRG451^{+}HI30^{+} was considered as non-modified WT form of CD45 and the MIRG451^{-}HI30^{-} population as KO. CD4 and CD8 cells were analyzed separately to see if we would observe differences of KO efficiency between the two types of cells (**Figure 32**).

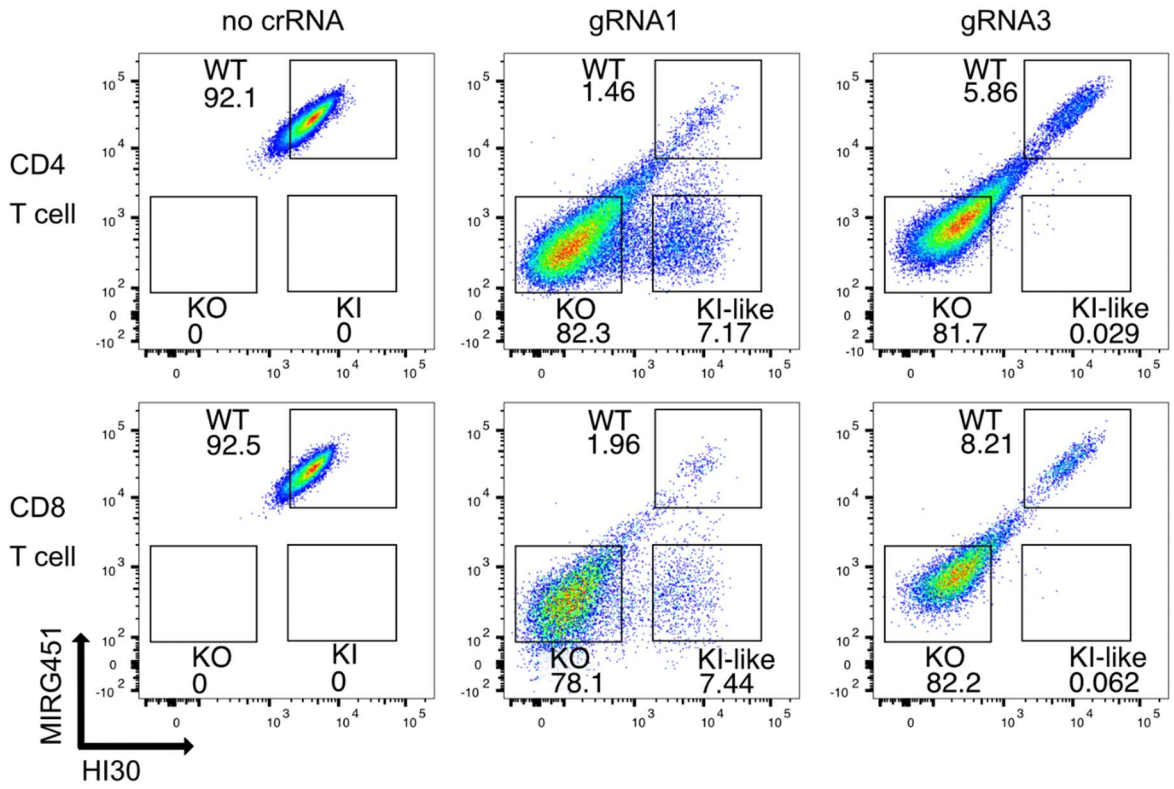

Figure 32: Testing of gRNA1 and gRNA2 cutting efficiency in human T cells

Representative flow cytometry plots of T cells knocked-out of CD45 with gRNA1 or gRN3. Flow cytometry analysis was performed using the anti-CD45 MIRG451 and HI30. MIRG451^{+}HI30^{+} population is considered as WT, MIRG451^{-}HI30^{-} is considered as KO and MIRG451^{-}HI30^{+} is considered as "KI-like". Control cells (no crRNA) were electroporated with Cas9 and tracrRNA but no crRNA. CD4 and CD8 cells were electroporated mixed but analyzed separately.

We observed similar KO efficiencies between gRNA1 and gRNA3. However, we observed a population HI30^{+}MIRG451^{-} when the cells were electroporated with gRNA1. Binding of HI30 means that the cells express the protein. However, loss-of-binding of MIRG451 means that its epitope is disrupted. This was unexpected as we did not intend to insert variants. NHEJ repair process is error-prone and can randomly insert or delete nucleotides around the DSBs generated by CRISPR/Cas9 [123]. We supposed that this random mechanism led to in-frame repairs with deletion of amino acids close or belonging to MIRG451 epitope, leading to a loss-of-binding of MIRG451 but a conserved binding of HI30. Identification of the mutations which led to this profile could be done by polymerase chain reaction (PCR) amplicons and Sanger sequencing but would be very time consuming. Other strategies would be to use NGS or single cell sequencing. As analyzing the introduced mutations was not the aim of our project, we did not

pursue further. To introduce only selected variants with HDRT, we decided to use the gRNA3, which did not show the variant "KI-like" population.

In order to introduce variants with CRISPR/Cas9 cut and HDR recombination, we designed HDRTs symmetrical around the Cas9 cut with a length around 100bp (**Figure 33**).

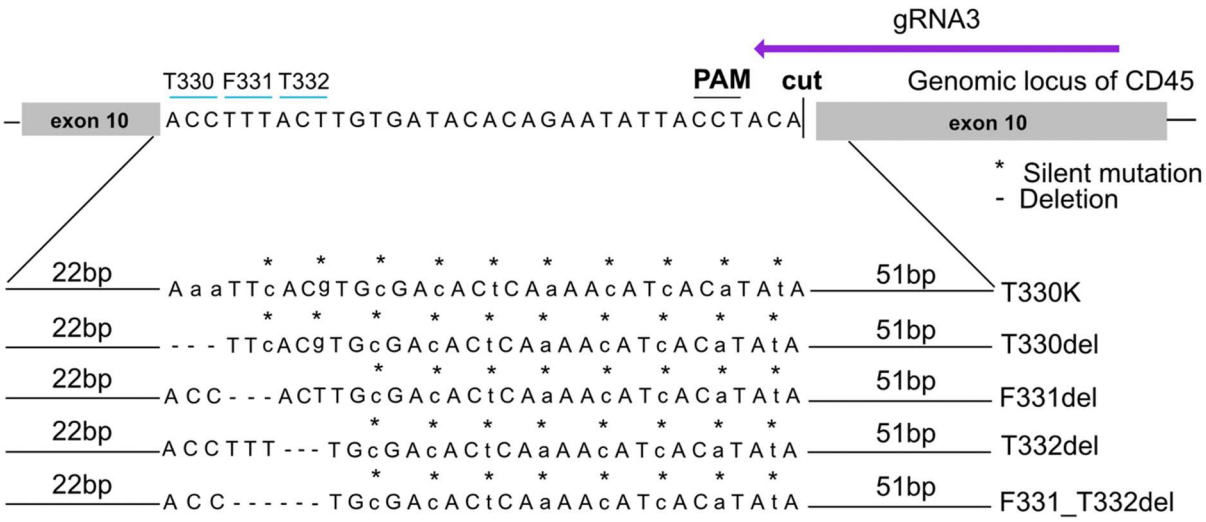

Figure 33: ssDNA HDRTs design for genome engineering of CD45 variants in primary human T cells

*Schematic of the ssDNA HDRTs designed to insert CD45 variants after cutting by gRNA3. * signals a silent mutation encoded in the HDRT. – signals a deletion encoded in the HDRT.*

In these templates, we inserted a PAM mutation in order to avoid re-cutting by Cas9 after insertion of the variants. In addition, we inserted silent point mutations between the cut site and the substitution in order to avoid the repair machinery switching to using the WT sequence and not integrating the full template sequence [96]. After electroporation of primary human T cells with RNPs and the designed HDRTs, we measured KO and KI efficiency by flow cytometry using the antibody combination described above. The KI population was identified as MIRG451^{-}HI30^{+} (**Figure 34**).

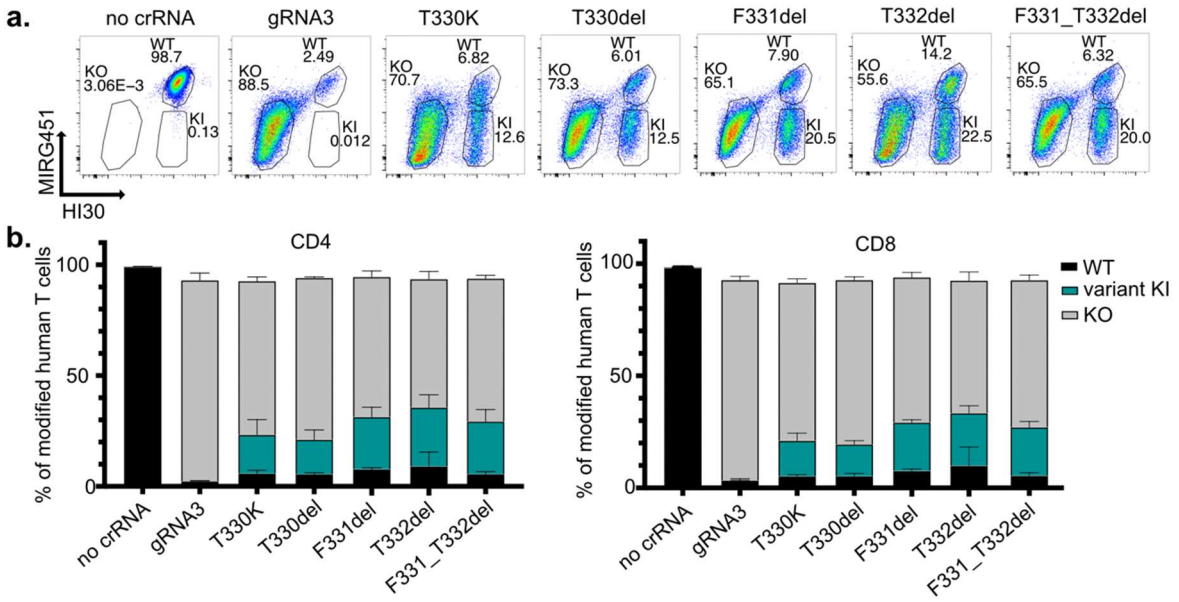

Figure 34: CD45 variants were efficiently engineered in human T cells

a. *representative flow cytometry plot of human T cells engineered with CD45 variants. KO and KI efficiency were analyzed by flow cytometry using the anti-CD45 MIRG451 and HI30 clones. Negative control cells (no crRN A) were electroporated with RNP and tracrRNA but no crRNA. KO control cells (gRNA3) were electroporated with RNPs complexed with gRNA3 but without HDRT.* ***b.*** *percentages of WT, variants KI, and KO population 4 days after electroporation in CD4 and CD8 populations. Data represent mean ± s.e.m (2 independent experiments)*

We observed a high KO efficiency for the cells electroporated with the gRNA3 without HDRT with about 90% of cells showing absence of CD45 at the surface across experiments. Similarly to previous studies [122], we observed a KI efficiency dependent on the distance between the variants inserted and the Cas9 cut. The closest variant, T332del, showed 22% of KI efficiency, while the variants F331_T332del and F331del showed 20% of KI and the furthest away variants, T330K and T330del, showed around 12% of KI efficiency. Similar efficiencies were observed in CD4 and CD8 T cells (**Figure 34b**). In order to confirm these observations, KI T-cells were sorted by flow cytometry and sequenced by Sanger sequencing (**Figure 35**).

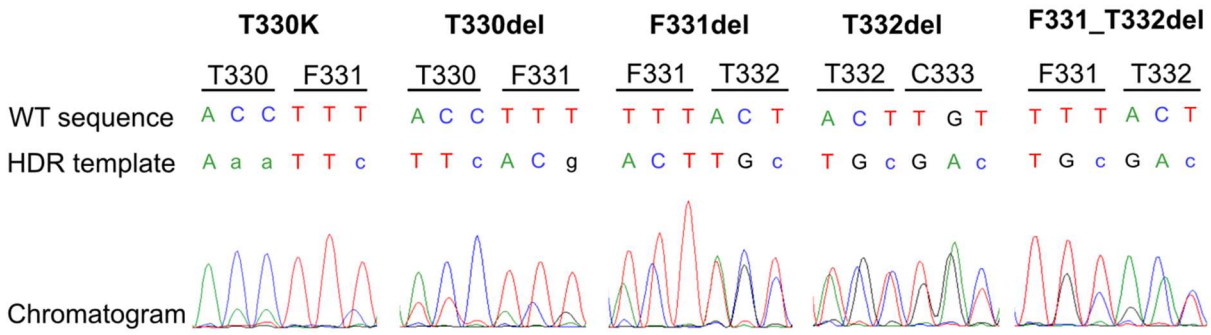

Figure 35: Sanger sequencing of KI human T cells

KI human T cells were flow cytometry sorted as HI30^{+}MIRG451^{-} and sequenced as bulk cells by Sanger sequencing.

We observed a similar trend as what we observed with flow cytometry: the variants localized the closest to the Cas9 cut site showed higher signal of the HDRT sequence. Despite the flow cytometry sorting of HI30^{+}MIRG451^{-} cells, a high proportion of WT sequence was observed by Sanger sequencing for all the variants. The "WT sequences" observed here cannot be pure WT, otherwise the cells would have bound MIRG451. We supposed that these sequences have indels not detected here that could have created upstream premature STOP codons. Thus, WT sequences in this sequencing likely indicate hemizygous cells KO/KI. To confirm this hypothesis and to identify the proportion of KI/KI cells, we could use single cell sequencing or NGS. However, we just aimed to confirm the cells enrichment with this sequencing analysis. To conclude, we successfully engineered primary human T cells with CD45 variants T330K, T330del, F331del, T332del and F331_T332del, and confirmed enrichment of the KI cells after flow cytometry sort with Sanger sequencing. Engineered primary human T could thus be used for shielding assay.

II.3.5.2- CD45 variants shield T cells from MIRG451-SAP killing

In order to demonstrate the shielding of the variants, we sorted engineered human T cells shown in **Figure 34** as variant KI, KO, or WT populations and each population was mixed with PBS, streptavidin-SAP, or MIRG451-SAP (**Figure 36**).

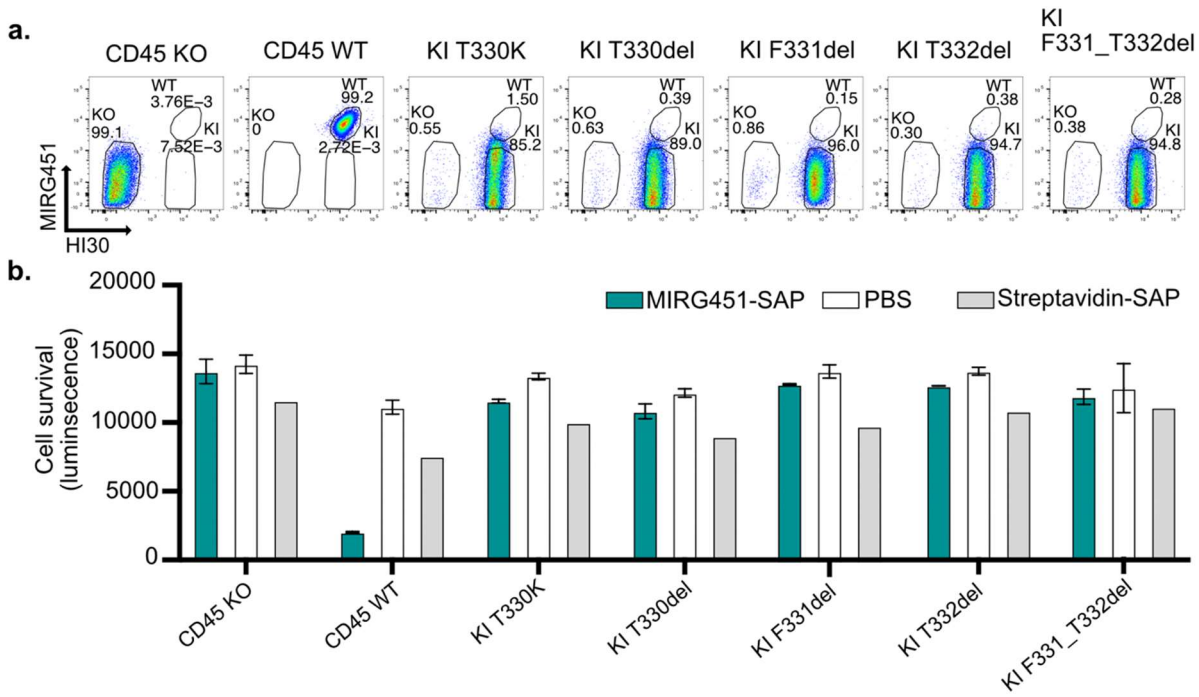

Figure 36: Shielding of engineered human T cells from MIRG451-SAP killing

***a**. representative flow cytometry plots of engineered T cells sorted for WT(MIRG451^{+}HI30^{+}), KO (MIRG451^{-}HI30^{-}) or variants KI (MIRG451-HI30+) profile. **b.** sorted human T cells incubated 3 days with 50 nM of MIRG451-SAP, 50 nM of unbound streptavidin-SAP or PBS. Cell survival was measured by luminescence. Data represent mean ± s.e.m (2 independent experiments).*

Sorting of cells allowed us to obtained populations highly enriched for WT, KO or KI profile (**Figure 36a**). We observed killing when the WT cells were incubated with MIRG451-SAP, but not when CD45 was knocked-out from the surface. Thus, absence of target protected cells from ADC killing, confirming the specific targeting of the therapy. No killing was observed for the cells expressing T330K, T330del, F331del, T332del and F331_T332del variants when they were incubated with MIRG451-SAP (**Figure 36b**). Thus, the CD45 variants shielded the primary human T cells from ADC killing. With this experiment we made the proof-of-concept that CD45 can be targeted with potent targeted therapies and that we can protect healthy cells by introducing point mutations in CD45.

To conclude, we established a highly efficient system of recombinant CD45 expression to screen available antibodies against the CD45 variants. The screening allowed to identified one anti-human mouse clone, QA17A19, which showed disrupted binding for several variants and was *de novo* sequenced to allow the generation of a chimeric antibody with a human Fc part and the variable chains of QA17A19: MIRG451. MIRG451 bound to saporin toxin was shown

to kill T cells but couldn’t kill them when they were engineered with the selected variants, showing in an *in vitro* proof-of-concept that CD45 variants could shield primary cells from targeted therapy.

II.4- Methods

Cloning of CD45RO in pCMV3 vector

DNA sequences primers used to clone the CD45RO from the CD45RABC isoform are listed in **Annex Table 4**. All DNA analysis were performed with DNASTAR Lasergene Version 17.2.1.61 and primers were ordered at Microsynth. All polymerase chain reactions (PCRs) described here were performed with the Phusion^{TM} High-Fidelity DNA Polymerase (F350, ThermoFischer).

CD45RABC is the full-length isoform of CD45. In the CD45RO isoform, exons A (exon 4), B (exon 5), C (exon 6) are not transcribed [100]. Coding DNA of full length CD45 (NM_002838.4) cloned in a pCMV3 vector was purchased from (Sino Biological, # HG14197-UT) and named pCMV-CD45RABC. In order to obtain the CD45RO form of the protein, the variable exons 4, 5 and 6 were removed from the pCMV-CD45RABC by two steps PCR. First, we amplified CD45RABC coding DNA (cDNA) from the leader peptide to the exon 3 before amplifying in another PCR the exon 7 to the C-terminus. PCR products were loaded on 2% agarose gel for a migration of 40 min at 110 V. The sequences were then purified using Nucleospin gel and PCR clean up (#740609, Macherey-Nagel) and the two fragments were mixed together for a third PCR with the forward primer of the leader peptide amplicon and the reverse primer of the C-terminus amplicon. The newly generated amplicon and the pCMV-CD45RABC plasmid were digested with XcmI and HindIII and the vector was dephosphorylated using Thermosensitive Alkaline Phosphatase (#M9910, Promega). Amplicon and vector were ligated using T4 DNA ligase (#EL0011, ThermoFischer), generating pCMV-CD45RO which was used for cloning of the point mutations.

Cloning of CD45 variants into pCMV-CD45RO

Primers used to insert point mutations are listed in **Annex Table 4**. Point mutations were inserted as following: (1) E329 was mutated to I and K, (2) T330 was mutated to E, D, R, K, I and deleted, (3) F331 was mutated to A, S, I, L and deleted, (4) T332 was mutated to A and deleted, (5) F331_T332 was deleted using the two steps PCR (**Figure 37**).

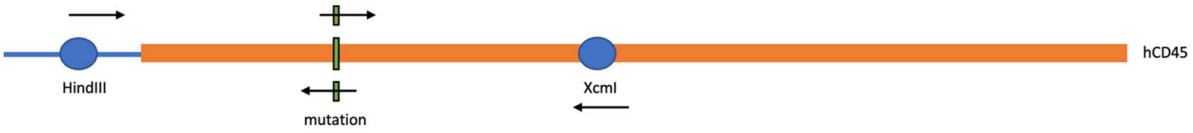

Figure 37: Two steps PCR for insertion of variants into CD45RO cDNA

Schematic representation of the two steps PCR strategy used to insert variants in the cDNA of CD45. The orange strand indicates CD45 cDNA. The blue rounds indicate restriction enzymes binding sites. Arrows indicate primers. The green band indicates the localization of the mutations inserted.

All point mutations were introduced into pCMV-CD45RO by two steps PCR. For each variant, the CD45RO cDNA was amplified from N-terminus to the point mutation with a generic forward primer encoding a HindIII restriction site and a reverse primer encoding for the variant. The sequence from the point mutation to C-terminus to was amplified with a forward primer encoding for the variant and a generic reverse primer encoding for XcmI restriction site. PCR products were loaded on a gel and purified on spin columns. The two amplicons were then mixed at a ratio 1:1 and amplified by PCR using the forward primer of the N-terminus sequence and the reverse primer of the C-terminus sequence. The final amplicon was cloned with the help of XcmI and HindIII into the pCMV-CD45RO.

De novo sequencing and production of MIRG451 antibody

QA17A19 antibody clone (biolegend, Cat#393402) was sent to RapidNovor Inc for *de novo* sequencing of the variable heavy and the variable light chain (sequences in supplementary **Annex Table 5**). The DNA sequence of the variable heavy chain (VH) was codon optimized and synthetized at GenScript® (**Annex Table 5**). The VH chain DNA sequence was amplified by PCR using a forward primer added with an AgeI restriction site and three amino acids from the leader peptide as AgeI cuts three amino acids before its end. The reverse primer encoded for a restriction site for SalI followed by two nucleotides in order to keep the sequence in frame with the constant part of the heavy chain encoded in the plasmid. VH sequence was cloned under hCMV promoter in plasmid 80795 from Addgene, encoding for human IgG1 isotype constant heavy chain [116] The new plasmid was named hCMV-VHQA17A19

The DNA sequence of the variable kappa light chain (VKL) was codon optimized and synthetized at GenScript® (**Annex Table 5**). VKL DNA sequence was amplified by PCR using a forward primer added with an AgeI restriction site and three amino acids and a reverse primer encoding for the restriction site for BsiWI. PCR amplified VKL sequence was cloned under hCMV promoter in plasmid 80796 from Addgene encoding for Human kappa constant light

chain [116]. The new plasmid was named hCMV-VKLQA17A19. Both plasmids were co-transfected in CHO-S cells for expression of secretory immunoglobulin heavy and light chain.

CHO-S cell culture and transfection for MIRG451

CHO-S were thawed and grown in roller bottles at 37°C and 5% CO_2 in PowerCHO^{TM} 2 Serum-free medium (Lonza: BELN12-771Q), supplemented with 2 mM GlutaMAX^{TM} (#35050-038, Gibco), 100 µM HT supplements (#41065012, Gibco) and 1 X Antibiotic-antimycotic (# 15240-062, Gibco)) for 10 days until they reached the number of of $2x10^9$ cells. The day of the transfection, $2x10^9$ cells were centrifuged and resuspended in 500 ml ProCHO^{TM} 4 Protein-free CHO medium (Lonza #BEBP12-029Q supplemented with 1X HT, 2 mM GlutaMAX^{TM} and 1X Antibiotic-antimycotic). Cells were added with a mixture of 0.8 mg of hCMV-VHQA17A19 plasmid and 0.8 mg of hCMV-VKLQA17A19 plasmid added slowly to 5 ml of Polyethylenimine (PEI), linear, MW 25000 (#23966, Polysciences) at 1 mg/ml. CHO-S cells were then distributed in four 500 ml roller bottles and let grown for six days at 31°C, 140 rpm, in a 5% CO_2 incubator.

MIRG451 purification

After six days of production, CHO-S cells were centrifuged for 20min at 3000rpm. Supernatant was filtered through a 0.22 µm filter and applied on a Protein A-Sepharose^{TM} 4B (#101042, ThermoFischer) column prewashed with PBS. Column was then washed with 100 ml PBS and MIRG451 was eluted using an elution buffer made of 0.1 M glycine pH=2.2. Fractions of 0.5 ml were collected and antibody concentration in the fractions was measured at OD 280 nm considering a molar adsorption coefficient of 210,000M^{-1} cm^{-1}. The final amount was calculated considering that 1 OD = 1.4 mg/ml. High concentration fractions were pooled and dialyzed twice overnight against PBS.

K562 CD45 KO cell line generation

K562 were maintained in RPMI-1640 medium (#R8758, Sigma-Aldrich) supplemented with 10% heat-inactivated FCS and 1% GlutaMAX^{TM} and splitted every 2-3 days at the density $1x10^6$ cells/ml. K562 $CD45^+$ cells were sorted as bulk with flow cytometry (BD Aria III) and were electroporated three days later with RNPs targeting CD45 locus using the Neon^{TM} Transfection System. RNPs were prepared as described in "RNPs preparation for KO and KI experiments" from chapter I. Briefly, crRNA and tracrRNA were annealed in a 1:1 molar ratio

in order to complex into a 80 µM gRNA solution. They were then mixed 1:1 by volume to 40 µM recombinant Cas9 (University of California Berkeley) in order to get a 2:1 gRNA:Cas9 ratio [124] then complexed for 30 min at room temperature (RT) in the dark.
Following RNPs preparation, two millions of $CD45^+$ cells were washed two times in PBS then re-suspended in 100 µl R buffer. Re-suspended cells were mixed with 10 µl of RNPs and electroporated using the program 1450 V, 10 ms, 3 pulses. Cells were kept in 1 ml of fresh medium in 24 well plate at 37C 5%CO_2 for 4 days before sort of the knocked-out cells by flow cytometry.

Expression of CD45 variant plasmids
The HEK293 was a kind gift of M. Zavolan (Biozentrum Basel). The cells were cultured in Dulbecco's Modified Eagle's Medium - high glucose (#D5796 Sigma-Aldrich) supplemented with 10% heat-inactivated FCS and 2 mM GlutaMAX™ at 37°C with 5% CO_2. One day before electroporation, cells were seeded at 50% confluency in fresh medium. For each electroporation, $2x10^6$ HEK293 cells were washed twice in FACS buffer (PBS with 2% FCS) then re-suspended in 110 µl of R buffer. For each electroporation, a mixture of 5.85 µg of plasmid encoding for one CD45RO variant and 0.65 µg of plasmid encoding for G418 resistance gene were added to the cells. Plasmid encoding for 418 resistance gene used was the pEGFP-N1 vector, a kind gift from Simona Rossi, where green fluorescent protein (GFP) was removed. Cells were electroporated at 1100 V, 20 ms, 2 pulses conditions. Two days after electroporation, they were put under G418 selection with the addition of Geneticin G418 (#4-15F01-H, Bioconcept) at the concentration of 350 µg/ml. At the end of the selection, 19 days after incubation with G418, electroporated HEK293 cells were stained with the anti-CD45 HI30 and sorted by clow cytometry for high expression of CD45.
Electroporation of plasmids encoding for the CD45 variants in K562 CD45KO bulk was performed as following. Two millions of cells were washed two times in PBS then re-suspended in 100 µl R buffer. Re-suspended cells were mixed with 6.5 µg of plasmid and electroporated using the K562 program 1450 V, 10 ms, 3 pulses. Cells were kept in 1 ml of fresh medium in 24 well plate at 37C 5% CO_2 for 1 day before staining of $0.25x10^6$ cells with anti-CD45 antibodies for flow cytometry analysis.

ADCC on transiently electroporated K562
ADCC assay was performed as described in chapter I.

Primary human T cells isolation and activation

Human T cell isolation was performed as described in chapter I.

Human T cells engineering with variants

Human T cells were electroporated after activation using the 4D-Nucleofector™ system (Lonza) as described in chapter I. Briefly, for each electroporation, $1x10^6$ activated T cells were washed once in PBS and resuspended in 20 µl Lonza supplemented P3 electroporation buffer (#V4XP-3032, Lonza). Freshly prepared RNPs added with PGA (Sigma-Aldrich) were mixed with 50 pmols of 100 bp single-stranded oligodeoxynucleotides HDRT (Ultramer DNA Oligonucleotides, IDT) encoding for a variant. The two gRNA 1 and 3 sequences tested are listed in **Annex Table 6**. All HDRTs used are listed in **Annex Table 7.** The T cells were then added and the whole volume was transferred into the 16-well Nucleocuvette™ strips for electroporation with the program Program EH-115. Immediately following electroporation, 80 µl of prewarmed supplemented medium was added to each cuvette and cells were incubated at 37°C. After 20 min the cells were transferred into 48-well culture plates at $1x10^6$ cells/ml and replenished with IL-2 500 U/ml. The medium and IL-2 were replenished every two days, and the cells were kept at a cell density of $1x10^6$ cells/ml. Four days after electroporation cells were scanned with flow cytometry and five days post-electroporation, they were flow sorted as CD45 WT cells ($HI30^+$, $MIRG451^+$), CD45KO cells ($HI30^-$, $MIRG451^-$) or CD45KI cells ($HI30^+$, $MIRG451^-$). Immediately after the sorting the supplemented medium was complemented with 1% Penicillin-Streptomycin and IL-2 (50U/ml) and the cells were rested for one day until they were used for killing assay.

Human T cells MIRG451-SAP killing assay

Killing curve was performed in order to determine the best condition for killing of human T cells knocked-in with CD45 variants. Prior to killing curve assay, human T cells were activated in order to mimic the conditions of engineered cells. Following activation, the T cells were separated from the dynabeads and dispersed as 5000 cells per well in 100 µl in fresh medium containing 500U/ml IL-2. Assay was developed according to the protocol presented in the paper from Palchaudhuri et al [21]. Cells were plated into wells of white cell culture microplate with clear bottom (mCLEAR®, CELLSTAR®, greiner bio-one). MIRG451-biotinilated and streptavidin-SAP (#IT-27, ATSbio) were mixed at the ratio 1:1 in PBS as a stock solution of 1 pmol/µl then added to the cells. Various volumes were taken from the stock solution in order to reach the final concentrations 0.1 nM, 0.5 nM, 1 nM, 5 nM, 10 nM, 50 nM, 100 nM of

MIRG451-SAP in the wells. Cells were incubated three days at 37C 5% CO_2 and amount of living cells was measured with CellTiter-Glo® 2.0 (#G9241, Promega) according to the following protocol: 100 µl of RT equilibrated CellTiter-Glo® 2.0 were added to 100 µl of RT equilibrated cells and were shaked 2 min then incubated 10 min at RT. Luminescence was read with the Synergy H1 (BioTek) with an integration time of 1 s.

Human T cells engineered with CD45 variants and sorted were cultured overnight with supplemented medium complemented with 1% Penicillin-Streptomycin and IL-2 (50U/ml) before killing assay. Killing assay of engineered cells was performed as described above with 50 nM of MIRG451-biot:strep-SAP mixed at ratio 1:1.

Flow cytometry and cell sorting

All antibodies used for flow cytometry staining are listed in **Annex Table 8**.

Flow cytometry was performed as described in chapter I. Data acquisition was performed on BD LSRFortessa with the BD FACSDiva Software, and data were analyzed with FlowJo Software (FlowJo version 10.7.1).

The primary T cells were stained as in chapter I. Briefly, they were successively stained with fixable viability dye then with fluorescently labelled antibodies for 20 min at RT in the dark. Fort the biotin-labelled MIRG451, the secondary staining with streptavidin was performed with the same incubation conditions. The stained cells were washed once in FACS buffer and then acquired immediately.

For flow cytometry cell sorting the cells were stained with anti CD45 HI30 (FITC) and anti-CD45 MIRG451 (biotin) before being stained with strep-PE. They were then sorted using the BD FACSMelody^{TM} Automated Cell Sorter. Three populations were sorted per sample: CD45 WT cells ($HI30^+$, $MIRG451^+$), CD45KO cells ($HI30^-$, $MIRG451^-$) and CD45KI cells ($HI30^+$, $MIRG451^-$).

Chapter III:
Optimization of base editors for CD45 genome engineering

III.1- Introduction

In this chapter, we aimed to optimize base editing as an alternative genome engineering approach to insert the desired variants in the CD45 endogenous genomic DNA. In the first two chapters we established the feasibility and potential benefit to shield cells by introducing CD123 and CD45 variants in the cells' DNA. Due to its relative ease of use we employed CRISPR/Cas9 and HDR. However, HDR relies on the generation of DSBs which results in indels that bear the risk of unwanted mutations, p53 activation and an increased risk for chromosomal translocations. In addition, the DNA HDRT is toxic to cells [74]. Therefore, avoiding DSBs and delivery of the genome editing tools as mRNA/RNA which results in higher cell viability would be desirable. In contrast to nucleases, BEs introduce only one cut to the DNA strand (a nick) and can edit Adenines (As) into Guanines (Gs) with the ABEs, or Cytosines (Cs) into Thymines (Ts) with the CBEs. Thus, they may represent a valuable alternative to the use of HDR to introduce amino acid substitutions. However, they face many restrictions due to their mechanism of action. BEs are complex molecules composed of several distinct proteins. They contain a deaminase, a nickase, which is a Cas9 engineered to cut only one DNA strand (Cas9n) and in the case of CBE, an uracil DNA glycosylase inhibitor (UGI). During the editing by the CBE, the cytidine deaminase APOBEC edits Cs on one strand of DNA by removing their amine group, turning them into Uracils (U) (**Figure 38**).

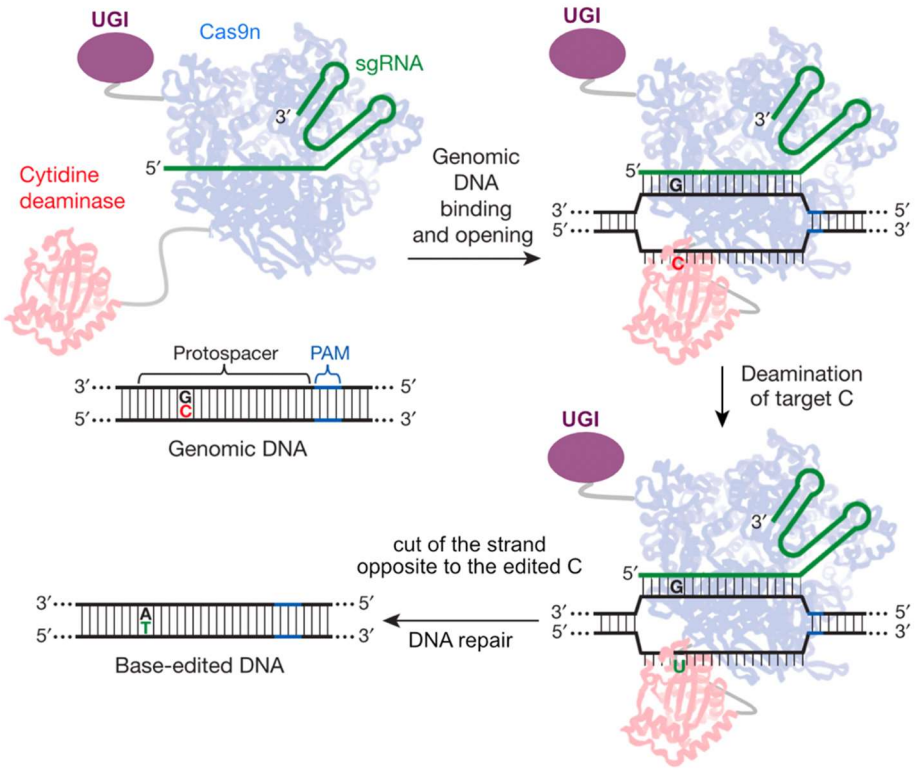

Figure 38: Base editing mechanism of C to T

CBE turn C into T by deamination of C, leading to U. Cas9n: nickase. UGI: Uracil DNA glycosylase inhibitor. Figure adapted from [69] *license nr: 5421380816180*

Following the deamination of the C, the opposite strand is cut by the nickase. This nicking is immediately followed by a repair using the deaminated strand as template. During this restoration, A, the nucleotide complementary to U, is inserted in the repaired DNA strand instead of the original G. Thus, the DNA is repaired with complementary nucleotides, but still contains a U. Later, the U is corrected from the edited strand and is replaced by a T by complementarity with the A previously inserted. Thus, Cs are deaminated by the CBE and turned into Ts. UGI is attached to the Cas9n-deaminase complex to prevent the cells from correcting the U before the end of the full process [69]. ABEs works similarly. Their deaminase, the TadA, removes the amine group from As and turn them into Inosines. Then, the nickase cuts the non-edited strand and the full resolution of the editing leads to the exchange of the original As with Gs [70]. However, BEs face restrictions in editing and cannot edit all C or A from the genome. They recognize the DNA strand thanks to their Cas9n which, similarly to the original Cas9, needs a protospacer followed by a PAM sequence to initiate the cut. Thus, similarly to Cas9, not all protospacers and PAM associated allow an efficient recognition and cut. In addition, the structure of the BE allows editing only in a region within the protospacer,

named editing windows which can vary between 4 and 12nt depending on the BE [125] (**Figure 39**).

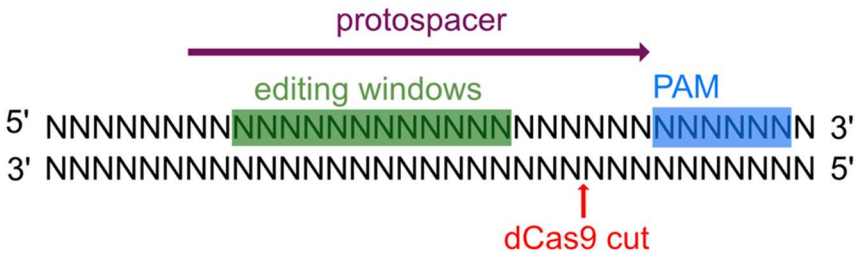

Figure 39: Editing windows of the CBE BE3

Editing by BEs occurs within protospacer in the editing window which is can vary between 4nt and 12nt length.

Thus, nucleotide editing is limited to small regions near PAM sequences, within protospacer allowing efficient binding of the Cas9n to DNA. These restrictions explain why many projects focused on engineering the most used S. *pyrogenes* Cas9 in order to increase the potentially recognized PAMs. Optimization studies allowed to reach the following PAMs: NRRH, NRCH, NRTH[126], NGN, NYN[127] and NG [128]. Here, N stands for any nucleotides, R for G or A and H for A, C or T. Another study also exchanged the *S. pyrogenes* Cas9n with *S. aureus* Cas9n to hit the PAM NNNRRT. This led to the generation of the CBE SaKKH-BE3 [129]. These new PAMs mean that more bases are in regions accessible for BE. This is key for the introduction of point mutations for shielding: this increase of possibilities increases our chances to hit an amino acid preserving the function of the protein but leading to a loss-of-binding of an antibody. To conclude, BEs are powerful tools with a potentially better safety profile than CRISPR/Cas9 HDR but introducing amino acids substitutions with BEs faces restrictions. Thus, they must be carefully chosen and optimized in order to insert the wanted mutations.

III.2- Aims and objectives of the chapter

In this chapter, we aimed to optimize base editing strategies to insert point mutations in the CD45 locus. To reach this goal we set up several aims:

- Optimize base editing of the FANCF locus with SaKKH-BE3 in K562 cells to establish a positive control for SaKKH-BE3 editing
- Test base editing of T330I in CD45 with SaKKH-BE3 in K562
- Screen available protospacers/BEs around the positions E328, T330, F331, T332 in the CD45 locus and assess the editing efficiencies associated
- Test if primary human T cells could be edited in the CD45 locus by electroporation of BE mRNA

III.3- Results

III.3.1- SaKKH-BE3 allowed 100% base editing efficiency of FANCF locus in K562 cells

Instead of CRISPR/Cas9, BEs can be used to edit point mutations. They do not generate DSBs, and are thus safer to use than CRISPR/Cas9. In order to have an alternative to CRISPR/Cas9, we aimed to develop base editing of the CD45 locus amino acid positions E329, T330, F331 or T332. However, BEs come with a lot of restrictions. These restrictions made that when the project started, only T330 was potentially editable by the available CBE SaKKH-BE3 which turns C into T and recognizes the PAM NNRRT [129]. The mutation potentially inserted by SaKKH-BE3 editing was T330I.

To gain experience with this BE, we first wanted to validate a positive control. It was shown that SaKKH-BE3 can edit the FANCF locus when used in HEK293 cells. SaKKH-BE3 edited three Cs of the DNA sequence CCAATC into Ts when electroporated with the single guide RNA (sgRNA) FANCF1, leading to TTAATT sequence [129] (**Figure 40a**). As we aimed to use SaKKH-BE3 for editing of CD45 in further steps, we first optimized base editing of FANCF in a cell line highly expressing CD45 and easy to transfect. Therefore, we selected the K562 cell line. The cells were electroporated with two plasmids: one encoding for the BE and one encoding for the sgRNA FANCF1. In the BE plasmid, expression of SaKKH-BE3 was linked to GFP in order to assess its expression. Thus, following transfection, K562 cells expressing GFP were sorted and we compared the editing efficiency between non-sorted and sorted cells. Two types of cells were sorted: GFP^- (no expression of SaKKH-BE3) and GFP^+ (high expression of SaKKH-BE3). This protocol allowed to test several optimizations of the BE plasmid (**Figure 40**).

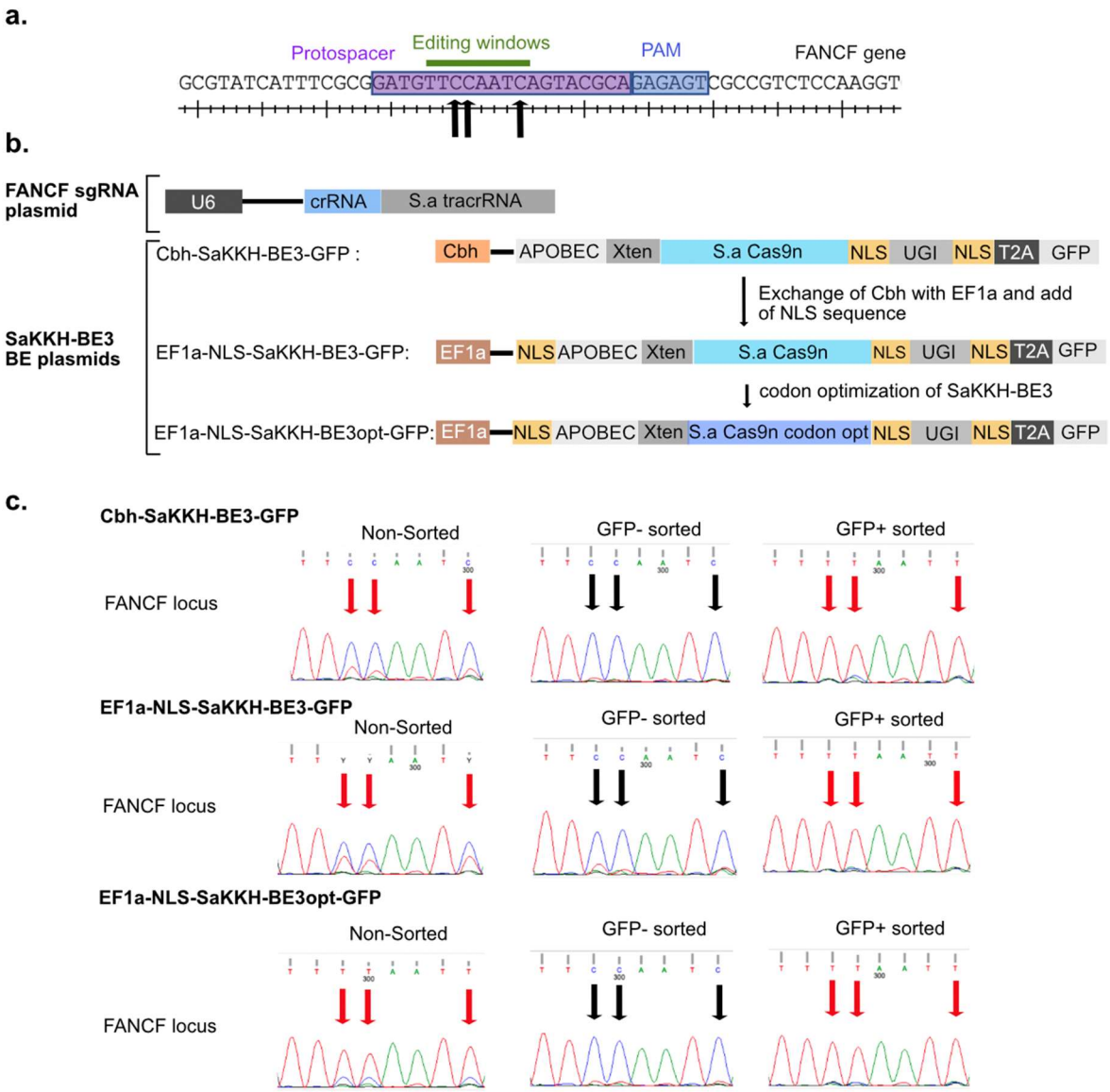

Figure 40: Optimization of SaKKH-BE3 editing of FANCF in K562 cells

a. *Schematic crRNA FANCF1 editing. Protospacer (purple), PAM (blue) and editing windows (green) of crRNA FANCF1 are represented in the FANCF gene. Black arrows indicate nucleotides potentially edited by SaKKH-BE3* ***b****. Plasmid optimization strategy. FANCF sgRNA plasmid: plasmid encoding for the protospacer presented in (a) followed by S. aureus tracrRNA under the control of U6 promoter. SaKKH-BE3 BE plasmids: plasmids used to express SaKKH-BE3 in K562 cells. Arrows between SaKKH-BE3 base editor plasmids indicates optimizations. NLS: nuclear localization signal. APOBEC: Deaminase turning C into U. S.a Cas9n: S. aureus Cas9 nickase. Xten: linker. UGI: Uracil DNA Glycosylase inhibitor. T2A: self-cleaving peptide* ***c****. Sanger sequencing of K562 electroporated with plasmids described in (b). The nucleotides showed correspond to the editing windows of SaKKH-BE3 with crRNA FANCF1. Black arrows indicate nucleotides potentially edited. Red arrows indicate nucleotides edited*

In the unsorted bulk cells electroporated with Cbh-SaKKH-BE3-GFP, an estimated 20% of editing was observed for the targeted Cs. In contrast, in the sorted GFP^+ cells, base editing efficiency was 100%. Ratio of electroporated BE plasmid:sgRNA plasmid in moles is 1:1. As all GFP^+ cells were edited, we concluded that gRNA was present in necessary quantities for editing (**Figure 40c**). The 20% of editing in the bulk cells reflect the cells that efficiently expressed the BE as we observed around 20% of GFP^+ cells by flow cytometry (data not shown). This is supported by the finding that no editing occurred in the GFP- cells. In order to increase the base editor expression, we exchanged the Cbh promoter with EF1α as it was shown to induce high transgene expression in $CD34^+$ [130] and K562 cell line was isolated from a patient with CML, so may have similar properties to hematopoietic stem cells [114]. We also added a nuclear localization signal (NLS) sequence on the N-terminus of SaKKH-BE3 as it was shown to improve base editing efficiency [131] (**Figure 40b**), leading to the generation of the optimized plasmid EF1a-NLS-SaKKH-BE3-GFP. After transfection with EF1a-NLS-SaKKH-BE3-GFP, we observed an increased editing efficiency in the bulk of non-sorted cells compared to the non-optimized plasmid with around 40% of sequences edited (**Figure 40c**).

Cas9 are proteins of bacterial origin, and it was shown before that codon optimization increases expression of *S. Pyrogenes* Cas9 in mammalian cells [131132]. We therefore codon-optimized the *S. aureus* Cas9 of SaKKH-BE3 for use in mammalian cells (**Figure 40b**). Electroporation of K562 cells with the EF1a-NLS-SaKKH-BE3opt-GFP plasmid dramatically increased editing efficiency even in unsorted cells. To conclude, we efficiently optimised the SaKKH-BE3 plasmid for BE expression in transfected K562, allowing us to reach a high base editing efficiency of the FANCF locus (**Figures 40c**). The optimized EF1a-NLS-SaKKH-BE3opt-GFP plasmid could be used for editing of other loci.

III.3.2- CD45 locus of interest cannot be edited by SaKKH-BE3 but is efficiently edited by ABEs

III.3.2.1- SaKKH-BE3 showed no editing of T330I

Using the optimised EF1a-NLS-SaKKH-BE3opt-GFP plasmid, we tested the base editing of T330I in K562 (**Figure 41**).

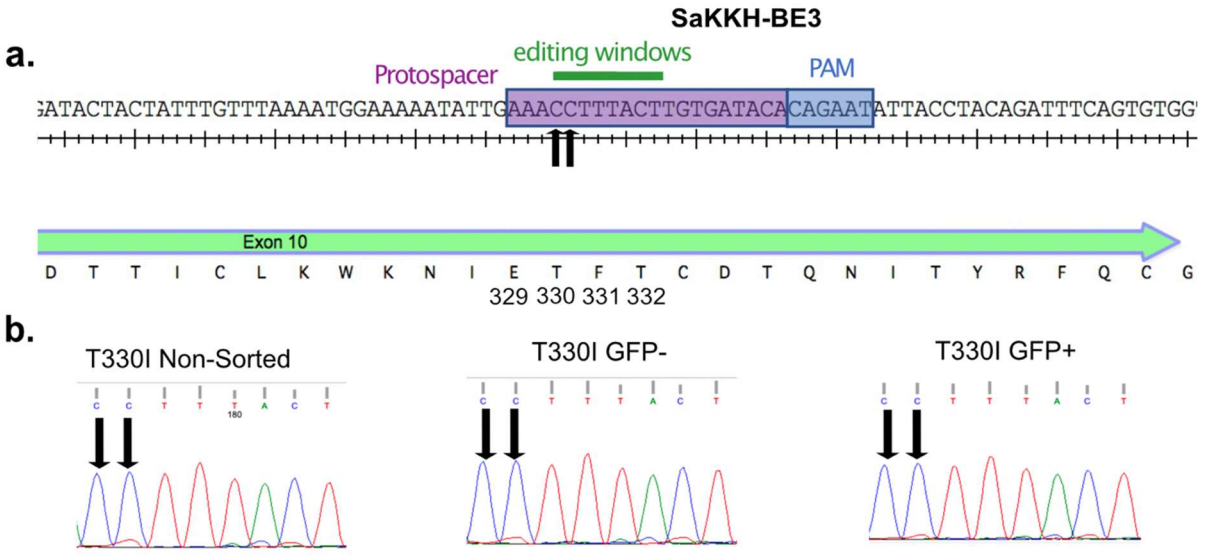

Figure 41: Comparison of Thr330Ile editing efficiencies between GFP sorted and non-sorted cells

a. *Schematic of crRNA T330I editing. Protospacer (purple), PAM (blue) and editing windows (green) of crRNA T330I are represented in the exon 10 of CD45 gene.* ***b.*** *Sanger sequencing of the editing window of crRNA T330I of non-sorted, GFP⁻ and GFP⁺ sorted cells after SaKKH-BE3 editing. Black arrows indicate nucleotides potentially edited by SaKKH-BE3.*

Despite use of the highly active, optimized EF1a-NLS-SaKKH-BE3opt-GFP plasmid, no editing was observed in non-sorted bulk cells as well as in GFP^+ sorted bulk cells. This result suggested that although SaKKH-BE3 can efficiently edit the FANCF locus using crRNA FANCF1, the T330 position cannot be edited with the current combination of base editor/sgRNA.

III.3.2.3- CD45 exon 10 was efficiently edited with several ABEs

Our previous results are highly encouraging because we found a BEs that can edit up to almost 100% of cells and the editing was very clean. Thus, this strategy could be very attractive. However, we also found that the particular edit we wanted to introduce, T330I, did not work at all. Therefore, we looked for alternatives to see if BEs could work in amino acids located around the position 330, 331 and 332. We screened several CBEs and ABEs adapted for different PAMs around the positions 329-331. We tested ABE 7.10 [70], SaKKH-ABE8 [129], ABE8e-NG [128], ABEmax-SpG, ABEmax-SpRY, CBEmax-SpRY [127], CBE-NRRH and CBE-NRCH [126]. The screening revealed that ABE 7.10 allowed editing of Y340C and ABEmax-SpG and ABE8e-NG allowed editing of I328V (**Figure 42**).

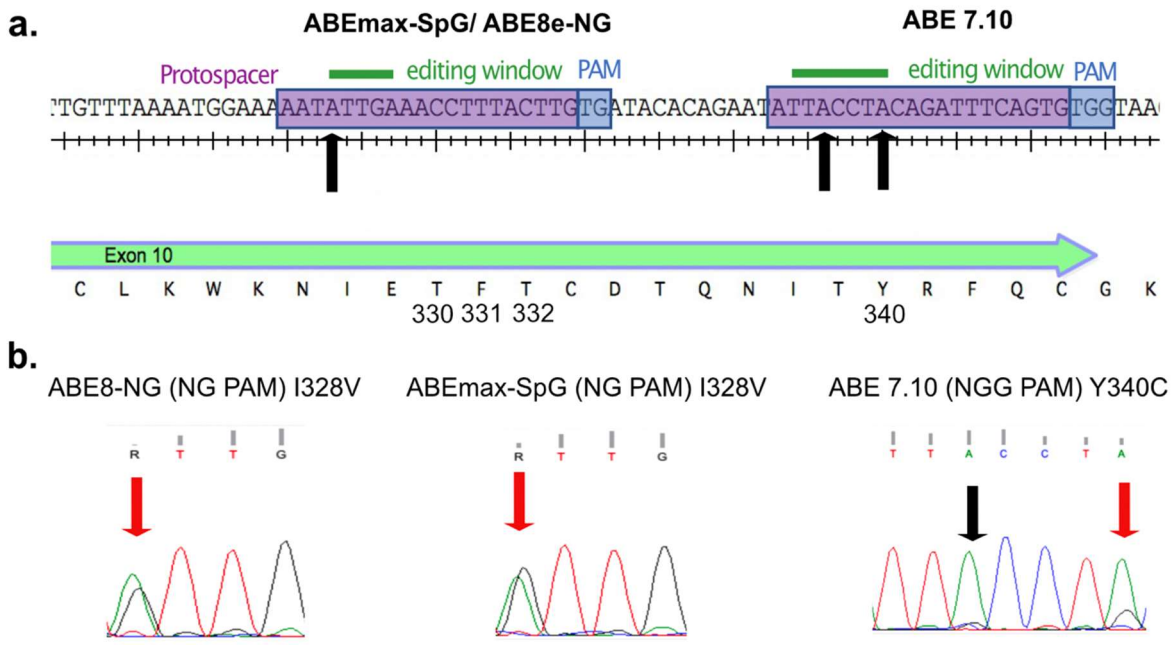

Figure 42: Editing of ABEmax-SpG, ABE8e-NG and ABE 7.10 on CD45

a. *Schematic of the binding site of ABEmax-SpG, ABE8e-NG and ABE 7.10 in the exon 10 of CD45. Black arrows indicate nucleotides potentially edited by BEs.* ***b.*** *Sanger sequencing of non-sorted cells after base editing. Red arrows indicate nucleotides edited. Area of Sanger sequencing displayed correspond to the editing windows of the BE.*

ABE8e-NG and ABEmax-SpG showed the same editing of almost 50%, indicating a good editing efficiency. Thus, we showed that the CD45 locus could be edited by BEs, but we were unable to edit the variant T330I. In addition, there is no strategy available with BEs to edit the variant of interest T330K: we would need to edit ACC into AAA or AAG and we can only turn C into T or A into G. We concluded that BEs are of interest but due to their limitations (low flexibility, low efficiency depending on the target) not straightforward. Nevertheless, the results triggered a separate project to screen base editable sites of CD45 with the goal to identify shielding variants (Garaudé, unpublished results).

III.3.2.4- ABEmax-SpG edited human T cells when electroporated as mRNA

Plasmids are often not suitable for clinical translation due to the risk of persistence of the DNA and insertion into the endogenous DNA. Moreover, plasmid transfection often results in reduced viability of primary cells. In contrast, purified recombinant proteins which will be rapidly degraded are preferred. In the case of BEs, expression as recombinant protein is complex due to the composition of the BEs themselves: they often contain a bacterial part (Cas9) and a mammalian part (APOBEC for CBE). In order to use BEs to edit therapeutic cells,

mRNA would be the ideal format for electroporation as it would overcome the issues linked to production of recombinant protein expression but would be degraded soon after injection, avoiding the issues of DNA insertion into the genome. In order to demonstrate that BEs as mRNA could be ready for translation, we developed a protocol of BE ABEmax-SpG mRNA electroporation in T cells for I328V editing (**Figure 43**).

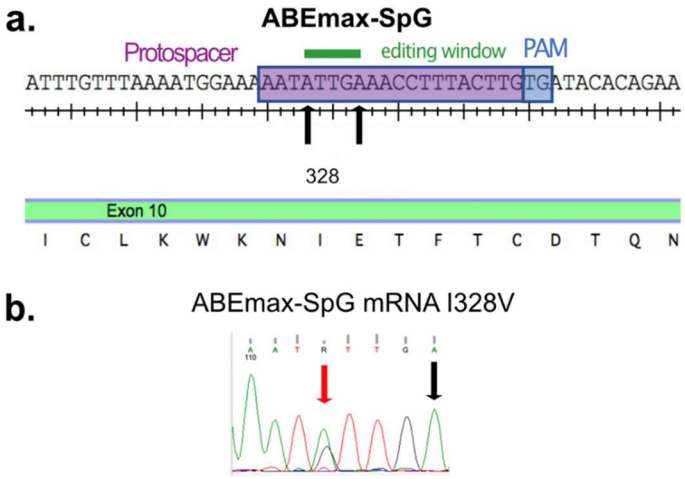

Figure 43: Editing of primary human T cells with ABEmax-SpG mRNA

a. *Schematic of the binding site of ABEmax-SpG in the exon 10 of CD45.* ***b****. Sanger sequencing of non-sorted cells after base editing. Black arrow: nucleotides potentially edited. Red arrow: nucleotides edited*

Base editing of 20% was reached in T cells, demonstrating that we could introduce a selected mutation into the genome of primary human T cells using BE mRNA.

To conclude, we showed that BEs can be highly effective with 100% of FANCF locus editing with SaKKH-BE3 and 50% of CD45 locus editing with ABEmax-SpG and ABE8e-NG. In addition, we showed that BEs can be electroporated as mRNA in primary cells and edit the CD45 locus. This is an advantage for translation as mRNA is safer than DNA and easier to produce than recombinant protein. However, it was not trivial to find the BE that installs the precise edit we want. Thus, although base editors are promising, for now CRISPR/Cas9 and HDR provides more flexibility since the template allows to install any desired amino acid substitution, particularly deletion which were shown to shield cells from MIRG451 but cannot be inserted by BEs.

III.4- Methods

Base editors cloning

Sequence of SaKKH-BE3 was copied from the paper of Kim et al [129] and inserted into px458 plasmid backbone which was a gift from Feng Zhang (#48138, addgene) [133] after digestion with AarI and NotI (done by R. M), resulting in Cbh-SaKKH-BE3-GFP plasmid.

Exchange of the CBh promoter with EF1a-NLS was started with a PCR amplification of the EF1a sequence from the plasmid lenti dCAS-VP64_Blast which was a gift from Feng Zhang (Addgene #61425) [134] with a forward primer containing an XbaI restriction site and a reverse primer containing a NLS sequence and a NheI restriction site. The plasmid backbone was amplified from Cbh-SaKKH-BE3-GFP with a forward primer encoding for a NheI restriction site and a reverse primer encoding for an XbaI restriction site. Both amplicons were loaded on a 1% agarose gel and ran 40 min at 110 V then cut and purified. Purified DNA sequences were digested with XbaI and NheI and ligated together after dephosphorylation of the Cbh-SaKKH-BE3-GFP backbone amplicon and the phosphorylation of EF1a-NLS fragment with T4 PNK (#M0201, NEB), generating the plasmid EF1a-NLS-SaKKHBE3-GFP.

In order to improve protein expression, the sequence of SaKKH-BE3 was codon optimised using the GenSmart™ Codon Optimization tool from GeneScript® and synthetized at GeneScript® as plasmid. It was exchanged with the SaKKH-BE3 sequence of the EF1a-NLS-SaKKH-BE3-GFP plasmid by enzymatic digestion of the two plasmids with BamHI and PpuMI, creating the new plasmid EF1a-NLS-SaKKH-BE3opt-GFP.

gRNA expression plasmids for co-transfection with SaKKH-BE3 plasmids were constructed by ligation of protospacers into BPK2660 which was a gift from Keith Joung (plasmid #70709) [135] after digestion of both with BsmBI. Protospacers were ordered as complementary primers and were prepared for the digestion with a phosphorylation step of 30 min at 37°C with T4 PNK and an annealing step of 5 min a 95°C, 20 min at 65°C and 10°C as final temperature.

sgRNA plasmids encoding for S.Pyrogenes Cas9 tracRNA were constructed by ligation of protospacers into px458 where Cas9 and GFP genes were removed. Ligation was performed as described above using digestion with BsmBI. They were co-transfected with BE4max-NRRH (#136918, Addgene) , BE4max-NRCH (#136920, Addgene), NG-ABE8e (#138491, Addgene), or ABE7.10 (#102919, Addgene) which are gift from David Liu [126] [128] [70] but as well with ABEmax-SpG (#140002, Addgene) , ABEmax-SpRY (#140003, Addgene), CBE4max-SpRY (#139999, Addgene) which are gifts of Benjamin Kleinstiver [136].

List of BE protospacers tested for screening of base editing on CD45 can be found in **Annex Table 9**.

BEs electroporation in K562 and primary human T cells

For each plasmid BEs electroporation, $2x10^5$ K562 cells were washed twice in FACS buffer (PBS and 2% FCS) and re-suspended in 11 µl of R buffer. Cells were then mixed with 0.65 µg of DNA containing 487.5 ng of BE plasmid and 165.2 ng of sgRNA plasmid. The mixture was electroporated using K562 program (1450 V, 10 ms, 3 pulses) and cells were re-suspended in 100 µl medium then transferred in a 96 well plate. Electroporated K562 were cultured three days before harvest, gDNA extraction and sequencing of the base edited loci. GFP^+ K562 cells were sorted one day after electroporation and cultured two more days before sequencing.

For mRNA BEs electroporation, human T cells were electroporated using the 4D-Nucleofector™ system (Lonza) as described in chapter I. Activated T cells were electroporated with 5.2 pmol of 5664bp mRNA base editor (**Annex Table 10**) and 120 pmol of 100 bp sgRNA (BE:sgRNA ratio 1:23). gDNA was extracted from the cells five days after electroporation.

DNA sequencing

Collected cells were washed with PBS and 30 µl of QuickExtract™ DNA (Biosearch) were added before to transfer the mixtures into PCR tubes. gDNA extraction was processed as follow: samples were vortexed 1 min and incubated 5 min at 60°C, then were vortexed again 1 min before a final incubation of 90°C for 10 min. Locus of interest were amplified by PCR using the GoTaq®G2 Green Master Mix (M782B, Promega) with the primers listed in **Annex Table 4** and was purified then sent for Sanger sequencing

Discussion

In this works, we aimed to see if we could shield cells from antibody-based targeted therapy by introducing point mutations in their antigens. Shielding of therapeutic cells would allow to deplete diseased cells while preserving healthy cells from off-tumor on-target toxicity. Thus, this strategy has an enormous potential. It could be used to treat any blood disease as they could all be possibly cured by replacing a cell subset.

The question was asked with two different proteins. First, we tested the shielding concept with CD123. This protein is a target of choice for myeloid malignancies as it is expressed on AML [137] and leukemic stem cells [82]. Several targeted therapies were developed against it, showing that CD123 can be targeted to deplete cells. However, it was observed that anti-CD123 CAR-T cells can lead to myelotoxicity. HSCs shielding would be beneficial when treating patients with targeted therapies [53]. To finish, we had the crystal structure of the CD123 bound to the anti-CD123 CSL362 published [93], which allowed us to deduce the amino acids of CD123 involved in the epitope of CSL362. Thus, it seemed more straightforward to start assessing the shielding concept with this target. We tested in a second time if shielding could be done by introducing point mutations in the protein CD45. This protein has a broader expression than CD123 as it is expressed on all nucleated cells on the hematopoietic system. It could have a much broader application than CD123 and be used to treat blood cancers other than myeloid malignancies as well as systemic autoimmune diseases. In addition, KO of CD45 could not be used to protect HSCs as the protein is essential and its absence it will prevent T cells maturation[138]. Thus, shielding could open the use of this promising antigen and this is why we explored the feasibility for this target.

Challenges associated with targeting CD123 in a therapy

Surprisingly, many single amino acid substitutions in CD123 led to shielding from CSL362 binding. However, it is difficult to predict how a mutation will affect the function of a protein [139]. For instance, we found shielding variants that likely resulted in non-binding due to protein instability. As such variants could not be used for therapeutics, we aimed to characterize the biophysical properties and to test the functionality of the selected variants. After having compared the biophysical properties of all the non-binding variants and of the WT protein we selected two variants showing properties similar to WT protein for further functionality assessments: E51K and E51T. We selected E51K because it is a naturally occurring variant

(Allele frequency: 3.59e-5, from The Genome Aggregation Database v2 [140]). As no pathology was so far associated with the variant, it could be that it is functional. However, its frequency is low in the population, we could not be sure that it is not pathogenic. In addition, we could not know if the individuals from whom the sequencing stems were truly healthy. Thus, this variant needed to be characterized as much as E51T. We showed preserved functionality of the two variants by IL-3 response of a CD123-dependent cell line. To conclude, we selected two mutations which shielded from targeted therapies while preserving the function of the protein. These results were highly encouraging and could lead to more sophisticated applications.

As targeting of CD123 with targeted therapies leads to myeloablation [53], CD123-targeted therapies could be used for host HSCs depletion before allogeneic HSCT (i.e. targeting HSCs on purpose). Thus, targeted therapy could be used to depleted myeloid cancer cells and HSCs, making space for the graft [92]. Such a treatment strategy requires use of allogeneic HSCs as the myeloid malignancy means that the stem cells are diseased. It also needs to include a lymphodepletion, otherwise the graft will be rejected [141]. Thus, anti-CD123 targeted therapies could be used as conditioning before HSCT, but they would need to be combined with a lymphodepletion strategy.

Shielding of the cells would allow to approach differently the conditioning step coming before the transplantation. Current treatment of cancer with HSCT can be divided into several phases: mobilization of the graft cells, conditioning, reinfusion of the graft, neutropenic phase, engraftment/recovery and follow-up [19]. Use of CD123-targeted therapies with shielded cells would involve different phases. There may no longer be the need to eliminate all cancer cells before the HSCT: the therapy could be continuously applied without harming the new HSCs. The treatment will not need to be stopped to protect graft HSCs. Then, the actual tumor and remaining HSCs eradication would happen after the transplant, during the hematopoietic reconstitution phase. With this system, patients could experience a shorter neutropenic phase and risk of relapses would be reduced compared to current strategies. In addition, a milder conditioning would turn more frail patients eligible and could therefore provide them new therapeutic options. However, this strategy is limited to malignancies due to the reduced expression of CD123 on healthy cell lineages, this is why it was interesting to develop the same concept with a protein more broadly expressed such as CD45.

Challenges associated with targeting CD45 in a therapy

It is more challenging to prove functionality of CD45 variants than CD123 variants. First, the role of the extracellular domain of CD45 in its function is not well known and controversial. Chang et al showed that the size of the ECD is important to trigger TCR activation as it allows CD45 exclusion from the synapse. This exclusion allows the gathering of activated Lck and TCR and leads to the phosphorylation of the CD3 subunits[142] [108]. However, it was shown that CD45 ECD could be exchanged with EGFR and that this chimeric protein restored TCR signaling in a CD45-deficient cell line [143] [144]. Thus, it seems that the TCR signaling read-out may not be sensitive enough to detect CD45 dysfunctions associated with point mutations. The repartition and the mobility of CD45 at the surface of the cells seem crucial for its function [108]. We emitted the hypothesis that point mutations could disrupt its structure and therefore impair its mobility, reducing the accessibility to some proteins. To verify this hypothesis, we could test CD45 main targets phosphorylation such as Lck or CD3ζ [102]. However, it was shown in B cells and macrophages that CD148 and CD45 have redundancy [145]. It may be that other proteins will replace CD45 if the protein cannot reach all of its targets. To finish, it was shown that a reduced amount of the protein led to impaired T cell development in mice [146]. We could quantify the number of variants and of WT protein at the surface of the cells, and exclude the variants showing a reduced expression. To conclude, demonstrating the functionality of CD45 variants is not straightforward.

The CD45 antigen we selected has limitations that prevent from developing targeted therapies against it. We saw that MIRG451 could not trigger ADCC against cells expressing CD45. We supposed that the lack of efficiency to trigger immune cells was due to a too big distance between the targeted cell and the depleting cell. MIRG451 targets an epitope far away from the membrane on a large protein, and it was shown that if the targeting antibody cannot bring the target cell and the killer cell close enough together, the killer cells will not get activated [117]. This was demonstrated for ADCC as well as for TCE killing [119]. Thus, it is likely that TCE and CAR-T cells derived from MIRG451 will also fail to activate T cells. In order to engineer functional CAR-T cells or TCE targeting CD45, we would need to use another antibody clone binding an epitope closer to the membrane, in the d4 or d3 domain. This issue was not observed with CD123, which is smaller than CD45 and for which we could generate mAbs triggering ADCC, TCE and CAR-T cells.

Use of CD45-targeted therapies with shielded cells could be advantageous for cancer treatment. Similarly to CD123 targeted therapies, this strategy would allow continuous application of the

therapy and reduced doses of conditioning. Nonetheless, CD45 is more promising than CD123 for several reasons. First due to its broad expression, several cancer types can be targeted. Then targeting CD45 will allow to deplete tumor cells together with HSCs and lymphocytes. On the contrary to anti-CD123 targeted therapies, no lymphodepletion would be needed before allogeneic HSCT. Thus, targeting of CD45 would be extremely powerful for the treatment of many cancers. Combination of CD45 targeted therapies and shielded cells could also be interesting to treat autoimmune diseases. Autoimmune lymphocytes are pathogenic. By targeting CD45 one would directly eliminate the autoreactive lymphocytes as well as the HSCs to prepare for transplantation. Therefore, this strategy would be attractive but so far but risky since it would be very new. The main drawback would be that it would greatly increase the risk for infections, particularly if T cells are deeply depleted.

Targeting of CD45 with targeted therapies is associated with several risks due to the broad expression of the target. First, expression of CD45 on T cells bring the risk of self-limitation of treatment strategies relying on these cells. For instance, injection of CAR-T cells targeting CD45 will likely lead to fratricide killing as the protein is highly expressed on this cell subset. However, several studies showed that CAR-T cells can be shielded from fratricide killing by KO of their target[14714814963]. As it seems that CD45 cannot be KO in T cells without impairing their function, they could be engineered with the shielding variants to protect the CAR-T cells from fratricide killing.

Use of TCE and CAR-T cells can be very toxic due to their mode of action and this toxicity can be exacerbated by the targeting of CD45. TCE and CAR-T cells break the tumor-mediated immunosuppression by forcing the activation of T cells. Even if such a reaction is an advantage in the treatment of tumor, it can also be deleterious if it leads to an uncontrolled cell killing and inflammation. Two syndromes are associated with the uncontrolled inflammation triggered by cells killing: the tumor lysis syndrome (TLS) and the CRS [4842]. The TLS is associated with hyperuricemia, hyperkalemia, hyperphosphatemia, and hypocalcemia and occurs when the tumor cells release their content in the blood[150]. The CRS is associated with the high release of the toxic cytokines IL-6, TNF-α and IFN-γ driven by an uncontrolled activation of the T cells. CD45 is a highly abundant target. If T cells targeted therapies such as TCE or CAR-T cell would target CD45, we suppose that the T cells involved in the therapy could be quickly over stimulated and lead to the CRS. Thus, it would be preferable to target this antigen with a therapeutic not relying on T cells in order to avoid this major risk for the patient. In order to avoid the TLS, it would be preferable to have a killing not too acute but rather gradual. Otherwise, the patient will likely experience the release syndrome maybe even without a tumor,

just because the amount of cells that express CD45 is very large. Therefore, instead of TCE or CAR-T cells, ADC could be dosed repetitively. However, the use of ADC to target CD45 has also drawbacks. It seems that internalization of the anti-CD45 ADC is passive due to the high presence of the target at the surface of the cells rather than active [21]. Then, it could be that anti-CD45 ADCs will have bystander effects.

Limitations associated with the introduction of variants in the hematopoietic system

Assessing the safety of the variants *in vivo* is challenging due to the limitations of the currently available mouse models. One way to test the functionality of the variants *in vivo* consists in analyzing the development of *ex vivo* engineering human HSCs compared to the non-modified HSCs. Study of human cells requires the use of immunodeficient mice to avoid rejection. Several immunodeficient mouse models were developed in order to allow a cell development as close as possible to what would happen in humans such as the NOD severe combined immunodeficiency (SCID) gamma mouse or the NOD SCID gamma mouse SGM3 [151]. However, the development of the human cells in these models is highly incomplete. For instance, as the human T cells from the graft develop in a mouse thymus, they fail to recognize HLA, and thus T cells and B cells from these model do not become functionally mature [152]. This is particularly problematic for the *in vivo* testing of CD45 variants. T cells maturation seems highly affected by a loss-of-function of CD45 [138]. However, we cannot assess T cells development with the current immunodeficient mouse model.

Introduction of a new protein isoform in the patient bring a risk of immunogenicity. To reduce the risks that the cells bearing the variants will be rejected by host cells, several strategies can be used. First, in the case of allogeneic transplantations, T cells will be depleted before the injection of the donor HSCs. Full depletion of host T cells is not necessary as it was shown that the establishment of a mixed chimerism between donor and host cells can protect from immune rejection [153]. In addition, we know that adoptive transfer of congenic mouse cells is possible in fully immunocompetent mice, demonstrating that not every variant will immediately get rejected [105].

Following engraftment, the donor engineered HSCs will develop into T cells that will mature in the thymus. However, the thymic cells do not express the new protein isoform. How can we reduce the risks that the variant will be recognized as “non-self” after T cell maturation? First, we know that in current allogeneic HSCT, the few mismatches do not impair the complete immune reconstitution of the patients and do not lead to graft auto-rejection [154]. Thus, we supposed that the point mutations will be accepted through the same mechanisms. In addition,

negative selection in the thymus was shown to be supported by dendritic cells (DCs) [155]. Following HSCT, we hypothesize that DCs expressing the variants will infiltrate the thymus and will do negative selection on T cells reacting against the introduced mutation.

Due to the possibility to continuously apply the targeted therapy, relapses due to remaining cancers cells are less likely to happen. The main risk in this case would be a relapse with downregulation of the receptor [156]. There, targeting two targets instead of one would be interesting [157]. For instance, CD123 could be combined with CD45. However, in this case the shielding would require multiplexing of HSCs, which is more delicate.

Can we safely engineer the genome of HSCs cells?

In order to introduce point mutations in the endogenous DNA of the cells, we chose to use HDR since it is readily accessible to labs. However, us of HDR for engineering therapeutic cells has limitations. It relies on the introduction of DSBs which is toxic and needs to be repaired immediately. Two main mechanisms are involved in the resolution of the breaks : NHEJ and HDR [73]. So far, we cannot control which mechanism will be used by the cells. However, the error-prone NHEJ repair mechanism presents a risk. If no premature STOP codon is inserted, it can introduce uncontrolled mutations in the protein, leading to changes of function [139]. In addition, the off-target of Cas9 cut and the consequent several DSBs generated can lead to chromosomal translocation, which is oncogenic [74] [158]. BEs are promising for the engineering of therapeutic point mutations as they can modify the genome without introducing DSBs and have thus a reduced off-targeting [125]. However, on the contrary to HDR based approaches, BEs use faces many restrictions. First, they can edit only A to G or C to T if these nucleotides are localized in the editing window of a protospacer. However, some protospacers work well, but others very little and it is so far not possible to accurately predict which one will actually work. In addition, editing by BEs is not always restricted to the editing windows. Sometimes bystanders edit can happen and nucleotides around the base editing window could be edited. Such an editing can bring unwanted mutations and is difficult to predict [125]. These limitations were illustrated with the attempt to introduce variants in CD45. None of the selected variants could be introduced by BE. Therefore, the alternative strategy to use BE to shield cells from targeted therapies would require to first search for editable positions, then raise mAbs that deplete WT cells but not cells edited with BEs. This editing strategy is attractive but may be challenging as variants edited by BEs could be not functional and the substitution possibilities are very restricted since only A to G and C to T mutations can be inserted. It may

be that no substitution editable by BE would allow good loss-of-binding of antibodies together with preserved function of the protein.

DSBs are unwanted in therapeutic cells due to the risks of repair errors which can lead to new cancer generation. However, when we compare the safety of the shielding/targeted depletion strategy to chemotherapy in terms of DNA breaks, the shielding/targeted depletion strategy is safer. Use of HDR lead to DSBs, but chemotherapy as well. However, break introduced by chemotherapy are done in an unspecific way and in different types of cells. Thus, following chemotherapy, many cells will have random DSBs, increasing the chances of relapse due to a secondary cancer. While in the shielding strategy DSBs are limited to a specific type of cells and these breaks can be predicted with informatic tools. Thus, despite the remaining challenges, use of shielded cells/targeted therapy is promising compared to chemotherapy.

The rise of cell technologies and of the available treatment strategies offers the opportunity to customize the blood cells therapies to the cancers and the patients. This increase of the therapeutic options will come with more treatment opportunities and shielded cells/targeted therapy strategy will take part of this tool arsenal. Thus, we can hope that in the future patients will be treated with more personalized drugs, reducing toxicities, improving the recovery and most important, allowing to target blood diseases so far untreated.

Conclusion

In this work, we tested the feasibility of shielding cells from antibody-based targeted therapies. To do so, we aimed to introduce point mutations in the antigen targeted by the therapies, disrupting the binding of the antibody while preserving the function of the protein.

In the first chapter, we showed that:

- Using the crystal structure of CD123 (IL-3rα) bound to the anti-CD123 CSL362 we could design *in silico* variants of CD123 which protected from binding of the antibody
- The non-binding CD123 variants protected from killing by ADCC, TCE and CAR-T cells *in vitro*
- Two non-binding variants E51K and E51T E51K and E51T, showed preserved biophysical properties and function of the receptor *in vitro*
- E51K and E51T variants could be engineered into HSPCs and protected the cells from TCE killing while allowing their normal development *in vivo*

In the second chapter we showed that:

- By screening CD45 designed variants vs. anti-CD45 antibodies we could identify pairs of antibody/variants leading to a loss-of-binding of the antibody clone QA17A19
- Engineering of selected variants T330K, T330del, F331del, F331del_T332del and T332del into human T cells protected them from QA17A19-derived ADC killing

In the third chapter we showed that:

- BEs can edit the CD45 locus but are too restricted to introduce selected variants

To conclude, we showed that cells could be shielded from antibody-based targeted therapies. The shielding/targeted therapy system would allow to target any hematopoietic cell subset with a reduced toxicity. While the diseased cells will be depleted by the targeted therapy, the shielded cells will reconstitute the subset. Shielding from CD123 targeted therapies would be advantageous for the treatment of myeloid malignancies, while shielding from CD45 targeted therapies would be interesting for several blood diseases. Thus, this system combined with the future improvement of genome engineering strategies could increase the therapeutic options for blood diseases, allowing fragile patients not eligible for hard conditioning to be treated.

Disclosure

A patent application related to the findings described in chapter I was filed

A patent application related to the findings described in chapter II and III was filed

I, Anna Devaux, declare holding Cimeio equity

Bibliography

1. Wang, L.D., and Wagers, A.J. (2011). Dynamic niches in the origination and differentiation of haematopoietic stem cells. Nat. Rev. Mol. Cell Biol. *12*, 643–655. 10.1038/nrm3184.
2. Ford, C.E., Hamerton, J.L., Barnes, D.W.H., and Loutit, J.F. (1956). Cytological identification of radiation-chimæras. Nature *177*, 452–454. 10.1038/177452a0.
3. Becker, A.J., Mcculloch, E.A., and Till, J.E. (1963). Spleen Colonies Derived From Transplanted Mouse Marrow Cells. Nature *197*, 452–454.
4. TILL, J.E., and McCULLOCH, E.A. (1961). A direct measurement of the radiation sensitivity of normal mouse bone marrow cells. Radiat. Res. *14*, 213–222. 10.2307/3570892.
5. Osawa, M., Hanada, K., Hamada, H., and Nakaucji, H. (1996). Long-Term Lymphohematopoietic Reconstitution by a Single CD34-Low /negative Hematopoietic Stem Cell. Science (80-.). *273*, 242–246.
6. Kiel, M.J., Yilmaz, Ö.H., Iwashita, T., Yilmaz, O.H., Terhorst, C., and Morrison, S.J. (2005). SLAM family receptors distinguish hematopoietic stem and progenitor cells and reveal endothelial niches for stem cells. Cell *121*, 1109–1121. 10.1016/j.cell.2005.05.026.
7. Christensen, J.L., and Weissman, I.L. (2001). Flk-2 is a marker in hematopoietic stem cell differentiation: A simple method to isolate long-term stem cells. Proc. Natl. Acad. Sci. U. S. A. *98*, 14541–14546. 10.1073/pnas.261562798.
8. Kondo, M. (2010). Lymphoid and myeloid lineage commitment in multipotent hematopoietic progenitors. Immunol. Rev. *238*, 37–46. 10.1111/j.1600-065X.2010.00963.x.Lymphoid.
9. Middlebrook, A.J., Snowden, E., Porter, W., Hahn, F., Ferguson, M., Soper, B., Keck, J., Malcolm, J., Dillmore, S., Ghanekar, S., et al. (2017). Comprehensive evaluation of human immune system reconstitution in NSGTM and NSGTM-SGM3 toward the development of a novel Onco-HuTM xenograft model. Cancer Res. *77*, 1656–1656. 10.1158/1538-7445.am2017-1656.
10. Crane, G.M., Jeffery, E., and Morrison, S.J. (2017). Adult haematopoietic stem cell niches. Nat. Rev. Immunol. *17*, 573–590. 10.1038/nri.2017.53.
11. Zhou, B.O., Yue, R., Murphy, M.M., Peyer, J.G., and Morrison, S.J. (2014). Leptin-receptor-expressing mesenchymal stromal cells represent the main source of bone formed by adult bone marrow. Cell Stem Cell *15*, 154–168. 10.1016/j.stem.2014.06.008.
12. Adams, G.B., Chabner, K.T., Alley, I.R., Olson, D.P., Szczepiorkowski, Z.M., Poznansky, M.C., Kos, C.H., Pollak, M.R., Brown, E.M., and Scadden, D.T. (2006). Stem cell engraftment at the endosteal niche is specified by the calcium-sensing receptor. Nature *439*, 599–603. 10.1038/nature04247.
13. Yamazaki, S., Ema, H., Karlsson, G., Yamaguchi, T., Miyoshi, H., Shioda, S., Taketo, M.M., Karlsson, S., Iwama, A., and Nakauchi, H. (2011). Nonmyelinating schwann cells maintain hematopoietic stem cell hibernation in the bone marrow niche. Cell *147*, 1146–1158. 10.1016/j.cell.2011.09.053.
14. Naveiras, O., Nardi, V., Wenzel, P.L., Hauschka, P. V., Fahey, F., and Daley, G.Q. (2009). Bone-marrow adipocytes as negative regulators of the haematopoietic microenvironment. Nature *460*, 259–263. 10.1038/nature08099.
15. Winkler, I.G., Sims, N.A., Pettit, A.R., Barbier, V., Nowlan, B., Helwani, F., Poulton, I.J., Van Rooijen, N., Alexander, K.A., Raggatt, L.J., et al. (2010). Bone marrow

macrophages maintain hematopoietic stem cell (HSC) niches and their depletion mobilizes HSCs. Blood *116*, 4815–4828. 10.1182/blood-2009-11-253534.
16. Robb, L. (2007). Cytokine receptors and hematopoietic differentiation. Oncogene *26*, 6715–6723. 10.1038/sj.onc.1210756.
17. Passweg, J.R., Baldomero, H., Chabannon, C., Basak, G.W., de la Cámara, R., Corbacioglu, S., Dolstra, H., Duarte, R., Glass, B., Greco, R., et al. (2021). Hematopoietic cell transplantation and cellular therapy survey of the EBMT: monitoring of activities and trends over 30 years. Bone Marrow Transplant. *56*, 1651–1664. 10.1038/s41409-021-01227-8.
18. Balassa, K., Danby, R., and Rocha, V. (2019). Haematopoietic stem cell transplants : Br. J. Hop. Med. *80*, 33–39.
19. Galgano, L., and Hutt, D. (2018). The European Blood and Marrow Transplantation Textbook for Nurses. Eur. Blood Marrow Transplant. Textb. Nurses. 10.1007/978-3-319-50026-3.
20. Copelan, E.A. (2006). Hematopoietic Stem-Cell Transplantation. N. Engl. J. Med. *354*, 1813–1826.
21. Palchaudhuri, R., Saez, B., Hoggatt, J., Schajnovitz, A., Sykes, D.B., Tate, T.A., Czechowicz, A., Kfoury, Y., Ruchika, F.N.U., Rossi, D.J., et al. (2016). Non-genotoxic conditioning for hematopoietic stem cell transplantation using a hematopoietic-cell-specific internalizing immunotoxin. Nat. Biotechnol. *34*, 738–745. 10.1038/nbt.3584.
22. Dominici, M., Rasini, V., Bussolari, R., Chen, X., Hofmann, T.J., Spano, C., Bernabei, D., Veronesi, E., Bertoni, F., Paolucci, P., et al. (2009). Restoration and reversible expansion of the osteoblastic hematopoietic stem cell niche after marrow radioablation. Blood *114*, 2333–2343. 10.1182/blood-2008-10-183459.
23. Mohty, M., Hübel, K., Kröger, N., Aljurf, M., Apperley, J., Basak, G.W., Bazarbachi, A., Douglas, K., Gabriel, I., Garderet, L., et al. (2014). Autologous haematopoietic stem cell mobilisation in multiple myeloma and lymphoma patients: A position statement from the European Group for Blood and Marrow Transplantation. Bone Marrow Transplant. *49*, 865–872. 10.1038/bmt.2014.39.
24. Miller, J.P., Perry, E.H., Price, T.H., Bolan, C.D., Karanes, C., Boyd, T.M., Chitphakdithai, P., and King, R.J. (2008). Recovery and Safety Profiles of Marrow and PBSC Donors: Experience of the National Marrow Donor Program. Biol. Blood Marrow Transplant. *14*, 29–36. 10.1016/j.bbmt.2008.05.018.
25. Horowitz, M.M., Gale, R.P., Sondel, P.M., Goldman, J.M., Kersey, J., Kolb, H.J., Rimm, A.A., Ringden, O., Rozman, C., Speck, B., et al. (1990). Graft-versus-leukemia reactions after bone marrow transplantation. Blood *75*, 555–562. 10.1182/blood.v75.3.555.555.
26. Glucksberg, H., Storb, R., Fefer, A., Buckner, C.D., Neiman, P.E., Clift, R.A., Lerner, K.G., and E.D.Thomas (1974). Clinical manifestations of graft-versus-host disease in human recipients of marrow from HLA-matched sibling donors. Transplantation *18*, 295–304.
27. Arnaout, K., Patel, N., Jain, M., El-Amm, J., Amro, F., and Tabbara, I.A. (2014). Complications of allogeneic hematopoietic stem cell transplantation. Cancer Invest. *32*, 349–362. 10.3109/07357907.2014.919301.
28. Kolb, H.J., Socié, G., Duell, T., Van Lint, M.T., Tichelli, A., Apperley, J.F., Nekolla, E., Ljungman, P., Jacobsen, N., Van Weel, M., et al. (1999). Malignant neoplasms in long-term survivors of bone marrow transplantation. Ann. Intern. Med. *131*, 738–744. 10.7326/0003-4819-131-10-199911160-00004.
29. Van Den Brink, M.R.M., Velardi, E., and Perales, M.A. (2015). Immune reconstitution

following stem cell transplantation. Hematol. (United States) *2015*, 215–219. 10.1182/asheducation-2015.1.215.
30. Czyz, A., and Nagler, A. (2019). The role of measurable residual disease (MRD) in hematopoietic stem cell transplantation for hematological malignancies focusing on acute leukemia. Int. J. Mol. Sci. *20*. 10.3390/ijms20215362.
31. Gatta, G., Capocaccia, R., Botta, L., Mallone, S., De Angelis, R., Ardanaz, E., Comber, H., Dimitrova, N., Leinonen, M.K., Siesling, S., et al. (2017). Burden and centralised treatment in Europe of rare tumours: results of RARECAREnet—a population-based study. Lancet Oncol. *18*, 1022–1039. 10.1016/S1470-2045(17)30445-X.
32. Passweg, J.R., Baldomero, H., Bader, P., Bonini, C., Cesaro, S., Dreger, P., Duarte, R.F., Dufour, C., Falkenburg, J.H.F., Farge-Bancel, D., et al. (2015). Hematopoietic SCT in Europe 2013: Recent trends in the use of alternative donors showing more haploidentical donors but fewer cord blood transplants. Bone Marrow Transplant. *50*, 476–482. 10.1038/bmt.2014.312.
33. Weiner, L.M., Surana, R., and Wang, S. (2010). Monoclonal antibodies: Versatile platforms for cancer immunotherapy. Nat. Rev. Immunol. *10*, 317–327. 10.1038/nri2744.
34. Saijo, N. (2010). Progress in cancer chemotherapy with special stress on molecular-targeted therapy. Jpn. J. Clin. Oncol. *40*, 855–862. 10.1093/jjco/hyq035.
35. Kantarjian, H., Stein, A., Gökbuget, N., Fielding, A.K., Schuh, A.C., Ribera, J.-M., Wei, A., Dombret, H., Foà, R., Bassan, R., et al. (2017). Blinatumomab versus Chemotherapy for Advanced Acute Lymphoblastic Leukemia. N. Engl. J. Med. *376*, 836–847. 10.1056/nejmoa1609783.
36. Kochenderfer, J.N., Dudley, M.E., Feldman, S.A., Wilson, W.H., Spaner, D.E., Maric, I., Stetler-Stevenson, M., Phan, G.Q., Hughes, M.S., Sherry, R.M., et al. (2012). B-cell depletion and remissions of malignancy along with cytokine-associated toxicity in a clinical trial of anti-CD19 chimeric-antigen-receptor-transduced T cells. Blood *119*, 2709–2720. 10.1182/blood-2011-10-384388.
37. Brentjens, R.J., Davila, M.L., Riviere, I., Park, J., Wang, X., Cowell, L.G., Bartido, S., Stefanski, J., Taylor, C., Olszewska, M., et al. (2013). CD19-targeted T cells rapidly induce molecular remissions in adults with chemotherapy-refractory acute lymphoblastic leukemia. Sci. Transl. Med. *5*. 10.1126/scitranslmed.3005930.
38. Yu, J., Song, Y., and Tian, W. (2020). How to select IgG subclasses in developing anti-tumor therapeutic antibodies. J. Hematol. Oncol. *13*, 1–10. 10.1186/s13045-020-00876-4.
39. Goede, V., Fischer, K., Busch, R., Engelke, A., Eichhorst, B., Wendtner, C.M., Chagorova, T., de la Serna, J., Dilhuydy, M.-S., Illmer, T., et al. (2014). Obinutuzumab plus Chlorambucil in Patients with CLL and Coexisting Conditions. N. Engl. J. Med. *370*, 1101–1110. 10.1056/nejmoa1313984.
40. Dean, A.Q., Luo, S., Twomey, J.D., and Zhang, B. (2021). Targeting cancer with antibody-drug conjugates: Promises and challenges. MAbs *13*. 10.1080/19420862.2021.1951427.
41. Carter, P.J., and Rajpal, A. (2022). Designing antibodies as therapeutics. Cell *185*, 2789–2805. 10.1016/j.cell.2022.05.029.
42. Strohl, W.R., and Naso, M. (2019). Bispecific t-cell redirection versus chimeric antigen receptor (car)-t cells as approaches to kill cancer cells. Antibodies *8*. 10.3390/antib8030041.
43. D.Staerz, U., Kanagawa, O., and Bevan, M.J. (1985). Hybrid antibodies can target sites for attack by T cells. Lett. to Nat., 3–6.

44. Müller, C., Murawski, N., Wiesen, M.H.J., Held, G., Poeschel, V., Zeynalova, S., Wenger, M., Nickenig, C., Peter, N., Lengfelder, E., et al. (2012). The role of sex and weight on rituximab clearance and serum elimination half-life in elderly patients with DLBCL. Blood *119*, 3276–3284. 10.1182/blood-2011-09-380949.
45. Zhu, M., Wu, B., Brandl, C., Johnson, J., Wolf, A., Chow, A., and Doshi, S. (2016). Blinatumomab, a Bispecific T-cell Engager (BiTE®) for CD-19 Targeted Cancer Immunotherapy: Clinical Pharmacology and Its Implications. Clin. Pharmacokinet. *55*, 1271–1288. 10.1007/s40262-016-0405-4.
46. Gross, G., Waks, T., and Eshhar, Z. (1989). Expression of immunoglobulin-T-cell receptor chimeric molecules as functional receptors with antibody-type specificity. Proc. Natl. Acad. Sci. U. S. A. *86*, 10024–10028. 10.1073/pnas.86.24.10024.
47. Eshhar, Z., Waks, T., Gross, G., and Schindler, D.G. (1993). Specific activation and targeting of cytotoxic lymphocytes through chimeric single chains consisting of antibody-binding domains and the γ or ζ subunits of the immunoglobulin and T-cell receptors. Proc. Natl. Acad. Sci. U. S. A. *90*, 720–724. 10.1073/pnas.90.2.720.
48. Finck, A. V., Blanchard, T., Roselle, C.P., Golinelli, G., and June, C.H. (2022). Engineered cellular immunotherapies in cancer and beyond. Nat. Med. *28*, 678–689. 10.1038/s41591-022-01765-8.
49. Melenhorst, J.J., Chen, G.M., Wang, M., Porter, D.L., Chen, C., Collins, M.K.A., Gao, P., Bandyopadhyay, S., Sun, H., Zhao, Z., et al. (2022). Decade-long leukaemia remissions with persistence of CD4+ CAR T cells. Nature *602*, 503–509. 10.1038/s41586-021-04390-6.
50. Hill, J.A., Giralt, S., Torgerson, T.R., and Lazarus, H.M. (2019). CAR-T – and a side order of IgG, to go? – Immunoglobulin replacement in patients receiving CAR-T cell therapy. Blood Rev. *38*. 10.1016/j.blre.2019.100596.
51. Perna, F., Berman, S.H., Soni, R.K., Mansilla-Soto, J., Eyquem, J., Hamieh, M., Hendrickson, R.C., Brennan, C.W., and Sadelain, M. (2017). Integrating Proteomics and Transcriptomics for Systematic Combinatorial Chimeric Antigen Receptor Therapy of AML. Cancer Cell *32*, 506-519.e5. 10.1016/j.ccell.2017.09.004.
52. Strassberger, V., Gutbrodt, K.L., Krall, N., Roesli, C., Takizawa, H., Manz, M.G., Fugmann, T., and Neri, D. (2014). A comprehensive surface proteome analysis of myeloid leukemia cell lines for therapeutic antibody development. J. Proteomics *99*, 138–151. 10.1016/j.jprot.2014.01.022.
53. Gill, S., Sarah K. Tasian, Ruella, M., Shestova, O., Li, Y., Porter, D.L., Carroll, M., Danet-Desnoyers, G., Scholler, J., Grupp, S.A., et al. (2014). Preclinical targeting of human acute myeloid leukemia and myeloablation using chimeric antigen receptor–modified T cells. J. Cancer *123*, 2343–2354. 10.7150/jca.28952.
54. Kenderian, S.S., Ruella, M., Shestova, O., Klichinsky, M., Aikawa, V., Morrissette, J.J.D., Scholler, J., Song, D., Porter, D.L., Carroll, M., et al. (2015). CD33-specific chimeric antigen receptor T cells exhibit potent preclinical activity against human acute myeloid leukemia. Leukemia *29*, 1637–1647. 10.1038/leu.2015.52.
55. Mullard, A. (2021). FDA approves fourth CAR- T cell therapy The. Nat. Rev., 2018.
56. Mullard, A. (2022). FDA approves second BCMA- targeted CAR- T cell therapy. Nat. Rev. Drug Discov. *21*, 2022.
57. Kim, M.Y., Yu, K.R., Kenderian, S.S., Ruella, M., Chen, S., Shin, T.H., Aljanahi, A.A., Schreeder, D., Klichinsky, M., Shestova, O., et al. (2018). Genetic Inactivation of CD33 in Hematopoietic Stem Cells to Enable CAR T Cell Immunotherapy for Acute Myeloid Leukemia. Cell *173*, 1439-1453.e19. 10.1016/j.cell.2018.05.013.
58. Laszlo, G.S., Estey, E.H., and Walter, R.B. (2014). The past and future of CD33 as therapeutic target in acute myeloid leukemia. Blood Rev. *28*, 143–153.

10.1016/j.blre.2014.04.001.
59. Borot, F., Wang, H., Ma, Y., Jafarov, T., Raza, A., Ali, A.M., and Mukherjee, S. (2019). Erratum: Gene-edited stem cells enable CD33-directed immune therapy for myeloid malignancies (Proceedings of the National Academy of Sciences of the United States of America (2019) 116 (11978–11987) DOI: 10.1073/pnas.1819992116). Proc. Natl. Acad. Sci. U. S. A. *116*, 14780–14781. 10.1073/pnas.1909768116.
60. Humbert, O., Laszlo, G.S., Sichel, S., Ironside, C., Haworth, K.G., Bates, O.M., Beddoe, M.E., Carrillo, R.R., Kiem, H.P., and Walter, R.B. (2019). Engineering resistance to CD33-targeted immunotherapy in normal hematopoiesis by CRISPR/Cas9-deletion of CD33 exon 2. Leukemia *33*, 762–808. 10.1038/s41375-018-0277-8.
61. Kim, M.Y., Cooper, M.L., Jacobs, M.T., Ritchey, J.K., Hollaway, J., Fehniger, T.A., and DiPersio, J.F. (2021). CD7-deleted hematopoietic stem cells can restore immunity after CAR T cell therapy. JCI Insight *6*. 10.1172/jci.insight.149819.
62. Haynes, B.Y.B.E., Martin, M.E., Kay, H.H., and Kurtzberg, J. (1988). EARLY EVENTS IN HUMAN T CELL ONTOGENY Phenotypic Characterization and Immunohistologic Localization of T Cell Precursors in Early Human Fetal Tissues. J. Exp. Med. *168*.
63. Cooper, M.L., Choi, J., Staser, K., Ritchey, J.K., Devenport, J.M., Eckardt, K., Rettig, M.P., Wang, B., Eissenberg, L.G., Ghobadi, A., et al. (2018). An "off-the-shelf" fratricide-resistant CAR-T for the treatment of T cell hematologic malignancies. Leukemia *32*, 1970–1983. 10.1038/s41375-018-0065-5.
64. Newby, G.A., Yen, J.S., Woodard, K.J., Mayuranathan, T., Lazzarotto, C.R., Li, Y., Sheppard-Tillman, H., Porter, S.N., Yao, Y., Mayberry, K., et al. (2021). Base editing of haematopoietic stem cells rescues sickle cell disease in mice. Nature *595*, 295–302. 10.1038/s41586-021-03609-w.
65. Kim, Y.G., Cha, J., and Chandrasegaran, S. (1996). Hybrid restriction enzymes: Zinc finger fusions to Fok I cleavage domain. Proc. Natl. Acad. Sci. U. S. A. *93*, 1156–1160. 10.1073/pnas.93.3.1156.
66. Smith, J., Bibikova, M., Whitby, F.G., Reddy, A.R., Chandrasegaran, S., and Carroll, D. (2000). Requirements for double-strand cleavage by chimeric restriction enzymes with zinc finger DNA-recognition domains. Nucleic Acids Res. *28*, 3361–3369. 10.1093/nar/28.17.3361.
67. Cermak, T., Doyle, E.L., Christian, M., Wang, L., Zhang, Y., Schmidt, C., Baller, J.A., Somia, N. V., Bogdanove, A.J., and Voytas, D.F. (2011). Efficient design and assembly of custom TALEN and other TAL effector-based constructs for DNA targeting. Nucleic Acids Res. *39*, 1–11. 10.1093/nar/gkr218.
68. Jinek, M., Chylinski, K., Fonfara, I., Hauer, M., Doudna, J.A., and Charpentier, E. (2012). A Programmable Dual-RNA – Guided. *337*, 816–822.
69. Komor, A.C., Kim, Y.B., Packer, M.S., Zuris, J.A., and Liu, D.R. (2016). Programmable editing of a target base in genomic DNA without double-stranded DNA cleavage. Nature *533*, 420–424. 10.1038/nature17946.
70. Gaudelli, N.M., Komor, A.C., Rees, H.A., Packer, M.S., Badran, A.H., Bryson, D.I., and Liu, D.R. (2017). Programmable base editing of A T to G C in genomic DNA without DNA cleavage. Nature *551*, 464–471. 10.1038/nature24644.
71. Kuscu, C., Parlak, M., Tufan, T., Yang, J., Szlachta, K., Wei, X., Mammadov, R., and Adli, M. (2017). CRISPR-STOP: Gene silencing through base-editing-induced nonsense mutations. Nat. Methods *14*, 710–712. 10.1038/nmeth.4327.
72. Anzalone, A. V., Randolph, P.B., Davis, J.R., Sousa, A.A., Koblan, L.W., Levy, J.M.,

Chen, P.J., Wilson, C., Newby, G.A., Raguram, A., et al. (2019). Search-and-replace genome editing without double-strand breaks or donor DNA. Nature *576*, 149–157. 10.1038/s41586-019-1711-4.
73. Ceccaldi, R., Rondinelli, B., and D'Andrea, A.D. (2016). Repair Pathway Choices and Consequences at the Double-Strand Break. Trends Cell Biol. *26*, 52–64. 10.1016/j.tcb.2015.07.009.
74. Bernard, B.E., Landmann, E., Jeker, L.T., and Schumann, K. (2022). CRISPR/Cas-based Human T cell Engineering: Basic Research and Clinical Application. Immunol. Lett. *245*, 18–28. 10.1016/j.imlet.2022.03.005.
75. Heyer, W.D., Ehmsen, K.T., and Liu, J. (2010). Regulation of homologous recombination in eukaryotes. Annu. Rev. Genet. *44*, 113–139. 10.1146/annurev-genet-051710-150955.
76. Brandsma, I., and Gent, D.C. (2012). Pathway choice in DNA double strand break repair: Observations of a balancing act. Genome Integr. *3*, 1–10. 10.1186/2041-9414-3-9.
77. Haapaniemi, E., Botla, S., Persson, J., Schmierer, B., and Taipale, J. (2018). CRISPR-Cas9 genome editing induces a p53-mediated DNA damage response. Nat. Med. *24*, 927–930. 10.1038/s41591-018-0049-z.
78. Hollstein, M., Rice, K., Greenblatt, M.S., Soussi, T., Fuchs, R., Sørlie, T., Hovig, E., Smith-Sørensen, B., Montesano, R., and Harris, C.C. (1994). Database of p53 gene somatic mutations in human tumors and cell lines. Nucleic Acids Res. *22*, 3551–3555.
79. Jost, M., Santos, D.A., Saunders, R.A., Horlbeck, M.A., Hawkins, J.S., Scaria, S.M., Norman, T.M., Hussmann, J.A., Liem, C.R., Gross, C.A., et al. (2020). Titrating gene expression using libraries of systematically attenuated CRISPR guide RNAs. Nat. Biotechnol. *38*, 355–364. 10.1038/s41587-019-0387-5.
80. Broughton, S.E., Dhagat, U., Hercus, T.R., Nero, T.L., Grimbaldeston, M.A., Bonder, C.S., Lopez, A.F., and Parker, M.W. (2012). The GM-CSF/IL-3/IL-5 cytokine receptor family: From ligand recognition to initiation of signaling. Immunol. Rev. *250*, 277–302. 10.1111/j.1600-065X.2012.01164.x.
81. Oon, S., Huynh, H., Tai, T.Y., Ng, M., Monaghan, K., Biondo, M., Vairo, G., Maraskovsky, E., Nash, A.D., Wicks, I.P., et al. (2016). A cytotoxic anti-IL-3Rα antibody targets key cells and cytokines implicated in systemic lupus erythematosus. JCI Insight *1*. 10.1172/jci.insight.86131.
82. Jordan, C.T., Upchurch, D., Szilvassy, S.J., Guzman, M.L., Howard, D.S., Pettigrew, A.L., Meyerrose, T., Rossi, R., and Grimes, B. (2000). 2401903-1. 1777–1784.
83. Dolgin, E. (2019). First CD123-targeted drug approved after wowing in rare cancer. Nat. Biotechnol. *37*, 202–203. 10.1038/s41587-019-0056-8.
84. Busfield, S.J., Biondo, M., Wong, M., Ramshaw, H.S., Lee, E.M., Ghosh, S., Braley, H., Panousis, C., Roberts, A.W., He, S.Z., et al. (2014). Targeting of acute myeloid leukemia in vitro and in vivo with an anti-CD123 mAb engineered for optimal ADCC. Leukemia *28*, 2213–2221. 10.1038/leu.2014.128.
85. Smith, B.D., Roboz, G.J., Walter, R.B., Altman, J.K., Ferguson, A., Curcio, T.J., Orlowski, K.F., Garrett, L., Busfield, S.J., Barnden, M., et al. (2014). First-in Man, Phase 1 Study of CSL362 (Anti-IL3Rα / Anti-CD123 Monoclonal Antibody) in Patients with CD123+ Acute Myeloid Leukemia (AML) in CR at High Risk for Early Relapse. Blood *124*, 120–120. 10.1182/blood.v124.21.120.120.
86. Uy, G.L., Aldoss, I., Foster, M.C., Sayre, P.H., Wieduwilt, M.J., Advani, A.S., Godwin, J.E., Arellano, M.L., Sweet, K.L., Emadi, A., et al. (2021). Flotetuzumab as salvage immunotherapy for refractory acute myeloid leukemia. Blood *137*, 751–762. 10.1182/blood.2020007732.

87. Chichili, G.R., Huang, L., Li, H., Burke, S., He, L., Tang, Q., Jin, L., Gorlatov, S., Ciccarone, V., Chen, F., et al. (2015). A CD3xCD123 bispecific DART for redirecting host T cells to myelogenous leukemia: Preclinical activity and safety in nonhuman primates. Sci. Transl. Med. *7*, 1–14. 10.1126/scitranslmed.aaa5693.
88. Mardiros, A., Dos Santos, C., McDonald, T., Brown, C.E., Wang, X., Budde, L.E., Hoffman, L., Aguilar, B., Chang, W.C., Bretzlaff, W., et al. (2013). T cells expressing CD123-specific chimeric antigen receptors exhibit specific cytolytic effector functions and antitumor effects against human acute myeloid leukemia. Blood *122*, 3138–3148. 10.1182/blood-2012-12-474056.
89. Tettamanti, S., Marin, V., Pizzitola, I., Magnani, C.F., Giordano Attianese, G.M.P., Cribioli, E., Maltese, F., Galimberti, S., Lopez, A.F., Biondi, A., et al. (2013). Targeting of acute myeloid leukaemia by cytokine-induced killer cells redirected with a novel CD123-specific chimeric antigen receptor. Br. J. Haematol. *161*, 389–401. 10.1111/bjh.12282.
90. Baroni, M.L., Sanchez Martinez, D., Gutierrez Aguera, F., Roca Ho, H., Castella, M., Zanetti, S.R., Velasco Hernandez, T., Diaz de la Guardia, R., Castaño, J., Anguita, E., et al. (2020). 41BB-based and CD28-based CD123-redirected T-cells ablate human normal hematopoiesis in vivo. J. Immunother. cancer *8*. 10.1136/jitc-2020-000845.
91. Gill, S., Tasian, S.K., Ruella, M., Shestova, O., Li, Y., Porter, D.L., Carroll, M., Danet-Desnoyers, G., Scholler, J., Grupp, S.A., et al. (2019). Preclinical targeting of human acute myeloid leukemia using CD4-specific chimeric antigen receptor (CAR) T cells and NK cells. J. Cancer *10*, 4408–4419. 10.7150/jca.28952.
92. Czechowicz, A., Daniel Kraft, I.L.W., and Bhattacharya†, D. (2007). Efficient Transplantation via Antibody-Based Clearance of Hematopoietic Stem Cell Niches. Science (80-.). *318*, 1296–1300.
93. Broughton, S.E., Hercus, T.R., Hardy, M.P., McClure, B.J., Nero, T.L., Dottore, M., Huynh, H., Braley, H., Barry, E.F., Kan, W.L., et al. (2014). Dual Mechanism of Interleukin-3 Receptor Blockade by an Anti-Cancer Antibody. Cell Rep. *8*, 410–419. 10.1016/j.celrep.2014.06.038.
94. Toshio Kitamura, Tsuyoshi Tange, Takashi Terasawa, Shigeru Chiba, Tomoaki Kuwaki, Kiyoshi Miyagawa, Yun-Feng Piao, Kohei Miyazono, Akio Urabe, F.T. (1989). Establishment and Characterization of a Unique Human Cell Line That Proliferates Dependently on GM-CSF, IL-3 or Erythropoietin. J. Cell. Physiol. *140*, 323–334.
95. Nguyen, D.N., Roth, T.L., Li, P.J., Chen, P.A., Apathy, R., Mamedov, M.R., Vo, L.T., Tobin, V.R., Goodman, D., Shifrut, E., et al. (2020). Polymer-stabilized Cas9 nanoparticles and modified repair templates increase genome editing efficiency. Nat. Biotechnol. *38*, 44–49. 10.1038/s41587-019-0325-6.
96. Bak, R.O., Dever, D.P., and Porteus, M.H. (2018). CRISPR/Cas9 genome editing in human hematopoietic stem cells. Nat. Protoc. *13*, 358–376. 10.1038/nprot.2017.143.
97. Kluesner, M.G., Nedveck, D.A., Lahr, W.S., Garbe, J.R., Abrahante, J.E., Webber, B.R., and Moriarity, B.S. (2018). EditR: A Method to Quantify Base Editing from Sanger Sequencing. Cris. J. *1*, 239–250. 10.1089/crispr.2018.0014.
98. Al Barashdi, M.A., Ali, A., McMullin, M.F., and Mills, K. (2021). Protein tyrosine phosphatase receptor type C (PTPRC or CD45). J. Clin. Pathol. *74*, 548–552. 10.1136/jclinpath-2020-206927.
99. Rheinländer, A., Schraven, B., and Bommhardt, U. (2018). CD45 in human physiology and clinical medicine. Immunol. Lett. *196*, 22–32. 10.1016/j.imlet.2018.01.009.
100. Tchilian, E.Z., and Beverley, P.C.L. (2006). Altered CD45 expression and disease. Trends Immunol. *27*, 146–153. 10.1016/j.it.2006.01.001.

101. Hermiston, M.L., Xu, Z., and Weiss, A. (2003). CD45: A Critical Regulator of Signaling Thresholds in Immune Cells. Annu. Rev. Immunol. *21*, 107–137. 10.1146/annurev.immunol.21.120601.140946.
102. Courtney, A.H., Shvets, A.A., Lu, W., Griffante, G., Mollenauer, M., Horkova, V., Lo, W.L., Yu, S., Stepanek, O., Chakraborty, A.K., et al. (2019). CD45 functions as a signaling gatekeeper in T cells. Sci. Signal. *12*. 10.1126/scisignal.aaw8151.
103. Zebedee, S.L., Barritt, D.S., and Raschke, W.C. (1991). Comparison of Mouse Ly5a and Ly5h Leucocyte Common Antigen Alleles. Dev. Immunol. *1*, 243–254. 10.1155/1991/52686.
104. Kornete, M., Marone, R., and Jeker, L.T. (2018). Highly Efficient and Versatile Plasmid-Based Gene Editing in Primary T Cells. J. Immunol. *200*, 2489–2501. 10.4049/jimmunol.1701121.
105. Mercier, F.E., Sykes, D.B., and Scadden, D.T. (2016). Single targeted exon mutation creates a true congenic mouse for competitive hematopoietic stem cell transplantation: The C57BL/6-CD45.1STEM mouse. Stem Cell Reports *6*, 985–992. 10.1016/j.stemcr.2016.04.010.
106. Symons, A., Willis, A.C., and Barclay, A.N. (1999). Domain organization of the extracellular region of CD45. Protein Eng. *12*, 885–892. 10.1093/protein/12.10.885.
107. Bork, P., and Doolittle, R.F. (1992). Proposed acquisition of an animal protein domain by bacteria. Proc. Natl. Acad. Sci. U. S. A. *89*, 8990–8994. 10.1073/pnas.89.19.8990.
108. Chang, V.T., Fernandes, R.A., Ganzinger, K.A., Lee, S.F., Siebold, C., McColl, J., Jönsson, P., Palayret, M., Harlos, K., Coles, C.H., et al. (2016). Initiation of T cell signaling by CD45 segregation at "close contacts." Nat. Immunol. *17*, 574–582. 10.1038/ni.3392.
109. Quan, L., Lv, Q., and Zhang, Y. (2016). STRUM: Structure-based prediction of protein stability changes upon single-point mutation. Bioinformatics *32*, 2936–2946. 10.1093/bioinformatics/btw361.
110. Eyrich, V.A., and Rost, B. (2003). META-PP: Single interface to crucial prediction servers. Nucleic Acids Res. *31*, 3308–3310. 10.1093/nar/gkg572.
111. James, J.R., and Vale, R.D. (2012). Biophysical mechanism of T-cell receptor triggering in a reconstituted system. Nature *487*, 64–69. 10.1038/nature11220.
112. Pulido, R., and Sánchez-Madrid, F. (1992). Glycosylation of CD45: carbohydrate processing through Golgi apparatus is required for cell surface expression and protein stability. Eur. J. Immunol. *22*, 463–468. 10.1002/eji.1830220226.
113. Medzihradszky, K.F., Kaasik, K., and Chalkley, R.J. (2015). Tissue-specific glycosylation at the glycopeptide level. Mol. Cell. Proteomics *14*, 2103–2110. 10.1074/mcp.M115.050393.
114. Lozzio, C.B., and Lozzio, B.B. (1975). Human chronic myelogenous leukemia cell line with positive Philadelphia chromosome. Blood *45*, 321–334. 10.1182/blood.v45.3.321.321.
115. Scheid, M.P., and Triglia, D. (1979). Further description of the Ly-5 system. Immunogenetics *9*, 423–433. 10.1007/BF01570435.
116. Tiller, T., Meffre, E., Yurasov, S., Tsuiji, M., Nussenzweig, M.C., and Wardemann, H. (2008). Efficient generation of monoclonal antibodies from single human B cells by single cell RT-PCR and expression vector cloning. J. Immunol. Methods *329*, 112–124. 10.1016/j.jim.2007.09.017.
117. Cleary, K.L.S., Chan, H.T.C., James, S., Glennie, M.J., and Cragg, M.S. (2017). Antibody Distance from the Cell Membrane Regulates Antibody Effector Mechanisms. J. Immunol. *198*, 3999–4011. 10.4049/jimmunol.1601473.
118. Penninger, J.M., Irie-Sasaki, J., Sasaki, T., and Oliveira-dos-Santos, A.J. (2018).

CD45: new jobs for an old acquaintance. Nat. Immunol. *2*, 389–396. 10.1038/87687.
119. Li, J., Stagg, N.J., Johnston, J., Harris, M.J., Menzies, S.A., DiCara, D., Clark, V., Hristopoulos, M., Cook, R., Slaga, D., et al. (2017). Membrane-Proximal Epitope Facilitates Efficient T Cell Synapse Formation by Anti-FcRH5/CD3 and Is a Requirement for Myeloma Cell Killing. Cancer Cell *31*, 383–395. 10.1016/j.ccell.2017.02.001.
120. Douglas, A.L., Fred, S.E., Luigi Barbieri, Fiorenzo Stirpe, and Marco Soria (1985). Characterization of a Saponaria officinalis seed ribosome-inactivating protein: Immunoreactivity and sequence homologies. Biochem. Biophys. Res. Commun. *129*, 934–942. 10.1016/0006-291X(85)91981-3.
121. Gillis, S., and Watson, J. (1980). Biochemical and biological characterization of lymphocytes regulatory molecules. J. Exp. Med. *152*, 413–420.
122. Paquet, D., Kwart, D., Chen, A., Sproul, A., Jacob, S., Teo, S., Olsen, K.M., Gregg, A., Noggle, S., and Tessier-Lavigne, M. (2016). Efficient introduction of specific homozygous and heterozygous mutations using CRISPR/Cas9. Nature *533*, 125–129. 10.1038/nature17664.
123. Chang, H.H.Y., Pannunzio, N.R., Adachi, N., and Lieber, M.R. (2017). Non-homologous DNA end joining and alternative pathways to double-strand break repair. Nat. Rev. Mol. Cell Biol. *18*, 495–506. 10.1038/nrm.2017.48.
124. Roth, T.L., Puig-Saus, C., Yu, R., Shifrut, E., Carnevale, J., Li, P.J., Hiatt, J., Saco, J., Krystofinski, P., Li, H., et al. (2018). Reprogramming human T cell function and specificity with non-viral genome targeting. Nature *559*, 405–409. 10.1038/s41586-018-0326-5.
125. Rees, H.A., and Liu, D.R. (2018). Base editing: precision chemistry on the genome and transcriptome of living cells. Nat. Rev. Genet. *19*, 770–788. 10.1038/s41576-018-0059-1.
126. Miller, S.M., Wang, T., Randolph, P.B., Arbab, M., Shen, M.W., Huang, T.P., Matuszek, Z., Newby, G.A., Rees, H.A., and Liu, D.R. (2020). Continuous evolution of SpCas9 variants compatible with non-G PAMs. Nat. Biotechnol. *38*, 471–481. 10.1038/s41587-020-0412-8.
127. Walton, R.T., Christie, K.A., Whittaker, M.N., and Kleinstiver, B.P. (2020). Unconstrained genome targeting with near-PAMless engineered CRISPR-Cas9 variants. Science (80-.). *368*, 290–296. 10.1126/science.aba8853.
128. Richter, M.F., Zhao, K.T., Eton, E., Lapinaite, A., Newby, G.A., Thuronyi, B.W., Wilson, C., Koblan, L.W., Zeng, J., Bauer, D.E., et al. (2020). Phage-assisted evolution of an adenine base editor with improved Cas domain compatibility and activity. Nat. Biotechnol. *38*, 883–891. 10.1038/s41587-020-0453-z.
129. Kim, Y.B., Komor, A.C., Levy, J.M., Packer, M.S., Zhao, K.T., and Liu, D.R. (2017). Increasing the genome-targeting scope and precision of base editing with engineered Cas9-cytidine deaminase fusions. Nat. Biotechnol. *35*, 371–376. 10.1038/nbt.3803.
130. Salmon, P., Kindler, V., Ducrey, O., Chapuis, B., Zubler, R.H., and Trono, D. (2000). High-level transgene expression in human hematopoietic progenitors and differentiated blood lineages after transduction with improved lentiviral vectors. Blood *96*, 3392–3398.
131. Zafra, M.P., Schatoff, E.M., Katti, A., Foronda, M., Breinig, M., Schweitzer, A.Y., Simon, A., Han, T., Goswami, S., Montgomery, E., et al. (2018). Optimized base editors enable efficient editing in cells, organoids and mice. Nat. Biotechnol. *36*, 888–896. 10.1038/nbt.4194.
132. Cong, L., Ran, F.A., Cox, D., Lin, S., Barretto, R., Habib, N., Hsu, P.D., Wu, X., Jiang, W., Marraffini, L.A., et al. (2013). Multiplex Genome Engineering Using

CRISPR/Cas Systems. Science (80-.)., 819–824.
133. Ran, F.A., Hsu, P.D., Wright, J., Agarwala, V., Scott, D.A., and Zhang, F. (2013). Genome engineering using the CRISPR-Cas9 system. Nat. Protoc. *8*, 2281–2308. 10.1038/nprot.2013.143.
134. Konermann, S., Brigham, M.D., Trevino, A.E., Joung, J., Abudayyeh, O.O., Barcena, C., Hsu, P.D., Habib, N., Gootenberg, J.S., Nishimasu, H., et al. (2015). Genome-scale transcriptional activation by an engineered CRISPR-Cas9 complex. Nature *517*, 583–588. 10.1038/nature14136.
135. Kleinstiver, B.P., Prew, M.S., Tsai, S.Q., Nguyen, N.T., Topkar, V. V., Zheng, Z., and Joung, J.K. (2015). Broadening the targeting range of Staphylococcus aureus CRISPR-Cas9 by modifying PAM recognition. Nat. Biotechnol. *33*, 1293–1298. 10.1038/nbt.3404.
136. Kleinstiver, B.P., Sousa, A.A., Walton, R.T., Tak, Y.E., Hsu, J.Y., Clement, K., Welch, M.M., Horng, J.E., Malagon-Lopez, J., Scarfò, I., et al. (2019). Engineered CRISPR–Cas12a variants with increased activities and improved targeting ranges for gene, epigenetic and base editing. Nat. Biotechnol. *37*, 276–282. 10.1038/s41587-018-0011-0.
137. Bras, A.E., de Haas, V., van Stigt, A., Jongen-Lavrencic, M., Beverloo, H.B., te Marvelde, J.G., Zwaan, C.M., van Dongen, J.J.M., Leusen, J.H.W., and van der Velden, V.H.J. (2019). CD123 expression levels in 846 acute leukemia patients based on standardized immunophenotyping. Cytom. Part B - Clin. Cytom. *96*, 134–142. 10.1002/cyto.b.21745.
138. K.F., B., L.A., C., S, H., A.J.H., S., J, M., D.R., A., and N, H. (2013). CD45-Null Transgenic Mice Reveal a Positive Regulatory Role for CD45 in Early Thymocyte Development, in the Selection of CD4+CD8 + Thyrnocytes, and in B Cell Maturation. J. Chem. Inf. Model. *53*, 1689–1699. 10.1017/CBO9781107415324.004.
139. Reva, B., Antipin, Y., and Sander, C. (2011). Predicting the functional impact of protein mutations: Application to cancer genomics. Nucleic Acids Res. *39*, 37–43. 10.1093/nar/gkr407.
140. Gudmundsson, S., Karczewski, K.J., Francioli, L.C., Tiao, G., Cummings, B.B., Alföldi, J., Wang, Q., Collins, R.L., Laricchia, K.M., Ganna, A., et al. (2021). Erratum: Addendum: The mutational constraint spectrum quantified from variation in 141,456 humans (Nature (2020) 581 7809 (434-443)). Nature *597*, 3–4. 10.1038/s41586-021-03758-y.
141. Persaud, S.P., Ritchey, J.K., Kim, S., Lim, S., Ruminski, P.G., Cooper, M.L., Rettig, M.P., Choi, J., and DiPersio, J.F. (2021). Antibody-drug conjugates plus Janus kinase inhibitors enable MHC-mismatched allogeneic hematopoietic stem cell transplantation. J. Clin. Invest. *131*. 10.1172/JCI145501.
142. Davis, S.J., and van der Merwe, P.A. (2006). The kinetic-segregation model: TCR triggering and beyond. Nat. Immunol. *7*, 803–809. 10.1038/ni1369.
143. Desai, D.M., Sap, J., Schlessinger, J., and Weiss, A. (1993). Ligand-mediated negative regulation of a chimeric transmembrane receptor tyrosine phosphatase. Cell *73*, 541–554. 10.1016/0092-8674(93)90141-C.
144. Majeti, R., Bilwes, A.M., Noel, J.P., Hunter, T., and Weiss, A. (1998). Dimerization-induced inhibition of receptor protein tyrosine phosphatase function through an inhibitory wedge. Science (80-.). *279*, 88–91. 10.1126/science.279.5347.88.
145. Zhu, J.W., Brdicka, T., Katsumoto, T.R., Lin, J., and Weiss, A. (2008). Structurally Distinct Phosphatases CD45 and CD148 Both Regulate B Cell and Macrophage Immunoreceptor Signaling. Immunity *28*, 183–196. 10.1016/j.immuni.2007.11.024.
146. Zikherman, J., Jenne, C., Watson, S., Doan, K., Raschke, W., Goodnow, C.C., and

Weiss, A. (2010). CD45-Csk Phosphatase-Kinase Titration Uncouples Basal and Inducible T Cell Receptor Signaling during Thymic Development. Immunity *32*, 342–354. 10.1016/j.immuni.2010.03.006.
147. Rasaiyaah, J., Georgiadis, C., Preece, R., Mock, U., and Qasim, W. (2018). TCRαβ/CD3 disruption enables CD3-specific antileukemic T cell immunotherapy. JCI insight *3*, 1–13. 10.1172/jci.insight.99442.
148. Georgiadis, C., Rasaiyaah, J., Gkazi, S.A., Preece, R., Etuk, A., Christi, A., and Qasim, W. (2021). Base-edited CAR T cells for combinational therapy against T cell malignancies. Leukemia *35*, 3466–3481. 10.1038/s41375-021-01282-6.
149. Chun, I., Kim, K.H., Chiang, Y.-H., Xie, W., Lee, Y.G.G., Pajarillo, R., Rotolo, A., Shestova, O., Hong, S.J., Abdel-Mohsen, M., et al. (2020). CRISPR-Cas9 Knock out of CD5 Enhances the Anti-Tumor Activity of Chimeric Antigen Receptor T Cells. Blood *136*, 51–52. 10.1182/blood-2020-136860.
150. Howard, S.C., Jones, D.P., and Pui, C.-H. (2011). The tumor lysis syndrome. N. Engl. J. Med. *364*, 1844–1854. 10.7326/0003-4819-114-9-808_2.
151. Ito, M., Hiramatsu, H., Kobayashi, K., Suzue, K., Kawahata, M., Hioki, K., Ueyama, Y., Koyanagi, Y., Sugamura, K., Tsuji, K., et al. (2002). NOD/SCID/γcnull mouse: An excellent recipient mouse model for engraftment of human cells. Blood *100*, 3175–3182. 10.1182/blood-2001-12-0207.
152. Shultz, L.D., Saito, Y., Najima, Y., Tanaka, S., Ochi, T., Tomizawa, M., Doi, T., Sone, A., Suzuki, N., Fujiwara, H., et al. (2010). Generation of functional human T-cell subsets with HLA-restricted immune responses in HLA class I expressing NOD/SCID/IL2rγnull humanized mice. Proc. Natl. Acad. Sci. U. S. A. *107*, 13022–13027. 10.1073/pnas.1000475107.
153. Sachs, D.H., Kawai, T., and Sykes, M. (2014). Induction of tolerance through mixed chimerism. Cold Spring Harb. Perspect. Med. *4*, 1–19. 10.1101/cshperspect.a015529.
154. Mackall, C., Fry, T., Gress, R., Peggs, K., Storek, J., and Toubert, A. (2009). Background to hematopoietic cell transplantation, including post transplant immune recovery. Bone Marrow Transplant. *44*, 457–462. 10.1038/bmt.2009.255.
155. Klein, L., Kyewski, B., Allen, P.M., and Hogquist, K.A. (2014). Positive and negative selection of the T cell repertoire: What thymocytes see (and don't see). Nat. Rev. Immunol. *14*, 377–391. 10.1038/nri3667.
156. Grupp, S.A., Kalos, M., Barrett, D., Aplenc, R., Porter, D.L., Rheingold, S.R., Teachey, D.T., Chew, A., Hauck, B., Wright, J.F., et al. (2013). Chimeric Antigen Receptor–Modified T Cells for Acute Lymphoid Leukemia. N. Engl. J. Med. *368*, 1509–1518. 10.1056/nejmoa1215134.
157. Perna, F., Berman, S.H., Soni, R.K., Mansilla-Soto, J., Eyquem, J., Hamieh, M., Hendrickson, R.C., Brennan, C.W., and Sadelain, M. (2017). Integrating Proteomics and Transcriptomics for Systematic Combinatorial Chimeric Antigen Receptor Therapy of AML. Cancer Cell *32*, 506-519.e5. 10.1016/j.ccell.2017.09.004.
158. Richardson, C., Moynahan, M.E., and Jasin, M. (1998). Double-strand break repair by interchromosomal recombination: Suppression of chromosomal translocations. Genes Dev. *12*, 3831–3842. 10.1101/gad.12.24.3831.

Annexes

Table 4: Primers

Aim	forward /reverse	Sequence
Amplify EF1a + NLS and add XbaI	forward	ATCTCTAGAGAATTGGCTCCGGTGC CCGTCA
Amplify EF1a + NLS and add NheI	reverse	ATCGCTAGCgactttcctcttcttcttgggTCAC GACACCTGAAATGGAAGAAA
Amplify Cbh-SaKKH-BE3-GFP backbone for EF1a-NLS cloning	forward	atcgctagcgccaccatgag
Amplify Cbh-SaKKH-BE3-GFP backbone for EF1a-NLS cloning	reverse	ATCTCTAGAGCCATTTGTCTGC
Amplify CD45 leader peptide for CD45RO isoform cloning and used as generic primer for variants insertion, addition of HindII	forward	ACCAAGCTTGGTACATGACCATGTA TTTGT
Amplify leader peptide CD45 for CD45RO isoform cloning	reverse	ATTAAGGTAGGCATC AGTGGGGGAAGGTGTTGGGC
Amplify the CD45RO part from exon 7 for CD45RO isoform cloning	forward	CCAACACCTTCCCCCACT GATGCCTACCTTAATGCCTC
Amplify the CD45RO part from CD45 Cter for CD45RO isoform cloning and used as generic primer for variants insertion	reverse	TGATGTCATGGAGACAGTCAT
Insert the variant E329I	forward	TGGAAAAATATTattACCTTTACT
Insert the variant E329I	reverse	AGTAAAGGTaatAATATTTTTCCA
Insert the variant E329K	forward	TGGAAAAATATTaaaACCTTTACT
Insert the variant E329K	reverse	AGTAAAGGTtttAATATTTTTCCA
Insert the variant T330E	forward	AAAAATATTGAAgaaTTTACTTGT
Insert the variant T330E	reverse	ACAAGTAAAttcTTCAATATTTTT
Insert the variant T330D	forward	AAAAATATTGAAgatTTTACTTGT
Insert the variant T330D	reverse	ACAAGTAAAatcTTCAATATTTTT
Insert the variant T330R	forward	AAAAATATTGAAcgtTTTACTTGT
Insert the variant T330R	reverse	ACAAGTAAAacgTTCAATATTTTT
Insert the variant T330K	forward	AAAAATATTGAAaaaTTTACTTGT
Insert the variant T330K	reverse	ACAAGTAAAtttTTCAATATTTTT
Insert the variant T330I	forward	AAAAATATTGAAattTTTACTTGT
Insert the variant T330I	reverse	ACAAGTAAAaatTTCAATATTTTT
Insert the variant F331T332del	forward	GAAACCTGTGATACACAGAATATT
Insert the variant F331T332del	reverse	TGTATCACAGGTTTCAATATTTTTC
Insert the variant F331del	forward	GAAACCACTTGTGATACACAGAAT ATT
Insert the variant F331del	reverse	TGTATCACAAGTGGTTTCAATATTT TTC
Insert the variant T332del	forward	GAAACCTTTTGTGATACACAGAATA TT
Insert the variant T332del	reverse	TGTATCACAAAAGGTTTCAATATTT TTC
Insert the variant T330A	forward	AAAAATATTGAAgccTTTACTTGT
Insert the variant T330A	reverse	ACAAGTAAAggcTTCAATATTTTT
Insert the variant F331S	forward	AATATTGAAACCagcACTTGTGATA

Insert the variant F331S	reverse	TATCACAAGTgctGGTTTCAATATT
Insert the variant F331I	forward	AATATTGAAACCattACTTGTGATA
Insert the variant F331I	reverse	TATCACAAGTaatGGTTTCAATATT
Insert the variant F331L	forward	AATATTGAAACCcttACTTGTGATA
Insert the variant F331L	reverse	TATCACAAGTaagGGTTTCAATATT
Insert the variant T330del	forward	AAAAATATTGAATTTACTTGT
Insert the variant T330del	reverse	ACAAGTAAATTCAATATTTTT
Insert the variant F331A	forward	AATATTGAAACCgctACTTGTGATA
Insert the variant F331A	reverse	TATCACAAGTagcGGTTTCAATATT
Insert the variant T332A	forward	AAACCTTTgctTGTGATACA
Insert the variant T332A	reverse	TGTATCACAagcAAAGGTTT
Amplify CD45 locus for Sanger sequencing	forward	CCATAGCAATCTCAATCCTTGCC
Amplify CD45 locus for Sanger sequencing	reverse	TGCCTGTGTATAACAATTGCCAAG

Table 5: QA17A19 sequencing

Variable heavy chain amino acid sequence	EVQLVESGGDLVKPGGSLKLSCAASGFAFSNYDMSWVRQTPEKRLEW VAYISSGGVSTYYPDTVKGRFTISRDNAKNTLYLQMSSLKSEDTAMYY CARRYDVWWYFDVWGAGTTVTVSSAKTTPPSVYPLAPGSAAQTNSM VTLGCLVKGYFPEPVTVTWNSGSLSSGVHTFPAVLQSDLYTLSSSVTVP SSTWPSETVTCNVAHPASSTKVDKKIVPRDCGCKPCICTVPEVSSVFIFP PKPKDVLTITLTPKVTCVVVDISKDDPEVQFSWFVDDVEVHTAQTQPR EEQFNSTFRSVSELPIMHQDWLNGKEFKCRVNSAAFPAPIEKTISKTKG RPKAPQVYTIPPPKEQMAKDKVSEEQFNSTFRSVSELPIMHQDWLNGK EFKCRVNSAAFPAPIEKTISKTKGRPKAPQVYTIPPPKEQMAKDKVSLT CMITDFFPEDITVEWQWNGQPAENYKNTQPIMDTDGSYFVYSKLNVQ KSNWEAGNTFTCSVLHEGLHNHHTEKSLSHSPGK
Variable heavy chain nucleotide sequence used for cloning	Gacgtgctgatgacccagactccgcttagtctccctgtctctcttggggatcaggccagtatttcctgtcgatcaag ccagtcaattgtgcattcaaatggtaacacctacctggagtggtatctccaaaagccgggccaatcccccaagct gctcatctataaagtatccaaccgctttagtggcgtgccggaccgcttctctggcagtggatctggcaccgacttta ctctcaagatttccagagttgaggcggaggacctcggagtctattactgcttccaggggtcccatgtgcccatgta caccttcggtgggggaaccaagcttgagataaaa
Variable kappa light chain amino acid sequence	DVLMTQTPLSLPVSLGDQASISCRSSQSIVHSNGNTYLEWYLQKPGQSP KLLIYKVSNRFSGVPDRFSGSGSGTDFTLKISRVEAEDLGVYYCFQGSH VPMYTFGGGTKLEIKRADAAPTVSIFPPSSEQLTSGGASVVCFLNNFYP KDINVKWKIDGSERQNGVLNSWTDQDSKDSTYSMSSTLTLTKDEYER HNSYTCEATHKTSTSPIVKSFNRNEV
Variable kappa light chain nucleotide sequence	gaggtgcagctggtggagagcggcggcgacctggtgaagcccggcggcagcctgaagctgagctgcgccg ccagcggcttcgccttcagcaactacgacatgagctgggtgagacagaccccgagaagagactggagtggg tggcctacatcagcagcggcggcgtgagcacctactaccccgacaccgtgaagggcagattcaccatcagcag agacaacgccaagaacaccctgtacctgcagatgagcagcctgaagagcgaggacaccgccatgtactactg cgccagaagatacgacgtgtggtggtacttcgacgtgtggggcgccggcaccaccgtgaccgtgagcagcg

Table 6: crRNA used for CRISPR/Cas9 KO

Name	**sequence**	**purpose**
CD45 exon 10 crRNA1	ATTCTGTGTATCACAAGTAA	gRNA used to KO CD45 using CRISPR/Cas9
CD45 exon 10 crRNA3	CTTACCACACTGAAATCTGT	gRNA used to KO CD45 using CRISPR/Cas9

Table 7: HDR templates

Name	Sequence
ssDNA CD45 gRNA3 F331del	/Alt-R-HDR1/T*T*TAAAATGGAAAAATATTGAAACCACTTGcGAcACtCAaAAcATcACaTAtAGATTTCAGTGTGGTAAGAATATAACATTGACCAGAGAATTTTTTTTTGT*G*G/Alt-R-HDR2/
ssDNA CD45 gRNA3 F331_T332del	/Alt-R-HDR1/T*T*TAAAATGGAAAAATATTGAAACCTGcGAcACtCAaAAcATcACaTAtAGATTTCAGTGTGGTAAGAATATAACATTGACCAGAGAATTTTTTTTTGT*G*G/Alt-R-HDR2/
ssDNA CD45 gRNA3 T330del	/Alt-R-HDR1/T*T*TAAAATGGAAAAATATTGAATTcACgTGcGAcACtCAaAAcATcACaTAtAGATTTCAGTGTGGTAAGAATATAACATTGACCAGAGAATTTTTTTTTGT*G*G/Alt-R-HDR2/
ssDNA CD45 gRNA3 T330K	/Alt-R-HDR1/T*T*TAAAATGGAAAAATATTGAAAAATTcACgTGcGAcACtCAaAAcATcACaTAtAGATTTCAGTGTGGTAAGAATATAACATTGACCAGAGAATTTTTTTTTGT*G*G/Alt-R-HDR2/
ssDNA CD45 gRNA3 T332del	Alt-R-/HDR1/T*T*TTAAAATGGAAAAATATTGAAACCTTTTGcGAcACtCAaAAcATcACaTAtAGATTTCAGTGTGGTAAGAATATAACATTGACCAGAGAATTTTTTTTTGT*G*G/Alt-R-HDR2/

Table 8: Antibodies

Target	**clone**	**Cat number**	**color**	**company**	**concentration**
CD45	2D1	368507	FITC	Biolegend	1:200
CD45	HI30	304005 304014	FITC APC-Cy7	Biolegend	1:200
CD45	QA17A19	393411	PE	Biolegend	1:200
CD45	F10-89-4	GTX76581	APC	GeneTex/lucerna	1:100
CD45	MEM-28	GTX79950	PerCP	GeneTex/lucerna	1:100
CD45	B-A11	ab27287	FITC	Abcam	1:100
CD45	10B1611	C2399-07G2-Biotin	No/strep-PE	USBiological/lucerna	1:200, Strep-PE dil 1:200
CD45	5K237	C2399-14G	Cy5	USBiological/lucerna	1:100
CD45	15j36	C2400-10R	FITC	USBiological/lucerna	1:100
CD45	YAML 501.4	CL7605APC-S	APC	Cedarlane/ Bioconcept	1:200
CD45	5B1	130-113-676	APC	Miltenyi Biotech	1:500
CD45	BRA-11	MAB12142	no/Cy5	Abnova	1:100, 2nd dil 1:100
CD45	MIRG451	Produced in the lab	Ax647 Biotin/Strep-PE for sort	N/A	1:100
CD4	OKT4	317443	BV510	Biolegend	1:100
CD8	RPA-T8	301031	PercP-Cy5.5	Biolegend	1:100

Table 9: crRNAs used for BE

Name	aa aimed	Aimed editing	BE used	sequence	purpose
crRNA FANCF1	N/A	C to T	SaKKH-BE3	GATGTTC CAATCAG TACGCA	edit FANCF locus with SaKKH-BE3
T330I CD45 exon 10	T330	C to T	SaKKH-BE3	AAACCTT TACTTGT GATACA	edit T330I in CD45 locus with SaKKH-BE3
Y340C CD45 exon 10	Y340	A to G	ABE 7.10	ATTACCT ACAGATT TCAGTG	edit Y340C in CD45 locus with ABE7.10
Mutation A	N327,I 328, E329, T330	C to T	SaKKH-ABE8	AAAATAT TGAAACC TTTACT	screen base editable sites around E329-T332 in CD45
Mutation B	I328	A to G	ABE8e-NG, ABEmax-SpG	AATATTG AAACCTT TACTTG	screen base editable sites around E329-T332 in CD45, ordered as gRNA to edit I328V with ABEmax-SpG mRNA
Mutation C1	E329,T 330	A to G	ABEmax-SpRY	ATTGAAA CCTTTAC TTGTGA	screen base editable sites around E329-T332 in CD45
Mutation C2	E329,T 330	A to G	ABEmax-SpRY	ATATTGA AACCTTT ACTTGT	screen base editable sites around E329-T332 in CD45
Mutation C3	E329,T 330	A to G	ABEmax-SpRY	TGAAACC TTTACTT GTGATA	screen base editable sites around E329-T332 in CD45
Mutation D	E329	C to T	CBEmax-SpRY	GTTTCAA TATTTTT CCATTT	screen base editable sites around E329-T332 in CD45
Mutation E	F331	A to G	ABEmax-SpRY	GTAAAGG TTTCAAT ATTTTT	screen base editable sites around E329-T332 in CD45
Mutation F,G	F331, C333	(F) A to G, (G) C to T	(F)ABEmax-SpRY, (G)CBEmax-SpRY	ATCACAA GTAAAGG TTTCAA	screen base editable sites around E329-T332 in CD45
Mutation H	T332	A to G	ABEmax-SpRY	TTTACTT GTGATAC ACAGAA	screen base editable sites around E329-T332 in CD45
Mutation I	T332	C to T	CBEmax-SpRY	TTTACTT GTGATAC ACAGAA	screen base editable sites around E329-T332 in CD45

Table 10: mRNA construct

ABEmax-SpG	ATGAAACGGACAGCCGACGGAAGCGAGTTCGAGTCACCAAAGAAGA AGCGGAAAGTCTCTGAAGTCGAGTTTAGCCACGAGTATTGGATGAGG CACGCACTGACCCTGGCAAAGCGAGCATGGGATGAAAGAGAAGTCCC CGTGGGCGCCGTGCTGGTGCACAACAATAGAGTGATCGGAGAGGGAT GGAACAGGCCAATCGGCCGCCACGACCCTACCGCACACGCAGAGATC ATGGCACTGAGGCAGGGAGGCCTGGTCATGCAGAATTACCGCCTGAT CGATGCCACCCTGTATGTGACACTGGAGCCATGCGTGATGTGCGCAGG AGCAATGATCCACAGCAGGATCGGAAGAGTGGTGTTCGGAGCACGGG ACGCCAAGACCGGCGCAGCAGGCTCCCTGATGGATGTGCTGCACCAC CCCGGCATGAACCACCGGGTGGAGATCACAGAGGGAATCCTGGCAGA CGAGTGCGCCGCCCTGCTGAGCGATTTCTTTAGAATGCGGAGACAGGA GATCAAGGCCCAGAAGAAGGCACAGAGCTCCACCGACTCTGGAGGAT CTAGCGGAGGATCCTCTGGAAGCGAGACACCAGGCACAAGCGAGTCC GCCACACCAGAGAGCTCCGGCGGCTCCTCCGGAGGATCCTCTGAGGT GGAGTTTTCCCACGAGTACTGGATGAGACATGCCCTGACCCTGGCCAA GAGGGCACGCGATGAGAGGGAGGTGCCTGTGGGAGCCGTGCTGGTGC TGAACAATAGAGTGATCGGCGAGGGCTGGAACAGAGCCATCGGCCTG CACGACCCAACAGCCCATGCCGAAATTATGGCCCTGAGACAGGGCGG CCTGGTCATGCAGAACTACAGACTGATTGACGCCACCCTGTACGTGAC ATTCGAGCCTTGCGTGATGTGCGCCGGCGCCATGATCCACTCTAGGAT CGGCCGCGTGGTGTTTGGCGTGAGGAACGCAAAAACCGGCGCCGCAG GCTCCCTGATGGACGTGCTGCACTACCCCGGCATGAATCACCGCGTCG AAATTACCGAGGGAATCCTGGCAGATGAATGTGCCGCCCTGCTGTGCT ATTTCTTTCGGATGCCTAGACAGGTGTTCAATGCTCAGAAGAAGGCCC AGAGCTCCACCGACTCCGGAGGATCTAGCGGAGGCTCCTCTGGCTCTG AGACACCTGGCACAAGCGAGAGCGCAACACCTGAAAGCAGCGGGGG CAGCAGCGGGGGGTCAGACAAGAAGTACAGCATCGGCCTGGCCATCG GCACCAACTCTGTGGGCTGGGCCGTGATCACCGACGAGTACAAGGTG CCCAGCAAGAAATTCAAGGTGCTGGGCAACACCGACCGGCACAGCAT CAAGAAGAACCTGATCGGAGCCCTGCTGTTCGACAGCGGCGAAACAG CCGAGGCCACCCGGCTGAAGAGAACCGCCAGAAGAAGATACACCAGA CGGAAGAACCGGATCTGCTATCTGCAAGAGATCTTCAGCAACGAGAT GGCCAAGGTGGACGACAGCTTCTTCCACAGACTGGAAGAGTCCTTCCT GGTGGAAGAGGATAAGAAGCACGAGCGGCACCCCATCTTCGGCAACA TCGTGGACGAGGTGGCCTACCACGAGAAGTACCCCACCATCTACCACC TGAGAAAGAAACTGGTGGACAGCACCGACAAGGCCGACCTGCGGCTG ATCTATCTGGCCCTGGCCCACATGATCAAGTTCCGGGGCCACTTCCTG ATCGAGGGCGACCTGAACCCCGACAACAGCGACGTGGACAAGCTGTT CATCCAGCTGGTGCAGACCTACAACCAGCTGTTCGAGGAAAACCCCAT CAACGCCAGCGGCGTGGACGCCAAGGCCATCCTGTCTGCCAGACTGA GCAAGAGCAGACGGCTGGAAAATCTGATCGCCCAGCTGCCCGGCGAG AAGAAGAATGGCCTGTTCGGAAACCTGATTGCCCTGAGCCTGGGCCTG ACCCCCAACTTCAAGAGCAACTTCGACCTGGCCGAGGATGCCAAACT GCAGCTGAGCAAGGACACCTACGACGACGACCTGGACAACCTGCTGG CCCAGATCGGCGACCAGTACGCCGACCTGTTTCTGGCCGCCAAGAACC TGTCCGACGCCATCCTGCTGAGCGACATCCTGAGAGTGAACACCGAG ATCACCAAGGCCCCCCTGAGCGCCTCTATGATCAAGAGATACGACGA GCACCACCAGGACCTGACCCTGCTGAAAGCTCTCGTGCGGCAGCAGCT GCCTGAGAAGTACAAAGAGATTTTCTTCGACCAGAGCAAGAACGGCT ACGCCGGCTACATTGACGGCGGAGCCAGCCAGGAAGAGTTCTACAAG TTCATCAAGCCCATCCTGGAAAAGATGGACGGCACCGAGGAACTGCT CGTGAAGCTGAACAGAGAGGACCTGCTGCGGAAGCAGCGGACCTTCG ACAACGGCAGCATCCCCCACCAGATCCACCTGGGAGAGCTGCACGCC ATTCTGCGGCGGCAGGAAGATTTTTACCCATTCCTGAAGGACAACCGG

	GAAAAGATCGAGAAGATCCTGACCTTCCGCATCCCCTACTACGTGGGC CCTCTGGCCAGGGGAAACAGCAGATTCGCCTGGATGACCAGAAAGAG CGAGGAAACCATCACCCCCTGGAACTTCGAGGAAGTGGTGGACAAGG GCGCTTCCGCCCAGAGCTTCATCGAGCGGATGACCAACTTCGATAAGA ACCTGCCCAACGAGAAGGTGCTGCCCAAGCACAGCCTGCTGTACGAG TACTTCACCGTGTATAACGAGCTGACCAAAGTGAAATACGTGACCGA GGGAATGAGAAAGCCCGCCTTCCTGAGCGGCGAGCAGAAAAAGGCCA TCGTGGACCTGCTGTTCAAGACCAACCGGAAAGTGACCGTGAAGCAG CTGAAAGAGGACTACTTCAAGAAAATCGAGTGCTTCGACTCCGTGGA AATCTCCGGCGTGGAAGATCGGTTCAACGCCTCCCTGGGCACATACCA CGATCTGCTGAAAATTATCAAGGACAAGGACTTCCTGGACAATGAGG AAAACGAGGACATTCTGGAAGATATCGTGCTGACCCTGACACTGTTTG AGGACAGAGAGATGATCGAGGAACGGCTGAAAACCTATGCCCACCTG TTCGACGACAAAGTGATGAAGCAGCTGAAGCGGCGGAGATACACCGG CTGGGGCAGGCTGAGCCGGAAGCTGATCAACGGCATCCGGGACAAGC AGTCCGGCAAGACAATCCTGGATTTCCTGAAGTCCGACGGCTTCGCCA ACAGAAACTTCATGCAGCTGATCCACGACGACAGCCTGACCTTTAAAG AGGACATCCAGAAAGCCCAGGTGTCCGGCCAGGGCGATAGCCTGCAC GAGCACATTGCCAATCTGGCCGGCAGCCCCGCCATTAAGAAGGGCAT CCTGCAGACAGTGAAGGTGGTGGACGAGCTCGTGAAAGTGATGGGCC GGCACAAGCCCGAGAACATCGTGATCGAAATGGCCAGAGAGAACCAG ACCACCCAGAAGGGACAGAAGAACAGCCGCGAGAGAATGAAGCGGA TCGAAGAGGGCATCAAAGAGCTGGGCAGCCAGATCCTGAAAGAACAC CCCGTGGAAAACACCCAGCTGCAGAACGAGAAGCTGTACCTGTACTA CCTGCAGAATGGGCGGGATATGTACGTGGACCAGGAACTGGACATCA ACCGGCTGTCCGACTACGATGTGGACCATATCGTGCCTCAGAGCTTTC TGAAGGACGACTCCATCGACAACAAGGTGCTGACCAGAAGCGACAAG AACCGGGGCAAGAGCGACAACGTGCCCTCCGAAGAGGTCGTGAAGAA GATGAAGAACTACTGGCGGCAGCTGCTGAACGCCAAGCTGATTACCC AGAGAAAGTTCGACAATCTGACCAAGGCCGAGAGAGGCGGCCTGAGC GAACTGGATAAGGCCGGCTTCATCAAGAGACAGCTGGTGGAAACCCG GCAGATCACAAAGCACGTGGCACAGATCCTGGACTCCCGGATGAACA CTAAGTACGACGAGAATGACAAGCTGATCCGGGAAGTGAAAGTGATC ACCCTGAAGTCCAAGCTGGTGTCCGATTTCCGGAAGGATTTCCAGTTT TACAAAGTGCGCGAGATCAACAACTACCACCACGCCCACGACGCCTA CCTGAACGCCGTCGTGGGAACCGCCCTGATCAAAAAGTACCCTAAGCT GGAAAGCGAGTTCGTGTACGGCGACTACAAGGTGTACGACGTGCGGA AGATGATCGCCAAGAGCGAGCAGGAAATCGGCAAGGCTACCGCCAAG TACTTCTTCTACAGCAACATCATGAACTTTTTCAAGACCGAGATTACC CTGGCCAACGGCGAGATCCGGAAGCGGCCTCTGATCGAGACAAACGG CGAAACCGGGGAGATCGTGTGGGATAAGGGCCGGGATTTTGCCACCG TGCGGAAAGTGCTGAGCATGCCCCAAGTGAATATCGTGAAAAAGACC GAGGTGCAGACAGGCGGCTTCAGCAAAGAGTCTATCCTGCCCAAGAG GAACAGCGATAAGCTGATCGCCAGAAAGAAGGACTGGGACCCTAAGA AGTACGGCGGCTTCCTGTGGCCCACCGTGGCCTATTCTGTGCTGGTGG TGGCCAAAGTGGAAAAGGGCAAGTCCAAGAAACTGAAGAGTGTGAA AGAGCTGCTGGGGATCACCATCATGGAAAGAAGCAGCTTCGAGAAGA ATCCCATCGACTTTCTGGAAGCCAAGGGCTACAAAGAAGTGAAAAAG GACCTGATCATCAAGCTGCCTAAGTACTCCCTGTTCGAGCTGGAAAAC GGCCGGAAGAGAATGCTGGCCTCTGCCAAGCAGCTGCAGAAGGGAAA CGAACTGGCCCTGCCCTCCAAATATGTGAACTTCCTGTACCTGGCCAG CCACTATGAGAAGCTGAAGGGCTCCCCCGAGGATAATGAGCAGAAAC AGCTGTTTGTGGAACAGCACAAGCACTACCTGGACGAGATCATCGAG CAGATCAGCGAGTTCTCCAAGAGAGTGATCCTGGCCGACGCTAATCTG GACAAAGTGCTGTCCGCCTACAACAAGCACCGGGATAAGCCCATCAG

	AGAGCAGGCCGAGAATATCATCCACCTGTTTACCCTGACCAATCTGGG AGCCCCTGCCGCCTTCAAGTACTTTGACACCACCATCGACCGGAAGCA GTACAGAAGCACCAAAGAGGTGCTGGACGCCACCCTGATCCACCAGA GCATCACCGGCCTGTACGAGACACGGATCGACCTGTCTCAGCTGGGA GGTGACTCTGGCGGCTCAAAAAGAACCGCCGACGGCAGCGAATTCGA GCCCAAGAAGAAGAGGAAAGTC
sgRNA (protospacer)	AATATTGAAACCTTTACTTG

CV

Anna Devaux

92A avenue de Bâle,
68300 Saint Louis, France
(+33) 06 80 67 94 42
anna.devaux@unibas.ch

Profile:

I am very interested about Immunology and genome engineering strategies and I enjoy working on translational projects with a clear impact on patients. In addition, I like to work in highly collaborative environments.

Skills

Sterile Cell culture techniques	Primary cells: human and mouse T cells, PBMCs Human cell lines adherent and in suspension: K562, Jurkat, HEK293, TF-1 Mouse cell lines: Ba/F3, EL4
Cell based assays	ADCC reporter Bioassay (Promega) CellTiter-Glo® Luminescent Cell Viability Assay Flow Cytometry scanning (BD LSR Fortessa), Flow Cytometry sorting (BD FACSMelody)
Immunoassays	Western Blot, ELISA
Molecular Biology	Cloning by restriction enzymes, cloning by Gibson Assembly PCR, Sanger sequencing analysis
Gene editing technologies	CRISPR/Cas9 knock-out, CRISPR/Cas9 knock-in with Homology Directed Repair template Cytosine Base editing, Adenine Base editing
Software	FlowJo Graphpad prism DNASTAR Lasergene, Snapgene Microsoft Office (Word, Excel, PowerPoint), Affinity Designer
Languages	French (mother tongue) English (fluent) German (starter)

Experience

PhD student (08/2018 - Current, 4 years, full-time)
Laboratory of Molecular Immune Regulation of Prof. Dr. Lukas T. Jeker
Department of Biomedicine, University of Basel, Basel, Switzerland

- Engineered safe mutations to protect cells from antibody-based targeted therapy
- Optimized Base Editing strategies to insert point mutations into a protein target
- Presented talks (FOCIS 2022, Wolfsberg meeting 2020-2021) and posters (Ubico retreat 2019; DBM PhD retreat and URI meeting 2019-2021)
- Led student association organizing monthly seminars for students (ImmunoPhD club) for 4 years and participated to the preparation and execution of the Day of Immunology 2022

Master Student (09/2017 - 06/2018, 6 months, internship)
Laboratory for Systems and Synthetic Immunology of Dr. Prof. Sai Reddy
D-BSSE, ETH Zürich, Basel, Switzerland

- Engineered doxycycline inducible constructs in Jurkat cells with CRISPR/Cas9 to discover novel genomic safe harbor loci

Scientific Associate (11/2016 - 06/2017, 9 months, full-time)
Protein Production and Antibody unit
NBC (NIBR Biologics Center), NIBR (Novartis Institute for Biomedical Research), Novartis, Basel, Switzerland

- Generated stable cell line for protein expression
- Produced proteins in small scale and analysed their expression by Western Blot

Research Associate (02/2015 - 09/2016, 10 months, full-time)
Protein Expression and Cell Line Generation
Glenmark Pharmaceuticals, La Chaux-de-Fonds, Switzerland

- Produced proteins in CHO and HEK cells before to purify them with resins and Akta

Education

- **Doctoral degree in Biology,** Molecular Immune Regulation, Lukas T. Jeker (2019-Current)
  University of Basel, Department of Biomedicine (Basel, Switzerland)
- **M.Sc. in Immunology,** Research in Innovative Immunotherapies and Vaccinations (2017-2018)
  Sorbonne University, Paris (France)
- **M.Sc in Biotechnology Engineering** (2012-2015)
  Polytech Marseille engineering school in biotechnology (ex-ESIL), Marseille (France)

Publications and patents

Epitope Engineered Human Haematopoietic Stem Cells are Shielded from CD123-targeted Immunotherapy
Emmanuelle Landmann*, **Anna Devaux***, Rosalba Lepore*, Romina Marone*, Corinne Engdahl, Giuseppina Capoferri, Alessandro Dell'Aglio, Amélie Wiederkehr, Alessandro Sinopoli, Valentin Do Sacramento, Anna Haydn, Laura Garcia-Prat, Christopher Divsalar, Anna Camus, Liwen Xu, Lorenza Bordoli, Torsten Schwede, Matthew Porteus, Stefanie Urlinger and Lukas T. Jeker (in revision)
* These authors contributed equally

Co-inventor on a patent aiming to shield cells from targeted therapies by introduction of point mutations in CD45

Co-inventor on a patent aiming to shield cells from targeted therapies by introduction of point mutations in CD123

Discovery and validation of human genomic safe harbor sites for gene and cell therapies
Erik Aznauryan, Alexander Yermanos, Elvira Kinzina, **Anna Devaux,** Edo Kapetanovic, Denitsa Milanova, George M. Church, and Sai T. Reddy, Cell Reports Method (2022)

Additional

Sport: Badminton (competition), hiking, reading

References

1. **Dr. Bernd Voedisch, Investigator III**
   Novartis Institutes for BioMedical Research
   NIBR Biologics Center (NBC) / PPA, Novartis Pharma AG
   Novartis Campus CH-4056 Basel (Switzerland)
   bernd.voedisch@novartis.com
   Phone: +41 61 529 21 39

2. **Prof. Dr. Sai Reddy**
   D-BSSE
   Laboratory for Systems and Synthetic Immunology
   Mattenstrasse 26
   4058 Basel (Switzerland)
   sai.reddy@bsse.ethz.ch
   Phone: +41 61 387 33 68

3. **Prof. Dr. Lukas T. Jeker (current employer)**
   Departement Biomedizin
   Hebelstrasse 20
   4031 Basel (Switzerland)
   lukas.jeker@unibas.ch
   Phone : +41 61 328 50 27